UNIVERSITY OF LONDON THESIS

Degree PhD Year 2008 Name of Author HUANG, ZHUO

Title

Properties of NMDA receptors in the rat basal ganglia

By

Zhuo Huang

A thesis submitted to the

University of London

in partial fulfillment of the requirements for the degree of

Doctor of Philosophy

Department of Pharmacology
UCL
2008

ProQuest LLC
789 East Eisenhower Parkway
P.O. Box 1346
Ann Arbor, MI 48106-1346

Abstract

Native subtypes of NMDA receptors with distinct developmental and anatomical distribution are present in the brain. Knowledge of their function and pharmacology greatly helps in understanding the involvement of NMDA receptors in physiological and pathological processes in the central nervous system.

Multiple patch-clamping methods were carried out in my experiments. First, the single-channel properties of native NMDA receptors were studied in outside-out patches excised from neuronal cell bodies in substantia nigra pars compacta (SNc) and subthalamic nucleus (STN) from 7-day old rats. The steady state channel activations produced by NMDA (100 nM or 200 μM) and glycine (10 μM) were studied at -60 mV. The results showed that both large and small conductance channels are present on STN and SNc neurons. These large conductance NMDA channels from SNc and STN display a high ifenprodil sensitivity, suggesting NR2B-containing NMDA receptors are present on SNc and STN neurons. In addition, direct transition analysis suggests that the small conductance channels may be due to NR2D-containing NMDA receptors.

Second, whole-cell patch-clamp recording of bath application-induced NMDA receptor-mediated currents (I_{NMDA}) in dopaminergic neurons of SNc in brain slices from P7 rats was used to characterize the ifenprodil inhibition and voltage-dependence of Mg^{2+} block of NMDA receptors. The NMDA-induced whole-cell currents were evoked by NMDA (10 μM or 200 μM) and glycine (10 μM). There are two main findings from the whole-cell experiments. (1) The NMDA-induced whole-cell currents display a high ifenprodil sensitivity, suggesting the presence of NR2B-containing NMDA receptors on P7

rat SNc neurons. (2) The combined application of Mg^{2+} and ifenprodil reduced the voltage-dependent Mg^{2+} block, which is consistent with recombinant NR2D-containing NMDA receptors that have a lower affinity for Mg^{2+}. This suggests that NR2D-containing NMDA receptors are present in P7 rat SNc.

Third, in order to evaluate the deactivation kinetics of extrasynaptic NMDARs, outside-out patches containing multiple channels were obtained from P7 rat dopaminergic neurons of SNc and stimulated with a brief synaptic-like (1-4ms) pulse of 1mM glutamate. The results suggested that the triheteromeric NR1-NR2B-NR2D rather than diheteromeric NR1-NR2D NMDA receptors are present on extrasynaptic sites of SNc neurons.

In addition, in order to investigate voltage-dependent Mg^{2+} block and memantine block, several channel block models were developed to evaluate multiple Mg^{2+} effects on native NMDA receptors and competition between Mg^{2+} and memantine for block of NMDAR channels.

Table of contents

List of Figures

List of Tables

Acknowledgements

I would like to express appreciation to my supervisor Alasdair J. Gibb for his patient guidance and continuous support, for being always kind and for his hard work, for his efforts in obtaining financial support to allow me to finish my PhD and achieve my dream, for his thoughtful consideration to my study and life, for his good sense of humor and his invaluable friendship. Whenever I had problem, he was always there to listen and to give me advice to solve the problems in my experiments and in my life. He taught me how to treat people sincerely, how to face and solve problems with optimistic attitude, how to become a good researcher. Without his encouragement and help, I could not have finished this thesis. I'll cherish the opportunity of being part of the world of young neuroscientists.

I would like to thank my parents, Guizhi Huang and Jing Liu, for giving me life in the first place and educating me with aspects of both science and ethics. Thanks for their unconditional support and encouragement to pursue my dream even when the dream went beyond boundaries of language, field and geography. Thanks for all their love and their confidence in me when I doubted myself.

I would like to thank my girl friend, Ye Cao, for all her love, continuous support, encouragement and understanding. Thanks for always being present in the airports or train stations when I came back from meetings, for all the delicious lunches and soups that she made for me, for all the happy times that she have given to me. She is making me the happiest man on earth.

I would like to thank my colleagues, Francisco Suarez and Michicko Takahashi, for their care, support, encouragement, enthusiasm and friendship. They offered me valuable ideas, suggestions and criticism with profound knowledge in a rich research experience. Their patience and kindness are greatly appreciated.

I am also grateful to Tina Tong, Seb Karcun and Kieran Boyle for their care and friendship. They are making the environment here fun and enjoyable.

Finally, I would like to thank the Overseas Research Association and UCL Graduate School for their financial support.

List of abbreviations

AIDS : Acquired Immunodeficiency syndrome
AMPA: : α-amino-3-hydroxy-5-methyl-4-isoxazolepropionic acid
CA1: Cornu Ammon region 1
Ca^{2+}: Calcium ions
cAMP: cyclic Adenosine monophosphate
cDNA: complementary Deoxyribonucleic acid
CONSAM: Continuous sampling program
DNQX: 6,7-Dinitroquinoxaline-2,3-dione
EGTA: Ethylene Glycol-bis(β-aminoethyl Ether) N,N,N',N'-Tetraacetic acid
EKDIST: Single-channel distribution program
EPSC: Excitatory post-synaptic current
GPe: external segment of globus pallidus
GPi: internal segment of globus pallidus
GABA: γ-aminobutyric acid
GluR: Glutamate receptor
HEK 293 cells: Human embryonic kidney 293 cells
HEPES: N-[2-Hydroxyethyl]piperazine-N'-[2-ethanesulfonic acid]
IC_{50}: Concentration giving 50% inhibition
K^+: Potassium ions
KA: Kainate
KA1: Kainate receptor subunit 1
KA2: Kainate receptor subunit 2
LTD: Long term depression
LTP: Long term potentiation
Mg^{2+}: Magnesium ions
mGluR1: Metabotropic glutamate receptor 1
mGluR2: Metabotropic glutamate receptor 2
mGluR3: Metabotropic glutamate receptor 3
mGluR4: Metabotropic glutamate receptor 4
mGluR5: Metabotropic glutamate receptor 5
mGluR6: Metabotropic glutamate receptor 6
mGluR7: Metabotropic glutamate receptor 7
mGluR8: Metabotropic glutamate receptor 8
mGluRs: Metabotropic glutamate receptors
mRNA: Messenger ribonucleic acid
Na^+: Sodium ions
NMDA: N-Methyl-d-Aspartic acid
NMDAR: *N*-Methyl-d-Aspartate receptor
NMDAR1, NR1: *N*-Methyl-d-Aspartate receptor subunit 1
NMDAR2A, NR2A: *N*-Methyl-d-Aspartate receptor subunit 2A
NMDAR2B, NR2B: *N*-Methyl-d-Aspartate receptor subunit 2B
NMDAR2C, NR2C: *N*-Methyl-d-Aspartate receptor subunit 2C
NMDAR2D, NR2D: *N*-Methyl-d-Aspartate receptor subunit 2D
NMDAR3A, NR3A: *N*-Methyl-d-Aspartate receptor subunit 3A
NMDAR3B, NR3B: *N*-Methyl-d-Aspartate receptor subunit 3B

P7: Post-natal day 7
P14: Post-natal day 14
P_{open}: Probability of being open
pS: picoSiemen
PD: Parkinson's disease
PSD-95: Post-synaptic density protein 95
SCAN: Single-channel analysis program
SCN: Central nervous system
SNc: substantia nigra pars compacta
SNr: substantia nigra pars reticulata
STN: subthalamic nucleus
TTX: Tetrodotoxin (anhydrotetrodotoxin 4-epitetrodotoxin, tetrodonic acid)
t_{crit_2}: Critical time
Zn^{2+}: Zinc ions

Chapter 1: Introduction

1.1 Glutamate receptors

In the central nervous system (CNS), L-glutamate is major excitatory neurotransmitter and mediates its actions via activation of both ionotropic and metabotropic receptor families. Metabotropic glutamate receptors are coupled to intracellular effector systems via G-proteins (Conn & Pin 1997) and ionotropic glutamate receptors are responsible for fast changes in membrane permeability (Ozawa *et al.* 1998; Dingledine *et al.* 1999; Kew & Kemp 2005).

1.1.1 Classification of glutamate receptors

1.1.1.1 Metabotropic glutamate receptors

Metabotropic glutamate receptors (mGluRs) play an important role in the transduction of glutamate-mediated signalling via coupling through G-proteins to intracellular second messenger cascades. They have been classified into groups 1, 2 and 3. Group 1 (mGluR1 and mGluR5) receptors are coupled to phospholipase C mediating increases in intracellular calcium and protein kinase C activation. Group 2 (mGluR2 and mGluR3) and group 3 (mGluR4, mGluR6, mGluR7, mGluR8) are negatively coupled to adenylate cyclase, producing a decrease in cAMP and reduced protein kinase A activation (Conn & Pin 1997).

1.1.1.2 Ionotropic glutamate receptors

1.1.1.2.1 Structure of ionotropic glutamate receptors

All subunits of ionotropic glutamate receptors are listed in Figure 1.1 and they all share a similar structure. The transmembrane topology of ionotropic glutamate receptors is shown in Figure 1.2 which is different from the classic four transmembrane domain model of the nicotinic acetylcholine receptors (Unwin 1989; Hollmann *et al.* 1994). Ionotropic glutamate receptor subunits possess an extracellular N terminus domain followed by a first transmembrane domain and then a pore forming membrane-residing domain that does not cross the membrane but forms a re-entrant loop entering from and exiting to the cytoplasm. The second and third transmembrane domains are linked by a large extracellular loop and the third transmembrane domain is followed by an intracellular C terminus. The crystal structure of the iGluR ligand binding domains, which comprise polypeptides in both the amino terminus (S1 domain) and the extracellular loop between transmembrane domains 3 and 4 (S2 domain), has confirmed this topology model for the ionotropic glutamate receptor family (Armstrong *et al.* 1998; Mayer & Armstrong 2004; Chen & Wyllie 2006; Mayer 2006).

Based on pharmacology, ionotropic glutamate receptors have been classified according to their agonist selectivity into three major sub-classes: α-amino-3-hydroxy-5-methyl-4-isoxazole propionate (AMPA) receptors, kainate receptors and N-methyl-D-aspartate (NMDA) receptors.

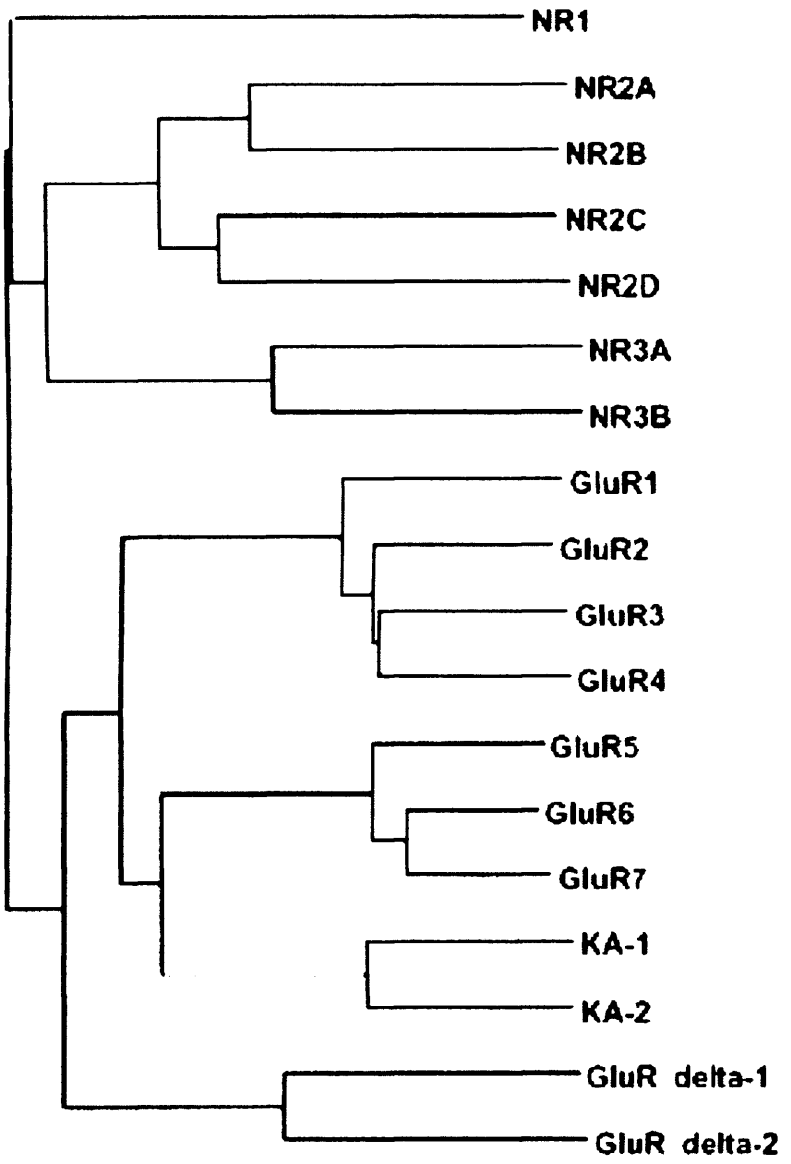

Figure 1.1 The subunit families of ionotropic glutamate receptors (Figure is taken from Wollmuth & Sobolevsky, 2004)

Seven NMDA receptor subunits have been identified: NR1 subunit, a family of NR2 subunits (NR2A, NR2B, NR2C and NR2D) and a pair of NR3 subunits (NR3A and NR3B). AMPARs are composed of four types of subunits, designated as GluR1, GluR2, GluR3, and GluR4. There are five types of kainate receptor subunits, GluR5, GluR6, GluR7, KA1 and KA2, which are similar to AMPA and NMDA receptor subunits and can be arranged in different ways to form a tetramer: a four subunit receptor (Wollmuth & Sobolevsky 2004).

Figure 1.2 The common structure of subunits of ionotropic glutamate receptors (The figure is taken from Paoletti & Neyton, 2007)

Each subunit has an extracellular N-terminus followed by the first transmembrane domain and then a pore-forming domain which does not cross the membrane. The second and third transmembrane domains have a large extra cellular S2 loop which forms the agonist binding site with the S1 region of the extracellular N-terminus. The third transmembrane domain is followed by an intracellular C-terminus that contains important phosphorylation sites that regulate receptor distribution and trafficking

1.1.1.2.2 NMDA receptors

NMDA receptors (NMDARs) are the most complex ionotropic glutamate receptors, differing from AMPA and kainate receptors in many ways. First, NMDA receptors show slow gating kinetics and a high permeability to calcium ions. The activation of NMDA receptors allows the flow of Na^+ and Ca^{2+} ions into the cell and K^+ out of the cell. The calcium flux through NMDARs is thought to contribute to a cascade of intracellular events that transduces the synaptic event into a cellular change that may trigger long-term potentiation (LTP) and long-term depression (LTD) of synaptic transmission. Second, NMDA receptors need both agonist and co-agonist to effectively activate the receptor. It has been suggested that endogenous agonists of NMDA receptors are L-glutamate and L-aspartate (Patneau & Mayer 1990) although the kinetics of aspartate-activated receptors do not match the kinetics of synaptic currents (Lester & Jahr 1992). Glycine was first reported to potentiate NMDA receptor activation (Johnson & Ascher 1987) although the endogenous co-agonist is thought to be D-serine (Wolosker 2006). Third, the NMDA receptors undergo a voltage-dependent block by physiological levels of extracellular Mg^{2+} (Ault *et al.*, 1980; Mayer *et al.*, 1984; Nowak *et al.*, 1984). The voltage-dependent Mg^{2+} block means that at resting potential, the NMDAR-mediated current is nearly fully blocked by extracellular Mg^{2+} and the blockade is relieved during cell depolarization. Therefore, effective activation of NMDA receptors not only needs the binding of agonist and co-agonist but also needs depolarization of the postsynaptic membrane. Lastly, the activity of NMDA receptors is highly regulated by endogenous extracellular protons, zinc and polyamines.

The unique characteristics of NMDA receptors suggest its important role in central nervous system. Under physiological conditions, signalling through NMDA receptors mediates processes of neuronal cell migration (Komuro & Rakic 1993), synaptogenesis

(Constantine-Paton 1990), synaptic transmission (Herron *et al.*, 1986; Bliss & Collingridge, 1993) and synaptic plasticity (Bliss & Collingridge 1993) while their excessive activation is thought to be a major cause of neuronal cell damage during acute neurologic conditions such as brain trauma, cerebral ischaemia, hypoglycaemia, hypoxia and epileptic seizures; as well as during chronic neurodegenerative diseases such as Parkinson's disease, Huntington's chorea, AIDS encephalopathy and dementia complex, and neuropathic pain syndromes (Choi, 1992; Arundine & Tymianski, 2003; Lipton, 2006; Lipton, 2007).

1.2 Molecular biology of NMDA receptors

1.2.1 Molecular diversity

The first cDNA encoding an NMDA receptor subunit, the NR1 subunit, was identified by expression cloning in 1991 by Nakanishi and colleagues (Moriyoshi *et al.* 1991). The breakthrough was rapidly followed by the subsequent identification and cloning of other NMDA receptor subunits (Durand *et al.*, 1992; Ikeda *et al.*, 1992; Mishina *et al.*, 1992; Monyer *et al.*, 1992; Ishii *et al.*, 1993; Planells-Cases *et al.*, 1993; Nakanishi *et al.*, 1994; Mori & Mishina, 1995; Dingledine *et al.*, 1999). To date, seven NMDAR subunits have been identified: NR1, a group of NR2 (NR2A, NR2B, NR2C, NR2D) and a pair of NR3 subunits (NR3A and NR3B), which are all products of single genes. All subunits share a high degree of amino acid sequence similarity. There is about 20% of amino acid sequence identity between the NR1 and NR2 subunits. In the NR2 subunit family, NR2A and NR2B share about 70% identity while NR2A and NR2C or NR2D just about 55% (Stephenson 2001). In addition, all subunits have the same transmembrane topologies (Figure 1.2). The glutamate binding site is formed by the S1 and S2 regions of NR2 subunit while the glycine site is formed by the S1 and S2 regions of the NR1 subunit (Armstrong *et al.* 1998; Dingledine *et al.* 1999; Paoletti & Neyton 2007).

1.2.2 Heteromeric channels and subunit stoichiometry

Expression of NR2 subunits alone does not produce functional NMDA receptors while responses produced by expression of homomeric NR1 subunits in oocytes are about 100 times smaller than those obtained when pairs of NR1 and NR2 subunits are co expressed (Monyer *et al.* 1992). It was therefore proposed that native NMDA receptor-channels occur as heteromeric assemblies of NR1 and NR2 subunits. The hypothesis first was proved by electrophysiological studies using recombinant NMDA receptors. The results showed that co-expression of NR1 and NR2 subunits was necessary to produce native-like recombinant NMDA receptors (Monyer et al., 1992; Stern *et al.*, 1992; Wyllie *et al.*, 1996). Moreover, several groups also showed similar results using biochemical approaches. This approach involves NMDA receptor solubilization from brain membranes using non-denaturing detergents followed by either immunoprecipitation or immunoaffinity purification using subunit specific antibodies (Sheng *et al.*, 1994; Dunah *et al.*, 1996; Chazot & Stephenson, 1997; Dunah *et al.*, 1998). Then the isolated receptor or immune precipitate is analyzed by immunoblotting to determine which of the other subunits are coassociated. The immunoprecipitation with NR2 antibody suggested that the presence of NR1/NR2A in forebrain and cerebellum (Sheng *et al.*, 1994; Chazot & Stephenson, 1997; Luo *et al.*, 1997; Abdrachmanova *et al.*, 2000), NR1/NR2B in forebrain (Sheng et al., 1994; Chazot & Stephenson, 1997; Luo et al., 1997), NR1/NR2C in cerebellum (Sheng *et al.* 1994; Chazot & Stephenson 1997) and NR1/NR2D in the forebrain and thalamus (Dunah *et al.* 1998).

In addition, the evidence of association between NR2 subunits has also been described for both electrophysiological and biochemical data. Sheng *et al.* (1994) were the first group to show that immunoprecipitation with anti-NR2A antibodies resulted also in the precipitation

of NR2B subunit immunoreactivity, suggesting the presence of triheteromeric NMDA receptors NR1-NR2A-NR2B. The same combination latterly also was found by Luo *et al.* (1997) in forebrain and (Chazot & Stephenson 1997) and (Didier *et al.* 1995) in cerebellum. Moreover, evidence for functional triheteromeric NMDA receptors, NR1-NR2B-NR2D, was found in outside-out membrane patches by (Brickley *et al.* 2003) and (Jones & Gibb 2005) from both cerebellar Golgi cells and midbrain dopamine cells and Dunah *et al.* (1998) found NR1-NR2B-NR2D triheteromers in midbrain using co-immunoprecipitetion. Furthermore, these triheteromeric complexes such as NR1/NR2A/NR2B and NR1/NR2A/NR2C might also be expressed at synaptic sites in cerebellar granule cells (Cathala *et al.* 2000). All evidence taken together suggests that functional NMDA receptors can be formed by NR1 subunits with two different NR2 subunits and these trimers are present both at synaptic and extrasynaptic sites and contribute to synaptic transmission and synaptic plasticity.

Blahos and Wenthold (1996) reported the presence of NR1/NR2A/NR2B subunit associations in adult rat forebrain, but in much lower proportion than NR1/NR2A or NR1/NR2B subunit associations. They suggested that the fraction of NR2A and NR2B subunits present in a single receptor complex is probably very small and that most NMDA receptors in the adult rat forebrain contain only one type of NR2 subunit. In agreement with this report, (Chazot & Stephenson 1997) identified NR1/NR2A/NR2B NMDA receptors as a minor subpopulation compared with NR1/NR2A and NR1/NR2B receptors. In contrast with these reports, Luo *et al.* (1997) have suggested that the majority of native NMDA receptors in adult rat cerebral cortex are the result of a combination of at least three different subunits (NR1/NR2A/NR2B) while native NMDA receptors composed of two different subunits (NR1/NR2B or NR1/NR2A) are present in a much lower proportion. In summary, triheteromeric NMDA receptors are present in rat brain and the expression level

of triheteromers depends on the brain region.

The exact number of subunits which are present in one single NMDA receptor has been debated. Some previous studies suggested that the NMDA receptor is a pentameric structure based on the size of the receptor, the receptor potency to different receptor antagonists when native subunits and mutant subunits were coexpressed and the interpretation of single-channel conductance when native subunits and mutant subunits were coexpressed. For example, Premkumar & Auerbach (1997) suggested that three NR1 subunits and two NR2 subunits are present in one single recombinant NMDA receptor. However, Behe *et al.* (1995) used similar methods and suggested that only two NR1 subunits and probably three NR2 subunits are expressed by a single recombinant NMDA receptor.

Several groups, however, suggested a tetrameric structure with two NR1 subunits and two NR2 subunits for native NMDA receptors based on pharmacological evidence (Laube *et al.*, 1998; Mano & Teichberg, 1998). In addition, more recently data from expression studies showed that when truncated subunits obtained from truncation of NMDA receptor subunits before the third transmembrane domains were joined to full-length subunits to generate tandems, the functional expression of these tandems confirmed the tetrameric structure of NMDA receptors and also suggested that the subunits making up NMDA receptors are arranged as two NR1 and two NR2 subunits (Schorge & Colquhoun 2003). Furthermore, Furukawa *et al.* (2005) reported crystal structures of the ligand-binding core of NR2A with glutamate and that of NR1-NR2A heterodimer with glutamate and glycine. The NR1-NR2A heterodimer suggests a mechanism for ligand-induced ion channel opening. Also, the analysis of the heterodimer interface, together with biochemical and electrophysiological experiments, confirms that the NR1–NR2A heterodimer is the

functional unit in tetrameric NMDA receptors.

1.2.3 Molecular properties and expression of the NR1 subunit

NR1 is the most highly expressed gene of all ionotropic glutamate subunits and its expression can be detected in nearly every neuron in the brain (Moriyoshi *et al.* 1991), where its product, the NR1 subunit seems to be indispensable for the assembly, expression and functioning of NMDA receptors. The NR1 gene (GR1N1) has been mapped to chromosome 3 in rat (Location 3p13) (Kuramoto *et al.* 1994) and 9q34-3 in human (Takano *et al.* 1993). The NR1 subunit gene contains 22 exons with the possibility of alternative splicing of exons 5 (the N1 cassette), 21 and 22 (the C1 and C2 cassettes) where N1 and C1 can be present or absent and C2 can alternate with C2', resulting in 8 different splice variants (Figure 1.3 and Table 1). The NR1 splice variants are widely distributed in the central nervous system (CNS) and expression is developmentally regulated. In brief, NR1 mRNA is barely detectable at embryonic day 14, increases gradually during development until the third postnatal week, after which it declines slightly to adults levels (Watanabe *et al.* 1993; Laurie & Seeburg 1994; Watanabe *et al.* 1994; Laurie *et al.* 1995). The individual regional distributions of splice forms appear to be established around birth, with little change thereafter. The NRl-2 and NR1-a splice forms occur extensively and approximately homogeneously throughout brain gray matter. The NRl-b variant are found primarily in the sensorimotor cortex, neonatal lateral caudate, thalamus, hippocampal CA3 field, and cerebellar granule cells, but are absent from adult caudate. The NRl-1 and -4 splice forms are detected in almost complementary patterns; the former are concentrated in more rostral structures such as cortex, caudate, and hippocampus, while the latter are principally in more caudal regions such as thalamus, colliculi, and cerebellum. These two splice forms account for a greater proportion of the adult NRl mRNA than that of the

neonate. The NR1-3 mRNA variant is scarce, being detected only at very low levels in postnatal cortex and hippocampus. The different splice forms generate regional differences in NMDA receptor properties during development and in the adult CNS (Sugihara *et al.*, 1992; Durand *et al.*, 1993; Laurie & Seeburg, 1994; Laurie *et al.*, 1995; Zukin & Bennett, 1995; Dingledine *et al.*, 1999).

Figure 1.3 Splice variants of the NR1 subunit (Winkler *et al.* 1999)

Table 1.1 Nomenclature of NR1 subunit splice variants. The eight splice variants of the NR1 subunit have been named differently by several laboratories.

Sugihara 1992	000	001	010	011	100	101	110	111
Hollmann's nomenclature	NR1-4a	NR1-2a	NR1-3a	NR1-1a	NR1-4b	NR1-2b	NR1-3b	NR1-1b
Durand 1993	NR1E	NR1C	NR1D	NR1A	NR1G	NR1F	NR1H	NR1B

1.2.4 Molecular properties and expression of the NR2 subunits

To date, four NR2 subunits have been identified for the NR2 family and termed NR2A, NR2B, NR2C and NR2D (Monyer et al., 1992; Ishii *et al.*, 1993). It has been demonstrated that they do not form functional NMDA receptors when expressed alone but only when coexpressd with NR1 subunits (Ishii *et al.* 1993). Although NR1 subunits are essential for forming functional NMDA receptors, NR2 subunits confer diversity to functional and pharmacological properties of NMDA receptors (Monyer *et al.* 1994). They modulate voltage-dependent Mg^{2+} block, ifenprodil sensitivity, Zn^{2+} block, receptor kinetics and single-channel properties (Dingledine *et al.* 1999).

The NR2A, NR2B, NR2C, NR2D subunits are composed of 1445, 1456, 1218 and 1333 amino acids, respectively. The predicted molecular weights for NR2A to NR2D are 163, 163, 133 and 143 kDa, respectively (Monyer et al., 1992). Similar to NR1 subunits, the protein and mRNA expression of NR2 subunits are developmentally and regionally regulated (Watanabe *et al.* 1993; Monyer *et al.* 1994; Watanabe *et al.* 1994). In the embryonic brain, NR2B and NR2D subunit mRNA predominate, the NR2A and NR2C mRNA first detected after birth. After birth, the expression pattern of NR2 subunits mRNA changes during development. At birth, weak expression of NR2A protein is restricted to the hippocampus, cerebral cortex and striatum (Wenzel *et al.*, 1997; Okabe *et al.*, 1998) thereafter the NR2A expression increases gradually and peaks in the third postnatal week and remains high in the adult brain (Wenzel *et al.* 1997). In adult rat, the NR2A subunit mRNA is highly expressed in cereberal cortex, hippocampus and cerebellum while NR2C mRNA is restricted to the granule cell layer of the cerebellum (Monyer *et al.*, 1994; Watanabe *et al.*, 1994a; Watanabe *et al.*, 1994b). As with the NR2A protein expression, the

protein expression for NR2B subunits increases during first three postnatal weeks then decreases to adults level (Wenzel *et al.*, 1997; Paarmann *et al.*, 2000). NR2D protein reaches peak around first postnatal week and decrease gradually and remain a low level in adult brain (Wenzel *et al.* 1997). In adult rat, the NR2D immonoactivity is mainly restricted to diencephalic, mesencephalic, and brainstem structure, being more prominent early development (Ishii *et al.* 1993; Monyer *et al.* 1994).

1.2.5 Molecular properties and expression of the NR3 subunits

In the NR3 family, there are two NR3 subunits, NR3A and NR3B. The NR3 subunits do not form functional NMDA receptors when expressed with NR2 subunits (Das *et al.* 1998; Chatterton *et al.* 2002). Interestingly, when NR3A or NR3B is coexpressed with NR1 subunits, it can form an excitatory glycine receptor that is permeable to Ca^{2+}, resistant to Mg^{2+} block, and unaffected by glutamate, NMDA, or NMDA antagonists (Chatterton *et al.* 2002). When NR3 subunits are coexpressed with both NR1 and NR2 subunits, functional triheteromeric NMDA receptors (NR1/NR2/NR3) are formed and NR3 subunits decrease single-channel conductance and Ca^{2+} permeability, compared with diheteromeric NMDA receptors (NR1-NR2) (Das *et al.* 1998; Perez-Otano *et al.* 2001; Chatterton *et al.* 2002). This finding is consistent with coimmunoprecipitation experiments, suggesting NR1, NR2, and NR3 can coexist together and form functional native NMDA receptors (Perez-Otano *et al.* 2001).

NR3 subunits are not essential NMDA subunits to form functional NMDA receptors, but it has been suggested the NR3 subunits may play a very important role in early development. For example, when coexpressed with NR1 and NR2 subunits, NR3 subunits influence

surface expression of NMDA receptors (Perez-Otano *et al.* 2001). Also the expression of NR3 protein and mRNA is developmentally and regionally regulated. In rat, NR3A expression peaks between postnatal days 7 and 10 in the cortex, midbrain, and hippocampus and the expression level of these regions is higher than the levels in the olfactory bulb and cerebellum. Thereafter, the protein expression level of NR3A subunit decreases gradually and remain low expression level in rat brain (Andersson *et al.* 2001).

In situ hybridization and immunohistochemical experiments reveal that expression of NR3B subunits is very restricted in somatic motoneurons of the brainstem and spinal cord. Its expression in other types of motoneurons is significantly weaker. In the adult rat NR3B expression is predominant in the ventral horn of spinal cord and ficial, trigeminal, vestibular and reticular nuclei of the brainstem. All evidence taken together suggests that NR3B is important as a regulatory subunit that controls NMDA receptor transmission in motoneurons. It may be involved in the pathogenesis of neurodegenerative diseases involving motoneurons as well (Andersson et al., 2001; Nishi *et al.*, 2001; Chatterton et al., 2002).

1.2.6 Expression of NMDAR subunits in the basal ganglia

1.2.6.1 NMDA receptors in substantia nigra pars compacta

Excitatory afferents to dopaminergic neurons of SNc originate from various structures; medial prefrontal cortex, subthalamic nucleus (STN) and pedunculopontine tegmental nucleus. It has been suggested that during Parkinson's disease, these excitatory inputs might contribute excitotoxic cell death to the remaining dopaminergic neurons (Blandini *et al.* 2000). In adult rats, in situ hybridization studies have demonstrated that the most

abundant NR1 isoform in SNc is NR1-2a, which lacks N1 and C1 segments and contains the C2 segment (Standaert *et al.* 1994; Albers *et al.* 1999). Therefore, the N1 segment does not affect the kinetics of NMDA receptor in dopaminergic neurons.

Although in both P7 and adult rat, high levels of NR2D protein and mRNA and low levels of NR2B protein and mRNA are expressed in the midbrain (Standaert *et al.* 1994; Dunah *et al.* 1996; Dunah *et al.* 1998), the composition of functional NMDA receptors in dopaminergic neurons is still not known. It has been suggested that the binary NR1-NR2D NMDA receptor was not detected in the midbrain, because all NR2D subunits were coimmunoprecipitated with NR1 and NR2B subunits (Dunah *et al.* 1998). This evidence taken together suggests that triheteromeric NMDA receptors are present on dopaminergic neurons. Similar conclusions were supported by single-channel recording data (Jones & Gibb 2005).

1.2.6.2 NMDA receptors in the subthalamic nucleus (STN)

The subthalamic nucleus receives excitatory input (glutamatergic input) from the cerebral cortex and the pars parafascicularis of the central complex. Adult rat STN neurons express the NR1-2b NR1-isoform. High levels of NR2D protein and mRNA were detected in STN while a low level of NR2B mRNA was found (Standaert et al., 1994; Wenzel *et al.*, 1996).

1.2.6.3 NMDA receptors in globus pallidus and substantia nigra pars reticulata

NMDA receptors are present in the striatal output structures, the GPi and SNpr. Both structures express NR1 (principally the NR1-4b isoform) and have prominent expression of the NR2D subunit, which can be detected both at the mRNA and at a protein level

(Standaert et al., 1994; Wenzel et al., 1996).

1.2.6.4 NMDA receptors in striatum

The protein expression of NR1 isoforms in adult rat striatum was reported by (Kuppenbender *et al.* 1999). It has been suggested that projection neurons (medium spiny neurons) in striatum express high levels of NR1-1a isoform and low levels of NR1-2a isoform while high levels of NR1-4a and NR1-2a isoforms are expressed by striatal interneurons.

In P7 young animals, the NR1 and NR2B mRNA is highly expressed by striatal medium spiny neurons while low NR2D mRNA expression is found (Monyer *et al.* 1994). In adult rat striatum, NR2A expression is moderate in all striatal neurons except cholinergic interneurons, and NR2B shows strong labeling in the medium spiny neurons and cholinergic interneurons. No NR2C mRNA or protein was found in adult striatum and only some interneurons such as somatostatin- or acetylcholine- containing neurons express NR2D subunits (Hallett & Standaert 2004). In addition, diheteromeric NMDA receptors containing NR1 either NR2A or NR2B are widely expressed in striatum, but triheteromeric receptors composed of NR1-NR2A-NR2B also are found in striatum (Dunah & Standaert 2003).

1.3 Functional and pharmacological properties of recombinant NMDA receptors

The functional and pharmacological properties of NMDA receptors are largely determined by their subunit compositions (Cull-Candy *et al.*, 2001). The studies using recombinant

NMDA receptors allow us to understand the functional and pharmacological properties converted by specific subunits. In other words, the diversity of NMDA subunits might be a basis of regulation of synaptic transmission and functional plasticity of native NMDA receptors. In the brain, native NMDA receptors are expressed regionally and developmentally. The expression of different NMDA subunits may determine physiologically functional differences of native NMDA receptors in the different regions during development. Understanding the functional and pharmacological properties exhibited by different recombinant NMDA receptors also give us the information about native NMDA receptor composition in different brain regions during development, provided we can make appropriate measurement from identified neurons.

1.3.1 Single-channel properties

The single-channel properties of recombinant NR1/NR2 NMDA receptors that have been reported include single-channel conductance, open times, shut times, direct transitions from main conductance level to sub-conductance level. (Stern et al., 1992; Stern *et al.*, 1994; Wyllie et al., 1996; Cull-Candy et al., 2001). These properties of native and recombinant NMDA-receptor channels have been shown to be partly determined by the identity of NR2 subunits while the effects of NR1 splice variants on single-channel properties have not been studied.

1.3.1.1 Single-channel conductance

The recombinant NMDA receptors composed of NR1-NR2A and NR1-NR2B show large single-channel conductances, which are 50 pS for the main conductance level and 40 pS for the not common sub-conductance level while the recombinant NMDA receptors formed by NR1-NR2C and NR1-NR2D have lower single-channel conductances of 38 pS for the main

conductance level and 19 pS for the sub-conductance level (Stern et al., 1992; Stern et al., 1994; Wyllie et al., 1996; Cull-Candy et al., 2001). In addition, the triheteromeric NMDA receptors formed by NR1-NR2A-NR2D show both high and low single-channel conductances of 50 pS, 40 pS 30 pS and 18pS (Cheffings & Colquhoun 2000).

1.3.1.2 Direct transitions between main conductance and sub-conductance levels

There are some highly selective antagonists to identify NR2A-containing and NR2B-containing NMDA receptors such as Zn^{2+} for NR2A-containing NMDA receptors (Paoletti *et al.* 1997) and ifenprodil for NR2B-containing NMDA receptors (Williams, 1993; Cull-Candy et al., 2001). These highly selective antagonists allow us to distinguish native NR2A- or NR2B- containing NMDA receptors. However, the shortage of selective antagonists for NR2C- and NR2D- containing NMDA receptors imposes a difficulty in distinguishing native NR2C- and NR2D- containing NMDA receptors using electrophysiological methods.

However, the single-channel properties of recombinant NR1-NR2C and NR1-NR2D receptors provide us with the possibility of identifying them based on open times and temporal asymmetry of direct transition between conductance levels. First, the steady state single-channel recordings from NR1a/ NR2C show that main and sub-conductance levels of NR1a/NR2C channels have similar opening durations (Stern *et al.* 1992) while for NR1a/NR2D channels, the duration of sub-conductance levels is longer than the main conductance level (Wyllie *et al.* 1996). Second, the NR1a/NR2D channels show temporal asymmetry, which is absent in any of the other three diheteromeric recombinant NMDA receptors (Stern *et al.* 1992; Wyllie *et al.* 1996).

Single-channel properties of most of the likely triheteromeric NMDA receptors have not been reported.

1.3.2 Kinetics

The NMDA receptor channel opening peaks about 10ms after glutamate binds to NMDA receptors and it activates not just one channel opening, but the channel may re-open many times before the agonist dissociates. In other words, the event that underlies the synaptic current and macroscopic current is actually a burst that consists of many openings separated by brief shuttings (Gibb & Colquhoun 1992; Wyllie *et al.* 1998; Colquhoun 2007).

The decay time course and desensitization time course of NMDA currents have been well studied and they are largely determined by the identity of NR2 subunits but the decay time course of NMDA receptors is also influenced by the identity of the NR1 isoforms (Monyer et al., 1992; Monyer et al., 1994; Vicini *et al.*, 1998; Wyllie *et al.*, 1998; Rumbaugh *et al.*, 2000).

1.3.2.1 Recombinant NR1/NR2A NMDA receptors

NR1-NR2A NMDA receptors in outside-out patches show significant desensitisation when activated by glutamate or NMDA for 4 seconds (Wyllie *et al.* 1998). Compared with other NR2- containing NMDA receptors, the recombinant NR1-NR2A NMDA receptors show the fastest decay time course. Deactivation time constants from one or two exponential components have been reported: 120 ms (Monyer *et al.* 1994), 32 ms and 202 ms (Erreger *et al.* 2005), 33 and 247 ms (Vicini *et al.* 1998), 65 and 312 ms (Wyllie *et al.* 1996) (see

Table 1.2).

1.3.2.2 Recombinant NR1/NR2B NMDA receptors

As with the NR1/NR2A NMDA receptors, NR1/NR2B receptor-mediated currents from outside-out patches show a significant desensitization when activated by glutamate or NMDA for 4 seconds. The NMDA receptors formed by NR1-NR2B and NR1-NR2C have similar decay time course. Deactivation time constants from one or two exponential components have also been reported: 400 ms (Monyer *et al.* 1994), 71 and 538 ms (Vicini et al., 1998), 93 ms and 569 ms (Banke & Traynelis 2003) and 128 and 799 ms (see Table 1.2).

Table 1.2 Summary of deactivation time course of NMDA receptors from previous studies

Paper	Receptor	Application duration	τ_w (ms)	τ_{fast} (ms)	τ_{slow} (ms)	% fast
(Rumbaugh *et al.* 2000)	NR1a-NR2B (cell)		745	261	1239	49%
	NR1a-NR2B (patch)		603	250	1281	59%
	NR1b-NR2B (cell)		194	182	480	97%
	NR1b-NR2B (patch)		144	61	308	60%
	NR1e-NR2B (cell)		583	215	810	39%
	NR1g-NR2B (cell)		167	167	----	100%
(Banke *et al.* 2005)	NR1-1a/NR2B	1-4ms (1mM glutamate)	----	93-102	569-595	-----
(Horak *et al.* 2004)	NR1-1a/NR2B	6ms (1mM glutamate)	498	208	839	54%
(Banke & Traynelis 2003)	NR1-1a/NR2B	1-4ms (1mM glutamate)	184	95	617	83%
(Erreger *et al.* 2005)	NR1-1a/NR2A	1ms (1mM glutamate)		32	202	94% (Area)
	NR1-1a/NR2B	1ms (1mM glutamate)		128	799	82% (Area)
(Wyllie *et al.* 1998)	NR1-1a/NR2A	1ms (1mM glutamate)		65	312	33%
	NR1-1a/NR2D	1ms (1mM glutamate)			5162	0%
(Vicini *et al.* 1998)	NR1a/NR2A (lifted HEK)		54	33	247	90%
	NR1a/NR2B(lifted HEK)		342	71	538	42%
	NR1a/NR2C(lifted HEK)		260			
	NR1a/NR2D(lifted HEK)				1700	
(Gotz *et al.* 1997)	Dopamine cell on SNc P10-P15 rat	10ms (100μM glutamate)	456	150	1049	66%
	Striatal principal neuorn P10-P15 rat		401	147	1088	73%
	Striatal Cholinergic neurons P10-P15 rat		347	130	687	61%
	Nigra GABA cells P10-P15 rat		339	142	797	70%
	Globus pallidus neurons P10-P15 rat		196	67	382	59%
	Subthalamic nucleus P10-P15 rat		292	137	833	73%

1.3.2.3 Recombinant NR1/NR2C NMDA receptors

The NMDA receptors composed of NR1/NR2C have a fast rise time (Chen *et al.* 2006) and do not show any desensitization during 4 second exposure to glutamate or NMDA (Monyer *et al.* 1992; Chen *et al.* 2006) and have a similar deactivation time constant to NR1-NR2B NMDA receptors (Cull-Candy *et al.* 2001).

1.3.2.4 Recombinant NR1/NR2D NMDA receptors

Recombinant NR1/NR2D NMDA receptors also show no desensitization during long glutamate or NMDA applications (several seconds) (Monyer *et al.* 1992; Wyllie *et al.* 1998). Intriguingly, recombinant NR1/NR2D NMDA receptor-mediated currents show the slowest rise time of 45 ms (Wyllie *et al.* 1998) and deactivation time constants of all NR1/NR2 subunit combinations: 4800 ms (Monyer *et al.* 1994) and 4469 ms (Wyllie *et al.* 1998).

1.3.2.5 Decay time course of NMDA responses is influenced by NR1 isoform

As mentioned before, all NR1 isoforms are produced by a single gene. Three regions on the NR1 gene (exons 5, 20 and 21) are alternatively spliced, giving rise to eight distinct isoforms. It has been demonstrated that the N1 segment encoded by exon 5 influences the deactivation time constant of recombinant NMDA receptors (Prybylowski *et al.* 2000; Rumbaugh *et al.* 2000). NMDA receptors containing NR1 subunits with the N1 sequence present (NR1-1b, NR1-2b, NR1-3b, NR1-4b) show about 4 times faster decay time course

than receptors without the N1 segment.

1.3.3 Multiple effects of Mg^{2+} on recombinant NMDA receptors

1.3.3.1 Extracellular Mg^{2+} block of NMDA receptors

One unique feature of NMDARs compared with other ligand-gated ion channels is the dual dependence on agonist binding and membrane potential. In external medium containing physiological concentrations of Mg^{2+} (about 1mM), the inward current induced by NMDA is significantly blocked by extracellular Mg^{2+} at negative voltages while the block is relieved at positive voltages (Figure 1.4). This voltage-dependence dominates the physiological role of NMDA receptors. At resting membrane potential, NMDA receptors undergo rapid channel block by extracellular Mg^{2+}, which significantly reduces the NMDAR component of the synaptic current. However, when neurons are depolarized, for example, by activation of colocalized AMPA receptors, the voltage-dependent block by extracellular Mg^{2+} is rapidly reduced, allowing ion influx though activated NMDA receptors. The voltage-dependence of the block has been interpreted by assuming the Mg^{2+} binding site is situated in the NMDA channel, and the magnitude of the voltage dependence has been used to localize the Mg^{2+} site by estimating the fraction (δ) of the transmembrane field sensed by Mg^{2+}. The affinity of external Mg^{2+} for NMDA receptors was represented by the Mg^{2+} afiinity at 0 mV ($K_{Mg2+}(0mV)$).

Single-channel recording from outside-out patches demonstrated that the mean open time of NMDARs decreases with increasing extracellular Mg^{2+} concentrations, while mean closure time is independent of the Mg^{2+} concentrations (Nowak *et al.* 1984; Ascher &

Nowak 1988). Meanwhile, the values of δ and K_{Mg} (0mV) were calculated to be 1 and 8.8 mM, respectively. These results suggested that the binding site for Mg^{2+} is on the cytoplasmic side of the channel. However, electrophysiological and mutagenesis studies with recombinant receptors suggested that the blocking site can not be deep enough to account for the voltage dependence of external Mg^{2+} block (Wollmuth *et al.* 1998). Subsequently, (Antonov & Johnson 1999) demonstrated that occupation of the NMDAR channels by permeant ions, such as Na^+, K^+, can affect Mg^{2+} block and taking ion permeation into account, the Mg^{2+} binding site was placed at a much shallower position (δ = 0.47).

In NMDA receptor channels, the subtype-specific differences in Mg^{2+} block are determined by NR2 subunits (Kuner & Schoepfer 1996). Receptors assembled from NR1-NR2A and NR1-NR2B are blocked more strongly than those formed by NR1-NR2C and NR1-NR2D, reflecting a difference in voltage-dependence. Kuner and Schoepfer (1996) measured the subtype-specific differences of Mg^{2+} block. The δ and K_{Mg}(0mV) were obtained by fitting the current-voltage relation and gave, K_b(0mV) and δ to be 4.8mM and 1.05 for NR1-NR2A, and 3.7mM and 1.07 for NR1-NR2B. The receptors assembled from NR2C or NR2D subunits have lower sensitivity to extracellular Mg^{2+} block, with K_b(0mV) 3.5mM, 3.6mM and δ of 0.73, 0.75, respectively. Qian and Johnson (2005), using single-channel recording, explained the subunit-specific differences. They suggested that for recombinant NMDAR NR1-NR2D, the binding rate of Mg^{2+} block is similar to NMDAR assembled with NR1-NR2A or NR1-NR2B, while the unbinding rate was much faster than that for NR1-NR2A or NR1-NR2B.

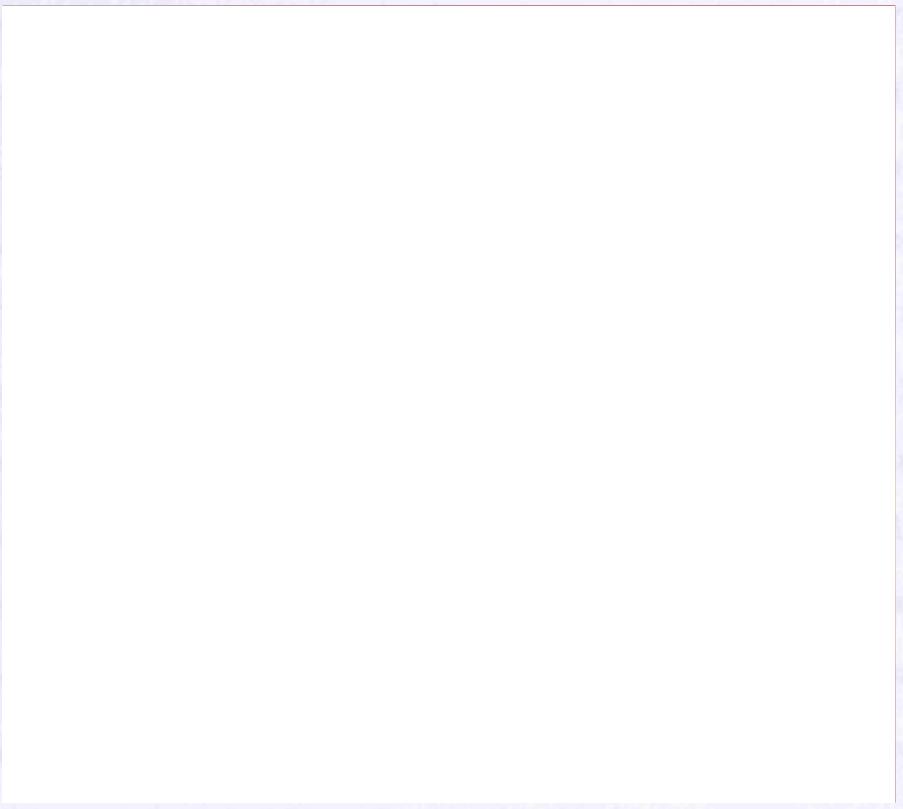

Figure 1.4 Multiple effects of Mg^{2+} on NMDA receptors

The figure shows that NMDA receptors can be blocked by intracellular and extracellular Mg^{2+}. Meanwhile, there is a Mg^{2+} potentiation binding site that exists on the NR2B subunit (http://www.securitylab.ru/_Article_Images/2005/10/nmda_receptor.gif).

1.3.3.2 Intracellular Mg^{2+} block of NMDA receptors

The intracellular free concentration of Mg_i^{2+} is regulated at approximately 5-10 % of the total concentration of Mg_i^{2+} through buffering, ion exchange and pumping. Mg_i^{2+} modulates diverse types of ionic channels, including NMDA receptors (Johnson & Ascher 1990). NMDA receptors are blocked by intracellular Mg^{2+} in a voltage dependent manner. The NMDA receptors are significantly blocked by millimolar internal Mg^{2+} at positive voltage and the effect is relieved at negative voltage. However, in normal physiological conditions, there is about 3mM of intracellular ATP that binds to intracellular Mg^{2+} and the free concentration of intracellular Mg^{2+} is evaluated at about 50 μM. Extracellular Mg^{2+} gives an apparent site of interaction between 0.8 and 1 across the transmembrane electric field whereas from the inside it is around 0.35. As pointed out by (Johnson & Ascher 1990), the overlap in the positioning of apparent blocking sites for intracellular and extracellular Mg^{2+} complicates definition of the mechanism of the block.

1.3.3.3 Glycine-independent and subunit-specific potentiation by extracellular Mg^{2+}

Extracellular Mg^{2+} potentiates the NMDA receptor response in a voltage-independent and subunit-specific manner at saturating glycine concentration (Paoletti *et al.* 1995). Wang & MacDonald (1995) suggested using whole-cell recording techniques with tissue-cultured neurons that the potentiation was due to a marked increase in glycine affinity on NMDA receptors. (Paoletti *et al.* 1995) compared the NMDAR currents recorded in the absence of Mg^{2+} and after addition of Mg^{2+} at a physiological concentration (2mM) and suggested that only oocytes expressing NR1/NR2B displayed a Mg^{2+} potentiation over the voltage range tested (from -50 mV to +50 mV). The mean value of potentiation (I_{mg}/I_o) was 2.55 ± 0.13

at negative voltages and 2.46 ± 0.07 at positive voltages. Outside-out patch-clamp experiments with recombinant NR1-NR2B receptors showed that the potentiation produced by extracellular Mg^{2+} was due to an increase in open probability, from 0.03 to 0.1. In addition, it has been found that extracellular Mg^{2+}, like spermine, partly relieves the inhibitory effect of protons observed at physiological pH and the potentiation produced by Mg^{2+} and spermine are not additive.

1.3.4 Ifenprodil block of NMDA receptors

Ifenprodil is an allosteric NMDA receptor antagonist with chemical structure unlike any of the common competitive or un-competitive antagonists. High affinity inhibition by ifenprodil depends critically on the presence of an NR2B subunit. It has significant affinity for NR1-NR2B receptors (IC_{50} = 0.29 μM), that is about 300-fold higher than NR1-2A, NR1-NR2C or NR1-NR2D receptors (Williams 1993; Williams 1995). Ifenprodil inhibits NR1-NR2B recombinant NMDAR currents, with a maximal inhibition of 91% (Williams 1993; Mott *et al.* 1998).

The major effect of ifenprodil on NMDA receptors is a high affinity, non-competitive, voltage-independent inhibition of receptors containing the NR2B subunit. It decreases the apparent association and dissociation rates of glutamate for NMDARs (Kew *et al.* 1996). Because the rate of agonist dissociation is decreased more than that of association, the apparent affinity of NMDA receptors for glutamate is increased (EC_{50} becomes smaller by approximately 3-6 fold). Thus, currents evoked by 0.3-1 μM NMDA were potentiated by 3μM ifenprodil to about 200% of control current level (Kew *et al.* 1996). With increasing concentration of NMDA the effect of ifenprodil on NMDA-evoked current changes from one of potentiation to one of increasing inhibition. When the NMDA binding sites are

saturated with a high concentration of NMDA, the ifenprodil-dependent increase in receptor affinity has no effect on the level of NMDA binding (Zhang *et al.* 2000). It has been suggested that ifenprodil inhibits NMDA receptor through shifting the pKa of the proton sensor to a more alkaline level, which would enhance tonic inhibition at physiological pH (Mott *et al.* 1998).

In diheteromeric NR1-NR2B receptors, by combining functional studies on recombinant NMDA receptors and biochemical studies on isolated domains, it has been shown that ifenprodil binds to the N-terminal leucine/isoleucine/valine-binding protein (LIVBP)-like domain of NR2B. In this domain, several residues, both hydrophilic and hydrophobic, were found to control ifenprodil inhibition (Perin-Dureau *et al.* 2002).

1.2 Parkinson's disease

1.2.1 Background of Parkinson's disease

Parkinson's disease (PD) is a common, disabling and degenerative disorder of central nervous system (CNS). It affects more than 1% of people aged over 65 in the world (Tanner 1992). In China, about 1,700,000 people have PD which is approximate half the number of PD patients in the world (4,000,000). Therefore, PD imposes a large economic cost on families and government. In addition, PD also decreases the quality of life of patients because the PD symptoms include tremor, muscle rigidity, slowness of movement and loss of postural balance leading to falls.

Thus, more attention needs to be put on PD. The primary pathology of PD is the loss of dopaminergic neurons in substantia nigra pars compacta (SNc), which project dopaminergic axons to the striatum. Since PD is both chronic and progressive, there are

two main therapeutic areas for this disease, symptomatic therapy and neuroprotective therapy. Currently, the symptomatic therapy is based primarily on replacing the dopaminergic deficit by use of levodopa, dopamine agonists or MAO-B inhibitors. L-Dopa is the most widely used PD treatment. It is transformed into dopamine in dopaminergic neurons by L-aromatic amino acid decayboxylase. However, only 1-5 % of L-DOPA enters into the dopaminergic neurons (http://viartis.net/parkinsons.disease/treatments.htm). The remaining L-Dopa is often metabolized to dopamine elsewhere, causing side effects. Due to feedback inhibition, L-DOPA reduces the formation of endogenous L-Dopa, and so eventually becomes counterproductive. The dopamine-agonists such as bromocriptine and pergolide are moderately effective. Dopamine agonists initially act by stimulating some dopamine receptors. However, they cause dopamine receptors to become progressively less sensitive, eventually increasing the symptoms (Radad *et al.* 2005). MAO-B inhibitors such as selegiline and rasagiline reduce the symptoms by inhibiting monoamine oxidase-B (MAO-B), which inhibits the breakdown of dopamine by the dopaminergic neurons. The metabolites of selegiline might result in side effects such as insomnia. In addition, to drug treatments deep brain stimulation is presently the most used surgical means of treatment in people with advanced PD for whom drug therapy is no longer sufficient (Kern & Kumar 2007). So far, there are no treatments that have been established to alter the progression of the underlying neurodegenerative process. However, NMDA receptor antagonists may contribute to this task. Next, the rationale for the use of NMDA receptor antagonists in Parkinson's disease will be described.

1.2.2 Neural basis of Parkinson's disease

Parkinson's disease was the first disease of the nervous system to be identified as a molecular disease. The pathological mechanism underlying this disease is that the dopaminergic neurons in substantia nigra pars compacta progressively degenerated and the

loss of dopaminergic neurons results in a profound loss of dopaminergic innervation of the striatum. The striatum and substantia nigra pars compacta are both part of basal ganglia which plays important roles in controlling voluntary movement. Next, the definition of basal ganglia and the function and role of basal ganglia in the normal conditions and in Parkinson's disease will be described.

1.2.2.1 What are the basal ganglia?

The basal ganglia are a group of nuclei in the basal telencephalon interconnected by multiple feedback loops with the cerebral cortex, thalamus and brainstem, associating with a variety of functions: motor control, cognition, emotions and learning. Unlike other components of the motor system, the basal ganglia do not make either direct input or indirect input connections with the spinal cord. The primary input for basal ganglia is from cerebral cortex and output is directed to prefrontal, premotor and motor cortices through the thalamus. The non-motor functions of the basal ganglia are achieved by the frontal cortex (See figure 1.5).

Figure 1.5 The basal ganglia consist of five nuclei: caudate nucleus, putamen, globus pallidus, subthalamic nucleus, substantia nigra

The basal ganglia comprise several interconnected brain areas deep in the brain, as shown here. First believed to be mainly involved in movement, the basal ganglia are now known to be also active in learning, habit formation, and certain psychiatric disorders. Image Credit: Ellen Davey (http://www.dana.org/news/brainwork/detail.aspx?id=6028)

1.2.2.2 The basal ganglia consist of five nuclei

There are two sets of basal ganglia in the mammalian brain, mirrored in the left and right hemispheres. Each of them consists of five nuclei: the caudate nucleus, putamen, globus pallidus (external segment and internal segment), subthalamic nucleus, and substantia nigra (pars compacta and pars reticulata). The two structures, the caudate and the putaman, together are generally referred to as striatum (see Figure 1.5).

1.2.2.2.1 Striatum

The striatum is a primary input structure of the basal ganglia circuit. It receives excitatory projections from almost all cortical areas (McGeorge & Faull 1989), midline and intralaminar nuclei of the thalamus (Berendse & Groenewegen 1990) and from limbic structures, particularly the amygdala (Kelley *et al.* 1982). Another important input to the striatum is from dopaminergic neurons in substantia nigra pars compacta and in ventral tegmental area, which is mediated by the monoamine transmitter dopamine.

The primary output targets of striatum projection neurons are the external segment of globus pallidus (GPe) and the internal segment of globus pallidus and substantia nigra pars reticulata (Gpi/SNr). These two striated outputs conceptually form the beginning of the direct and indirect pathways (Penney & Young 1986). The functional segmentation of basal ganglia output is mainly based on these direct and indirect pathways which are described later in more detail. It has been shown that neurons containing enkephalin project to Gpe, while the neurons containing substance P project to Gpi/SNr (Blandini *et al.* 2000). A large number of dopamine D1 and D2 receptors are expressed by the projection neurons and it has been suggested that D1 and D2 class receptors have a differential effect on the direct and indirect pathways.

The cellular composition of the striatum has been well studied. It has been shown that about 90% of striatum neurons are medium spinal neurons (medium-size 15-20 μm), containing GABA as transmitter while the remaining neurons are interneurons (Difiglia *et al.* 1980; Kawaguchi *et al.* 1995; Parent & Hazrati 1995; Holt *et al.* 1997).

1.2.2.2.2 Globus pallidus (GP)

The globus pallidus is divided into the GPe and the GPi. They all have similar main afferents from striatum, but the efferents for these two segments are different. The main output target of the external segment of globus pallidus is subthalamic nucleus, using GABA as a transmitter, while the GPi and SNr made up of the main output structure of basal ganglia and project GABAergic efferent back to frontal cortex thought thalamus. In addition, GPe and GPi also receive strong glutamatergic projection from the subthalamic neucleus.

1.2.2.2.3 Subthalamic nucleus (STN)

The subthalamic nucleus is a small lens-shaped nucleus in the brain where it is a part of the basal ganglia system. As suggested by its name, the subthalamic nucleus is located ventral to the thalamus and also is dorsal to the substantia nigra.

The subthalamic nucleus receives its main input from the external segment of the globus pallidus. This afferent is GABAergic, inhibiting the neurons of the subthalamic nucleus. Excitatory, glutamatergic inputs come from the cerebral cortex (particularly the motor cortex), and from the pars parafascicularis of the central complex. The subthalamic nucleus also receives neuromodulatory inputs, notably dopaminergic axons from the substantia

nigra pars compacta (Nakanishi *et al.* 1988; Parent & Hazrati 1995).

The efferent axons are glutamatergic. Except for the connection to the striatum (17.3% in macaques), most of the subthalamic neurons are multitargets and directed to the other elements of the basal ganglia. Some send axons to the substantia nigra. Some are di-target with the lateral pallidum and the substantia nigra (2.7%) (Nakanishi *et al.* 1988; Gotz *et al.* 1997) or the lateral pallidum and the medial (48%). Less are single target for the lateral pallidum (Parent & Hazrati 1995).

1.2.2.2.4 Substantia nigra compacta (SNc) and reticulata (SNr)

The substantia nigra is a major element of the basal ganglia and is subdivided into two segments, substantia nigra pars compacta and substantia nigra pars reticulata.

As mentioned before, the substantia nigra pars reticulata is part of the output nuclei of basal ganglia and it receives GABAergic afferents from the striatum and projects GABAergic efferents back to the thalamus (Parent & Hazrati 1995).

Neurons in the substantia nigra pars compacta contain neuromelanin and use dopamine as neurotransmitter (Parent & Hazrati 1995). The primary output targets are the striatum, subthalamic nucleus and globus pallidus. The afferents to these dopaminergic neurons in SNc originate from various structures. Both striatum and globus pallidus send GABAergic projections to nigra dopaminergic neurons while these neurons receive glutamatergic projections from the medial prefrontal cortex, subthalamic nucleus and pedunculopontine tegmental nucleus (Parent & Hazrati 1995).

1.2.2.3 Functional organization of the basal ganglia

The basal ganglia circuitry is a very popular model. This exciting model is proposed based on two central concepts. First, there are two parallel circuits converting information from different regions of the cortex though the basal ganglia and back to the cortex via the thalamus. Second, each circuit allows the information flow and can process information individually and the balance of activities from these two parallel circuits controls voluntary movement (Alexander & Crutcher 1990; Haber 2003). The two pathways in the basal ganglia circuit model are the direct and indirect pathways (Figure 1.6). According to this model, the striatum is the primary input nucleus receiving information from the cortex to the basal ganglia output nucleus (GPi/SNr) though the direct and indirect pathways. The two pathways originate from different neurons in the striatum. In the direct pathway, the striatal GABAergic neurons containing dynorphin and expressing D1 dopamine receptors, project to the output nucleus, GPi/SNr while the striatal GABAergic neurons containing substance P and expressing D2 dopamine receptor projects to GPe. The GPe sends an inhibitory projection to the STN. The STN, in turn, sends its excitatory glutamatergic efferents to the output nuclei, GPi/SNr.

The functional activity of this organization is that activation of the direct and indirect pathways give rise to opposite changes in the net output of the basal ganglia circuitry. In fact, in the direct pathway, activation of the striatal GABAergic neurons causes inhibition of the output nuclei of the basal ganglia, GPi/SNr and hence disinhibition of the thalamus. In contrast, in the indirect pathway, activation of striatal GABAergic neurons inhibits the GPe. This leads to disinhibition of the STN neurons. In turn, increased activity of STN neurons increases the activity of the output nuclei (Figure 1.6).

Figure 1.6 The functional organization of the basal ganglia (Figure is taken from Blandini *et al.* 2000)

There are two pathways in this basal ganglia circuit to process the information from the cortex; direct pathway and indirect pathway. Th striatum is the main input nuclei of the basal ganglia, which receives excitatory glutamatergic input from almost the entire cortex. In the direct pathway, the striatum projects GABAergic axons to the internal segment of the globus pallidus or substantia nigra pars reticulata (GPi/SNr) then output information is sent back to the cortex through the thalamus. In the indirect pathway, the information is projected to STN, then STN sends excitatory glutamatergic input to the output nuclei of basal ganglia (GPi/SNr). Therefore, the direct and indirect pathways have opposite effects on information from the cortex and the balance of activities of the two pathways determines the output of information from the basal ganglia.

1.2.2.4 Basal ganglia circuits in Parkinson's disease

In patients with Parkinson's Disease (PD), dopaminergic innervation of the caudate putamen is lost due to the progressive death of dopamine neurones in the SNc. As mentioned before, STN neurons project excitatory glutamatergic input to dopaminergic neurons of SNc (Nakanishi *et al.* 1988; Gotz *et al.* 1997). One result of the loss of dopamine is an increased excitatory drive from the subthalamic nucleus to the remaining dopamine neurones of the substantia nigra (Hamani *et al.* 2004). In effect, the basal ganglia neural circuit attempts to compensate for the loss of some dopamine neurones by driving the remaining neurones much harder. It has been hypothesised (Blandini *et al.* 2000; Hallett & Standaert 2004) that an increased excitatory drive may generate oxidative stress and excitotoxic cell death of dopamine neurones via excessive activation of NMDA receptors. This may contribute to the disease progression in PD (Blandini *et al.* 2000).

1.2.3 Excitotoxic cell death and the projects described in this thesis

Glutamate is an excitatory neurotransmitter that plays a very important role in the central nervous system, rapidly signalling sensory information and complex motor commands from one part of the body to another, contributing to maintaining homestasis in the body and contributing to consioursness and decision-making processes in the brain. Glutamatergic terminals in the brain contain high concentrations of glutamate, about 10mM. During synaptic transmission, the glutamate concentration in the synaptic cleft may be greater than 1mM for 1ms (Clements *et al.* 1992) to convey information to postsynaptic neurons. However, because glutamate has such profound postsynaptic effects, its presence in excessive amounts or for excessive periods of time can course excitotoxic cell death

(Choi 1992). Two different mechanisms may contribute to excitotoxic cell death, acute excitotoxic cell death and chronic excitotoxic cell death. For acute exitotoxic cell death, for example, in head or spinal cord injury, large amounts of glutamate are released from injured cells. This excessive amount of glutamate can cause prolonged activation of postsynaptic glutamate receptors, especially NMDA receptors. The excessive activation of NMDA receptors induces large amounts of Ca^{2+} influx into cells, causing cell death. In addition, a slow, subtle form of excitotoxic cell death also may contribute in a variety of slow neurodegenerative diseases, such as Parkinson's disease, Alzheimer's disease, multiple sclerosis, HIV-associated dementia and amylotrophic lateral sclerosis (Lipton 2006). In these diseases, excessive periods of exposure to glutamate may contribute to chronic excitotoxic cell death.

As mentioned before, in Parkinson's disease patients, the loss of dopaminergic neurons of SNc decreases the release of dopamine in the striatum. In order to compensate for the reduced level of dopamine in the striatum, the STN drives the remaining dopaminergic neurons much harder to increase dopamine release in the striatum (Blandini *et al.* 2000). This process uses glutamate as a transmitter and is partially mediated by NMDA receptors on dopaminergic neurons of SNc. The increased synaptic transmission may increase the probability of excitotoxic cell death thereafter accelerating the death of the remaining dopaminergic neurons. Therefore, it has been suggested that NMDA receptor antagonist might have therapeutic value in Parkinson's disease as neuroprotective drug (Hallett & Standaert 2004). From a drug discovery perspective it is clearly disable to know both the subunit composition of native NMDA receptor subtypes and their distribution in the brain. Such information is crucial to the development of new subtype-selective therapeutic compounds with improved pharmacological profiles.

1.3 Experiments conducted in this study

For my project, I focused on the subunit composition of NMDA receptors in P7 rat dopaminergc neurons. The functional and pharmacological characterization of NMDA receptors are applied as a basis of identification of NMDAR subunit composition. Through the identification and localization of NMDA receptor subtypes to specific neuronal populations it should be possible to improve our understanding of how NMDA receptor-mediated signalling is regulated in dopaminergic neurons of SNc and how subtype-selective drugs could be more efficiently used to target specific brain areas affected by particular neuropathological conditions such as Parkinson's disease, increasing therapeutic efficacy and reducing at the same time the potential side effects of drugs.

Chapter 2: Materials and Methods

2.1 Solutions

2.1.1 Slicing solution

A modified Krebs solution (Edwards *et al.* 1989) with the following composition was used for slicing (in mM): sucrose, 206; KCl, 2.5; $CaCl_2$, 1.0; $MgCl_2$, 4.0; NaH_2PO_4, 1.25; $NaHCO_3$, 26; glucose, 25; at pH 7.4 when bubbled with 95% O_2 and 5% CO_2..

2.1.2 External solution

A magnesium-free Krebs solution with the following composition was used for the external recording solution (in mM): NaCl, 125; KCl, 2.5; $CaCl_2$, 1.0; NaH_2PO_4, 1.25; $NaHCO_3$, 26; glucose, 25; pH 7.4. The external solution for recording was continuously gassed with a mixture of O_2 (95%) and CO_2 (5%) (BOC Gases, Manchester, UK). In my whole-cell experiments 200nM of TTX was added to the external recording solution to block action potentials in the slice and avoid excitotoxic effects.

2.1.3 Pipette solution

In order to minimize potassium currents, patch pipettes were filled with cesium chloride (CsCl) internal solution (Gibb & Colquhoun 1991). The composition of the internal solution was (in mM): $CsCl_2$, 140; EGTA, 10; HEPES, 10; NaCl, 10; adjusted to pH 7.4 with NaOH (1M). This solution was filtered and stored frozen in 1 ml aliquots.

For whole-cell recordings, ATP 1mM, GTP 0.5 mM and $MgCl_2$ 0.5mM were added to the pipette solution to avoid run-down of the whole-cell current and TEA 10mM was added to each 1ml aliquot to block potassium channels.

2.2 Drugs and chemicals

NaH_2PO_4 (500g, Prod. 301324Q), $CaCl_2$ (calcium chloride solution, 1.0M, 1L, Prod.190464k), $MgCl_2$ (magnesium chloride standard solution, 1.0M, 1L, EC No. 2320946), sucrose (1 Kg, Prod. 102745C), and CsCl (100g, Prod. 100675U) were purchased from BDH (Poole, England). NaCl (1Kg, SigmaUltra, minimum 99.5%, EC 231-589-3), $NaHCO_3$ (250 g, SigmaUltra,minimum 99.5% EC 205-633-8), KCl (250G, EC No. 2312118), glucose (250g, SigmaUltra, minimum 99.5% GC, EC 200-075-1), NMDA (N-methyl-D-aspartic acid, 250 mg, minimum 98% titration, 099F5805), HEPES (N-[2-hydroxyethyl] piperazine-N'-[2-ethanesulfonic acid], 100g, minimum 99.5%, Lot 48H5449), bicuculline methiodide (250 mg, Lot 36H3897), strychnine (25G, Lot 18H1178), EGTA (ethylene glycol tetraacetic acid, 100 g, 97%, Lot 17H5714), ATP (adenosine 5'-triphosphate disodium salt, 10g, 99%, Lot 17h7816), GTP (guanosine 5'-triphosphate sodium salt, 250 mg, 95%, CAS. 36051-31-7), nimodipine (100 mg, CAS 66085-59-4), ifenprodil tartrate salt (25mg, CAS. 23210-58-4), TEA (tetraethylammonium chloride, 25g, Lot 61K1464) and L-glutamic acid monosodium salt hydrate, glycine (100g, 99%, Lot 77H2512), cesium hydroxide (99%, 100g in water, CAS 21351-79-1), sodium hypochlorite (250ml, Batch U20738) and memantine hydrochloride (25mg, 98% GC, CAS 41100-52-1) were purchased from Sigma (St. Louis, MO, USA) were purchased from Tocris (Bristol, UK). TTX (tetrodoxin, 1mg, Batch APN06092-1-1), NBQX (10mg, Batch APN 06093-1-1) was purchased from Ascent Scientific.

2.3 Brain slice preparation

Coronal brain slices were prepared as previously described (Jones & Gibb, 2005). 7 day-old Sprague-Dawley rats were decapitated using a pair of surgical scissors (RS6930, Roboz, Germany) in accordance with the Animals Scientific Procedures Act, UK (1986). The skin was cut along the midline with a pair of small scissors. The skull was cut along the midline with a pair of fine scissors and the skull bones were removed using fine curved forceps. Within 60 seconds of decapitation the exposed brain was submerged in a 100 ml plastic weighting boat (Fisher Scientific, Loughborough, UK) containing ice-cold slicing solution continuously bubbled with a mixture of O_2 (95%) and CO_2 (5%).

The brain containing telencephalon, diencephalon and mesencephalon was isolated from the rostral part of the cerebellum and caudal part of the olfactory bulb. Then the brain was removed from the skull using a fine spatula. The brain was removed into ice-cold oxygenated slicing solution and allowed to cool down for 3-5 minutes.

For coronal brain slices, the rostral part of the telencephalon was glued, using cyanoacrylate instant adhesive (Loctite UK Ltd, Watchmead, Welwyn Garden City, Cat No. 40637), to the specimen bath of a vibroslicer (DTK 1000, Dosaka, Kyoto, Japan) with the dorsal side of the brain facing the cutting blade. Immediately, the specimen bath was filled with oxygenated ice-cold slicing solution until the tissue was completely covered. Slices were cut using carbon steel blades or ceramic blades (Campden Instruments Ltd, UK) at a thickness of 250- 300 μm. Hypodermic needles (Monoject, Ballymoney, UK) were used to dissect out the slices containing substantia nigra pars compacta from the adjacent cerebral cortex. Slices were transferred into an incubation chamber using a plastic disposable Pasteur pipette (Scientific Laboratory Supplies Ltd, Nottingham) cut to a tip opening of 3-5

mm across. The incubation chamber contained 100 ml external recording solution with additional 1 mM $MgCl_2$ added and was continuously bubbled with a mixture of O_2 (95%) and CO_2 (5%). Slices were incubated at room temperature (20 – 24 °C) for a period that ranged from 1 to 8 hours before experimenting.

2.4 Cell visualisation and identification of dopaminergic neurons in SNc (substantia nigra compacta)

The cell bodies of individual neurons in brain slices were visualised under Normaski differential interference contrast optics (Edwards *et al.* 1989) using an upright microscope (Axioskop FS, Zeiss, Oberkochen, Germany) with an achromat 40X water immersion objective with a numerical aperture of 0.75 and a working distance of 1.6 mm at a total magnification of 600X. Visualisation was carried out on a monochrome video monitor (VM-902K, Hitachi-Denshi, Tokyo, Japan) connected to CCD monochrome camera (RS Components, Corby, UK) mounted on top of the microscope trinocular head. Slice health was visually checked before patching and the presence of a considerable proportion of neurons with a smooth surface readily evident on the surface of the slice was used as an indicator of a good healthy slice. Individual healthy cells were identified by the smooth appearance of their surface.

Dopaminergic neurons were identified using a combination of morphological and electrophysiological criteria. Initially they were distinguished from interneurons in SNc by their large cell bodies, which were readily apparent under DIC optics. Dopaminergic neurons had ovoid, polygonal, or fusiform cell bodies that emitted 3-6 primary dendrites (Figure 2.1). In coronal sections, the dendrites of ovoid- or polygonal- shaped neurons in SNc are oriented mainly along the dorsoventral axis, whereas fusiform-shaped neurons

have dendrites that are oriented primarily mediolaterally (Tepper *et al.* 1987). In my experiments, the averaged cell capacitance of dopamine cells in P7 SNc was 53.2±2.5pF (mean ± S.E.; n=21) which is consistent with previous studies, 59.7±6.7pF from P5 rat (Washio *et al.* 1999).

Various electrophysiological characteristics of dopaminergic neurons were also used to identify dopamine cells in SNc. It is observed that dopaminergic neurons very often displayed spontaneous activity at a constant rate of 0.5-3.0 Hz. This activity is apparent upon suction to obtain the cell-attached gigaseal (>10GΩ) configuration. In the whole-cell configuration, dopaminergic cells possess a hyperpolarization-activated inward current (Counihan *et al.*) with characteristically slow kinetics. In our experiments, a voltage step from -60mV to -120mV was applied for 1.5s to activate a clear slow time-dependent inward current to identify dopaminergic neurons in SNc (see Figure 2.2). These observations are in good general agreement with previous descriptions of dopaminergic neurons in rat SNc (Yung *et al.* 1991; Hajos & Greenfield 1993).

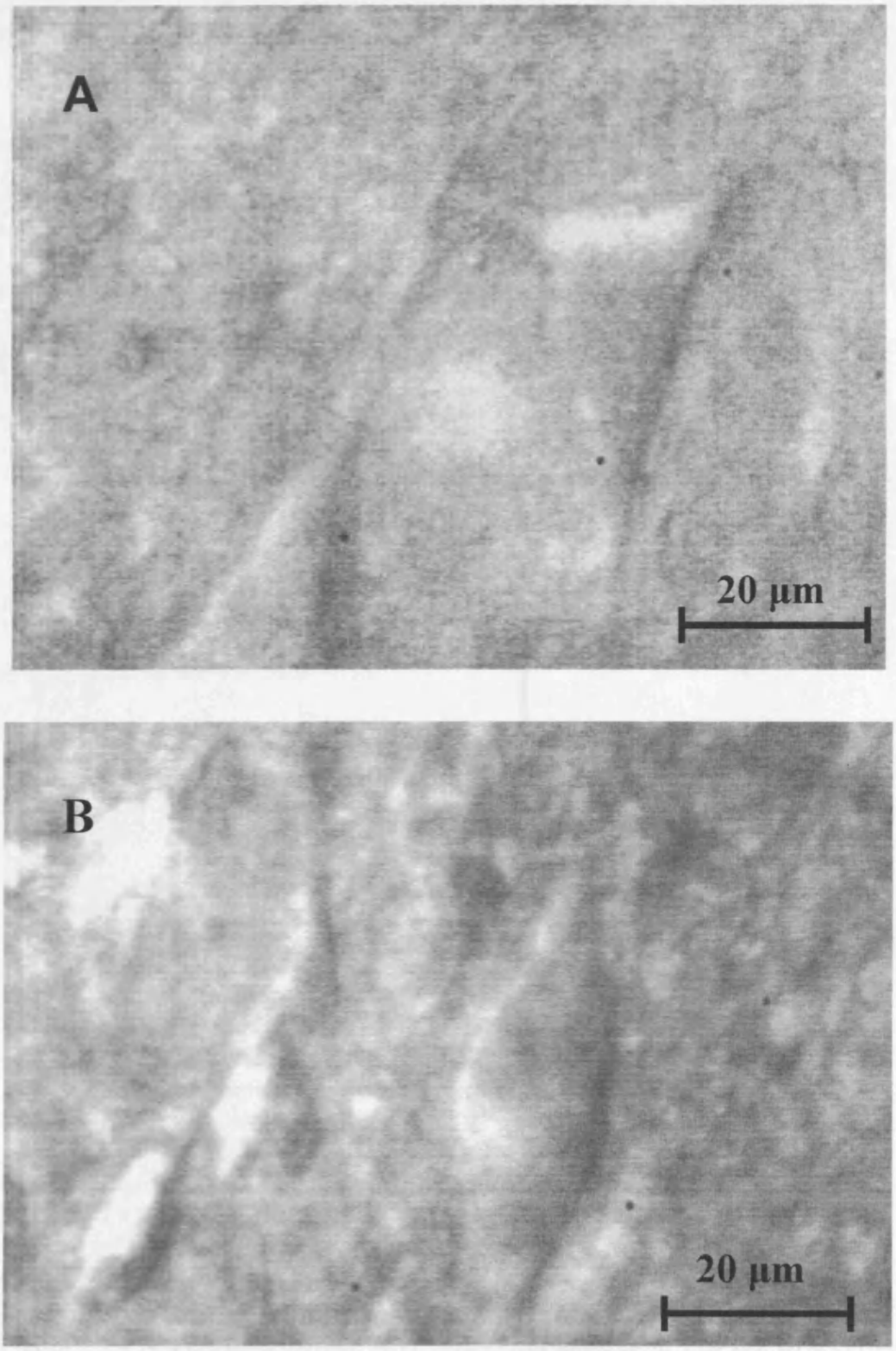

Figure 2.1 DIC images of dopaminergic neurons from P7 rat SNc.

A and B. two microscope images of dopaminergic neurons in P7 rat SNc. They are typical of SNc dopaminergic neurons in this study. A. The neuron had a polygonal cell body with three primary dendrites whereas B has an ovoid cell body

A

B

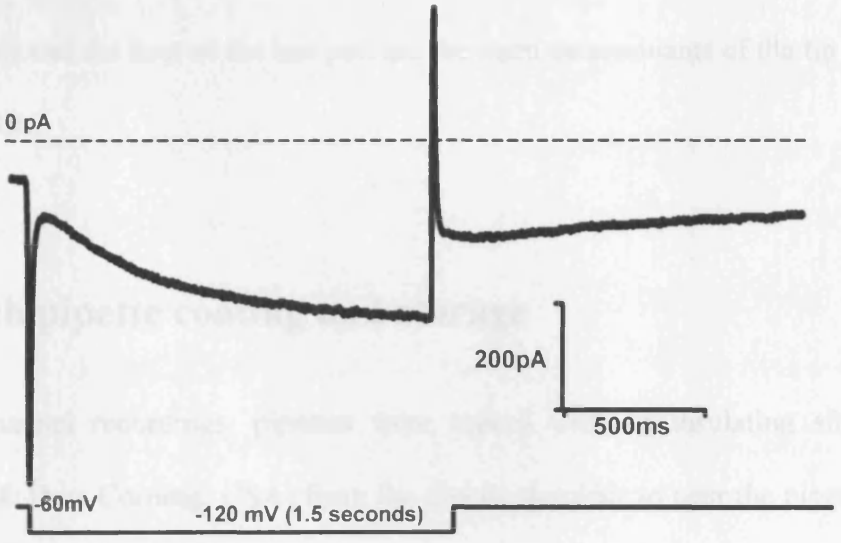

Figure 2.2 Identification of dopaminergic neurons in P7 rat SNc

Figure 2.2A is a detailed coronal slice map of rat brain from The Rat Brain Atlas (Paxinos and Watson, 1998, fourth edition), showing where the substantia nigra compacta (SNc) is in the coronal slices. This map was used as a guide to find dopaminergic neurons in SNc. Figure 2.2B shows a typical I_h current from an SNc dopamine cell. More than 85% of tested neurons in SNc possessed an I_h current, which was activated by a voltage-step from -60mV to -120mV for 1.5s. In this way, dopaminergic neurons in rat SNc could be distinguished from interneurons in SNc.

2.5 Patch-pipette making

2.5.1 Patch-pipette fabrication

Patch pipettes were made before patching cells in a vertical pipette puller (MF-83, Narishige, Tokyo, Japan) from thick-walled borosilicate glass capillaries containing an internal filament (GC150F-7.5, outer diameter 1.5 mm, inner diameter 0.86 mm, Harvard Apparatus Ltd). The pipettes were pulled in two stages. The first stage is to thin the glass to 200- 400 μm at the narrowest point over a 7- to 10-mm region. The second pull is to pull the two halves apart, leaving clean, symmetrical breaks. Both halves were used. The length of the first pull and the heat of the last pull are the main determinants of the tip diameter of the final pipette.

2.5.2 Patch pipette coating and storage

For single-channel recordings, pipettes were coated with an insulating silicone resin (Sylgard 184® Dow Corning, USA) from the pipette shoulder to near the pipette tip and then heated with a heated coil connected to a variable voltage source in order to cure the Sylgard. Then the tip of the pipette was cleaned and smoothed by fire polishing on a microforge (MF-83, Narishige, Tokyo, Japan) to a final resistance of 5-15 MΩ. Patch pipettes were stored horizontally mounted on a strip of Blu-Tack (Bostik, Leicester, UK) fixed to the base of a 90mm Petri dish (Sterilin, Staffs, UK).

2.6 Patching procedure

2.6.1 Whole-cell recordings

2.6.1.1 Procedure

Pipettes were back-filled with pipette solution and the level in the pipette was kept to a minimum to reduce electrical interference produced by solution creeping up the electrode or going into the suction line. Any bubbles left in the pipette can be removed by tapping the side of the pipette. Patch pipettes were positioned in an electrode holder connected to the head-stage of a patch-clamp amplifier (Axopatch 200A, Axon Instruments, Foster City, CA, USA) and some positive pressure was applied to the inside of the pipette to generate a tiny stream of solution at the tip of the pipette that prevented the accumulation of debris at the tip and the mixing of the pipette solution inside the pipette with the external solution in the recording chamber. The patch pipette was then lowered into the recording chamber. Once in solution, the pipette resistance was measured by passing a 5 mV rectangular pulse through the input using the patch-clamp amplifier. Patch pipettes usually had a final resistance of 10 - 15 MΩ for single-channel recordings and 5 – 10 MΩ for whole-cell recordings. Positioning of the patch pipette was carried out under the optical field of the microscope using a micromanipulator (Sutter Instrument, MP-225, England, UK) and under visual control the patch pipette was lowered further down until visual contact with the slice. Contact between the patch pipette and the cell was visually confirmed by the formation of a characteristic dimple on the cell surface caused by flow of solution from the pipette tip. Immediately, the positive pressure was released and a small amount of suction was applied to the back of the electrode. Then the cell membrane and the tip of the electrode begin to form a high resistance gigaohm seal. The membrane under the patch pipette was held at -60 mV and suction was applied through the tubing connected to the back of the electrode holder to break the membrane and gain electrical access to the cell

interior and then a whole-cell current can be recorded.

2.6.1.2 Compensation of series resistance

In whole-cell voltage-clamp recordings, the membrane potential of the cell was controlled by the potential applied to the pipette. The control of potential is not complete but depends on the access resistance between the pipette and the cell interior and on the size of the currents that must flow though this resistance.This access resistance is called series resistance (Rs). Series resistance arises from the pipette itself, but normally the major part arises from the residual resistance of the broken patch membrane. Series resistance not only slows the charging of the cell membrane capacitance because it impedes the flow of the capacitive charging current when a voltage step is applied to the pipette electrode, but also gives errors in membrane potential when large membrane currents flow.

In order to reduce the voltage error due to the series resistance existing in whole-cell experiments, more than 70% of the series resistance was compensated by the Axopatch -200 A before starting recordings. The voltage error can be calculated by Ohm's law ($V_{error} = I \times R_s$). The average series resistance (R_s) before compensation from my experiments was 20 MΩ (n = 150). The holding current ($I_{membrane}$) was usually less than 50 pA. Therefore, originally the voltage error ($V_e = I_{membrane} R_s$) was less than 1mV and reduced to -0.2 mV after 80% compensation. Although during the response evoked by 10μM NMDA application, the currents increased to 700.5 ± 64.6 (Mean ± S.E., n= 17) pA, the voltage error would be -2.8 mV after compensation. For experiments where ifenprodil inhibition of NMDAR, only dopamine cells with series resistance less than 10MΩ were used. In the presence of 250 μM of NMDA and 10μM of glycine, the whole-cell NMDA current increased to about 1500 pA and the voltage error is less than 4mV after 85%

compensation. Therefore in these experiments series resistance errors had little impact on the whole-cell recordings.

2.6.2 Single-channel recording

For single-channel recording, high resistance gigaohm seals with more than 40GΩ were required for low noise recording. After gaining a whole-cell configuration, the patch electrode was very slowly withdrawn away from the cell using the manipulator until an outside out patch was obtained. Electrical noise was reduced by bringing the patch pipette towards the surface of the bath leaving only its tip in the solution. The patch pipette was also brought toward the inlet of the recording chamber to improve contact between the patch and the incoming solutions. Before recording was attempted, the noise level was checked and an RMS noise level below 0.300 pA at a bandwidth of 5 kHz was considered acceptable for recording.

2.6.3 Concentration jump experiment

2.6.3.1 Theta glass tubing

Dual-channel theta glass tubing is provided by several different suppliers. The borosilicate theta glass from Hilgenberg (Malsfeld, Germany, outer diameter 2.0 mm, inner diameter 1.4mm, and septum thickness 0.1167 mm) and aluminosilicate theta glass tubing (Sutter Instrument, O.D. 1.5 mm, I.D. 1.0 mm, 10 cm length, catalog: AF150-100-10) were used in my experiments. The use of thick-walled glass tubing is advantageous because the application pipette is mechanically more stable, minimizing oscillations in the solution exchange. Thin septa are preferable because the interface between the solutions flowing down the two barrels of the application pipette is sharper.

2.6.3.2 Pulling and breaking

The theta glass tube was pulled to an outer diameter of about 300 μm in one step. Then the raw piece was cut into two parts under visual control of a 10× binocular microscope using a diamond pencil. This step was critical, because tip irregularities could cause turbulence of flow. Sometimes, it was just necessary to touch the glass, in other case the tubing had to be rotated and scratched again until the two parts separate. A typical theta glass pipette shows a tip outer diameter of 300 μm and a shank length of about 5 mm.

2.6.3.3 Tubing connection

To connect the two barrels of the application pipette with the solution reservoirs, polyethylene (PE) microtubing (Portex, England, O.D. 0.61 mm, I.D. 0.28 mm) was inserted into the back end of the application pipette barrels and moved as far as possible toward the tip. The space between the pipette wall and the PE tubing was filled with glue (Loctite UK Ltd, Watchmead, Welwyn Garden City, Cat No. 40637) by putting a drop of glue on the back end of the application pipette and allow the glue to flow as far as possible to the end of the PE tubing. The space between PE tubing and glass wall was filled almost entirely to minimize the dead volume in the pipette.

2.6.3.4 Mounting the application pipette to the Piezo translator

To fix the application pipette to the Piezo translator (EXFO Burleigh products Group Inc, LSS-3100 Ultrafast Solution-Switching System, Canada) and minimize the possibility of application pipette vibration, we use the following design. A trapeziform hard plastic piece

was mounted on the bottom of the Piezo translator using four screws. A 2.5 cm length groove was made on the one side of the trapezoform piece for mounting the application pipette.

2.6.3.5 Perfusion of application pipette

Two 10ml-syringes were loaded after slight modification of the original design and were connected to the back end of the application pipette with PE tubing (Potex Fine Bore Polythene Tubing, I.D. 0.38 mm, O.D. 1.09 mm, REF 800/100/120). One syringe contains control solution (external solution 20 μM glycine and 20 μM DNQX) and the other syringe contains glutamate solution (external solution with 1mM glutamate, 20 μM glycine and 20 μM DNQX). Both solutions were perfused into the application pipette by gravity. A flow velocity of about 100 μm / ms at the application pipette tip was used and flow rate was adjusted by moving the vertical position of the syringes and hence changing the level of the solution surface. For an application pipette with 120 μm barrel width, a perfusion rate of about 10 ml/hr was used. Bath perfusion was at 2-3 ml/min and roughly parallel to the direction of solution flow out of application pipette to avoid turbulence and to remove the agonist quickly from the recording bath.

Only filtered solutions were used for pipette perfusion using 0.22 μm syringe filters (Millipore Corporation, U.S.A, Cat No. SLGS033SS) to minimize the risk of destroying patches due to small particles in the perfusion solution. The perfusion solutions were held at room temperature for at least half an hour before use to avoid bubble formation.

2.6.3.6 Cleaning and storage of application pipettes

To avoid contamination with dirt and bacteria, application pipettes were rinsed with

distilled and deionised water containing 0.5% of sodium hypochlorite for at least 20 minutes after each experiment. The application pipettes were stuck inside a 60-ml plastic test tube using Blu-Tack (Bostic, Leicester, UK) and the tips of the application pipettes were submerged in distilled water to avoid contamination.

2.6.3.7 Open-tip response

In order to map out the optimal position of the recording pipette, open-tip experiments were performed every day before experiment. Theta glass application pipettes were perfused with 10mM NaCl solution and 1mM NaCl solution, respectively. To begin with, an open-tip recording pipette was positioned in the 1 mM NaCl solution, 100 μm away from application pipette tip and 20 μm away from the interface. The position of the recording pipettes was slightly below the center of the application pipette tip and the angle between the application pipette and the horizontal plane was about 20°. Then 5 volt electrical pulses for 1-4 ms which were generated by WinWCP (written by John Dempster, University of Strachclycle, 1991-2005) were filtered with a low-pass bessel filter at frequency of 0.5 kHz (Warner Instrument Corp.) to smooth the rising and falling phase of the voltage pulses then the filtered pulses were repeatedly applied to the Piezo translator and the open-tip response was observed as a change in current recorded by the patch-clamp amplifier. Once the optimal position of the recording pipette was found, it was documented in order to be able to reproducibly find it when a good outside-out patch was made. An example of an open tip experiment is shown in figure 2.3 and the measurement of the change in liquid junction potential for this experiment indicated that the 20-80 % rise-time for the exchange of control and test solutions was < 200 μs (fitting of the rising phase is shown in figure 2.3).

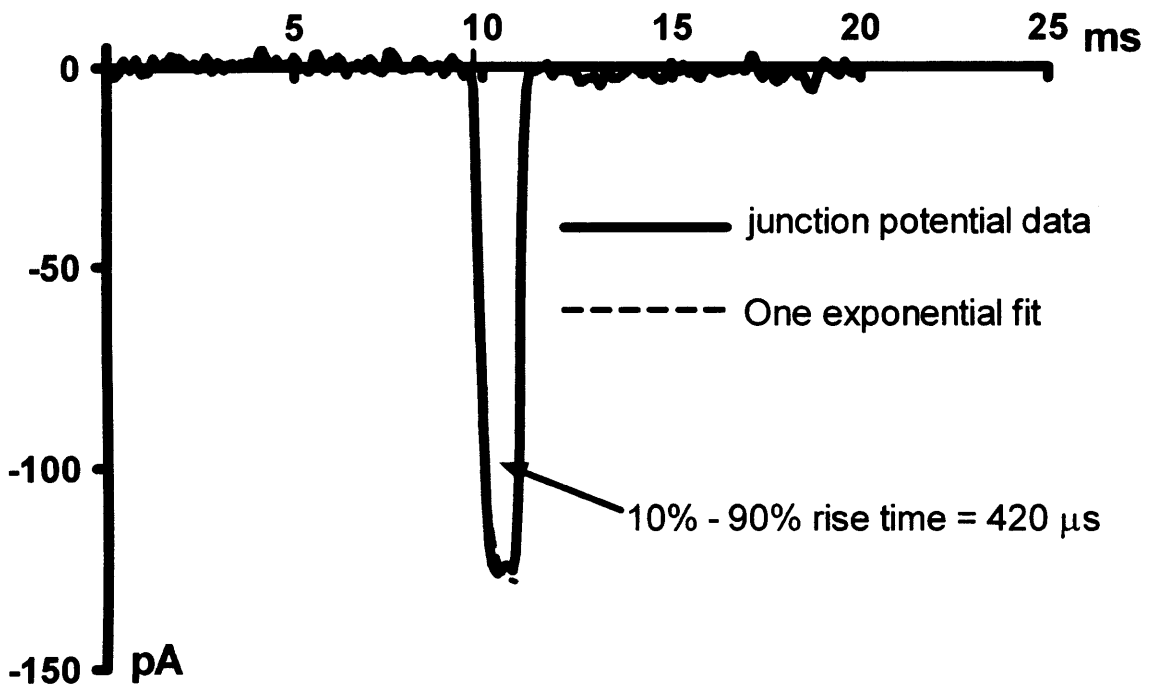

Figure 2.3 A example of open-tip experiments

Figure 2.3 shows the liquid junction potential between high and low concentrarion of NaCl which were purfused from a theta glass application pipettes. The 1-4 ms solution change between 1mM NaCl to 10 mM NaCl was achived by fast moving recording pipette using a Piezo translator. The rise time phase of this junction potential is well fitted with one exponential component with 10-90% rise-time of 420 μs for the exchange of control and test solutions.

2.6.3.8 Patching procedure and data analysis

To obtain good outside-out patchs, high resistance gigaohm seals of more than 40GΩ resistance were required for low noise recording. After gaining a whole-cell configuration, the patch electrode was very slowly withdrawn away from the cell using the manipulator until an outside out patch was obtained. Then the outside-out patch was positioned in the place where the pipette was in the open tip recording. Then 5 volt electrical pulses for 1 ms or 4 seconds duration were repeatedly applied to the Piezo translator using the program WinWCP to make fast applications of glutamate. All 10-second sweeps evoked by fast application of 1mM glutamate were recorded by WinWCP at a holding potential of -60 mV, filtered at 2 kHz and sampled at 10 kHz onto a computer hard disk via a CED 1401 plus interface (CED Instruments, Cambridge, UK).

During data analysis, all sweeps from one patch were averaged by WinWCP and the decaying phases of the averaged sweeps were well fitted with two exponential components (the equation for two exponential fitting is $y(t) = A_1\exp(-t/\tau_1) + A_2\exp(-t/\tau_2)$). Then all data from 6 individual patches were averaged by Mircsoft Excel and the decaying phase of the averaged curve was fitted with two exponential components.

2.7 Drug application and experimental design

All solutions were perfused into the recording chamber by gravity. The exchange between solutions was made by manually switching a two-way tap. Solution was removed from the recording chamber by suction supplied by a suction pump connected to a solution reservoir.

2.7.1 Whole-cell recordings

All whole-cell currents recorded were filtered on-line at 2 kHz, digitized at a sample rate of 10kHz and were recorded and analyzed using WinEDR-$V_{2.5.9}$ and WinWCP-$V_{3.5.9}$ (written by John Dempster, University of Strachclycle, 1991-2005)

2.7.1.1 Mg^{2+} block experiments

Slices were placed in a recording chamber on the stage of a Zeiss Axioskop microscope and were continuously bathed in the external solution at room temperature with 0.5μM of conotoxin MVIIC and 2μM of nimodipine to minimize the effect of voltage-gated calcium channels.

Following by a voltage-step from –60 mV to 0 mV for 1.5 seconds to inactivate voltage gated calcium channels and a voltage-ramp from -100 mV to +40 mV for 2 seconds (Figure 2.4), the NMDA-induced current and membrane current-voltage relationships were obtained for each cell at three different Mg^{2+} concentrations (contaminating concentration of Mg^{2+}, 100μM Mg^{2+}, and 1mM Mg^{2+}) using the following protocol.

As shown in figure 3.1A, after obtaining the whole-cell configuration, the cell was held at -60mV and the recording channels perfused with Mg^{2+}- free external solution. A few minutes later when the holding current reached steady state, four voltage changes were made using the protocol above to evoked control current-voltage relationships (I-V relations) which were stored on computer using the WinWCP program. Then application of 20μM NMDA and 10μM glycine evoked a whole-cell NMDA current, four voltage ramps were applied when the NMDA whole-cell current reached a steady state and NMDA I-V relations were recorded on computer. Afterwards, the NMDA response was washed out

followed by application of control Mg^{2+}- free external solution and four control I-V relations were recorded when the control current was stable. In order to the obtain NMDA I-V relation in the presence of a contaminating concentration of Mg^{2+}, eight control I-V relations obtained before and after application of NMDA and four I-V relations obtained during application of NMDA were averaged, then the averaged control ramp was substracted from averaged ramp recorded in the presence of NMDA. Using the same protocol, the NMDA I-V relations in the presence of 100μM and 1mM Mg^{2+} were obtained (Figure 2.4). For Mg^{2+} ramp experiments in the presence of 10μM ifenprodil, a saturating concentration of NMDA (200 μM) and 10μM glycine were applied to avoid the change in NMDA receptor affinity that occurs on coapplication of 10μM ifenprodil.

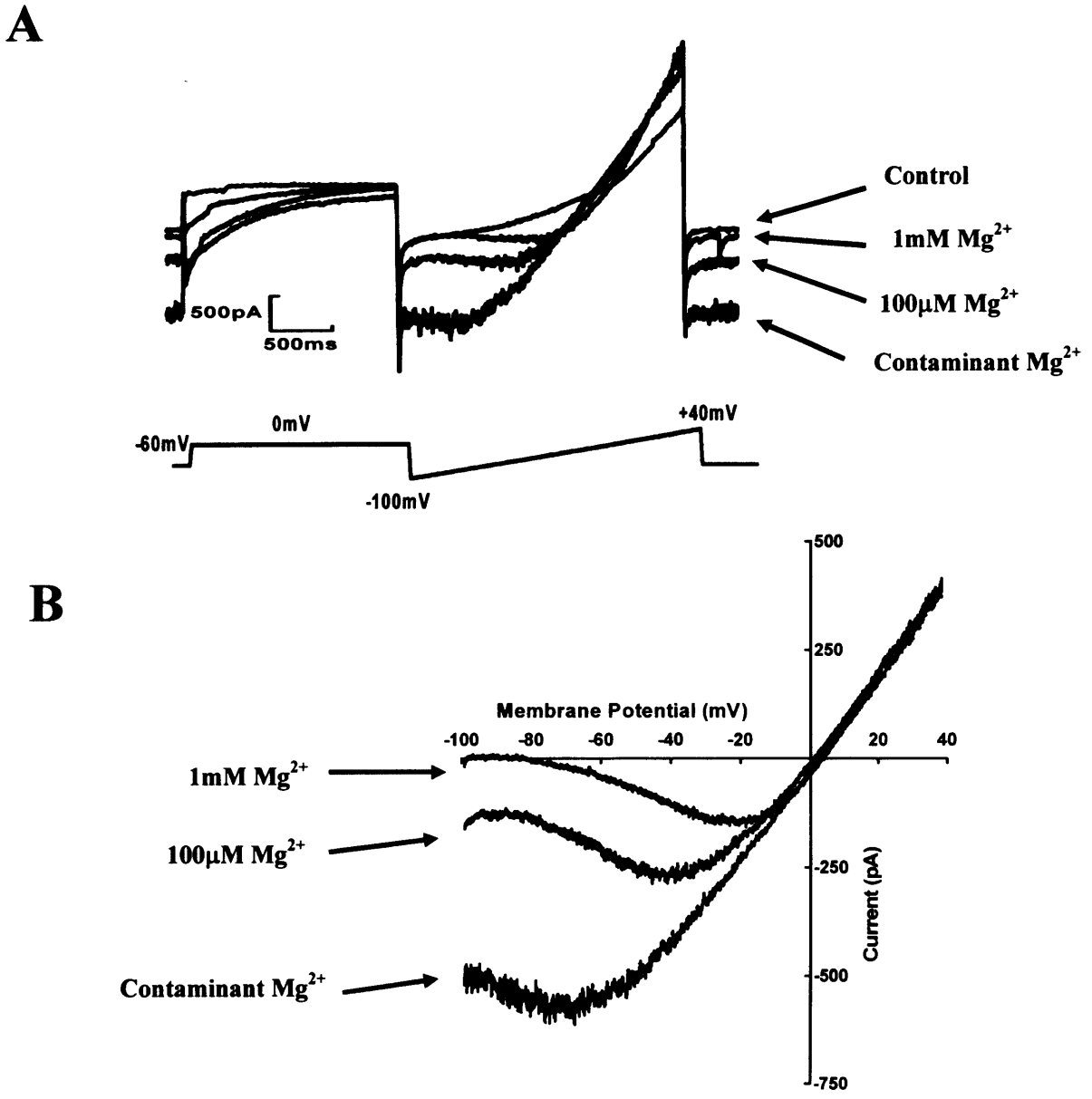

Figure 2.4 Experimental protocol for recording voltage-dependent Mg^{2+} block of NMDAR currents

A. Example currents recorded from whole-cell patch-clamp recordings from a P7 rat dopaminergic neuron in SNc. The cell was clamped and held at -60mV. Before voltage ramps from -100mV to +40mV, a voltage step to 0mV was added for 1.5s to inactivate voltage-gated calcium channels. This protocol was repeated before and during a steady-state NMDA current. For each Mg^{2+} concentration, four voltage ramps were made and the average of these four ramps was used to estimate the voltage-dependence of Mg^{2+} block. B. The control current trace was substracted from the traces recorded in the presence of NMDA. The resultant I_{NMDA} values were plotted versus membrane potential.

2.7.1.2 Ifenprodil inhibition experiments

Slices were placed in a recording chamber on the stage of a Zeiss Axioskop microscope and were continuously bathed in the external solution with 100 nM of TTX at a flow rate about 3-5 ml / min to reduce excitotoxic effects during application of 250 μM of NMDA.

As shown in figure 5.1, the dopamine cells were held at –60 mV during whole experiments and the application of 250 μM NMDA and 10 μM glycine produced an inward whole-cell NMDA current that was inhibited by coapplication of 1 μM and 10 μM of ifenprodil.

2.7.1.3 Memantine ramp experiment

The protocol for memantine ramp experiments is similar to the Mg^{2+} block experiment. Three concentrations of NMDA (100μM, 50 μM and 10 μM) and 10 μM glycine were used respectively to produce NMDA whole-cell currents and 1mM Mg^{2+} was coapplied during the whole experiment to study the effect of Mg^{2+} block on memantine. Taking the 100 μM NMDA experiment as an example, after obtained the whole-cell configuration, dopamine cells were held at –60 mV, then four voltage ramps as shown in figure 6.1 were applied to evoke I-V relations when the holding current reached a steady state. Then application of 100μM NMDA and 10μM glycine evoked a whole-cell NMDA current, four voltage ramps were applied when the NMDA whole-cell current reached a steady state and NMDA I-V relations were recorded on computer. Afterwards the NMDA response was washed out followed by application of control external solution with 1mM of Mg^{2+} and four control I-V relations were recorded when the current was stable. In order to obtain the NMDA I-V relation in the absence of memantine, eight control I-V relations obtained before and after application of NMDA and four I-V relations obtained during application of

NMDA were averaged, then the averaged control ramp was subtracted from the averaged ramp in the presence of NMDA. Using the same protocol, the NMDA I-V relations in the presence of 1μM, 5 μM and 50μM memantaine were obtained.

2.7.2 Single-channel recordings

2.7.2.1 Single-channel recording from subthalamic nucleus (STN)

In single-channel experiments each outside-out patch from P7 rat STN was firstly exposed to a constant concentration of NMDA (200μM) for 2-5 minutes in the presence of saturating concentrations of glycine (10 μM). Then ifenprodil (10 μM) was applied together with NMDA and glycine for 2-5 minutes.

2.7.2.2 Deactivation and desensitization experiment

Outside-out patches were obtained from P7 rat SNc dopaminergic neurons and each outside-out patch firstly was exposed to control solution which contained 20μM glycine and 20 μM DNQX (DNQX was used to block AMPA and kainate receptors). Then test solutions (1mM glutamate, 20μM glycine and 20 μM DNQX) were applied by Piezo translator for 1ms to measure the activation and deactivation time course and for 4 seconds to measure the desensitization time course.

2.7.2.3 Single-channel recording from P7 rat dopaminergic neurons

In single-channel recording experiments each outside-out patch from P7 rat dopamine cells was firstly exposed to a constant concentration of glutamate (100nM) for 2-5 minutes in the presence of saturating concentrations of glycine (10μM). During the

whole-expriements, 20μM DNQX, 1μM of strychnine and 10μM of bicuculline were coapplied to inhibit AMPA and kainate receptors, glycine receptors, and GABA receptors.

2.8 Whole-cell data acquisition and analysis

2.8.1 Whole-cell NMDA responses - WinEDR

Whole-cell currents evoked by NMDA and glycine application were recorded using an Axopatch 200A patch-clamp amplifier (Axon Instruments). Signals were amplified and filtered at 2 kHz (8 pole Bessel) and digitised at 20 kHz using an analogue-to-digital converter (CED micro 1401, Cambridge Electronics Design, UK). Whole-cell currents were stored on computer using the program WinEDR (V2.2.3) (available at http://spider.science.strath.ac.uk/PhysPharm /showPage.php?page Name=software_ses).

After recording the whole-cell currents traces were printed out using the program WinEDR and then the mean maximum currents manually measured with a ruler. Excel was used to organize and analyze all the data obtained from manually measured current traces. An average current was calculated and a percentage change from different responses was calculated.

2.8.2 Whole-cell Mg^{2+} ramp experiment- WinWCP

Whole-cell currents evoked by NMDA and glycine were recorded using an Axopatch 200A patch-clamp amplifier (Axon Instruments). Signals were amplified and filtered at 2 kHz (8 pole Bessel) and digitised at 20 kHz using an analogue-to-digital converter (CED micro 1401, Cambridge Electronics Design, UK).

The NMDA current ramps were evoked and recorded by WinWCP (available at http://spider.science.strath.ac.uk/sipbs/page.php?page=software_ses)

In order to measure the fractional block of NMDA whole-cell currents by external Mg^{2+} at -60 mV, NMDAR I-V relationships at positive voltages from 0 mV to +40 mV were extrapolated to -100 mV and the control current values at -60 mV, -80mV and -100 mV were calculated from the this line. The ratios of residual current in the presence of Mg^{2+} to control current were used to calculate external Mg^{2+} IC_{50} at different voltages.

2.9 Single-channel data analysis

2.9.1 Steady-state single-channel recordings – WinEDR

Steady state single-channel activity was produced by a constant concentration of glutamate 100nM or NMDA (200μM) and a constant saturating concentration of glycine (10 μM), and recorded using an Axopatch 200A patch-clamp amplifier (Axon Instruments). Signals were amplified and filtered at 2 kHz (8 pole Bessel) and digitised at 20 kHz using an analogue-to-digital converter (CED micro 1401, Cambridge Electronics Design, UK). Single-channel currents were stored on the computer using a program WinEDR.

2.9.2 Jump experiment recording – WinWCP

1ms or 4 second pulse of 1mM of glutamate was applied by Piezo translator which was driven by 5mV voltage pulse for 1ms added by WinWCP program (available at http://spider.science.strath.ac.uk/sipbs/page.php?page=software_ses). Each sweep of NMDA current evoked by fast application was recorded using an Axopatch 200A

patch-clamp amplifier (Axon Instruments) for 10 seconds to investigate whether there is any slow deactivation component in the response of NMDA receptors on dopaminergic neurons. Signals were amplified and filtered at 2 kHz (8 pole Bessel) and digitised at 20 kHz using an analogue-to-digital converter (CED micro 1401, Cambridge Electronics Design, UK). Single-channel currents were stored on the computer using the program WinWCP. For each experiment all NMDA current sweeps were averaged to obtain an averaged deactivation time course and averaged desensitization time course.

2.9.3 Detection and fitting of single-channel data - SCAN

Each digitised single-channel record was scanned and opening and closing transitions were detected, measured and fitted using an interactive computer program (SCAN, available at http://www.ucl.ac.uk/Pharmacology/dcpr95.html#scan) that carried out direct fitting of each event time-course based on the step response of the recording system (Colquhoun & Sigworth, 1995). Briefly, the digitised recording was displayed and scanned by scrolling it across the computer screen under visual inspection. Events were detected after crossing a threshold placed close to the baseline. Once it was decided that the event could be fitted, the program made initial guesses for the positions of all the transitions and amplitudes and performed a least-squares fit on the basis of these guesses; finally, it displayed the fitted curve superimposed on the digitised event. If the step-response function fitted poorly, the fit was adjusted to obtain the fit that best described the event. Fits were stored as a list of values with the amplitude and duration of each open period and the duration of each closed period. Incompletely resolved openings had their amplitude constrained to be the same as that of the closest opening longer than 2 filter rise-times if such an opening was present in the region of trace being fitted. If on the contrary, there were no openings with such characteristic in the section of trace being fitted, they were fitted as openings to the mean

amplitude level. After the record was fitted, a data file containing all the values describing the lifetime and amplitude of all single-channel events present in the record was created and stored as a computer file which was later used during the analysis of the single-channel data.

2.9.4 Analysis of single-channel distributions - EKDIST

Display and analysis of single-channel data distributions was done using the program 'EKDIST' (Available at http://www.ucl.ac.uk/Pharmacology/dcpr95.html#scan) designed by D. Colquhoun (Department of Pharmacology, University College London). Before analysis, a fixed resolution for open times and closed times that gave a false event rate less than 10^{-11} events per second was imposed, and a 'real' difference between adjacent amplitude levels defined as > 0.25 pA.

2.9.4.1 Stability plots

Stability plots (Weiss & Magleby 1989) for amplitudes were built by plotting the individual single-channel current amplitude of each opening against the interval number in which the opening was detected. The amplitude of each single opening longer than 2 rise-times (332 μs) was plotted. Each data point on the plot represented a single observation independently of its duration.

Before a patch was accepted for detailed analysis, the long term stability of the data records was checked by making stability plots for open times, shut times and P_{open}. Stability plots for open and shut times were made by calculating a moving average of 50 consecutive open or shut time intervals with an overlap of 25 events and plotting this

average against the interval number at the center of the averaged values. Stability plots for open probability were made by calculating a P_{open} value for each set of 50 open and shut times. Once the stability of the record was confirmed, values were sorted into bins and used in the construction of frequency distribution histograms.

2.9.4.2 Distribution of fitted amplitudes

The amplitude of channel openings can be measured accurately only if the duration is at least twice the rise-time (T_r) of the recording system (Colquhoun & Sigworth, 1995). Frequency distribution histograms containing individual open-channel amplitudes longer than 2 filter rise-times were constructed and fitted with the sum of three Gaussian components with their standard deviations constrained to be the same. The relative area occupied by each Gaussian component represents the relative frequency of events to each particular amplitude level rather than the relative time spent at each level. Each single-channel opening longer than 2 filter rise-times represented one observation independently of its duration.

2.9.4.3 Distributions of open times and shut times

As the duration of closed and open time intervals can vary from tens of microseconds to tens of seconds, frequency distribution histograms were constructed using a logarithmic transformation of the abscissa (Sigworth & Sine 1987) and a square root transformation of the ordinate (Sigworth & Sine 1987). Distributions were fitted using the maximum likelihood method with probability density functions that were a mixture of three exponential components for open times and five exponential components for closed times (Gibb & Colquhoun 1992).

2.9.4.4 Statistics (student t-test)

Statistical analysis (student's paired or unpaired t-test) was performed in Microsoft Excel and Graphpad Prism software, with a significance level of $p < 0.05$.

During fitting of Mg^{2+} block and memantine block data, in order to test which model is able to well explain the Mg^{2+} or memantine block data, we minimized the sum-of-squares values during the curve fitting then the model with minimal sum-of-squares value was considered as the best model to explain the block.

Chapter 3: Mg^{2+} block of NMDA receptors in dopaminergic neurons of rat substantia nigra pars compacta

3.1 Summary

1. Whole-cell patch-clamp recording of bath application-induced NMDA receptor-mediated currents (I_{NMDA}) in dopaminergic neurons of substantia nigra pars compacta in brain slices from P7 rats were used to characterize the voltage-dependence of Mg^{2+} block of NMDA receptors.

2. NMDA receptors on dopaminergic neurons undergo a significant voltage-dependent Mg^{2+} block. At resting potential (-60mV), the application of NMDA (10μM) and glycine (10μM) produced inward currents which were blocked by the physiological concentration of Mg^{2+} (1mM) by 85.2 ±0.1% (±SE, n=16) and at 100μM Mg^{2+} by 60.3 ± 0.1 % (±SE, n=9). The IC_{50} value for Mg^{2+} block at –60mV was 74.4μM.

3. Concentration-inhibition curves were constructed at each voltage selected. The IC_{50} of Mg^{2+} at each voltage was obtained by curve fitting of I_{Mg} / $I_{control}$ ratio at various concentrations of external Mg^{2+}. The Mg^{2+} IC_{50} values at -100mV, -80mV and -60mV were 7.9 μM, 18.8 μM and 74.4 μM, respectively (n=12). Compared with previous studies, these IC_{50} values suggest that NR2A- or NR2B-containing NMDA receptors

are present on dopaminergic neurons.

4. The application of the NR2B subunit-specific NMDA antagonist ifenprodil (10 μM) reduces the NMDA induced whole-cell current (75.7 ± 1.9%). The residual ifenprodil-insensitive I_{NMDA} component had a lower Mg^{2+} sensitivity than the total NMDA current. The Mg^{2+} IC_{50} values for the ifenprodil-insensitive current at -100mV, -80mV and -60mV were 46.6 μM, 97.3 μM and 259.3 μM, respectively (n=9). These data suggest that NR2C- or NR2D-containing NMDA receptors are expressed by P7 rat dopaminergic neurons.

5. Four Mg^{2+} block models were used to explain the voltage-dependent Mg^{2+} block of NMDA receptors on dopaminergic neurons. Fitting NMDAR I-V relationships with different models shows that trapping block model, potentiation model and proton block model all give same voltage-dependent block parameters, δ and K_{Mg2+} (0 mV), being 0.82 and 6 mM in the absence of ifenprodil and 0.64 and 4.87 mM in the presence of ifenprodil. The sequential block model stimates a higher Mg^{2+} affinity 432 μM in the absence of ifenprodil and 348 μM in the presence of ifenprodil.

6. The voltage-dependent Mg^{2+} block parameter for dopamienrgic neurons is 0.82, which is smaller than NR1-NR2A and NR1-NR2B NMDARs but higher than NR1-NR2C and NR1-NR2D NMDA receptors. This result suggests that a mixed population of NR2 subuntis is present in doapminergic neurons. The decrease in δ in the presence of ifenprodil suggests that NR2 subunits with a low Mg^{2+} sensitivity are expressed by dopamine cells.

3.2 Introduction

NMDA receptors are unique glutamate-gated ion channels in displaying a voltage-dependent Mg^{2+} block, and requiring the binding of both the transmitter and the co-agonist, glycine, for their activation (Mayer *et al.* 1984; Nowak *et al.* 1984; Johnson & Ascher 1987). The functional and pharmacological properties of NMDARs are mainly determined by NR2 subunits (Cull-Candy & Leszkiewicz 2004). For example, recombinant receptor channels assembled from NR1-NR2A and NR1-NR2B subunits are blocked more strongly by external Mg^{2+} than the channels formed by the NR1-NR2C and NR1-NR2D subunits (Monyer *et al.* 1994).

The voltage-dependent Mg^{2+} block of NMDARs has important physiological functions and pharmacological practical value. Firstly, at resting membrane potential, NMDARs undergo rapid channel block by physiological concentrations of Mg^{2+}, which significantly reduces the NMDAR component of the synaptic current (Herron *et al.* 1986; Forsythe & Westbrook 1988). However, when neurons are depolarized, for example, by activation of colocalized AMPA receptors, the voltage-dependent block by external Mg^{2+} is rapidly reduced, allowing Na^{+} and Ca^{2+} ion influx through activated NMDA receptors. It has been suggested that NMDA receptors in injured neurons decrease their sensitivity to voltage-dependent Mg^{2+} block (Furukawa *et al.* 2000). It is not clear yet that whether in PD the NMDARs in dopamine cells of SNc undergo a switch in sensitivity to Mg^{2+} block when the neurons are injured during disease progression. Secondly, the transition between membrane hyperpolarization and depolarization of dopamine cells in SNc is facilitated by voltage-dependent Mg^{2+} block (Hu & Bourque 1992). Finally, the subtypes of native NMDAR can be investigated by comparing voltage-dependent Mg^{2+} block in native cells

with that of recombinant receptors (Kirson *et al.* 1999).

The aim of this study is to characterize Mg^{2+} block of NMDAR on dopamine cells of SNc to investigate NMDAR composition and to add to information concerning the physiology of NMDA receptors in substantia nigra. My results and those from other studies support the idea that NR2B-containing and NR2D-containing NMDARs are present in SNc dopamine cells and dopamine cells experience a reduced Mg^{2+} block due to the presence of NR2D-containing NMDA receptors. In order to quantify the voltage dependent Mg^{2+} block, two Mg^{2+} block models are developed to accurately estimate the voltage dependent parameters for Mg^{2+} block.

3.3 Modelling and curve fitting

The blocking mechanism of NMDA channels by Mg^{2+} has been extensively investigated. In the widely accepted mechanism, Mg^{2+} is considered as an open channel blocker and can bind to an open NMDA receptor channel at a discrete site situated in the membrane electrical field, obstructing current flow. As a result, the affinity of Mg^{2+} for the binding site changes as a function of membrane voltage. There are three widely accepted models used to explain the interaction of Mg^{2+} with the NMDA channel. First is the sequential model (Scheme 3.1). It assumes that Mg^{2+} can only bind to an open NMDA channel. When Mg^{2+} is bound, ion flow is blocked and agonist cannot unbind from the receptor and so the channel stays in open (blocked) state until Mg^{2+} leaves the channel. This sequential blocking model is roughly consistent with single-channel data except that the burst length does not increase linearly with Mg^{2+} concentration (Nowak *et al.* 1984). Therefore, some modifications were made based on the sequential block model to produce the three-state

model (Scheme 3.2) and a trapping block model (Scheme 3.3) to provide a satisfactory explanation for the data. The three-state model was first pointed out by Jahr and Stevens (1990) and the predictions of this model for the distribution of open times, closed times, and number of interruptions per burst are in approximate agreement with previous studies. This model is considered as an embryo of the trapping block model. In the three-state model (Scheme 3.2), Mg^{2+} can only bind to the open NMDA channel (B) and the channel can close and the agonist can unbind from the NMDA channel before Mg^{2+} leaves the NMDA channel (C). However, the model did not distinguish the two NMDAR closed states between AR (agonist bound closed state without Mg^{2+} bound) and ARB (agonist bound closed state with Mg^{2+} bound). Then another modified symmetrical trapping block model was proposed by Sobolevsky and Yelshansky in 2000 (Scheme 3.3). In this trapping block model, Mg^{2+} allows the channel gate to close during the block and it can be subsequently trapped in the channel when the agonist dissociates. These models mentioned above failed to predict a slow component of Mg^{2+} unblock in response to a depolarizing voltage jump. In order to explain the observation of slow Mg^{2+} block, another two asymmetric trapping block models were proposed by Scheme 3.4 (Kampa *et al.* 2004) and Scheme 3.5 (Vargas-Caballero & Robinson 2004). Both models suggested that occupation of the channel by Mg^{2+} moderately accelerates only the rate of channel closure (Vargas-Caballero & Robinson 2004) or accelerates rates of channel closure and agonist unbinding, along with increasing the occupancy of desensitizated states (Kampa *et al.* 2004). These models predict accurately the appearance of a slow component of Mg^{2+} unblock.

In addition to subunit specific external Mg^{2+} block of NMDA receptors, multiple Mg^{2+} effects on NMDA receptors have been reported. For example, NMDA receptor channels are blocked by intracellular Mg^{2+} in a voltage-dependent manner (Johnson & Ascher 1990).

In the absence of extracellular Ca^{2+}, the block of NMDA receptor channels composed of NR1-NR2A by intracellular Mg^{2+} showed a voltage-dependence (δ) of around 0.38 and an affinity for the channel of 4mM at 0mV membrane potential (Johnson & Ascher 1990; Wollmuth *et al.* 1998). This effect, however, in my experiments is a minor effect because the presence of 3mM ATP and 10mM EGTA and 0.5mM GTP chelates the 0.5mM Mg^{2+} in the pipette solution. The free intracellular Mg^{2+} concentration was calculated to be 22.8 μM using the MaxChelator program (available from http://www.stanford.edu/~cpatton/maxc.html). In addition, external Mg^{2+} also potentiates NMDAR-mediated whole-cell currents in a subunit specific and voltage-independent manner. The effect has been reported both in oocytes and HEK cell expression systems (Paoletti *et al.* 1995) and in native hippocampal neurons in CA1 region (Wang & MacDonald 1995). Wang and MacDonald (1995) discovered that at positive potentials, Mg^{2+} potentiates NMDA responses recorded in low glycine concentration and they suggested that the potentiation is related to a significant increase in affinity of the NMDA receptor for glycine. However, in the meantime, Paoletti *et al.* (1995) suggested that the potentiation effect is still obvious in the presence of saturating concentrations of glycine and the effect is not mimicked by extracellular Ca^{2+} and Ba^{2+} and is dependent on the presence of NR2B subunits. In my experiments, the potentiation by Mg^{2+} might be considerable because of the presence of NR2B-containing NMDA receptors (see ifenprodil block, chapter 5 or Jones & Gibb, 2005). In order to accurately estimate Mg^{2+} block voltage-dependence (δ) and affinity for the NMDA receptor, K_{Mg2+}(0mV), and also to investigate if the NMDAR potentiation by Mg^{2+} influences the estimation of the voltage dependent Mg^{2+} block parameters, the potentiation model (Scheme 6) was developed based on the trapping block model to fit NMDA I-V relationships. In this model, there are two NMDA receptor open states, AR* and AR^{*M} (Mg^{2+} potentiation state). As with the trapping block model, Mg^{2+} allows the channel gate to close during the block and it can be

subsequently trapped in the channel when the agonist is removed.

Allosteric regulators such as polyamines acting at NR1/NR2B NMDA receptors (Traynelis *et al.* 1995), ifenprodil acting at NR1/NR2B NMDA receptors (Mott *et al.* 1998), and zinc acting at NR1/NR2A (Paoletti *et al.* 2000) have been suggested to exert their actions through modification of proton inhibition (Erreger & Traynelis, 1995, 1996). Proton-sensitive gating is therefore a feature of receptor activation that can be regulated by exogenous molecular or therapeutic agents. In order to investigate whether Mg^{2+} potentiation of NMDA receptors acts through modification of extracellular proton block, a proton block model (Scheme 3.7) was developed based on the trapping block (Scheme 3.3) and potentiation models (Scheme 3.6) and used to fit NMDA I-V relationships. In this proton block model (Scheme 3.7), we assume occupancy of the proton binding sites on the receptor is mutually exclusive with the Mg^{2+} potentiation sites. Once Mg^{2+} binds to the NR2B subunit potentiation site, protons can not bind and vice-versa. With the potentiation model, there are two NMDA receptor channel open states, AR* and AR^{*M} (the Mg^{2+} potentiation state).

3.3.1 Scheme 3.1 Sequential block model

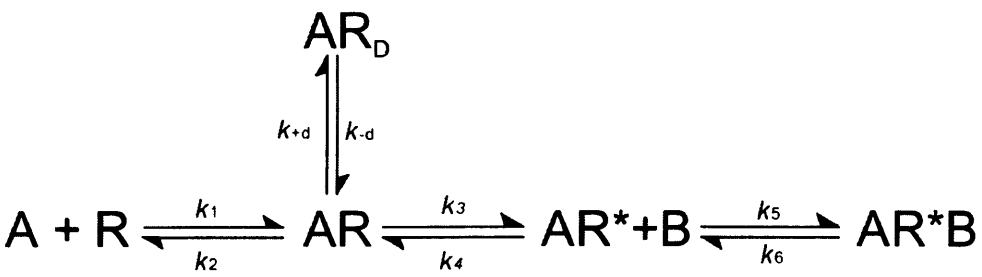

A sequential block mechanism used to describe channel block of ligand-gated ion channel receptors. Mg^{2+} can only bind to the receptor in the open state. When Mg^{2+} binds to the open state, ion flow through the channel is blocked. The NMDA receptor channel can not close until Mg^{2+} unbinds from the NMDA receptor. Here k_1 and k_2 refer to agonist binding and unbinding rates, respectively, k_3 and k_4 are channel opening and closing rates and k_5 and k_6 are Mg^{2+} microscopic association and dissociation rates.

AR_D refers to the NMDA receptor desensitized state.

3.3.1.1 Equations for the sequential block model

The open probability equation for the sequential block model is shown below [1].

$$P_{open} = \frac{[AR^*]}{[R_{Total}]} = \frac{1}{\frac{k_2}{k_1}\frac{k_4}{k_3}\frac{1}{[A]} + \frac{k_4}{k_3} + 1 + \frac{k_{+d}}{k_{-d}}\frac{k_4}{k_3} + \frac{k_5}{k_6}[Mg^{2+}]} \quad [1]$$

Here, k_1 and k_2 are agonist binding and unbinding rate constants, k_3 and k_4 are channel opening and closing rates, k_5 and k_6 are blocker microscopic association and dissociation rates and k_{+d} and k_{-d} refer to desensitization rate constants. [A] indicates agonist concentration and $[Mg^{2+}]$ refers to concentrations of extracellular Mg^{2+}.

The voltage dependence of Mg^{2+} block is expressed by [2]:

$$\frac{k_6}{k_5} = K_{Mg}(0mV)Exp(\frac{\delta_{Mg}VFz}{RT}) \quad [2]$$

Here k_5 and k_6 are antagonist microscopic association and dissociation rates. δ indicates the fraction of the membrane voltage at the blocking site and the sign of δ is determined by whether the blocking drug approaches the binding site from inside or outside of the membrane. K_{Mg}^{2+} (0mV) refers to the dissociation constant in the absence of a transmembrane voltage. z refers to the valence of the blocking drug and F, R and T have their usual meaning; Faraday constant (9.65×10^4 C mol^{-1}), the gas constant (8.23J K^{-1} mol^{-1}) and the absolute temperature (293K at room temperature) respectively.

Thus, the current at any particular voltage is described by equation [3]:

$$I_B = N(V_h - V_{rev})\gamma P_{open}$$

$$= \frac{\gamma(V_h - V_{rev})N}{\frac{k_2}{k_1}\frac{k_4}{k_3}\frac{1}{[A]} + \frac{k_4}{k_3} + 1 + \frac{k_{+d}}{k_{-d}}\frac{k_4}{k_3} + \frac{[Mg^{2+}]}{K_{Mg2+}(0mV)Exp(\frac{V\delta zF}{RT})}} \quad [3]$$

Here, γ stands for NMDA single-channel conductance. V_h and V_{rev} refer to holding potential and NMDA reversal potential, respectively. N indicates number of NMDA receptors on a tested neuron. k_1, k_2, k_3, k_4, k_{+d}, k_{-d}, [A] and $[Mg^{2+}]$ are defined on equation [1]. δ, z, *F*, *R* and *T* are defined on equation [2].

3.3.1.2 Curve fitting for the traditional sequential block model

There are several conditions which have been applied during the NMDA I-V curve fitting.

1. According to previous studies, we fixed the values of k_2/k_1, k_{+d}/k_{-d} and k_4/k_3 at 10μM, 5 and 2, respectively during curve fitting (Sobolevsky *et al.* 1998) (Benveniste & Mayer 1991) (Lester & Jahr 1992) in order to give a control open probability consistent with previous estimates.
2. There is always contaminating Mg^{2+} in rat brain slices which caused NMDA I-V curves obtained in zero-Mg^{2+} NMDA-containing solutions to bend at negative voltage. Therefore, the contaminating extracellular Mg^{2+} concentration is set to vary during curve fitting.
3. Since the different concentrations of external Mg^{2+} are assumed to not affect N (the total number of NMDAR on dopaminergic neurons), δ, $K_{Mg}^{2+}(0mV)$ and γ (single-channel conductance), N, γ, δ and $K_{Mg}^{2+}(0mV)$ were constrained to be the same for all Mg^{2+} concentrations during curve fitting.
4. Here, we assume that the single-channel conductances for all the receptors on SNc are the same, which are set to be 50pS during the curve fitting.

3.3.2 Scheme 3.2 The three-state model (Jahr & Stevens 1990)

3.3.3 Scheme 3.3 Symmetrical trapping block model

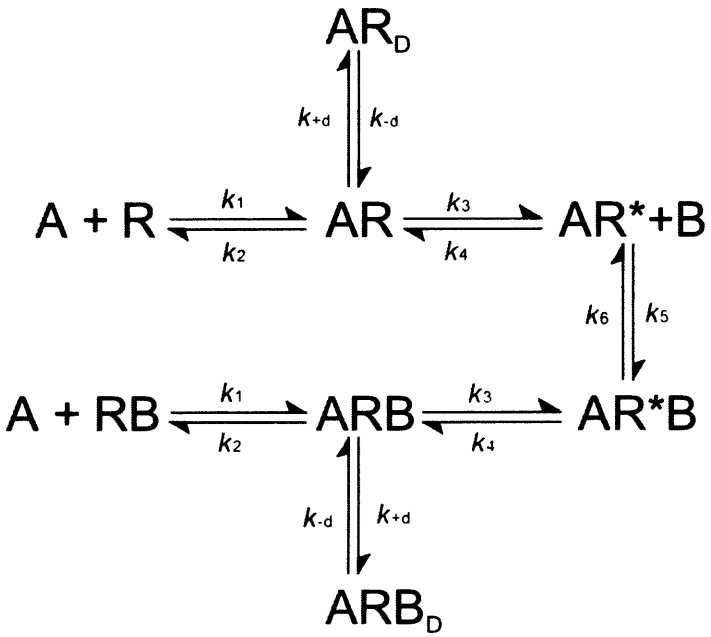

Mg^{2+} trapping block mechanism used to describe channel block of ligand-gated ion channel receptors. Mg^{2+} allows the channel gate to close during the block and it can be subsequently trapped in the channel when the agonist dissociates. Here, k_1, k_2, k_3, k_4, k_5, k_6, k_{+d} and k_{-d} are defined on section 3.1.1.1.

3.3.3.1 Equations for the traditional trapping block model

The open probability equation for the traditional trapping block model is shown below [4].

$$P_{open} = \frac{[AR^*]}{[R_{Total}]} = \frac{1}{(\frac{k_2}{k_1}\frac{k_4}{k_3}\frac{1}{[A]} + \frac{k_4}{k_3} + 1 + \frac{k_{d+}}{k_{d-}}\frac{k_4}{k_3})\quad(1 + \frac{k_5}{k_6}[Mg^{2+}])} \qquad [4]$$

Here, k_1, k_2, k_3, k_4, k_5, k_6, k_{d+}, k_{d-}, [A] and [Mg^{2+}] are defined on section 3.1.1.1.

The voltage dependence of Mg^{2+} block is expressed by relation [2]:

Thus, the current at any particular voltage is described by equation [5]:

$$I_B = N(V_h - V_{rev})\gamma P_{open} \qquad [5]$$

$$= \frac{\gamma(V_h - V_{rev})N}{(\frac{k_2}{k_1}\frac{k_4}{k_3}\frac{1}{[A]} + \frac{k_4}{k_3} + 1 + \frac{k_{+d}}{k_{-d}}\frac{k_4}{k_3})\quad(1 + \frac{[Mg^{2+}]}{K_{Mg2+}(0mV)\exp(\frac{V\delta zF}{RT})})}$$

Here, γ, V_h, V_{rev}, N, k_1, k_2, k_3, k_4, k_{+d}, k_{-d}, [A], [Mg^{2+}], δ, z, F, R and T are defined on section 3.1.1.1.

4.3.3.2 Curve fitting for the trapping block model

See the section 3.3.1.2

3.3.4 Scheme 3.4 Asymmetric trapping block model (Kampa *et al.* 2004)

Mg^{2+} block scheme shows two agonist molecules bind to an NMDA receptor (R) to form the A_2R state. Then the A_2R can open to open state (O) or goes to D_f (fast desensitisation state) and D_s (slow desensitisation state). Mg^{2+} can bind to all five states, although binding is much more rapid to the open state than to other states (dashed line).

3.3.5 Scheme 3.5 Asymmetric trapping block model (Vargas-Caballero & Robinson 2004)

Asymmetric trapping block kinetic scheme for the NMDA receptor. This model suggests that Mg^{2+} binding affects the NMDA receptor channel gating. Therefore, in this model, $K_A \neq K'_{A'}$, $K_E \neq K'_{E'}$, $K_D \neq K'_{D'}$.

3.3.6 Scheme 3.6 Potentiation model

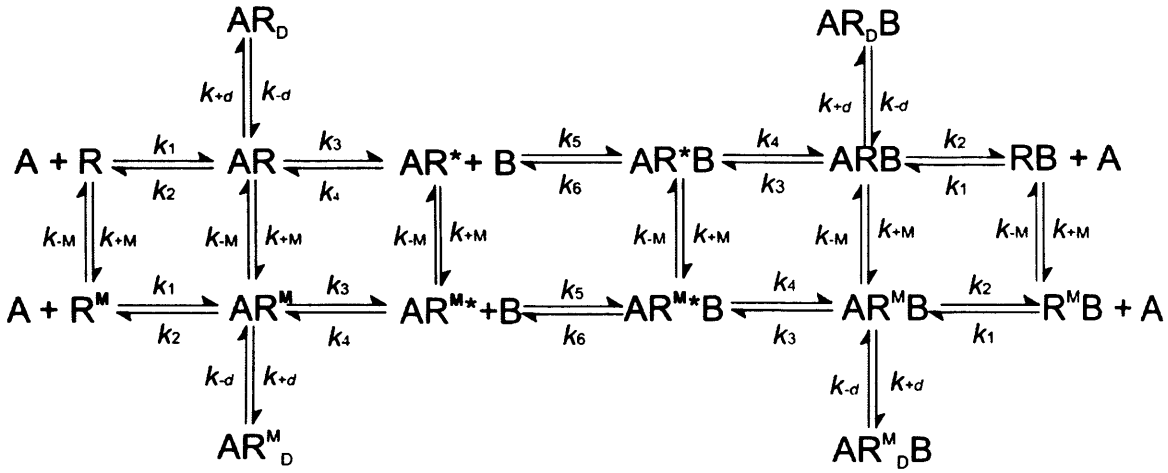

Mg^{2+} block and potentiation mechanism used to describe channel block of ligand-gated ion channel receptors. There are two NMDA receptor open states in this model (AR* and $AR^{*M}B$), in the trapping block model, NMDA receptors can close while Mg^{2+} blocked and Mg^{2+} can be subsequently trapped in the channel when the agonist dissociates. Here, k_{-M} and k_{+M} stand for microscopic association and dissociation rates for Mg^{2+} potentiation. k_1, k_2, k_3, k_4, k_5, k_6, k_{-d} and k_{-d} are defined on section 3.1.1.1.

3.3.6.1 Equations for the potentiation model

The open probability for the potentiation model is shown in equation [6].

$$P_{open} = \frac{[AR^*] + [AR^{*M}]}{[R_{Totala}]} = \frac{1 + \frac{k_{+M}}{k_{-M}}}{[1 + \frac{k_{+M}}{k_{-M}} + (\frac{k_4}{k_3} + \frac{k_4}{k_3}\frac{k_{+M}}{k_{-M}})(1 + \frac{k_{+d}}{k_{-d}} + \frac{k_2}{k_1}\frac{1}{[A]})](1 + \frac{k_5}{k_6}[Mg^{2+}])} \quad [6]$$

Here, k_1 and k_2, k_3, k_4, k_5, k_6, k_{+d}, k_{-d}, [A] and $[Mg^{2+}]$ are defined on section 3.3.1.1. k_{-M} and k_{+M} are defined on section 3.3.6.

The voltage dependence of Mg^{2+} block is expressed by relation [2]:

Thus, the current at any particular voltage is described by equation [7]:

$$I_B = N(V_h - V_{rev})\gamma P_{open} \qquad [7]$$

$$= \frac{(1+\frac{k_{+M}}{k_{-M}})\ \gamma(V_h - V_{rev})N}{[1+\frac{k_{+M}}{k_{-M}}+(\frac{k_4}{k_3}+\frac{k_4}{k_3}\frac{k_{+M}}{k_{-M}})(1+\frac{k_{+d}}{k_{-d}}+\frac{k_2}{k_1}\frac{1}{[A]})](1+\frac{[Mg^{2+}]}{K_{Mg2+}(0mV)\exp(\frac{V\delta zF}{RT})})}$$

Here, k_{-M} and k_{+M} are defined on section 3.3.6. γ, V_h, V_{rev}, N, k_1, k_2, k_3, k_4, [A], [Mg^{2+}], δ, z, F, R and T are defined on section 3.1.1.1.

3.3.6.2 Curve fitting for the Mg^{2+} potentiation and block model

The fitting conditions are similar to the method which is described on section 3.3.1.2 apart from the k_{+M} and k_{-M}. In this curve fitting, the k_{+M} and k_{-M} are set to vary.

3.3.7 Scheme 3.7 Mg^{2+} potentiation with proton block model

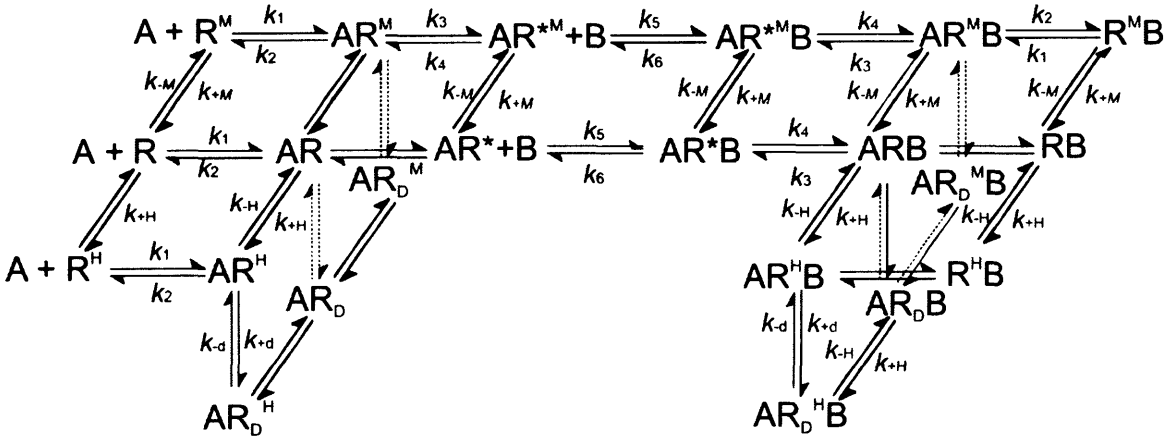

Combined Mg^{2+} block and potentiation due to relief of proton block mechanism, Mg^{2+} allows the channel gate to close during the block and it can be subsequently trapped in the channel when the agonist dissociates. Here k_1, k_2, k_3, k_4, k_5, k_6, k_{+d} and k_{-d} are defined on section 3.1.1.1. k_{+M} and k_{-M} stand for microscopic association and dissociation rates for Mg^{2+} potentiation, and k_{+H} and k_{-H} refer to microscopic association and dissociation rates for proton block.

3.3.7.1 Equations for Mg^{2+} potentiation with proton block model

The equation for traditional trapping block model is shown below [8].

$$P_{open} = \frac{[AR^*] + [AR^{*M}]}{[R_{Total}]} = \frac{1 + \frac{k_{+M}}{k_{-M}}}{[(1 + \frac{k_{+M}}{k_{-M}})(\frac{k_2}{k_1}\frac{1}{[A]}\frac{k_4}{k_3} + 1 + \frac{k_4}{k_3} + \frac{k_{+d}}{k_{-d}}\frac{k_4}{k_3}) + (\frac{k_4}{k_3}\frac{k_{+H}}{k_{-H}}[H^+])(1 + \frac{k_{d+}}{k_{d-}} + \frac{k_2}{k_1}\frac{1}{[A]})](1 + \frac{k_5}{k_6}[Mg^{2+}])} \quad [8]$$

Here k_1, k_2, k_3, k_4, k_5, k_6, k_{+d}, k_{-d}, [A] and [Mg^{2+}] are defined on section 3.1.1.1. k_{+M}, k_{-M}, k_{-H} and k_{-H} are defined on section 3.3.7.

The voltage dependence of Mg^{2+} block is expressed by relation [2]:

Thus, the current at any particular voltage is described by equation [9]:

$$I_B = N(Vh - Vre)\gamma Popen \quad [9]$$

$$= \frac{(1 + \frac{k_{+M}}{k_{-M}})\gamma(V_h - V_{rev})N}{[(1 + \frac{k_{+M}}{k_{-M}})(\frac{k_2}{k_1}\frac{1}{[A]}\frac{k_4}{k_3} + 1 + \frac{k_4}{k_3} + \frac{k_{+d}}{k_{-d}}\frac{k_4}{k_3}) + (\frac{k_4}{k_3}\frac{k_{+H}}{k_{-H}}[H^+])(1 + \frac{k_{d+}}{k_{d-}} + \frac{k_2}{k_1}\frac{1}{[A]})](1 + \frac{[Mg^{2+}]}{K_{Mg2+}(0mV)Exp(\frac{V\delta F}{RT})})}$$

Here k_1, k_2, k_3, k_4, k_5, k_6, k_{+d}, k_{-d}, [A], [Mg^{2+}],δ, z, F, R and T are defined on section 3.1.1.1. k_{-H} and k_{-H} are defined on section 3.3.7. k_{-M} and k_{+M} are defined on section 3.3.6.

3.3.7.2 Curve fitting for traditional trapping block model

1. During curve fitting, the k_{+M} and k_{-M} are set to vary.
2. Since all experiments were carried on at pH=7.4 condition, the proton concentration is 0.0398 at room temperature and the $K_{[H]}=k_{+H}/k_{-H}$ is set to be 0.1.
3. The values for other parameters are defined on the section 3.3.1.2.

3.4 Results

All experiments were carried out upon dopaminergic neurons of substantia nigra pars compacta in coronal brain slices from P7 rats. Dopaminergic neurons were voltage clamped at –60mV in the presence of TTX (100nM), nimodipine (2μM) and conotoxin MVIIC (0.5μM) to minimize the effect of voltage-gated sodium and calcium channels.

3.4.1 External Mg^{2+} inhibition of NMDA-mediated whole-cell currents at resting potential

In order to characterize external Mg^{2+} block of NMDAR at resting potential, three concentrations of Mg^{2+} (contaminating Mg^{2+}, 100μM and 1mM) were co-applied with 10μM NMDA and 10μM glycine.

Figure 3.1 shows that the application of external Mg^{2+} (100μM and 1mM) significantly decreased the NMDA-induced whole-cell currents. Figure 3.1A illustrates a current trace from a whole-cell recording, where the first NMDA response was evoked by application of NMDA (10μM) and glycine (10μM) in the presence of only contaminating Mg^{2+}. Then the whole-cell NMDA response was washed off by application of external solution in the absence of NMDA and glycine. The second and third NMDA response were evoked by coapplication of NMDA (10μM) and glycine (10μM) together with 100μM and 1mM Mg^{2+}, respectively. Details of whole-cell recordings are given in Table 3.1.

Figure 3.1B shows that external Mg^{2+} inhibits whole-cell NMDA currents in a concentration dependent manner. The physiological concentration of Mg^{2+}(1mM) blocked the NMDA current by 85.2 ± 0.1% (Mean ± S.E., n=16) while 100μM Mg^{2+} caused a 59.3

± 0.1% (Mean ± S.E., n=9) inhibition.

To further quantify Mg^{2+} inhibition of the NMDA-activated current at resting potential, concentration-inhibition curves were constructed at –60mV. The contaminating Mg^{2+} concentration was estimated from simultaneous fitting of the I-V curves to be 23.4μM (The method to obtain this result was described in 3.4.2 section of this chapter). The IC_{50} of Mg^{2+} at –60 mV was estimated to be 74.4 μM (Figure 3.1C).

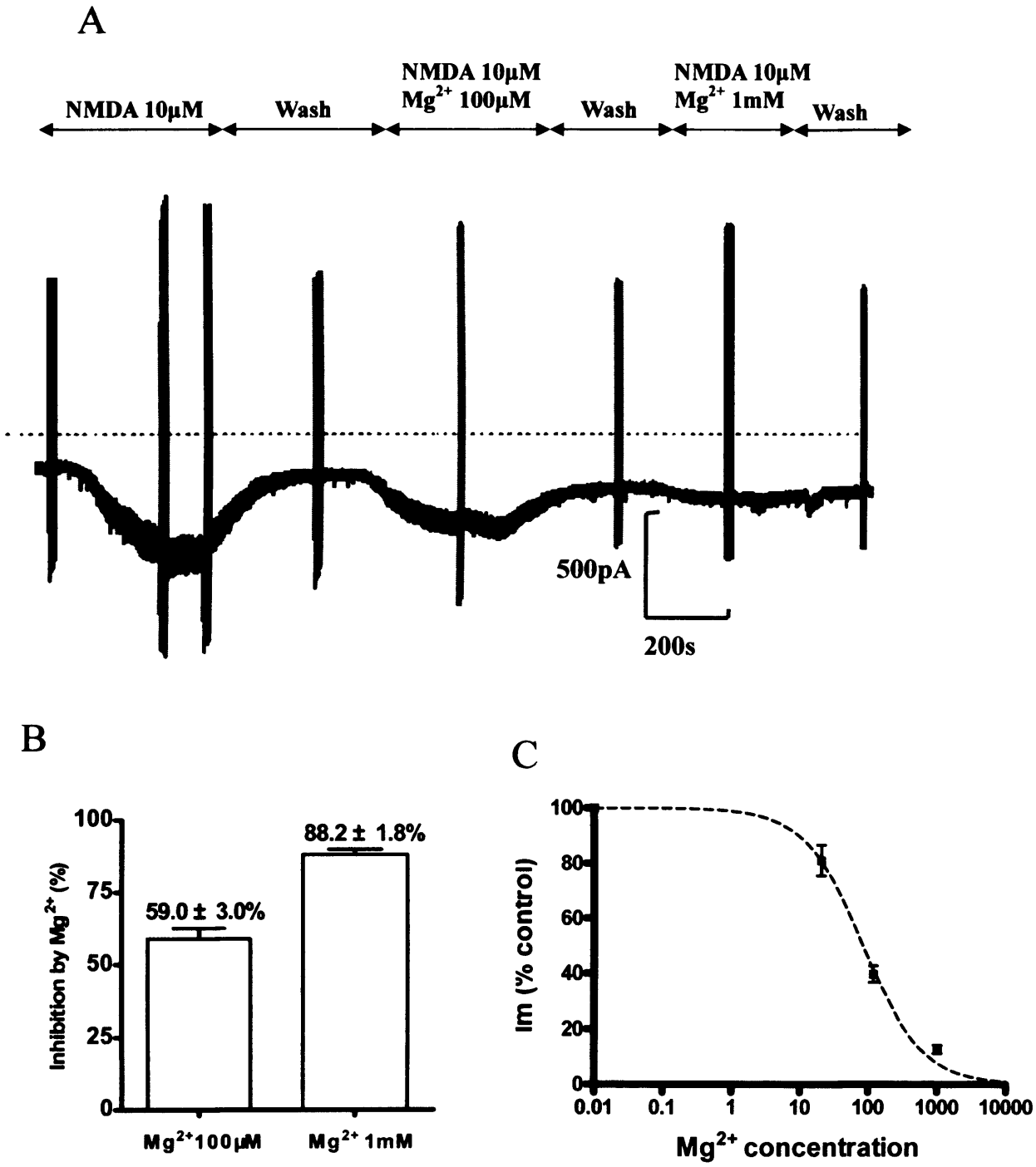

Figure 3.1 Mg^{2+} inhibition of NMDAR-mediated whole-cell currents at resting potential.

A. NMDA-mediated current trace evoked by application of 10μM NMDA and 10 μM glycine at -60mV. Bars above the current trace show the time of application of the indicated solutions. Upright lines on NMDA current trace are current traces evoked by voltage-ramps from -100mV to +40mV. In B, summary of results with Mg^{2+} inhibition at -60mV shows a significant inhibition of NMDA-evoked whole-cell current by different concentrations of Mg^{2+}. In C, external Mg^{2+} concentration-inhibition curve at -60mV constructed according to the Hill-Langmuir equation. IC_{50} value is estimated to be 74.4 μM.

	Control NMDA response (pA)	NMDA response with 100μM Mg^{2+} (pA)	Remaining current in the presence of Mg^{2+} 100 μM	NMDA response with 1mM Mg^{2+} (pA)	Remaining current in the presence of Mg^{2+} 1mM
02032006-1	177			42	23.7%
02032006-2	339			45	13.3%
10032006-1	557	216	38.8%	75.5	13.6%
15032006-1	1070	591	55.2%	42.3	4.0%
15032006-2	868	350	40.3%	112.5	13.0%
16032006-4	544	193	35.5%	56.1	10.3%
16032006-5	619	248	40.1%	67	10.8%
17032006-3	590			150	25.4%
17032006-4	685			100	14.6%
17032006-5	800	361	45.1%	117.1	14.6%
20032006-1	765	275	35.9%		
20032006-2	1219			230	18.9%
20032006-3	400	185	46.3%	15	3.8%
29032006-1	652			121	18.6%
29032006-2	938			165	17.6%
29032006-3	722			49	6.8%
29032006-4	963			156	16.2%
Average	**700.5**	**302.4**	**42. 2%**	**96.5**	**14. 1%**
count	**17**	**8**	**8**	**16**	**16**
SE	**64.6**	**47.4**	**0.02**	**14.5**	**0. 01**

Table 3.1 Results of Mg^{2+} inhibition experiments at resting potential.
Details are given of each whole-cell recording from 16 recordings in this experiment, which include the steady state NMDA currents in response to application of two concentrations of Mg^{2+} (100 μM and 1 mM) of each cell. ATP (3 mM) and GTP (1 mM) were in the pipette solution. 100μM of external Mg^{2+} cause 60.3% inhibition of the whole-cell NMDA current and 1mM of external Mg^{2+} inhibited the whole-cell NMDA current by 85.2%.

3.4.2 Voltage-dependence of Mg^{2+} block of NMDAR in dopamine cells of SNc

In order to investigate the voltage dependence of Mg^{2+} block of NMDA receptors on dopaminergic neurons and also to study the NMDA receptor subunit composition on doapminergic neurons, voltage-ramps from –100mV to +40mV were applied in the presence of 10μM NMDA, 10μM glycine and different concentrations of external Mg^{2+} (contaminating concentration, 100μM and 1mM Mg^{2+}). A typical NMDA current trace is shown in Figure 3.1A. The upright lines on the current trace indicate where voltage ramps from –100mV and +40mV were applied. Each protocol collected 4 ramps and the averaged data from the 4 ramps was used for analysis. All NMDA I-V relationships were obtained by subtracting control ramps from those ramps obtained in the presence of NMDA. Each NMDA I-V relationship obtained from one cell was normalized to +40 mV and averaged with I-V curves from other neurons (n=9). The averaged and normalized NMDA I-V relationships are shown in Figure 3.2 A and B.

Figure 3.2A shows typical exemplary NMDA I-V curves while averaged NMDA I-V curves obtained from 12 dopamine cells are shown in Fig.3.2 B. It is evident to see from the NMDAR I-V curves that NMDA receptors in 7-day-old rat dopaminergic neurons are already highly sensitive to extracellular Mg^{2+} and undergo significant voltage-dependent Mg^{2+} block. In the presence of 1mM of Mg^{2+}, NMDAR channels were largely blocked at negative voltage and passed maximal inward current at about -25mV. When 100μM and contaminating concentration of Mg^{2+} are present in recording solutions, the NMDAR maximal inward currents are found at -40mV and -60mV, respectively.

In order to quantify the voltage-dependent Mg^{2+} block of NMDAR in dopaminergic

neurons of P7 rat SNc, external Mg^{2+} concentration-inhibition curves were constructed at –60mV, -80mV and –100mV, respectively. As shown in Fig.3.2 C, the Mg^{2+} IC_{50} values at -100mV, -80mV and -60mV were 7.9 μM, 18.8 μM and 74.4 μM, respectively (n=12).

Then the averaged and normalized NMDA I-V relations were fitted with four Mg^{2+} block models; simple sequential block, simple trapping block, potentiation and proton block models using the Solver function in Microsoft Excel. The curve fitting details and parameters selection were introduced in mpdelling and curve fitting section. The curve fitting results are shown in Figure 3.5 and Table 3.2. The K_{Mg}(0mV) was estimated to be 432μM using the simple sequential block model while the values were found to be the 6mM using the trapping block, potentiation and proton block models. The value of δ, however, was the same for all four models, being 0.82. In addition, although the contaminating Mg^{2+} concentration was set to vary during curve fitting, the same contaminating concentration of Mg^{2+} were estimated from all four models to be 23.4μM. The potentiation constant k_{+M}/k_{-M} was estimated to be 0.86. By comparing fitting results between different models (Figure 3.5), we can see there is no significant difference between fitting results obtained from different models. All models did not give ideal fitting results for the100μM Mg^{2+} I-V relationship.

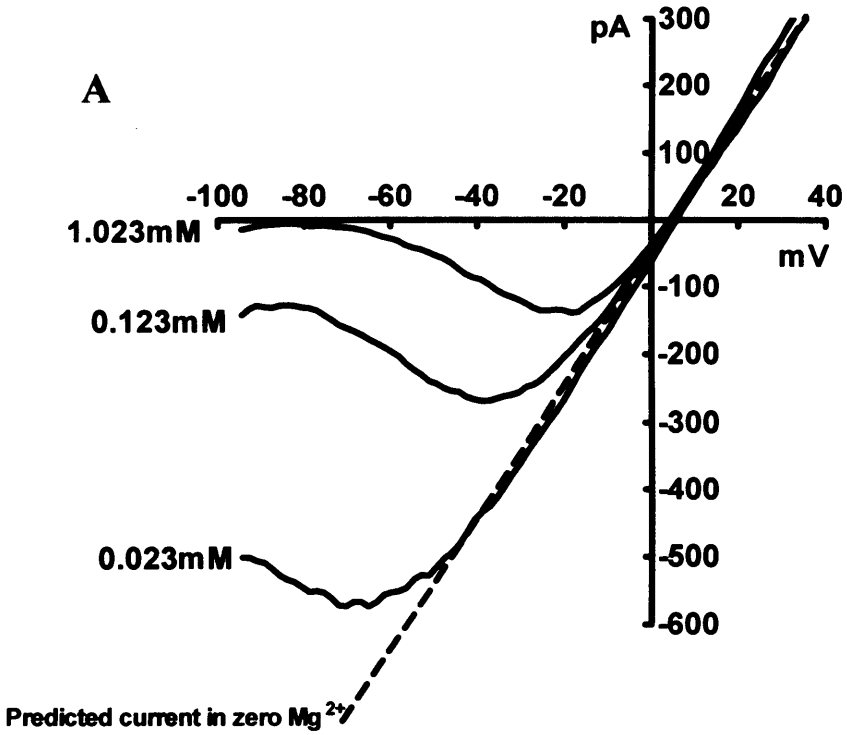
A
pA
300
200
100
-100 -80 -60 -40 -20 20 40
mV
1.023mM
0.123mM
0.023mM
-100
-200
-300
-400
-500
-600
Predicted current in zero Mg 2+

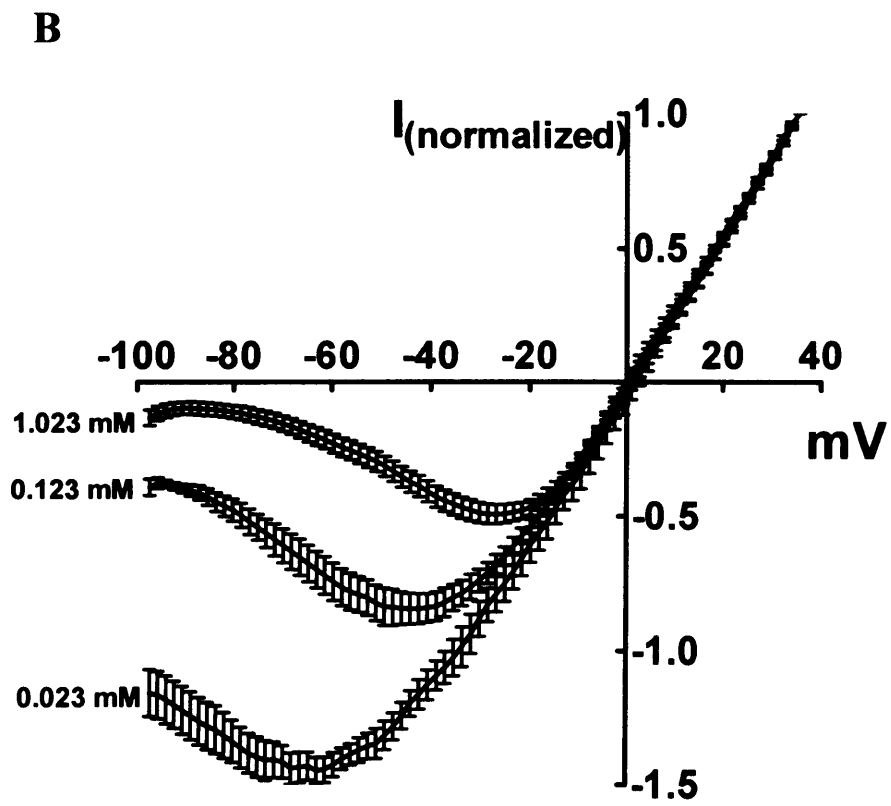
B
I(normalized)
1.0
0.5
-100 -80 -60 -40 -20 20 40
mV
1.023 mM
0.123 mM
0.023 mM
-0.5
-1.0
-1.5

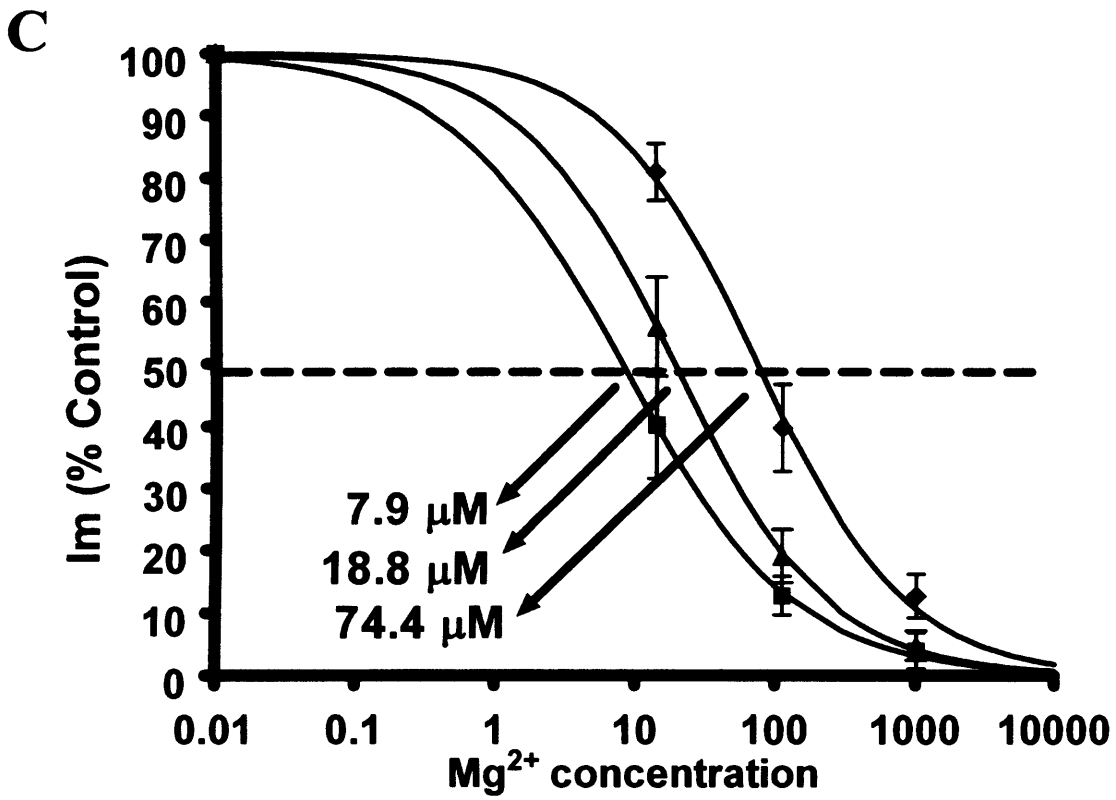

Figure 3.2 Voltage-dependence of Mg^{2+} block of NMDARs in dopamine cells of SNc

A. Example NMDA I-V curves recorded from P7 rat SNc dopaminergic neurons. The NMDA current trace was evoked by bath application of 10μM NMDA and 10μM glycine. 3μM Nimodipine and 0.5μM ω-conotoxin were used to inhibit voltage-gated calcium channel. 23 μM contaminating Mg^{2+} concentration was estimated in the brain slice. Since there are alwayse some contaiminatng concentration of Mg^{2+} in the slices, the dashed line was obtained by reversely extending positive curve of NMDA I-V relationships to predict the control NMDA current in the absence of Mg^{2+}.

B. Normalized and averaged NMDA I-V curves (n=9). In C, the predicted Mg^{2+} concentration-inhibition curves obtained from B are shown to estimate the Mg^{2+} IC_{50} at selected voltages. (-100mV; ■, -80mV; ▲, -60mV; ◆) The Mg^{2+} IC_{50} value at -100mV, -80mV and -60mV were 7.9 μM, 18.8 μM and 74.4 μM, respectively.

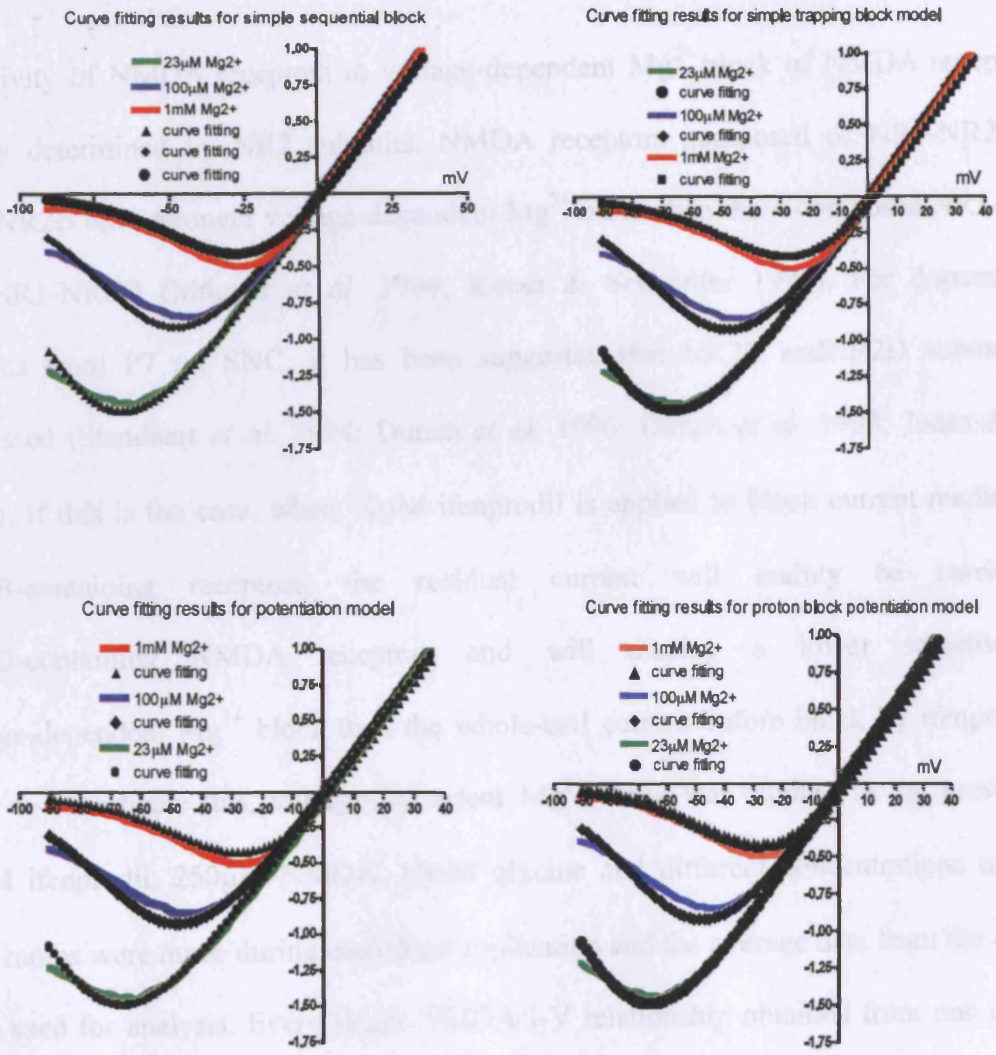

Figure 3.5 Comparison of curve fitting between different Mg^{2+} block models

Table 3.2 Summary of curve fitting results for NMDAR I-V relations in the absence of ifenprodil

	Simple sequential model	Simple trapping block model	Potentiation model	Proton block potentiation model
K_{Mg}(0mV)	432 μM	6 mM	6 mM	6 mM
δ	0.82	0.82	0.82	0.82
Contaminating [Mg^{2+}]	23.4 μM	23.4 μM	23.4 μM	23.4 μM
k_{+M}/k_{-M}	------	------	0.86	0.86

3.4.3 Voltage-dependence of Mg^{2+} block of ifenprodil-insensitive NMDA currents in dopamine cells of SNc

Sensitivity of NMDA receptors to voltage-dependent Mg^{2+} block of NMDA receptors is largely determined by NR2 subunits. NMDA receptors composed of NR1-NR2A and NR1-NR2B have stronger voltage-dependent Mg^{2+} block than those composed NR1-NR2C and NR1-NR2D (Monyer *et al.* 1994; Kuner & Schoepfer 1996). For dopaminergic neurons from P7 rat SNC, it has been suggested that NR2B andNR2D subunits are expressed (Standaert *et al.* 1994; Dunah *et al.* 1996; Dunah *et al.* 1998; Jones & Gibb 2005). If this is the case, when 10μM ifenprodil is applied to block current mediated by NR2B-containing receptors, the residual current will mainly be carried by NR2D-containing NMDA receptors and will display a lower sensitivity to voltage-dependent Mg^{2+} block than the whole-cell current before block by ifenprodil. In order to investigate this, voltage-dependent Mg^{2+} block was studied in the presence of 10μM ifenprodil, 250μM NMDA, 10μM glycine and different concentrations of Mg^{2+}. Four ramps were made during each drug application and the average data from the 4 ramps were used for analysis. Every single NMDA I-V relationship obtained from one cell was normalized to +40 mV and averaged with I-V curves from other neurons. The averaged and normalized NMDA I-V relationships are shown in Figure 3.3.

Figure 3.3A shows typical NMDAR I-V curves recorded in the presence of 10μM ifenprodil while averaged and normalized NMDA I-V curves obtained from 7 dopamine cells are shown in Figure 3.3B. As shown in Figure 3.3B, in the presence of 1mM external Mg^{2+}, the NMDA currents were largely blocked at negative voltage and passed maximal inward current at about -30mV. When 100μM or 10μM Mg^{2+} are present in the recording solutiosn, the NMDA maximal inward currents are found at -60mV and -80mV, respectively.

Averaged and normalized NMDA I-V relations were fitted with the four Mg^{2+} block models. The curve fitting results are shown in Figure 3.6 and Table 3.3. The $K_{Mg}(0mV)$ is estimated to be 348μM using the simple sequential block model while this was 4.87mM using the trapping block, potentiation and proton block models. The values of δ, however, are the same for all four models, being 0.64. In addition, the contaminating concentration of Mg^{2+} was estimated from all four models to be 23.4μM. The potentiation constant k_{+M}/k_{-M} was estimated to be 0.86. From Figure 4, we can see the four different models all give very good fitting results.

In addition, external Mg^{2+} concentration-inhibition curves were constructed at –60mV, -80mV and –100mV, respectively. As shown in Fig.3.2 C, the Mg^{2+} IC_{50} values at -100mV, -80mV and -60mV were 46.6 μM, 97.3 μM and 259.3 μM, respectively (n=9).

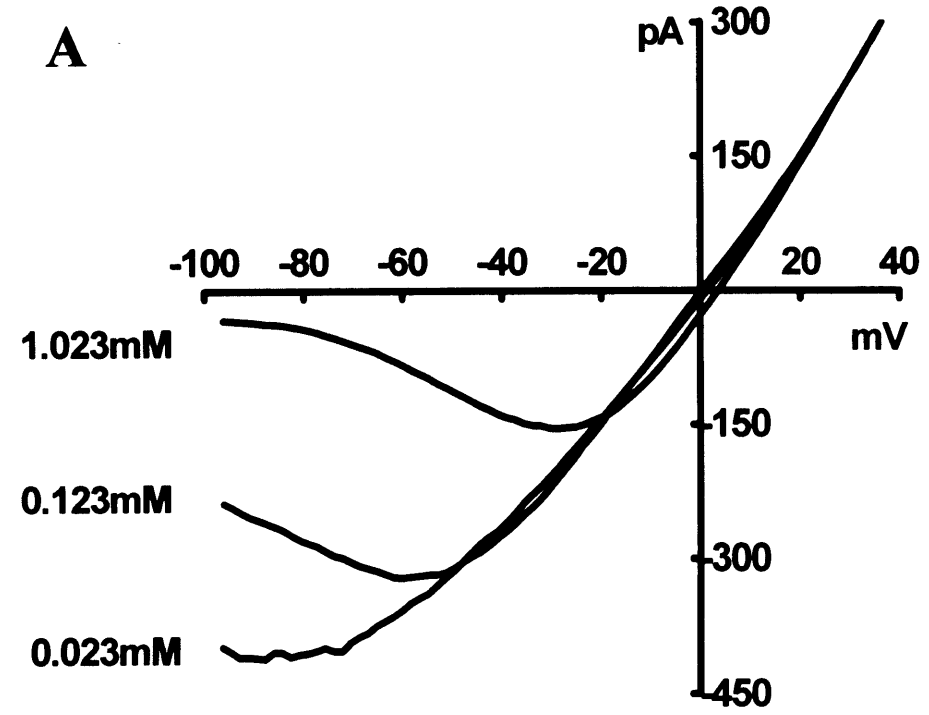
A
pA
300
150
-100
-80
-60
-40
-20
20
40
mV
1.023mM
0.123mM
0.023mM
150
300
450

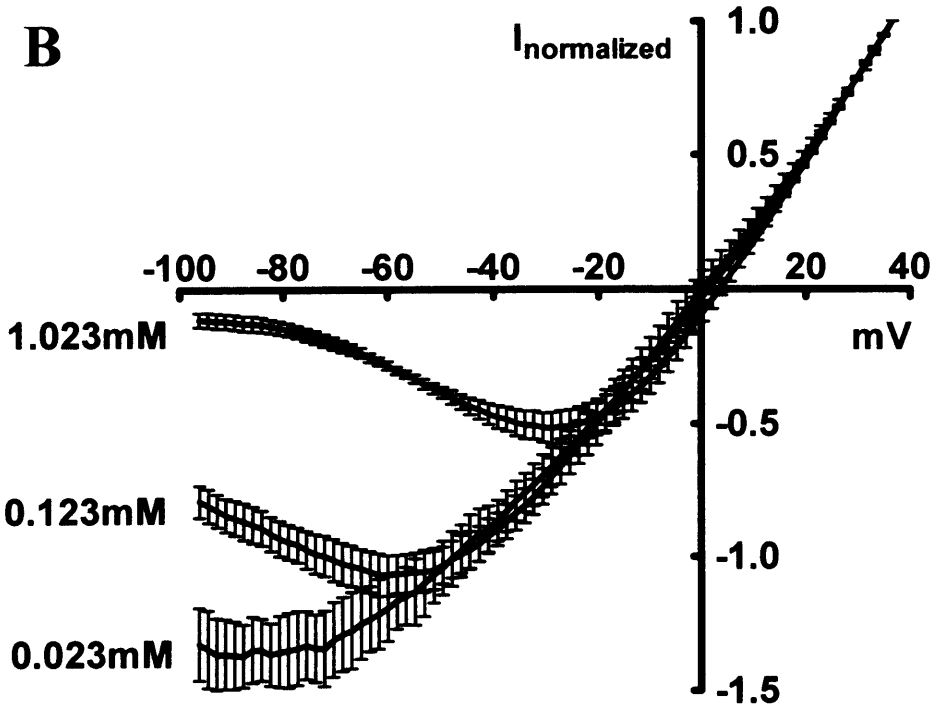
B
I normalized
1.0
0.5
-100
-80
-60
-40
-20
20
40
mV
1.023mM
0.123mM
0.023mM
-0.5
-1.0
-1.5

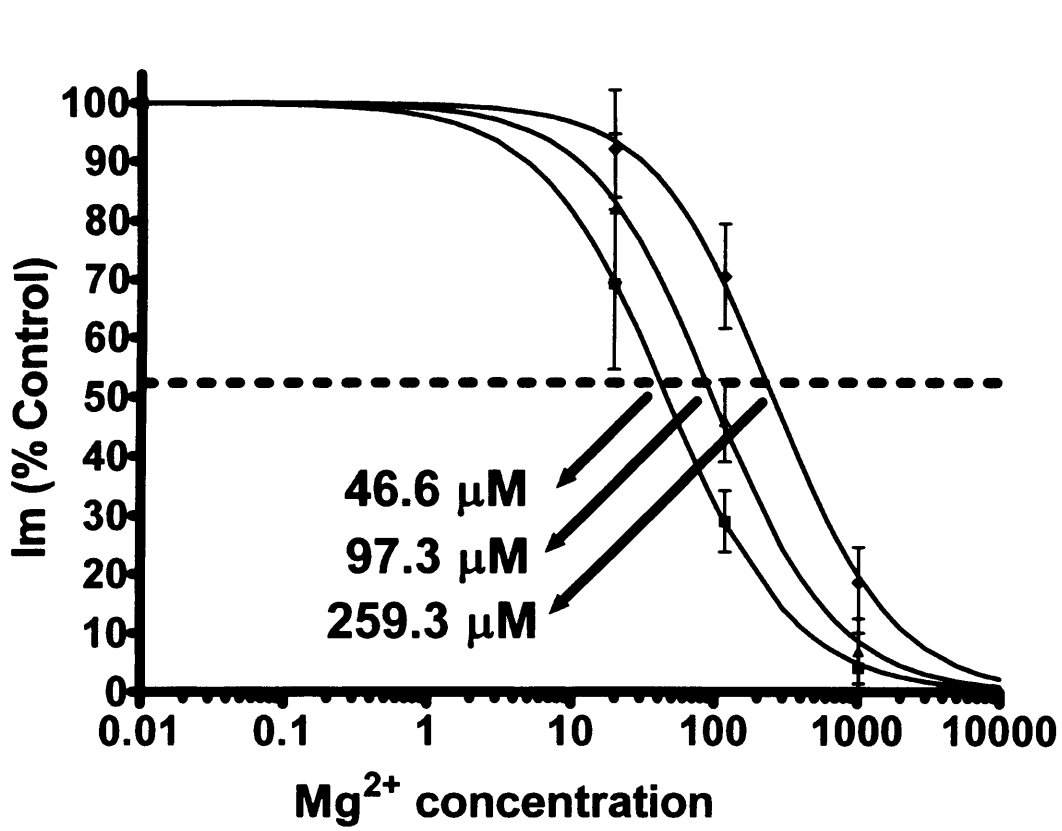

Figure 3.3 Voltage-dependence of Mg^{2+} block of ifenprodil-insensitive NMDAR in dopamine cells of SNc

A and B. Exemplary and averaged (mean ± S.E.; n=8) normalized NMDA I-V curves in the presence of 250μM NMDA, 10μM glycine and 10μM ifenprodil. The contaminating concentration of Mg^{2+} in the brain slice was estimated to be 23.4μM. (see methods) C. The predicted Mg^{2+} concentration-inhibition curves obtained from B to estimate Mg^{2+} IC_{50} at selected voltages (-100mV; ■, -80mV; ▲, -60mV; ◆). The IC_{50} values at -100mV, -80mV and -60mV were 46.6 μM, 97.3 μM and 259.3 μM, respectively.

3.4.4 Comparison of Mg^{2+} sensitivity between residual current in the presence of ifenprodil and normal whole-cell current

In order to compare Mg^{2+} sensitivity between normal NMDAR whole-cell currents from dopamine cells and residual whole-cell currents obtained in the presence of 10μM ifenprodil, the NMDAR I-V relationships obtained in the presence of the same concentrations of Mg^{2+} are ploted in the same figure (Figure 3.4).

It is clear to see that in Figure 3.4 at negative voltages the whole-cell NMDAR current evoked by 10μM NMDA and 10μM glycine (I_{normal}) is blocked more strongly by extracellular Mg^{2+} than the residual whole-cell NMDAR current evoked by 250μM NMDA and 10μM glycine in the presence of 10μM ifenprodil ($I_{ifenprodil}$). For example, in Figure 3.4B at –60mV the $I_{ifenprodil}$ is blocked by 100μM external Mg^{2+} by about 10% while 100μM external Mg^{2+} significantly blocked I_{normal} by about 45%.

A

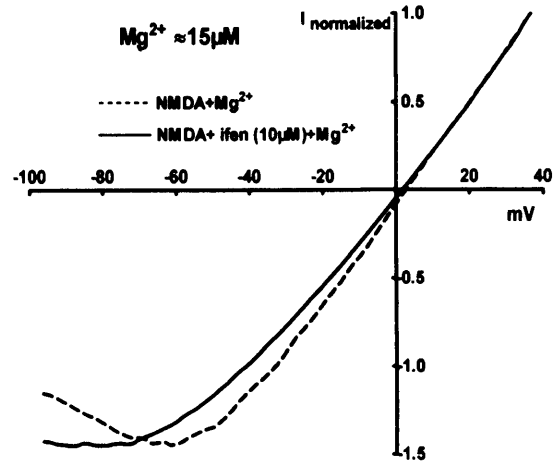

B

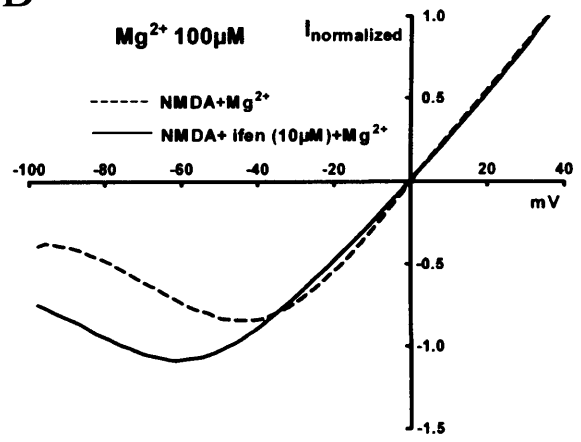

C

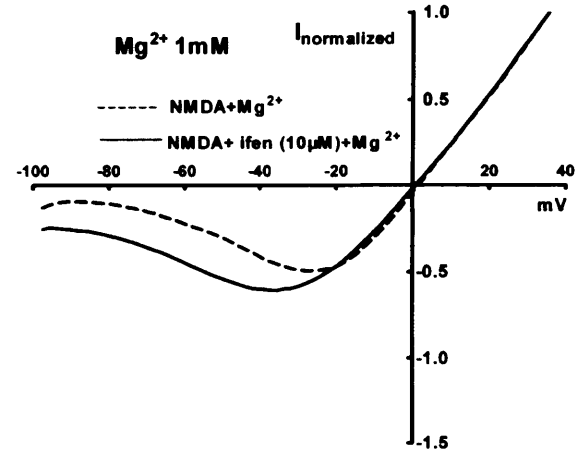

Figure 3.4 Comparison of Mg^{2+} sensitivity between residual current in the presence of ifenprodil and normal whole-cell current.

A.B.C. Normalized and averaged current curves show a significant difference in voltage-dependence of Mg^{2+} block of NMDAR currents in the presence of 10μM ifenprodil. The dashed lines indicate the I-V curves in the presence of 10μM NMDA, 10μM glycine and selected concentrations of Mg^{2+} whereas the solid lines show the I-V relations in the presence of 250μM NMDA, 10μM glycine and two concentrations of Mg^{2+} (100μM and 1mM).

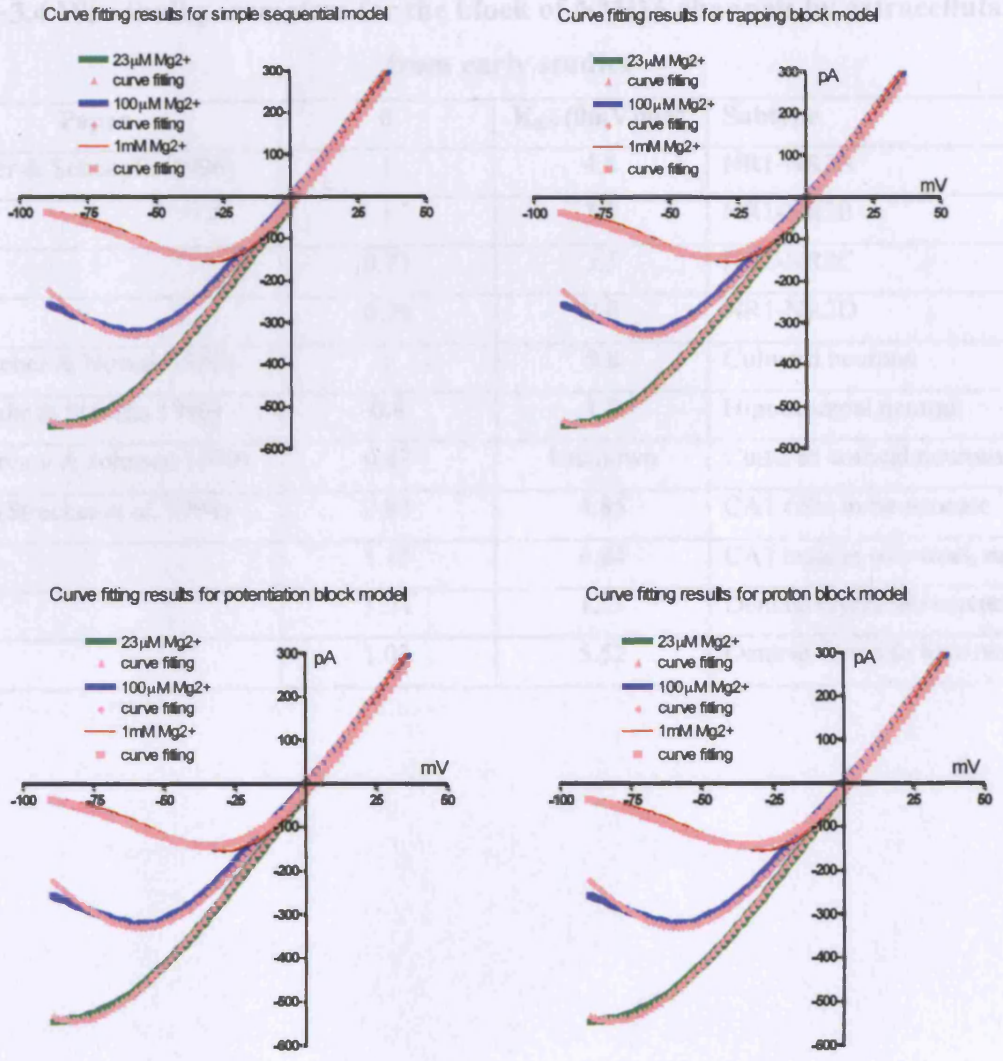

Figure 3.6 Comparing the fitting results from the four Mg^{2+} block models for NMDA I-V relations obtained in the presence of 10μM ifenprodil

Table 3.3 Summary of curve fitting results for NMDAR I-V relations in the presence of ifenprodil

	Simple sequential model	Simple trapping block model	Potentiation model	Proton block model
K_{Mg}(0mV)	348 μM	4.87 mM	4.87 mM	4.87 mM
δ	0.64	0.64	0.64	0.64
Contaminating Mg^{2+}	23.4 μM	23.4 μM	23.4 μM	23.4 μM
k_{+M}/k_{-M}	------	------	0.86	0.86

Table 3.4 Woodhull parameters for the block of NMDA channels by extracellular Mg^{2+} from early studies			
Paper	**δ**	**$K_{0.5}$ (0mV)mM**	**Subtype**
(Kuner & Schoepfer 1996)	1	4.8	NR1-NR2A
	1	3.7	NR1-NR2B
	0.73	3.5	NR1-NR2C
	0.75	2.6	NR1-NR2D
(Ascher & Nowak 1988)	1	8.8	Cultured neurons
(Jahr & Stevens 1990)	0.8	1.8	Hippocampal neuron
(Antonov & Johnson 1999)	0.47	Unknown	Cultured cortical neurons
(Strecker *et al.* 1994)	0.93	4.85	CA1 cells in rat neonate
	1.13	6.84	CA1 cells in two-week rats
	1.24	12.3	Dentate Gyrus in neonate
	1.03	5.52	Dentate Gyrus in four- week rats

3.5 Discussion

3.5.1 Functional high Mg^{2+} sensitivity and low Mg^{2+} sensitivity NMDARs are present

The external Mg^{2+} block of recombinant NMDA receptors has been characterized by Kuner and Schoepfer (1996) and Monyer *et al.*(1994). It has been shown that 100μM extracellular Mg^{2+} blocked NMDA-evoked responses from recombinant NR1-NR2A or NR1-NR2B receptor by 79.8% at -60mV while for recombinant NR1-NR2C or NR1-NR2D receptors by about 48% (Kuner & Schoepfer 1996). Moreover, 1mM extracellular Mg^{2+} blocked NMDA-evoked responses from recombinant NR1-NR2A or NR1-NR2B by 95.7% (Kuner & Schoepfer 1996) and by 92.8% (Monyer *et al.* 1994) and at -60mV while for recombinant NR1-NR2C or NR1-NR2D, by about 89% (Kuner & Schoepfer 1996) and 64% (Monyer *et al.* 1994), respectively.

In my experiments, the NMDA-evoked whole-cell current from dopamine cells in P7 rat SNc was significantly blocked by 100μM external Mg^{2+} by 57.8 ± 0.1% (Mean ± S.D., n=8) while 1mM Mg^{2+} blocked NMDAR currents by 85.9 ± 0.1% (Mean ± S.D., n=16). Comparing the data presented here with previous studies, these results suggested that NMDA receptors on dopamine cells have less Mg^{2+} sensitivity than NR2A- and NR2B-containing NMDA receptors and have more sensitivity than NR2C and NR2D-containing NMDA receptors. Therefore, it is suggested that the dopamine neurons on substantia nigra compacta express both high Mg^{2+} sensitivity subunits (NR2A, NR2B) and low Mg^{2+} sensitivity subunits (NR2C, NR2D) and the data are strongly supported by previous in situ hybridization and immunochemical and patch-clamping experiments, which demonstrated that high levels of NR2D mRNA and NR2D protein and low levels of NR2B mRNA were

found in SNc (Monyer *et al.* 1994; Dunah *et al.* 1996; Dunah *et al.* 1998). In addition, Patch-clamp single-channel recording experiments showed that both high and small-conductance NMDA channels (50pS, 41pS and 18pS conductance level) were found in outside-out patches form P14 rat dopaminergic neurons (See Chapter 4). The high conductance NMDA channels are ifenprodil-sensitive, which suggests NR2B subunits are present (Jones & Gibb 2005).

Previous studies also suggest that NR2B and NR2D may be present in the same NMDA receptor on dopaminergic neurons (Jones & Gibb 2005). These triheteromeric NR1-NR2B-NR2D complexes may have less sensitivity to Mg^{2+} than recombinant receptors composed of NR1-NR2A, NR1-NR2B (Hatton & Paoletti 2005). Therefore, the low Mg^{2+} sensitivity NMDA receptor on dopamine cells are likely to be NR2D- containing NMDA receptors (they might be NR1-NR2D diheteromers or NR1-NR2B-NR2D triheteromers).

3.5.2 Functional NR2D-containing receptors might be expressed by dopamine cells in SNc

Voltage-dependent channel block by external Mg^{2+} is an NMDA receptor property of critical physiological importance (Nevian & Sakmann 2004). In addition to its functional implications, block by external Mg^{2+} provides a means to explore the subunit composition and gating of NMDA receptors (Monyer *et al.* 1994; Kuner & Schoepfer 1996; Vargas-Caballero & Robinson 2004).

In my experiments, partial Mg^{2+} concentration-inhibition curves were constructed (Figure

3.2.C) and the magnitude of the IC_{50} for Mg^{2+} block at -60mV was estimated to be 74.4 μM. Compared with previous studies (40-106μM for NR1-NR2A and NR1-NR2B, 191-425μM for NR1-NR2C and NR1-NR2D) (Qian *et al.* 2005), these data suggest that although dopamine cells in SNc contain more than one type of NMDA receptor subunit, macroscopic NMDA-evoked currents exhibit more NR2B-like characteristics.

The coapplication of ifenprodil and Mg^{2+} reduced the voltage dependence of Mg^{2+} block of NMDA receptors, which suggests that both Mg^{2+}-sensitive (likely to be NR2B) and Mg^{2+}-insensitive (likely to be NR2D) NMDA receptors are expressed in dopamine cells in SNc. This result is consistant with a previous single-channel study, which showed small conductance NMDARs (NR2D) with asymmetric direct transition between main opening and sub-conductance levels are present (Jones & Gibb 2005). The smaller currents recorded in the presence of ifenprodil mean that the series resistance error in these recordings will be smaller than in control recordings and so it is unlikely that differences in series resistance can account for the lower voltage-dependence of the Mg^{2+} block in the presence of ifenprodil. In these experiments, the average series resistance was 19±4% (Mean±S.D., n=8) and in the presence ifenprodil 21±3% (Mean±S.D., n=9). The averaged current at -60mV in control experiments (10μM NMDA) was 700.5 ± 54.6 (±S.E., n=17) and in the presence of ifenprodil (250μM NMDA) was 171±12 (n=17). These series resistance errors are likely to be similar in these two experimental conditions.

The low Mg^{2+} sensitive and ifenprodil-insensitive current component may be from diheteromeric NR1-NR2D NMDA receptors or NR1-NR2B-NR2D NMDARs. The IC_{50} values for the Mg^{2+}-insensitive component determined in this study were 46.6.6 μM at -100mV, 97.3 μM at -80mV, and 259.3 μM at -60mV, respectively. These data are in good agreement with previous studies from recombinant NR1-NR2D NMDA receptors (Qian *et*

al. 2005).

So far, there is no evidence showing the Mg^{2+} sensitivity of thiheteromeric NR1-NR2B-NR2D NMDAR. However, Hatton and Paoletti (2005) used an mutagenesis approach to produce a triheteromeric NR1-NR2A$_{N614R}$-NR2B receptor. The mutation prevents external Mg^{2+} block for NR2A subunits while NR2B subunit sensitivity to Mg^{2+} has not changed. The results showed that although NR2B subunits still have high Mg^{2+} sensitivity, the triheteromeric NR1-NR2A$_{N614R}$-NR2B has low Mg^{2+} block properties due to NR2A subunits mutation. Thus, triheteromeric NR1-NR2B-NR2D NMDAR might have low Mg^{2+} sensitivity, which is similar to NR1-NR2D diheteromeric NMDA receptors.

The NR2D-containing receptors in dopaminergic neurons could have functional importance in excitotoxicity because of the long duration of NR2D receptor activations and high agonist affinity, as well as weak Mg^{2+} blockade and low sensitivity to inhibition by polyamines (Kuner & Schoepfer 1996; Cull-Candy *et al.* 2001). Our findings support the idea that NR2D subunits form functional NMDA receptors in dopaminergic neurons of SNc (possibly these are triheteromeric NR1-NR2B-NR2D receptors). These may provide a novel therapeutic target in Parkinson's disease (Hallett & Standaert 2004).

3.5.3 NMDA concentrations applied during experiment

In order to study voltage dependent Mg^{2+} block of NMDA receptors on dopamine cells, 10μM of NMDA and 10μM of glycine were applied to activate whole-cell NMDA currents. However, when the NMDA-induced ifenprodil-insensitive current was studied, 200μM of NMDA and 10μM of glycine were applied. There are two reasons for this NMDA concentration difference. First, the mean value of whole-cell NMDA-induced current

evoked by 10μM NMDA and 10μM is approximately 700 pA. Ifenprodil block experiments showed that 10μM of ifenprodil causes 86% inhibition of NMDA-induced whole-cell current (see ifenprodil inhibition; chapter 5). Therefore, only about 70pA of whole-cell NMDA current remains when 10μM ifenprodil is applied. This current is too small to quantify Mg^{2+} block of the ifenprodil-insensitive whole-cell NMDA current. Secondly, it has been shown that ifenprodil block is noncompetitive and is associated with an increase in NMDA affinity (Kew *et al.* 1996). In order to avoid an increase in NMDA open probability caused application of ifenprodil (10μM), a saturating concentration of NMDA (250μM) was applied during these experiments.

The trapping block model for Mg^{2+} block of NMDAR is widely accepted, which suggests that the extent of Mg^{2+} block of the steady-state NMDA whole-cell current is independent of NMDA concentration. Therefore, the concentration of NMDA used will not affect the voltage dependence of the NMDA receptor Mg^{2+} block. Moreover, it has been suggested that ifenprodil inhibits NMDA receptors through shifting the pKa of the proton sensor to a more alkaline level, which means the application of ifenprodil also does not affect Mg^{2+} block behaviour.

3.5.4 Comparison with recombinant NMDA receptors

In the oocyte expression system, a clear result has shown that NMDA receptors composed of NR1-NR2A, NR1-NR2B show a higher voltage-dependence of Mg^{2+} block than receptors composed of NR1-NR2C and NR1-NR2D (Kuner & Schoepfer 1996; Wrighton *et al.* 2008). However, different values for the voltage-dependence of Mg^{2+} block (δ) have been reported. Kuner and Schopfer (1996) reported that the δ value for NR1-NR2A and

NR1-NR2B NMDA receptors is about 1.05 and the δ value for NR1-NR2C and NR1-NR2D NMDA receptors is about 0.75. In another group (Wrighton *et al.* 2008), a similar result was obtained for NR1-NR2A NMDA receptors (δ=0.96) while a δ value higher than that of Kuner & Schopfer (1996) was reported for NR1-NR2D NMDA receptors (δ=0.91). We do not know what causes the δ value difference between these experiments. Assuming permeant ions might affect the voltage-dependent Mg^{2+} block (Antonov & Johnson 1999), a possible explanation for this inconsistency is that different ion concentrations of recording solution and inside the oocyte were present. For example, in Kuner and Schoepfer's experiment, 0.18mM Ca^{2+} was used in the external solution while 1.8mM Ba^{2+} used in the external solution in the experiments of Wrighton et al. (2008).

In my experiments, fitting NMDA I-V relations using different models permitted us to quantify the voltage-dependent Mg^{2+} block of NMDA channels in dopaminergic neurons. According to these models, the same δ value was found (0.82) independently of the model used in the presence of 20 μM NMDA, 10 μM glycine while δ=0.64 in the presence of 200 μM NMDA, 10 μM glycine and 10 μM ifenprodil. There are two reasons for different NMDA concentrations used in my experiments. Firstly, when a low concentration of NMDA was used, ifenprodil does not block NR2B-containing NMDAR-mediated currents but potentiates NMDA-induced whole-cell currents, because ifenprodil can increase the receptor affinity for agonists at the glutamate-site (Kew *et al.* 1996). (see also ifenprodil block chapter) Secondly, all Mg^{2+} block models derived from the traditional trapping block model suggest that the voltage-dependence of Mg^{2+} block will be independent of agonist concentration. This suggestion also was supported by experimental data (Qian *et al.* 2005; Wrighton *et al.* 2008). These results are consistent with the observation that Mg^{2+} does not alter channel gating in the sense that the durations of "bursts" of channel openings do not

change in the presence of Mg^{2+} (Ascher & Nowak 1988; Qian *et al.* 2005).

Comparing my data presented above with recombinant NMDA receptors reveals that the δ value (0.82) obtained in the absence of ifenprodil is in the range of previous studies and is higher than the δ value for NR1-NR2C and NR1-NR2D recombinant NMDA receptors (0.75) (Kuner & Schoepfer 1996) but smaller than the NR1-NR2D δ value obtained by Wrighton et al. (2008) and smaller than that for NR1-NR2A and NR1-NR2B recombinant NMDA receptors, 0.96 (Wrighton *et al.* 2008) and 1.05 (Kuner & Schoepfer 1996). This may suggest that native NMDA receptors on dopaminergic neurons express a mixed population of NMDA receptors, highly voltage-dependent Mg^{2+} block NMDA receptors (NR2A- and NR2B-containing NMDA receptors) and receptor less voltage-dependent Mg^{2+} block (NR2C- and NR2D- containing NMDA receptors). This evidence also is supported by previous electrophysiological experiments (Jones & Gibb 2005), in situ hybridization (Standaert *et al.* 1994) and western blot experiments (Dunah *et al.* 1996; Dunah *et al.* 1998). They suggested that both NR2B- and NR2D-containing NMDA receptors are expressed by dopaminergic neurons in adult SNc. If this is the case, in the presence of 10μM ifenprodil, the NMDA whole-cell current mediated by NR2D-containing NMDA receptors should be more obvious than before and the whole-cell current should display a lower voltage-dependence of Mg^{2+} block. In agreement with this idea, a smaller δ value (0.64) was observed in the presence of 10μM ifenprodil, suggesting that NR2D-containing NMDA receptors are expressed by P7 dopamine cells. However, the δ value (0.64) in my experiments is smaller than that of NR1-NR2D recombinant NMDA receptors, being 0.91 (Wrighton *et al.* 2007) and 0.75 (Kuner & Schoepfer 1996). The discrepancy might be due to the experimental conditions, because in my experiments, 1mM Ca^{2+} was added to the external recording solution and this external Ca^{2+} could cause an interaction between Ca^{2+} and Mg^{2+} (Mayer & Westbrook 1987; Ascher & Nowak 1988).

The discrepancy also might be due to receptor expression system differences. Therefore, I compared my data with previous experimental results from native NMDA receptors (See section 3.5.5).

The Mg^{2+} affinity parameter for NMDA receptors (K_{Mg}^{2+}(0mV)) also was obtained during fitting the NMDA I-V relations to different Mg^{2+} block models. Intriguingly, the traditional trapping block, potentiation and proton block models all gave the same results for K_{Mg}^{2+} (0mV), being 6mM (without ifenprodil) and 4.87mM (with ifenprodil) while the values of K_{Mg2+}(0mV) obtained from fitting data using the simple block model are smaller than values obtained using the other models. They are 432μM (without ifenprodil) and 348μM (with ifenprodil), respectively. These results are due to the fact that both the potentiation model and proton block models are based on the trapping block model and also proton block effect and Mg^{2+} potentiation effect only affect NMDA receptor open probability and do not influence Mg^{2+} block voltage-dependence (δ) and Mg^{2+} affinity at 0mV. However, compared with the trapping block model, the simple block model has less NMDA receptor closed states, which could cause the difference in Mg^{2+} affinity at 0mV.

In the Kuner and Schoepfer (1996) paper, they reported that K_{Mg2+}(0mV) values for NR1-NR2A and NR1-NR2B NMDA receptors are 4.87mM and 3.7mM, respectively and for NR1-NR2C and NR1-NR2D NMDA receptors are 3.5mM and 2.6mM, respectively. These results suggested that there are no significant differences in K_{Mg2+} (0mV) between different NR2-containing NMDA receptors. In agreement with previous reports, my data (6mM and 4.87mM) from the trapping block, potentiation and proton block models are similar to (somewhat higher than) data from recombinant NMDA receptors. My data also suggested that the traditional simple block model cannot accurately explain Mg^{2+} block voltage-dependence of NMDA receptors, especially for K_{Mg}^{2+}(0mV).

3.5.5 Comparison with native NMDA receptors

Voltage-dependent Mg^{2+} block has been widely investigated on native NMDA receptors in different brain areas during rat development. As indicated by previous studies, the values of δ and K_{Mg2+} (0mV) for exteral Mg^{2+} block were estimated to be 1 and 8.8mM for NMDA receptors in cultured rat neurons (1-8 weeks) (Ascher & Nowak 1988), 0.8 and 1.8mM for NMDA receptors in P3 rat CA1 hippocampal neurons (Jahr & Stevens 1990), 0.92 and 7.7mM for NMDA receptors in 180g rat CA1 pyramidal neurons and *et al.* (data from previous studies data were shown in Table 3). Table 3 shows that a large range of values of δ and K_{Mg2+} (0mV) have been reported, δ being from 0.65 to 1.24 and K_{Mg2+}(0mV) being from 1.6mM to 21mM. It is worth mentioning that Antonov and Johnson (1999) reported values of δ and K_{Mg2+}(0mV) was 0.47 and 0.1mM, respectively when the effect of permeant ions is taken into account. These data are considerably different from the data from other research groups because Antonov and Johnson introduced permeant ion effects into the study of voltage-dependent Mg^{2+} block of NMDA receptors and a new Mg^{2+} model was used in fitting their single-channel recording data. The values of δ and K_{Mg2+}(0mV) from my experiments are in the range of previous studies. It remains unclear what factors might be responsible for these wide ranges of reported δ and K_{Mg2+}(0mV) values, however, given that permeant ions influence δ and K_{Mg2+}(0mV) values (Antonov & Johnson 1999; Zhu & Auerbach 2001; Zhu & Auerbach 2001; Qian *et al.* 2002; Qian *et al.* 2005), the experimental conditions could contribute to this large range of δ and K_{Mg2+}(0mV) values.

3.5.6 Proton block and Mg^{2+} potentiation do not affect voltage-dependent Mg^{2+} block

In my experiments, two new Mg^{2+} block models were developed to investigate whether allowing for proton block of NMDA receptors and Mg^{2+} potentiation effects on NR2B-containing NMDA receptors influence estimation of the voltage-dependent Mg^{2+} block parameters, δ and $K_{Mg2+}(0mV)$.

Fitting NMDA receptor I-V relations using these two new models gave us the same results as those obtained from fitting data using the traditional trapping block model. This fact suggested that for estimating voltage-dependent Mg^{2+} block of NMDARs, there are no significant differences among these models; the trapping block, potentiation, and proton block models. In other words, allowing for the Mg^{2+} potentiation effect and proton block of NMDA receptors has no effect on voltage-dependent Mg^{2+} block of NMDA receptors.

Chapter 4: Kinetics of NMDA receptors in P7 rat dopaminergic neurons

4.1 Summary

1. Single-channel recording and concentration jump experiments were made using outside-out patches from P7 rat dopaminergic neurons of SNc to study the kinetics of NMDA receptors.

2. Single-channel results show that both large- (49 pS and 38 pS) and small- (38 pS and 18 pS) conductance NMDAR channels are expressed by P7 rat dopaminergic neurons. In the presence of 100 nM NMDA and 10 μM glycine, the mean open frequency was 7.5 ± 0.74 openings s^{-1}, the mean open time was 3.78 ± 0.64 ms and the mean open probability (P_{open}) was 0.026 ± 0.005.

3. Fast application (1-4 ms) of 1 mM glutamate to outside-out patches evoked macroscopic current responses with a main decay time constant of hundreds of milliseconds. The averaged macroscopic current response from 6 individual patches was well fitted with two exponential components with time constants of 129 ms (53%) and 1449 ms (47%). These results suggest that NR1-NR2D NMDA receptors are absent or at very low expression levels (less than 1% of total NMDA receptors) in extrasynaptic sites.

4. Four-second application of 1 mM glutamate to outside-out patches evoked a marked desensitization of NMDA receptors. The desensitization was well fitted with a mixture of

two components; a fast component with a time constant of 82.2 ms (30.8% charge) and slow component with time constant of 259 ms (69.2% charge). The macroscopic NMDA current approached a steady state level (21.5% of the peak current value).

4.2 Introduction

4.2.1 Deactivation kinetics of NMDA receptors are largely determined by NR2 subunits and NR1 isoforms

The NMDA receptor is one type of ionotropic glutamate receptor that is widely expressed in central nervous system (CNS) contributing to both excitatory synaptic transmission (Collingridge *et al.* 1988; Forsythe & Westbrook 1988) as well as synaptic plasticity (Collingridge 1987; Bliss & Collingridge 1993). So far, three main families of NMDAR subunits have been identified, NR1, NR2 (NR2A to NR2D) and NR3 (NR3A and NR3B) (Cull-Candy *et al.* 2001). It has been shown that many of the NMDA receptor properties are determined by the identity of the glutamate-binding NR2 subunits (Cull-Candy & Leszkiewicz 2004). The NMDA receptors composed of NR1a and NR2A show the fastest deactivation time course (50ms) while the NMDA receptors formed by NR1a/NR2B or NR1a-NR2C exhibit a similar deactivation time course (about 300ms). Intriguingly, the NR1a-NR2D NMDA receptors show a long deactivation time course, which is about 2-5 seconds (Vicini *et al.* 1998; Wyllie *et al.* 1998). The variation in NMDAR kinetic properties among NR2 subunits implies functional differences during synaptic transmission and also the possibility to use kinetic properties investigate NMDA receptor composition.

In addition, the deactivation time course also is determined by the NR1 subunit isoform

(Vicini *et al.* 1998). The NR1 subunit is the product of a single gene containing 22 exons with the possibility of alternative splicing of exons 5 (the N1 cassette), 21 and 22 (the C1 and C2 cassettes) where N1 and C1 can be present or absent and C2 can alternate with C2', resulting in 8 different splice variants. Previous studies demonstrated that the NMDA receptor deactivation kinetics did not change when NR1 isoforms were expressed with the NR2A subunit (Vicini *et al.* 1998). However, when NR2B subunits were expressed with different NR1 isoforms, the NMDA receptors with N1 cassette-containing-NR1 subunits show an about 4 times faster decay time course than NMDA receptor containing N1 cassette-lacking NR1-subunits.

In my experiments, the kinetics of extrasynaptic NMDA receptors in P7 rat dopaminergic neurons of SNc were investigated to determine the composition of NMDA receptors. From previous studies (Dunah *et al.* 1996; Dunah *et al.* 1998; Jones & Gibb 2005) (see also ifenprodil; chapter 5), we know that P7 rat dopaminergic neurons express NR2B subunits. Thus, the kinetics of NMDA receptors in dopaminergic neurons of SNc might be influenced by their NR1 isoform expression. Therefore, we reviewed previous studies about the expression of NR1 splice variants in SNc dopaminergic neurons (Laurie & Seeburg 1994; Standaert *et al.* 1994; Laurie *et al.* 1995; Albers *et al.* 1999). In situ hybridization experiments suggested that the expression of NR1 splice variants in rat SNc is development regulated. In P7 rat SNc neurons the NR1-2a isoform is dominant while SNc neurons in adult rat mainly express NR1-4a isoform (Laurie & Seeburg 1994; Standaert *et al.* 1994; Laurie *et al.* 1995). Similar results also were reported in immunohistochemistry experiments (Albers *et al.* 1999). Neither NR1-4a or NR1-2a subunits contain the N1-cassette. Thus, it may be concluded that the N1 cassette of NR1 subunits is absent in dopaminergic neurons of SNc during rat development. The effect of the N1 cassette of NR1 subunits on the deactivation kinetics of NMDA receptors in dopaminergic neurons can be disregarded.

4.2.2 Relationship between single-channel behavior of NMDAR and channel deactivation kinetics

Before Neher and Sakmann successfully observed single-channel openings (Neher & Sakmann 1976), it had been supposed that the synaptic current decay depended on the mean duration of openings of the individual ion channels (Magleby & Stevens 1972). This idea had been common until the giga-ohm seal method was discovered (Hamill *et al.*, 1980). The method makes it possible to get sufficient resolution to see the brief shuttings that separate individual openings (Colquhoun & Sakmann 1981). In this way, the mean opening duration was measured to be about 2 ms for acetylcholine, which was too brief to explain the frog endplate synaptic current decay.

Before this hypothesis was proposed that when the transmitter binds as fast as is physically possible, it will activate not just one channel opening, but that the channel will re-open a few times before the agonist dissociates (Colquhoun & Hawkes 1977). In other words, the event that underlies the synaptic current is actually a brief burst that consists of several openings separated by brief shuttings, though for NMDA receptors it wasn't until the 1990s that the formal relationship between burst length and synaptic current time course was elucidated (Gibb & Colquhoun 1991; Gibb & Colquhoun 1992; Wyllie *et al.* 1998).

4.2.3 Extrasynaptic and synaptic NMDA receptors

A comparison of synaptic and extrasynaptic NMDA receptors is shown in Table 4.1. Extrasynaptic NMDA receptors are expressed in dendrites outside spines or on the soma of neurons and they seem to be ubiquitously expressed throughout the nervous system. Thus they have less chance to be activated during synaptic transmission.

However, these extrasynaptic NMDA receptors can be activated by glutamate spillover induced by a high frequency trains of stimuli or by blocking glutamate uptake (Traynelis *et al.* 1993; Brickley *et al.* 2003) and they represent a potentially important threat to the neuron during stroke or some other pathologies. These extrasynaptic NMDA receptors can be investigated in membrane patches (Spruston *et al.* 1995; Clark *et al.* 1997; Jones & Gibb 2005) or in brain slices by using glutamate uncaging (Hayashi & Majewska 2005) or directly by activating extrasynaptic NMDA receptors by bath perfusion after block of synaptic NMDA receptors by a slow off-rate open channel blocker such as MK-801 (Tovar & Westbrook 2002). In contrast, the synaptic NMDA receptors are found in dendrite spines and can be activated during synaptic transmission. Therefore, they can be investigated by recording EPSCs (Brothwell *et al.* 2008) or spontaneous synaptic currents.

Table 4.1 Differences between synaptic and extrasynaptic NMDA receptors

	Location	Activation by synaptic transmission	Investigation Method
Synaptic NMDAR	Dendritic spines	Yes	EPSC, spontaneous NMDA current
Extrasynaptic NMDAR	Dendrite outside spines or soma	Difficult	Membrane patches

4.2.4 Aims of these experiments

In my experiments, to investigate the kinetics of extrasynaptic NMDA receptors and also to make inferences about the composition of extrasynaptic NMDA receptors, steady-state single-hannel recordings and concentration jump experiments were made for outside-out patches from P7 rat dopaminergic neurons of SNc. Three main results are reported here. First, NR1-NR2D NMDA receptors are absent or at very low expression levels (less than 1% of total NMDA receptors) in extrasynaptic sites. Second, a mixed population of NMDA receptors (NR1-NR2B and NR1-NR2B-NR2D) is present in extrasynaptic sites. Third, the kinetics of extrasynaptic NMDA receptors is similar to these of synaptic NMDA receptors, suggesting they have similar subunit composition.

4.3 Results

4.3.1 Single-channel recordings from outside-out patches of P7 rat dopaminergic neurons

4.3.1.1 Both large and small conductance NMDA receptors are present

The conductance of NMDA receptor channels is mainly determined by NR2 subunits (Stern *et al.* 1992; Wyllie *et al.* 1996). The NMDA receptors composed of NR1-NR2A and NR1-NR2B have similar channel conductance, 50pS for the main channel open level and 40pS for the main sub-conductance level while the NMDA receptors formed by NR1-NR2C and NR1-NR2D have smaller conductances, being 35pS for NR1-NR2C (Stern *et al.* 1992) and 39pS for NR1-NR2D (Wyllie *et al.* 1996; Chen *et al.* 2004) main open channel levels and 18pS for sub-conductance levels. Therefore, single-channel the conductance of NMDA receptor channels provides one possibility to investigate native NMDA receptor subunit composition.

Application of NMDA (100nM) and glycine (10 μM) to outside-out patches (n=5) from P7 rat SNc dopaminergic neurones activated individual NMDA receptor channels at –60 mV with three different amplitudes: 1.13 ± 0.09 pA, 2.27 ± 0.3 pA and 2.94 ± 0.17 pA (details are shown in Table 4.2). An example recording of NMDA receptor channel openings to all three amplitudes is shown in Figure 4.1a, and the stability of channel openings throughout a recording is shown in Figure 4.1b. In 5 patches, the mean opening frequency was 7.5 ± 0.74 openings s^{-1}, the mean open time was 2.78 ± 0.64 ms and the mean open probability (P_{open}) was 0.026 ± 0.005. The distribution of channel amplitudes activated by 100nM NMDA in 5 patches was fitted with the sum of three Gaussian components (an example is

shown in Figure 4.1c). The measured channel amplitudes correspond to chord conductances (and relative areas) of 18.8 ± 1.0 pS (6.28 ± 3.25%, n= 5), 37.8 ± 4.9 pS (25.7 ± 55.2%, n= 5) and 49.0 ± 2.8 pS (72.3 ± 5.1%, n= 5). The distribution of amplitudes for the recording illustrated in Figure 4.1a is shown in Figure 4.1c, with the superimposed fit of the three Gaussian components.

Analysis of the frequency of direct transition between conductance levels was used to test for evidence that NR2D subunits may be present in SNc dopamine cell NMDA receptors (Wyllie *et al.* 1996; Jones & Gibb 2005). In these data, transition from 19 pS to 38 pS were less frequent (44.3 ± 3.3%) than transition from 38 pS to 19 pS (55.7 ± 3.3%) and transition from 19 pS to 49 pS (46.5 ± 2.6%) were less frequent than transition from 49 pS to 19 pS (53.5 ± 2.6%) while transitions between 38 pS and 49 pS levels were almost symmetrical (48.9 ± 1.3% and 51.1 ± 1.3%).

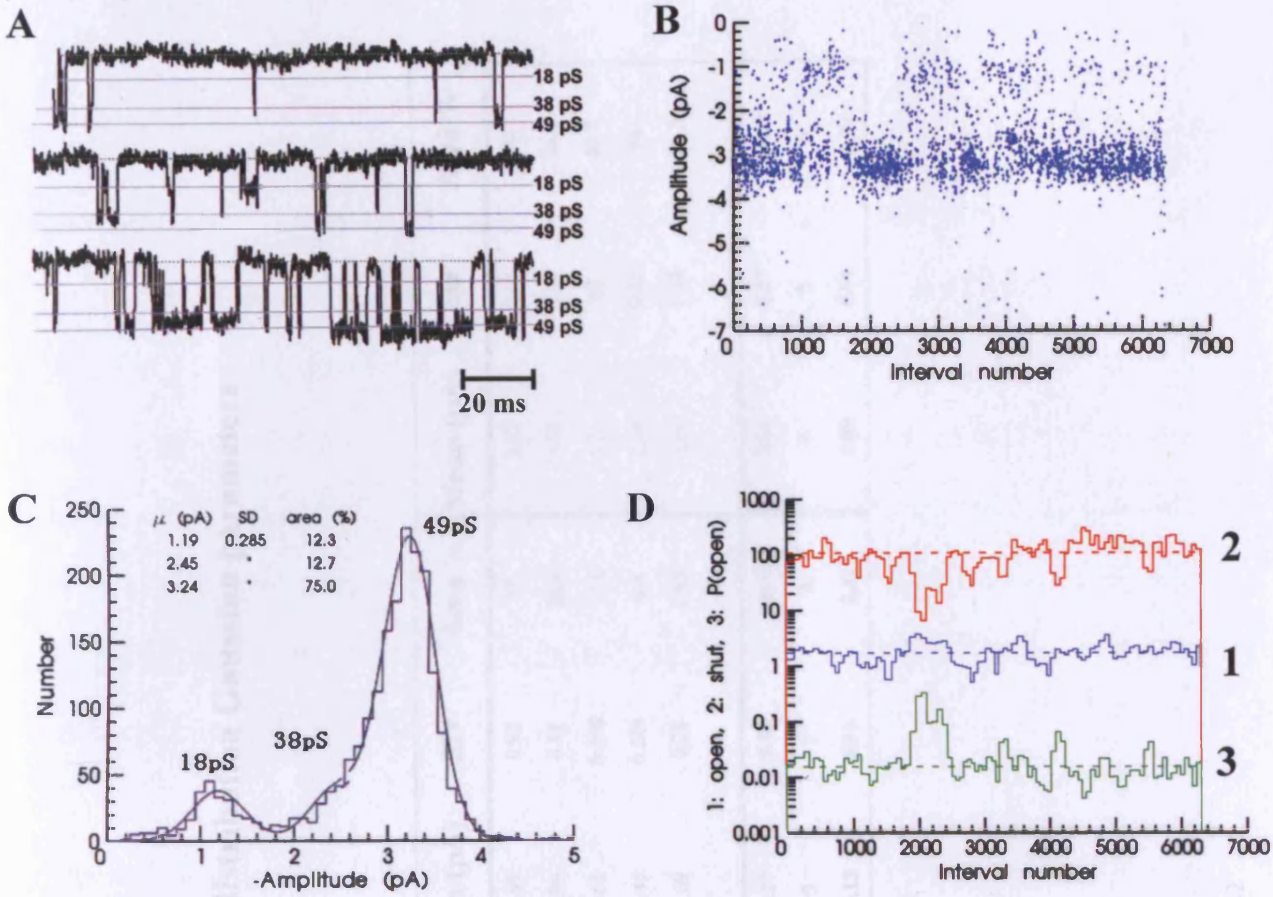

Figure 4.1 Large and small-conductance NMDA receptor channels in SNc dopaminergic neurons

A. Examples of NMDAR single-channel recordings . B. *S*tability plot of channel amplitudes throughout the duration of a recording. C. Amplitude distribution for the patch illustrated in *A*, fitted with the sum of three Gaussian components. The mean amplitude and relative area of each component are shown on the histogram, and correspond in this example to chord conductances of 20pS, 41 pS and 54 pS. D. Stability plots of P_{open}, mean open time and mean shut time for single-channel currents in the presence of 100 nM NMDA and 10 μM glycine.

Table 4.2 Summary of amplitude distribution Gaussian parameters

patch	Number of events	Mean (pA)	SD	Area %	Mean (pA)	SD	Area %	Mean (pA)	SD	Area %
1	2395	1.2	0.1	1.30	2.59	0.92	37	3.22	0.23	62
2	4990	1.29	0.39	4.4	2.99	0.57	28.9	3.18	0.27	66.7
3	2464	1.2	0.54	19.1	2.64	0.308	17.1	3.26	0.2	63.8
4	1032	0.8	0.289	2.6	1.45	0.228	6.4	2.44	0.35	91
5	2358	1.17	0.43	4	1.69	0.28	19.5	2.61	0.32	76.5
Average	**1439**	**1.13**	**0.35**	**6.28**	**2.27**	**0.46**	**21.70**	**2.94**	**0.27**	**72.02**
n	**5**	**5**	**5**	**5**	**5**	**5**	**5**	**5**	**5**	**5**
SE	**643**	**0.04**	**0.03**	**1.45**	**0.13**	**0.06**	**2.31**	**0.08**	**0.01**	**2.40**

4.3.1.2 Open times and shut times

The open times here are referred to as open periods because it is likely they often contain unresolved brief channel closings. Single-channel current open periods of NMDA receptors activated by 100nM NMDA and 10μM glycine were well fitted with a mixture of three exponential components (n = 5). An open period distribution from one recording is shown in Figure 4.2 and the summary details of open period distributions from 5 patches are shown in Table 4.3. The measured NMDAR channel open periods were well described by three components with time constants and relative areas of, 0.13 ± 0.04 ms (40.46 ± 3.4 %, *n*= 5), 1.52 ± 0.30 ms (29.7 ± 4.6 %, *n*= 5) and 3.9 ± 0.5 ms (29.3± 3.7 %, *n*= 5). The mean open time was 2.62 ms.

The shut time periods of single-channel current traces of NMDA receptors (n=5) evoked by 100nM NMDA and 10μM glycine were fitted with a mixture of five exponential components; 0.36 ± 1.03 ms (5.3 ± 1.9%, *n*= 5), 1.04 ± 0.21 ms (28.6 ± 6.2%, *n*= 5), 11.4 ± 1.02 ms (30.1 ± 2.6%, *n*= 5), 152 ± 28 ms (14.2 ± 1.0, *n*= 5) and 541 ± 144 ms (19.6 ± 3.6%, *n*= 5). The mean shut time was 122 ms. A summary of details of the shut time distributions from 5 patches is shown in Table 4.4.

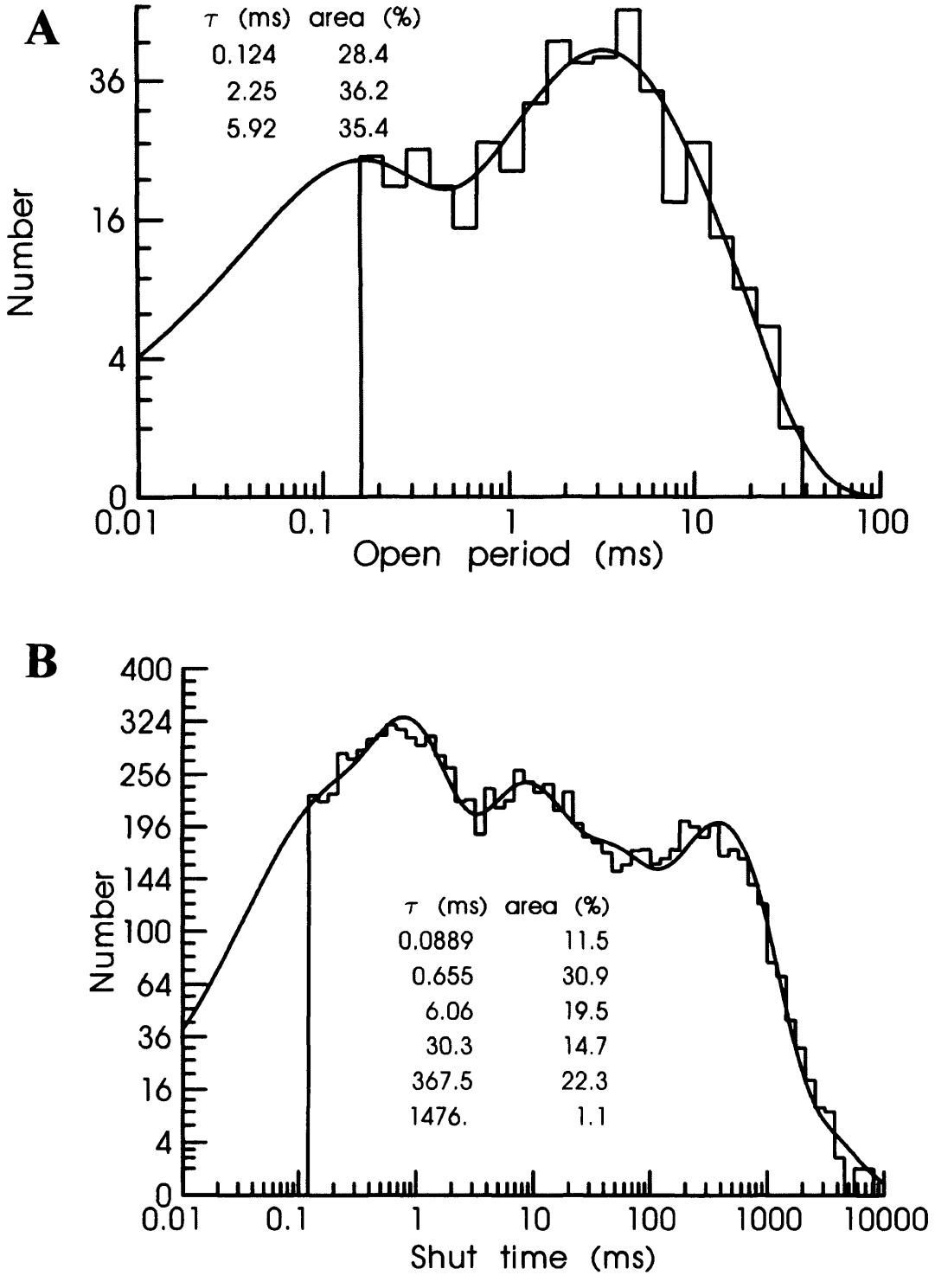

Figure 4.2 Analysis of the distribution of NMDA channel open periods and shut time

Figure 4.2 shows distributions of open periods to any amplitude level and and shut time from a single patch. The open time distribution has been fitted with a mixture of three exponential components with parameter shown in the inset. The shut time distribution has been fitted with a mixture of 6 exponential components (in the table 4.4, the shut time distribution for this patch has been fitted with 5 expoenential because the 1476 ms component is too small).

Table 4.3 Summary of open time distribution from 5 individual patches

	Patch	Number of Trans.	Length (min)	Resol. (μs)	TT	P_{open}	Opening Frequency (s^{-1})	Mean Open (ms)	1st Exponential (ms)	%	2nd Exponential (ms)	%	3rd Exponential (ms)	%
	1	8125	5	80	485	0.02	9.48	2.17	0.05	47	0.48	14	2.87	38
	2	14458	8.3	120	965	0.02	7.5	2.67	0.05	37.9	1.69	37.7	3.72	24.3
	3	11233	4.8	110	527	0.015	8.9	1.69	0.25	45	1.9	36	3.57	18
	4	2778	1	150	82	0.037	7.9	4.6	0.12	28.4	2.25	36.2	5.92	35.4
	5	8760	5.5	120	514	0.015	7.77	1.97	0.19	44	1.29	24.5	3.27	30.7
Average		9070.80	4.92		514	0.024	8.31	2.62	0.13	40.46	1.52	29.68	3.87	29.28
N		5			5	5	5	5	5	5	5	5	5	5
SE		1927			139	0.002	0.38	0.52	0.04	3.38	0.30	4.58	0.53	3.66

Table 4.4 Summary of shut time distributions from five individual patches

Patches	1st Exponential		2nd component		3rd component		4th component		5th component	
	(ms)	%	(ms)	%	(ms)	%	(ms)	%	(ms)	%
1	0.182	11	0.80	24	11.1	36	163	16	425	14
2	0.112	9	0.71	39	11.0	23	158	13	546	17
3	0.588	4	1.32	8	11.1	36	162	11	289	31
4	0.09	3	0.64	28	8.7	30	51	14	355	25
5	0.836	1	1.72	44	15.0	26	225	17	1090	12
Average	**0.36**	**5.3**	**1.04**	**28.6**	**11.4**	**30.1**	**151**	**14.2**	**541**	**19.6**
N	**5**	**5**	**5**	**5**	**5**	**5**	**5**	**5**	**5**	**5**
SE	**0.07**	**0.85**	**0.09**	**2.79**	**0.46**	**1.16**	**12.57**	**0.47**	**64.40**	**1.60**

4.3.2 Concentration jump experiments

In order to evaluate the deactivation kinetics of extrasynaptic NMDARs, outside-out patches containing multiple channels were obtained from P7 rat dopaminergic neurons of SNc and stimulated with a brief synaptic-like (1-4ms) pulse of 1mM glutamate. Saturating concentrations of glycine (10 μM), DNQX (20 μM) and strychnine (10μM) were always present both in control solution and in the solution containing glutamate (1mM).

Figure 4.3A and 4.3B show two individual responses recorded following a 1ms pulse of 1mM glutamate and 10 μM glycine. Several channels were present in this outside-out patch and single-channel currents are clearly visible in the current traces, containing both large- and small- conductance NMDA receptor channels. The averaged NMDAR current trace from six individual patches is shown in Figure 4.3c. To evaluate the NMDA receptor deactivation parameters, we fitted the averaged NMDAR current decay with a mixture of two exponential components. The fast component and slow component time constants were 128.8 ms and 1449 ms, respectively. The relative areas of the two decay components were 53% and 47% (charge), respectively. Interestingly, we can see that there is a slow component to the decay time course, about 1449 ms for NMDA receptors in dopaminergic neurons. Although the slow component contributes only about 9% of the current peak amplitude, it carries about 47% of the charge.

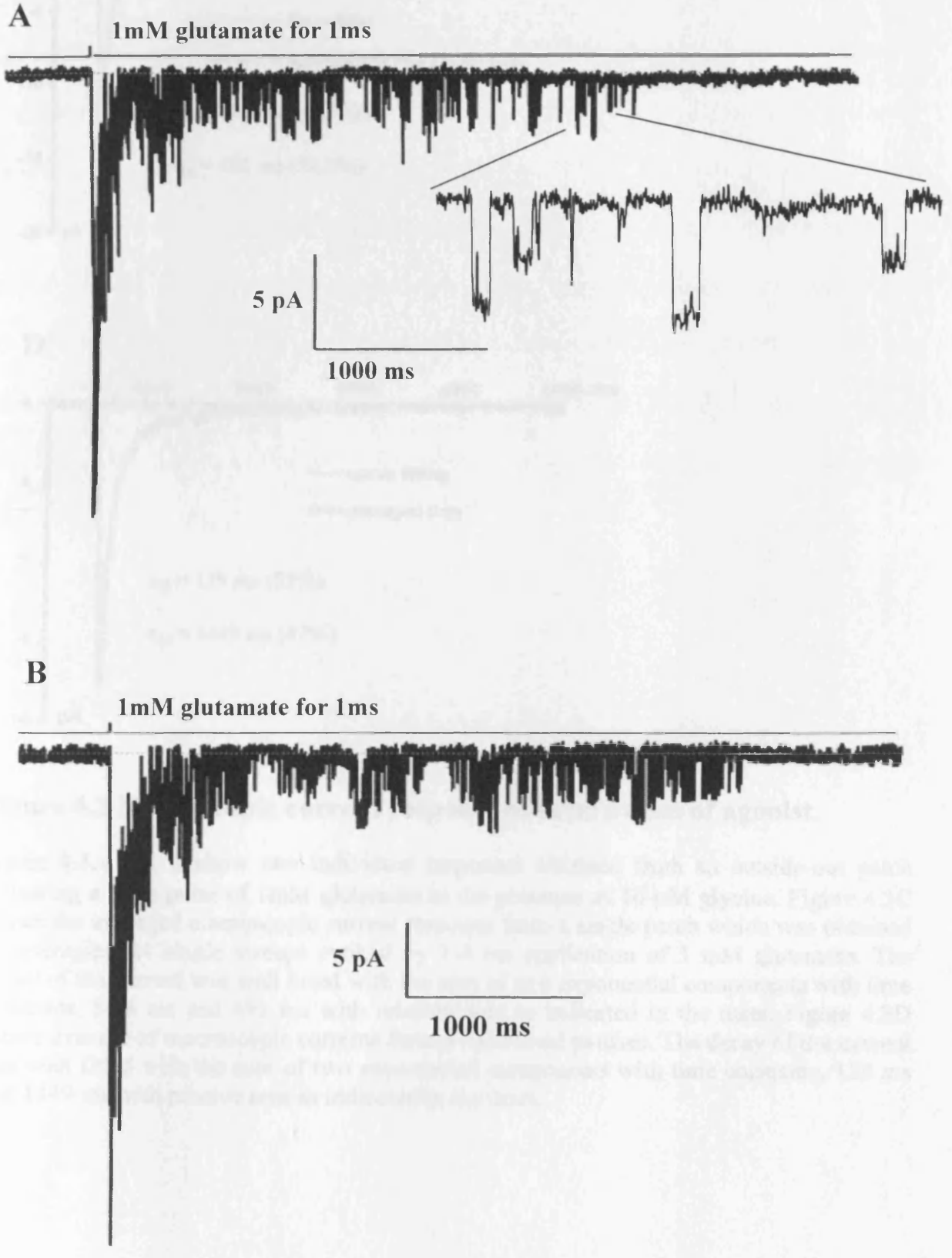
A
1mM glutamate for 1ms
5 pA
1000 ms
B
1mM glutamate for 1ms
5 pA
1000 ms

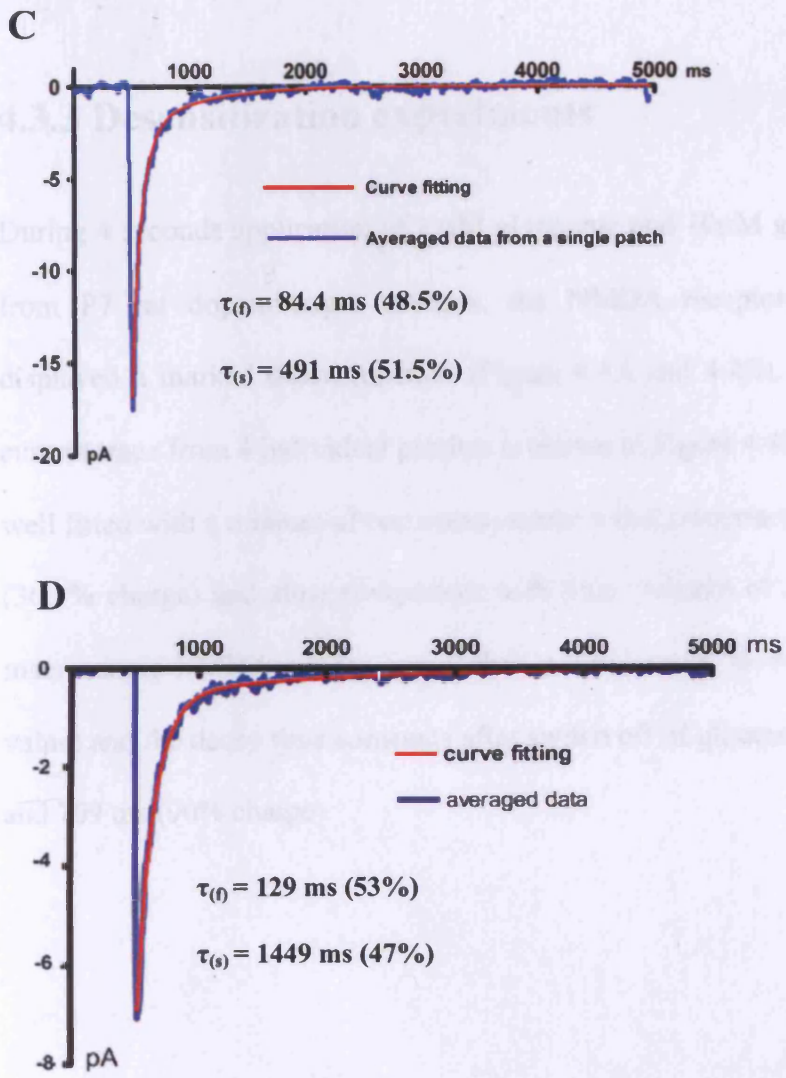

Figure 4.3 Macroscopic current response to brief pulses of agonist.

Figure 4.3A and B show two individual responses obtained from an outside-out patch following a 1 ms pulse of 1mM glutamate in the presence of 10 μM glycine. Figure 4.3C shows the averaged macroscopic current response from a single patch which was obtained by averaging 24 single sweeps evoked by 1-4 ms application of 1 mM glutamate. The decay of the current was well fitted with the sum of two exponential components with time constants, 84.4 ms and 491 ms with relative area as indicated in the inset. Figure 4.3D shows average of macroscopic currents from 6 individual patches. The decay of the current was well fitted with the sum of two exponential components with time constants, 129 ms and 1449 ms with relative area as indicated in the inset.

4.3.3 Desensitization experiments

During 4 seconds application of 1mM glytamate and 10μM glycine to outside-out patches from P7 rat dopaminergic neurons, the NMDA receptors in dopaminergic neurons displayed a marked desensitization (Figure 4.4A and 4.4B). The averaged dsensitization current trace from 4 individual patches is shown in Figure 4.4D and the desensitization was well fitted with a mixture of two components; a fast component with time constant 82.2 ms (30.8% charge) and slow component with time constant of 259 ms (69.2% charge). The macroscopic NMDA current approached a steady state level (21.5% of the peak current value) and the decay time constants after switch off of glutamate were 151 ms (10% charge) and 709 ms (90% charge).

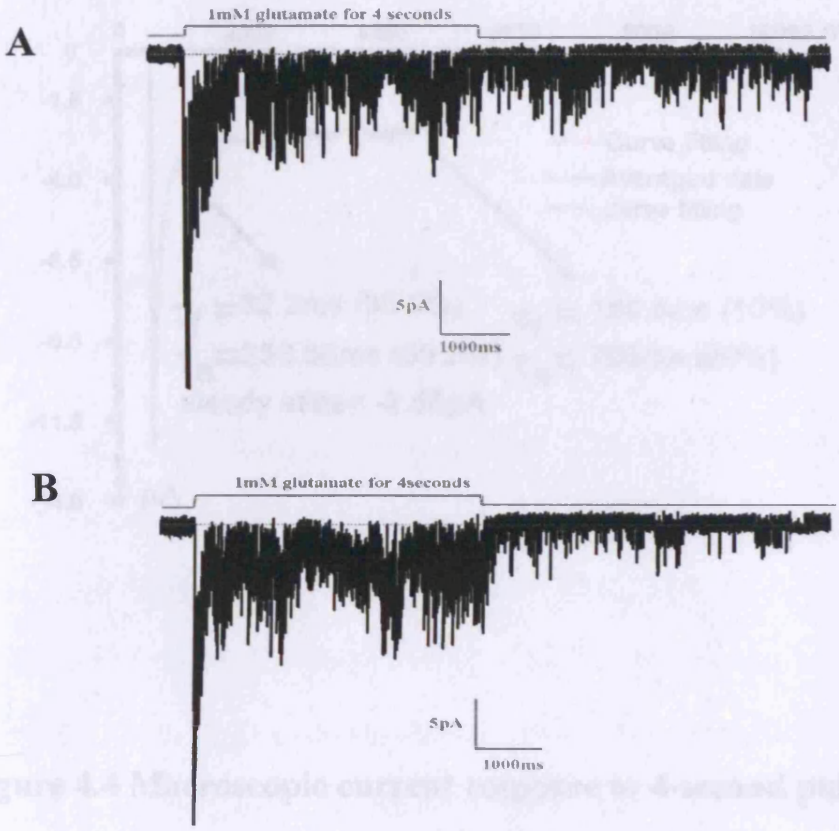
A
1mM glutamate for 4 seconds
5pA
1000ms
B
1mM glutamate for 4seconds
5pA
1000ms

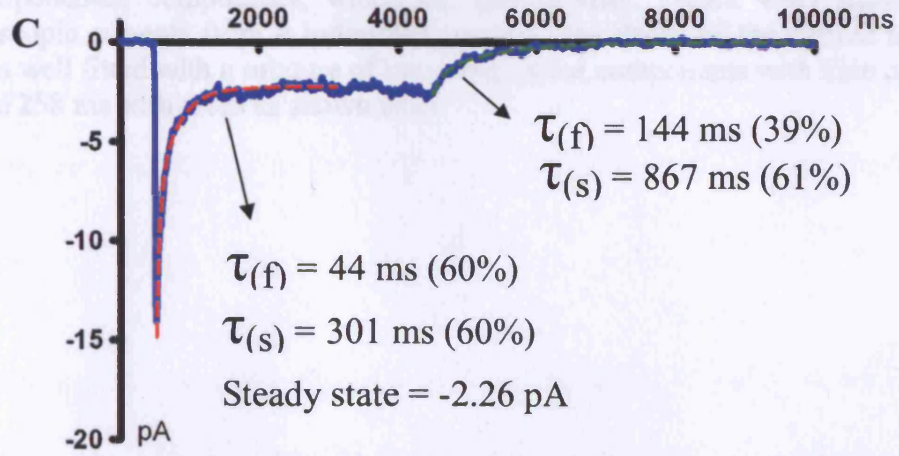
C
2000
4000
6000
8000
10000 ms
0
-5
-10
-15
-20
pA
τ(f) = 144 ms (39%)
τ(s) = 867 ms (61%)
τ(f) = 44 ms (60%)
τ(s) = 301 ms (60%)
Steady state = -2.26 pA

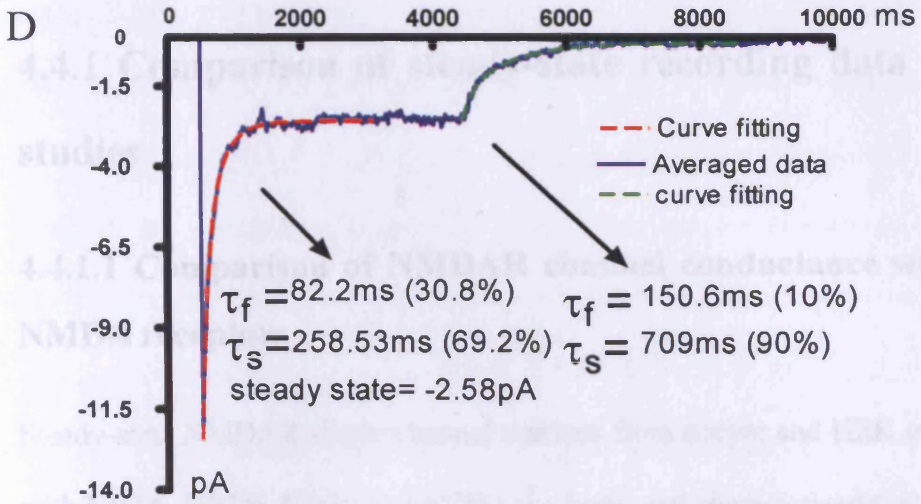

Figure 4.4 Macroscopic current response to 4-second pulses of agonist.

Figure 4.4A and 4.4B shows two individual response obtained from an outside-out patch during a 4 second pulse of 1mM glutamate in the presence of 10 μM glycine. Figure 4.4C shows an averaged macroscopic currnet from a single patch which was obtained by averaging 100 sweeps. The desensitization and decay time courses were well fitted with two exponential components, which are shown inset. Figure 4.4D shows average of macroscopic currents from 4 individual patches. The decay of the current to steady state level is well fitted with a mixture of two exponential components with time constants, 82.2 ms and 258 ms with areas as shown inset.

4.4 Discussion

4.4.1 Comparison of steady-state recording data with previous studies

4.4.1.1 Comparison of NMDAR channel conductance with recombinant NMDA receptors

Steady-state NMDAR single-channel currents from oocyte and HEK cells expressing NR1 with NR2A, NR2B, NR2C or NR2D have been well characterized (Stern *et al.* 1992; Stern *et al.* 1994; Wyllie *et al.* 1996; Anson *et al.* 1998; Cheffings & Colquhoun 2000; Banke *et al.* 2005; Chen & Wyllie 2006). Recombinant NMDA receptors composed of NR1-NR2A and NR1-NR2B have large conductance channels (50 pS with 40 pS sublevel) while NMDA receptors formed by NR1-NR2C or NR1-NR2D exhibit smaller conductance channels (38 pS with 19 pS sublevel). In addition, when NR1, NR2A and NR2D subunits were co-expressed in Xenopus oocytes, not only channel openings characteristic of NR1-NR2A (50 pS and 40 pS) receptors and channels characteristic of NR1-NR2D receptors were found but also a novel channel with a conductance of 30 pS, 40 pS and 50 pS was recorded, with direct transitions between all three levels (Cheffings & Colquhoun 2000).

Previous reports about the single-channel conductance of native NMDA receptors are summarized in Table 4.5. From Table 4.5, we know that single-channel properties of native NMDA receptors also were mimicked by recombinant NMDA receptors. For example, the outside-out patches obtained from dopaminergic neurons in P14 rat SNc contain NR2B subunits and display large 50pS conductance channel openings (Jones & Gibb 2005) and the patches excised from NR2D knock-out rat cerebellum containing only NR1 and NR2B subunits also showed large conductance channel openings (50pS and 40pS) (Brickley *et al.*

2003). Moreover, the outside-out patches containing NR2C subunits such as patches from cerebellar granule neurons (Farrant *et al.* 1994; Momiyama *et al.* 1996; Cathala *et al.* 2000) or NR2D subunits such as patches from P6 rat cerebellar Purkinje cells display small conductance NMDAR channels (39 pS and 19 pS). In my experiments, outside-out patches from P7 rat dopaminergic neurons show three conductance levels; 18pS (6.3%), 38pS (21.7%) and 49pS (72%). Comparison of my data presented here with previous studies using recombinant NMDA receptors shows that the 18pS NMDA channel and 38 pS channel are consistent with NR2C- or NR2D- containing NMDA receptors while the 38 pS and 49 pS channels are consistent with NR2A- and NR2B- containing NMDA receptors. Then, comparing my data with native NMDA receptors reported by other groups, our data are very similar to single-channel data from Golgi cell and Purkinje cells in rat cerebellum (Momiyama *et al.* 1996; Misra *et al.* 2000; Misra *et al.* 2000; Brickley *et al.* 2003). The neurons in Golgi cells and Purkinje cells of rat cerebellum express NR2B and NR2D subunits (Watanabe *et al.* 1994) and the patches from these neurons display three NMDA channel conductance levels; 50 pS, 40 pS and 19 pS.

The 30 pS conductance of NMDAR channels may be a characteristic of triheteromeric NMDARs and the 30pS channel has been reported both in recombinant putative triheteromeric NR1-NR2A-NR2D NMDA receptors (Cheffings & Colquhoun 2000) and in native triheteromeric NR1-NR2B-NR2D NMDA receptors in P14 rat dopaminergic neurons (Jones & Gibb 2005). My data using ifenprodil (chapter 5) and my Mg^{2+} block data (see chapter 3) are consistent with the hypothesis that NR1-NR2B-NR2D NMDA receptors are expressed by P7 rat dopaminergic neurons. However, a distinct 30 pS NMDAR component was not evident in amplitude distributions from P7 rat dopaminergic neurons. The absence of 30 pS conductance NMDAR channel openings might be due to the low percentage of 30pS openings expected for a triheteromer reported in the work of

Cheffings & Colquhoun (2000). There are two pieces of evidence to suggest that a lower level of functional NR2D-containing NMDA receptors are expressed in P7 rat dopaminergic neurons than in P14 rat. First, in the single-channel amplitude distribution, the NR2D component (18 pS) from P14 rats is larger than that in P7 rats, 13.3±4% vs. 6.3 ±1.5% (Mean±S.E.), suggesting a lower NR2D expression level for P7 rat dopaminergic neurons. Second, at P14, 10 μM ifenprodil inhibits NMDA-EPSCs by 55.1±2.7% which is significantly less than inhibition of EPSCs at P7 (73.5±2.7%) (Brothwell *et al.* 2008). These facts suggest that the percentage of functional NR2D-containing NMDA receptors is lower in P7 rat dopaminergic neurons and its level increases from P7 to P14. These receptors may be triheteromeric NR1-NR2B-NR2D receptors. Since the 30 pS conductance of triheteromeric NMDARs contributes only a small component to the amplitude distribution when triheteromeric NR1-NR2B-NR2D NMDA receptors are co-expressed with diheteromeric NMDA receptors, the 30 pS conductance may not be obvious in amplitude distributions when the proportion of triheteromeric NMDA receptors is low. Similar results were reported in new-born rat hippocampal granule cells where a triheteromeric NR1-NR2B-NR2D receptor may also be expressed (Pina-Crespo & Gibb 2002). Although the amplitude distribution is well fitted with four components, the 30pS conductance component is only about 3.7%, suggesting a low level of trimers is expressed extrasynaptically at this age.

Table 4.5 A summary of NMDA receptor conductance from previous studies

Paper	Receptor type	Possible composition	Conductance
(Cheffings & Colquhoun 2000)	Recombinant	NR1a-NR2A-NR2D	20pS, 30pS, 40pS, 50pS
(Stern *et al.* 1992)	Recombinant	NR1-NR2A, NR1-NR2B,	50pS, 40pS
		NR1-NR2C	36pS, 19pS
	large cerebellar neurons in culture	NR1-NR2C	38pS, 18pS
(Wyllie *et al.* 1996)	recombinant	NR1-NR2D	35pS, 17pS
(Jones & Gibb 2005)	Dopaminergic neuron in P14 rat SNc	NR1-NR2B-NR2D	18pS, 30pS, 41pS, 54pS
(Brickley *et al.* 2003)	NR2D-\- P7-P10 mice	NR1,NR2B and NR2D subunits	20pS, 40pS and 50pS
		NR1, NR2B	50pS and 40pS
(Misra *et al.* 2000)	Golgi cells in P7-P10 mice	NR1, NR2B and NR2D	50pS, 39pS and 19pS
(Misra *et al.* 2000)	P6 rat cerebellar Purkinje cells	NR1-NR2D	20pS and 40pS
(Green & Gibb 2001)	In laminae I and II of the dorsal horn of the neonatal rat spinal cord	NR1, NR2B and NR2D	19pS, 32pS, 42pS, 53pS and 68pS
(Pina-Crespo & Gibb 2002)	in new-born rat hippocampal granule cells	NR1, NR2B and NR2D	17pS, 33pS, 42pS and 50pS
(Farrant *et al.* 1994)	Developing cerebellum	NR1, NR2A or NR2B, NR2C,	48pS, 40pS, 30pS, 18 pS

4.4.1.2 Comparison of macroscopic currents with previous studies

Similar concentration jump experiments were reported by Gotz *et al.* (1997). They applied 100 μM glutamate, 10 μM glycine and 10 μM CNQX to outside-out patches from P10-P15 rat dopaminergic neurons of SNc for 10 seconds to activate NMDAR-mediated macroscopic currents. The decay of the macroscopic currents was fitted with a mixture of two exponential components. The time constants of both the fast and slow component were 150 ms and 1049 ms, contributing 66% and 34% to total current amplitude. Inspection of my decay time constants for macroscopic currents with this previous report shows that there are no significant differences in time constants between the two studies (128 ms vs 150ms for the fast component and 1449 and 1049 for the slow component). However, the amplitude carried by the slow component (34% of total amplitude) in the study of Gotz *et al.* (1997) is much bigger than that in my experiment (8.5%). The discrepancy might be due to the different experimental conditions, such as glutamate concentration (1mM in my study and 100μM in Gotz's study), or concentration jump duration (1-4 ms in my study and 10 ms in Gotz's study). Another possibility is that more NR2D-containing NMDA receptors are expressed by P10-P15 rat dopaminergic neurons or more heterotrimeric NR1-NR2B-NR2D receptors (Brothwell *et al.* 2008).

I also compared my results with previous studies from recombinant NMDA receptors. Table 1.2 shows that the decay time courses for NR1a-NR2A NMDA receptors are in the range from 32 ms to 65 ms for the fast component and in the range from 202 ms to 312 ms for the slow component with the fast component, contributing about 90% of the amplitude and 10% for the slow decay component. The fast decay component for NR1a-NR2B is in the range from 95 ms to 250 ms, contributing in the range from 59% to 83% of the amplitude, while the slow component is in the range from 569ms to 1281 ms. A large range

of variation for NR1-NR2B NMDA receptors also was reported by Vicini *et al.* (1998). The NR1a/NR2D NMDA receptors have the slowest decay time course, being in the range of from 1700 ms to 5162 ms. In my experiments, the fast decay component is 128 ms, which is much slower than NR1a-NR2A NMDA receptors and is similar to NR1a-NR2B NMDA receptors. Consistent with their ifenprodil sensitivity, this suggests that NR2B subunit containing NMDA receptors are expressed by P7 rat dopaminergic neurons. However, the slow decay component (1484 ms) from my experiments is slower than that for most recombinant NR1a-NR2B NMDA receptors, suggesting that the NMDA receptors in dopaminergic neurons are not homogenous. Taken together with the results from experiments with ifenprodil (see chapter 5), these data are consistent with the idea that 25% of NMDA receptors in P7 dopaminergic neurons may be NR1-NR2B-NR2D triheteromeric NMDA receptors with 75% being NR1-NR2B diheteromeric NMDA receptors.

4.4.2 Similar NMDA receptor composition for synaptic and extrasynaptic sites in P7 rat dopaminergic neurons

As mentioned before, extrasynaptic NMDA receptors in P7 rat dopaminergic neurons are suggested to be a mixture of NR2B- and NR2D-containing NMDA receptors with around 75% of NMDA receptors being diheteromeric NMDA receptors and 25% being triheteromeric NMDA receptors. Since synaptic NMDA receptors are more important for excitatory synaptic transmission as well as synaptic plasticity, it is worthwhile to understand the composition of synaptic NMDA receptors in P7 rat dopaminergic neurons.

It also has been estimated that following the synaptic release of glutamate, the concentration in the synaptic cleft rises rapidly to around 1-10 mM and then decays with a

time constant of about 1ms (Clements *et al.* 1992; Barbour 2001). Therefore, in my experiments, the protocol of a 1-4 ms application of glutamate (1mM) to outside-out patches pulled from P7 rat dopaminergic neurons was used to activate a synaptic-like NMDA receptor current and the kinetics of these extrasynaptic NMDA receptors were compared with the kinetics of excitatory postsynaptic currents to see whether synaptic NMDA receptors have similar kinetics and hence infer whether they have similar subunit composition to extrasynaptic NMDA receptors.

It has been reported that the EPSC of P7 rat dopaminergic neurons is described by a mixture of two exponential components. At 30°C the fast and slow component time constant are 43ms and 164 ms, respectively (Brothwell *et al.* 2008). Assuming a Q10 of 3.5 the EPSC fast and slow components would be 164 ms and 494 ms at room temperature, respectively. The EPSC fast decay component is very similar to the fast decay for extrasynaptic NMDA receptors in my experiments, which is 128 ms. Also both fast components for EPSC and extrasynaptic NMDARs carry similar charges, being 56% and 53%, respectively. These facts suggest that synaptic NMDA receptors have similar composition to extrasynaptic NMDA receptors, which are NR2B- and NR2D- containing NMDA receptors. This conclusion is supported by the results of Brothwell *et al.* (2008). They used UBP141, a selective NMDA antagonist with 7-fold higher selectivity for NR2C and NR2D NMDA receptors than NR2A and NR2B (Morley *et al.* 2005). EPSC from P7 rat dopaminergic neurons were tested and an IC_{50} close to the K_D value for NR2C and NR2D-containing NMDA receptors was found. In addition, the EPSC in P7 rats was inhibited by 72% by 10 μM ifenprodil. Taken together the evidence suggests that NR2B- and NR2D- containing receptors are present at synapse and they might form triheteromeric NMDA receptors (Brothwell *et al.* 2008).

Comparing the slow components of the macroscopic current with the EPSC slow component (Brothwell *et al.* 2008), shows that the slow decay of the macroscopic current (1449 ms) is slower than that for the EPSC (494 ms). There may be two possible explanations for this discrepancy. First, the EPSCs in their studies only were recorded for 200ms or 1 second and the slow decay component was difficult to observe over this timescale. Second, the extrasynaptic sites might express a greater percentage of NR1-NR2B-NR2D NMDA receptors than synaptic sites, which could contribute to the slow decay component. In fact, Brothwell *et al.* (2008) estimate that for P7 neurons 53.4% of synaptic receptors are triheteromeric.

4.4.3 The absence of NR1-NR2D diheteromeric NMDA receptors at extrasynaptic sites

My ifenprodil experiments show that 10μM ifenprodil produced a 75% inhibition of NMDA-induced whole-cell current. Allowing for 90% maximum inhibition of recombinant NR1-NR2B whole-cell currents by 10μM ifenprodil, we can suggest there is about 16% of NMDA-induced whole-cell current which is carried by ifenprodil-insensitive NMDA receptors. Alternately, the ifenprodil insensitive current may be partly due to the presence of triheteromeric NR1-NR2B-NR2D receptors which are likely to have a maximum inhibition of about 50% (Hatton & Paoletti 2005)

In order to know if the ifenprodil-insensitive NMDA receptors are diheteromeric NMDA receptors or triheteromeric NMDA receptors, 1mM glutamate and 10 μM glycine were applied for 1ms to outside-out patches from dopaminergic neurons of SNc. The results show that there is no NR2D-like long deactivation time course, suggesting that diheteromeric NR1-NR2D receptors are absent on dopaminergic neurons or are expressed

at very low levels.

4.4.4 Extrasynaptic and synaptic NMDA receptors

The presence of NR2D-containing NMDA receptors at synaptic sites is interesting, suggesting that NR2D-containing NMDA receptors also mediate synaptic transmission and might contribute synaptic plasticity (Vicini & Rumbaugh 2000). Over the past few years several studies showed that NR2D-containing NMDA receptors are present at extrasynaptic sites rather than synaptic sites. 1-10 ms application of 1mM glutamate to outside-out patches from cerebellar Purkinje neurons produces an extremely slow NR2D-like channel deactivation. This was the first report of an NR1-NR2D-like NMDA receptor deactivation in mammalian neurons (Misra *et al.* 2000). Excitatory synaptic transmission to neonatal cerebellar Purkinje cells does not involve NMDA receptors. Therefore, the presence of NMDA receptors in these neurons is likely to be mainly extrasynaptic (Misra *et al.* 2000). In addition, single-channel recordings from outside-out patches from cerebellar Golgi cells (Misra *et al.* 2000; Brickley *et al.* 2003), dopaminergic neurons of SNc (Jones & Gibb 2005) and new-born rat hippocampal granule cells (Pina-Crespo & Gibb 2002) suggested that NR2D-containing NMDA receptors are present at extrasynaptic sites. In my experiments, the results suggested that diheteromeric NR1-NR2D NMDA receptors are absence or present at very low percentage. Instead the NR2D subunits might form triheteromeric NR1-NR2B-NR2D NMDA receptors. It is likely that the triheteromer is also present at synaptic sites of dopaminergic neurons (Brothwell *et al.* 2008). Although the kinetics of triheteromeric NR1-NR2B-NR2D NMDA receptors are still not known, allowing for the NR1-NR2D NMDA receptor's slow deactivation time course, we could suggest that the slow decay component of the synaptic current might be slowed down by the expression of NR2D subunits as these subunits have the highest

glutamate affinity and the slowly decaying synaptic currents may increase the Ca^{2+} influx into neurons, have reduced voltage-sensitivity of Mg^{2+} block and contribute to synaptic plasticity in a different way to NR2A and NR2B receptors.

In previous studies, it has been shown that NR2B subunits are widely expressed by the central nervous system in young animals and the level of protein and mRNA decreases during development (Monyer *et al.* 1994). In addition, NR2B subunits were found to be present both at synaptic and extrasynaptic sites (Misra *et al.* 2000; Brickley *et al.* 2003; Janssen *et al.* 2005; Jones & Gibb 2005; Brothwell *et al.* 2008). In brain slices from cortex and dentate gyrus, NMDAR antagonists for NR2B subunits reduce evoked synaptic NMDA currents more effectively than NMDA currents generated by spontaneously released glutamate (Stocca & Vicini 1998; Dalby & Mody 2003). In cerebellar Golgi and hippocampal pyramidal CA1 cells, a higher contribution of NR2B and NR2D at extrasynaptic sites has been indicated during high frequency trains but not during single stimuli when glutamate spillover is restricted (Cathala *et al.* 2000; Brickley *et al.* 2003; Lozovaya *et al.* 2004).

Furthermore, glutamate spillover from synapses on neighboring CA1 cells or glutamate released from astrocytes activates extrasynaptic NMDARs sensitive to NR2B antagonists (Fellin *et al.* 2004; Scimemi *et al.* 2004). The above observations in brain slices indicate that NR2B-containing receptors in adult neurons can be selectively activated at extrasynaptic sites. However, NR2B subunits do not exclusively segregate to extrasynaptic compartments when NR2A expression increases developmentally (Monyer *et al.* 1994). Instead, NR2B remains present in synapses of neurons coexpressing, for example, NR2A (Fujisawa & Aoki 2003; Kohr *et al.* 2003), allowing NR2B within synaptic NMDARs to bind to molecules important for NMDAR signaling or internalization, e.g., binding to CaMKII (Bayer *et al.* 2001), rasGRF1 (Krapivinsky *et al.* 2003; Li *et al.* 2006), or to the

clathrin adaptor protein AP-2 (Roche *et al.* 2001). Furthermore, NR2A is not exclusively synaptic but is also found extrasynaptically, even in cultured neurons of wildtypes (Li *et al.* 1998) (Mohrmann *et al.* 2002; Thomas *et al.* 2006). Taken together, the segregation of NR2A, NR2B and NR2D to extrasynaptic or synaptic sites is not absolute. Therefore, the extrasynaptic NMDA receptors might provide a receptor pool that can transport to synaptic sites for receptor renewal or as part of synaptic plasticity.

Chapter 5: Ifenprodil inhibition of NMDA-induced whole-cell currents in dopaminergic neurons

5.1 Summary

1. Whole-cell patch-clamp recordings were made from dopaminergic neurons to test ifenprodil sensitivity in dopaminerfic neurons of SNc to investigate if NR2B-containing NMDA receptors are expressed.

2. The whole-current NMDAR currents were evoked by bath application of 250 μM NMDA and 10 μM glycine. The coapplication of 1 μM and 10 μM ifenprodil significantly reduced the NMDA-induced current with IC_{50} of 0.32 μM, which is similar to recombinant NR2B-containing NMDA receptors. This result suggests that NR2B-containing NMDA receptors are expressed by P7 rat dopaminergic neurons.

3. The maximum effect of ifenprodil on P7 rat dopamine cells was predicted to be 78%, which is significantly smaller than that for recombinant NR1-NR2B NMDA receptors. Allowing for the triheteromeric NR2B-containing NMDA receptors have less ifeprodil maximum block, we suggest that a mixture population of NR1-NR2B and NR1-NR2B-NR2D NMDARs are expressed.

5.2 Introduction

Ifenprodil is an allosteric NMDA receptor antagonist with chemical structure unlike any of the common competitive or un-competitive antagonists. High affinity inhibition by ifenprodil depends critically on the presence of an NR2B subunit. It has significant affinity for NR1 – NR2B receptors (IC_{50} = 0.29 μM), that is about 400-fold higher than NR1-2A, NR1-NR2C or NR1-NR2D receptors (Williams 1993; Williams 1995). Ifenprodil inhibits NR1-NR2B recombinant NMDAR currents with a maximal inhibition of 91% (Williams 1993; Mott *et al.* 1998; Hatton & Paoletti 2005).

Since the NR2B subunit can be coimmuniprecipitated with other NR2 subunits (Sheng *et al.* 1994; Chazot & Stephenson 1997), such as with NR2D in P7 rat dopamine cells of SNc (Dunah *et al.* 1998), it is important to know the NR1-NR2B-NR2D sensitivity to ifenprodil. Hattton and Paoletti (2005) used an approach combining mutagenesis and pharmacology which permits isolation of triheteromeric receptor populations when three subunits are expressed together in oocytes and they suggested that triheteromeric NR1-NR2A-NR2B NMDARs have similar ifenprodil sensitivity to diheteromeric NR1-NR2B NMDARs but they have a smaller maximum block (about 50%) than diheteromeric NR1-NR2B receptors (91%).

Ifenprodil, elipodril and some newer derivatives were found to be neuroprotective in whole animal models of cerebral ischemia (Gotti *et al.* 1988; Di *et al.* 1997) and traumatic brain injury (Zeevalk & Nicklas 1990; Toulmond *et al.* 1993; Okiyama *et al.* 1997; Dempsey *et al.* 2000), effects that may be due to blockade of NMDA receptors. These antagonists were also protective against glutamate- or hypoxia-induced toxicity in cultured neurons (Shalaby

et al. 1992; Tamura *et al.* 1993; Fischer *et al.* 1997; Hess *et al.* 1998) and in the retina (Zeevalk & Nicklas 1990). Thus, the ifenprodil site on NMDA receptors, like glutamate, glycine, MK-801, and possibly other sites, represents a target for neuroprotective agents, that could be used, for example after ischemic stroke. Several characteristics of the ifenprodil-site antagonists, including their subunit-selectivity, use-dependence, and mechanism of action make them particularly attractive candidates as potential neuroprotectants. NMDA antagonists are also potential therapeutic agents for a number of other diseases or pathologies. For example, ifenprodil can reduce Parkinsonian symptoms in animal models of Parkinson's disease (Mitchell & Carroll 1997; Blanchet *et al.* 1999; Nash *et al.* 1999) and a possible use for NMDA receptor antagonists as antidepressants also has been noted (Layer *et al.* 1995).

Previous studies suggested NR2B- and NR2D-containing NMDARs are expressed by P7 rat dopamine cells and they might form triheteromeric NR1-NR2B-NR2D NMDARs (Dunah *et al.* 1996; Dunah *et al.* 1998; Jones & Gibb 2005). I used whole-cell patch-clamp recordings to test ifenprodil sensitivity in dopaminergic cells of SNc of P7 rat to investigate if NR2B-containing NMDARs are expressed and possibly if the triheteromeric complex is expressed. My results are consistent with previous studies (Dunah *et al.* 1998; Jones & Gibb 2005), suggesting that diheteromeric NR1-NR2B and triheteromeric NR1-NR2B-NR2D NMDA receptors are present on dopamine cells of SNc.

5.3 Results

All experiments were carried out upon dopaminergic neurons of substantia nigra pars compacta in coronal brain slices from P7 rats. Dopaminergic neurons were voltage-clamped at –60mV in the presence of 100nM tetrodotoxin (TTX) to block action potentials in the slice and 1μM strychnine to block glycine receptors.

As mentioned in the introductory section of this thesis, ifenprodil potentiates NMDA-induced whole-cell currents when a low concentration of NMDA is used, because ifenprodil binding increases the receptor affinity at the glutamate-site for agonists, such as NMDA or glutamate (Kew *et al.* 1996). Thus, in my experiments, a saturating concentration (250μM) of NMDA was used to activate the whole-cell NMDA current without the complication of changes in agonist affinity caused by ifenprodil.

5.3.1 NMDA receptors in SNc dopaminergic neurons contain NR2B subunits

To determine the possible contribution of NR2B-containing receptors to the NMDA evoked response, I tested the effect of 1μM and 10μM ifenprodil on NMDA-induced whole-cell currents in 12 dopaminergic neurons. As shown in Figure 5.1, the first response was produced by bath application of 250μM NMDA and 10μM glycine, then co-application of 1μM followed by 10μM ifenprodil significantly reduced the NMDA-induced current. The second and third responses are for 1μM ifenprodil and the fourth and fifth responses are for 10μM ifenprodil, respectively. The first and second responses displayed a sharp peak on application of NMDA followed by a rapid decline or desensitization. However, the peak is absent for the rest of the responses. The details of whole-cell recording are presented in Table 5.1. 59.2 ± 3.1% (n=8) of the NMDA current was blocked by 1μM ifenprodil while 10μM ifenprodil caused 75.7±1.9% (n=12) inhibition (Figure 5.2).

In order to characterize the NMDA receptor sensitivity to ifenprodil, the observed % inhibition was matched to an ifenprodil concentration-inhibition curve constructed

according to the Hill-equation using the Solver function in Microsoft Excel. At -60mV, in the presence of 250μM NMDA and 10μM glycine, the IC_{50} for ifenprodil was estimated to be 0.32μM (n=12) and the maximum effect of ifenprodil was predicted to be 78% (Figure 5.3).

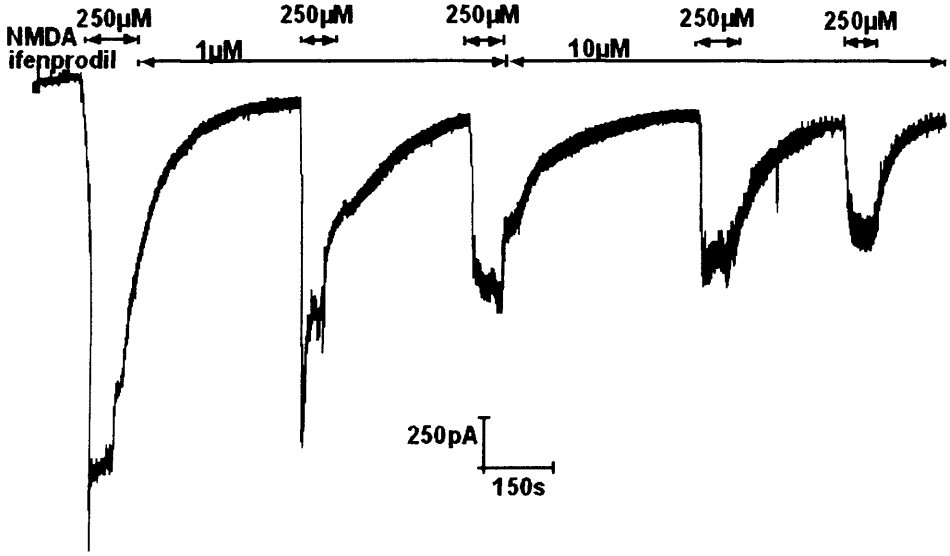

Figure 5.1 Ifenprodil inhibition of NMDA receptors on SNc dopaminergic neurons

An example NMDA-mediated current trace from a whole-cell patch-clamp recording from an SNc dopaminergic neuron. The dopaminergic neuron was clamped at -60mV and bath application of 250μM of NMDA (together with 10μM of glycine) evoked an inward current. The co-application of 1μM and 10μM of ifenprodil caused a significant inhibition of the NMDA-evoked whole-cell current. The bars above the current trace show the time of application of individual solutions.

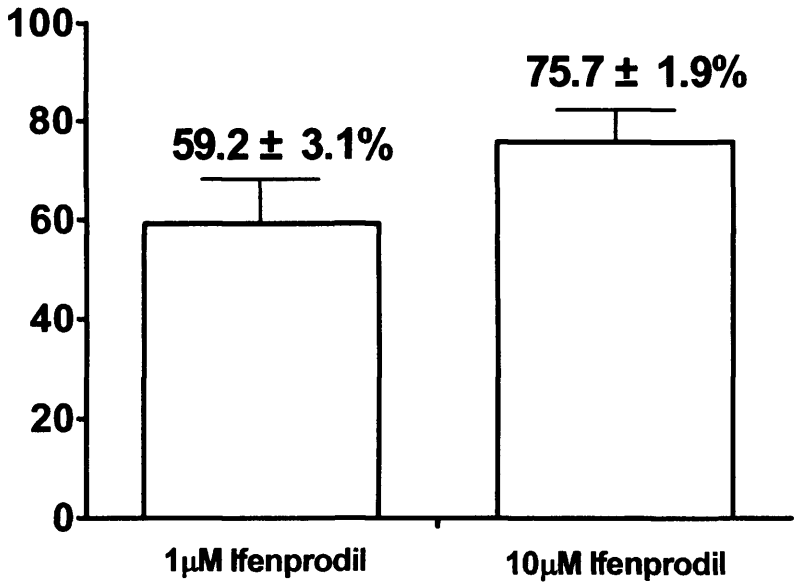

Figure 5.2 Summary of results with ifenprodil inhibition

This figure shows a significant inhibition of NMDA-mediated whole-cell current with both 1μM and 10μM ifenprodil. 59.2±3.1% (n=8) of NMDA current was blocked by 1μM of ifenprodil while 10μM of ifenprodil caused 75.7±1.9% (n=12).

.

	NMDA 250μM	1μM ifenprodil + NMDA 250μM	% control	10μM ifenprodil + NMDA 250μM	% control	Rs (MΩ)
	1330	735	55.3%	339	25.5%	23.2
	1030			253	24.6%	21
	1500	609	40.6%			22
	2114.7			353	16.7%	16.2
	1375	609	44.3%	459	33.4%	17.5
	775	362	46.8%	265	34.2%	21.6
	2064	577	28%	270.3	13.1%	15.3
	2226	757	34.1%	460	20.7%	12.8
	1877			531.2	28.3%	21
	1649			358	21.7%	16.9
	1119			220	19.7%	24.2
	1985	887.2	44.7%	596	30%	15.6
	1879	607	32.3%	453	24.1%	13.9
Count	13	8	8	12	12	13
Average (pA)	1610	643	41%	380	24%	19
S.E.	128	55	3%	35	2%	1

Table 5.1 Details of whole-cell patch-clamp recording to test the effect of ifenprodil on NMDARs of dopaminergic neurons

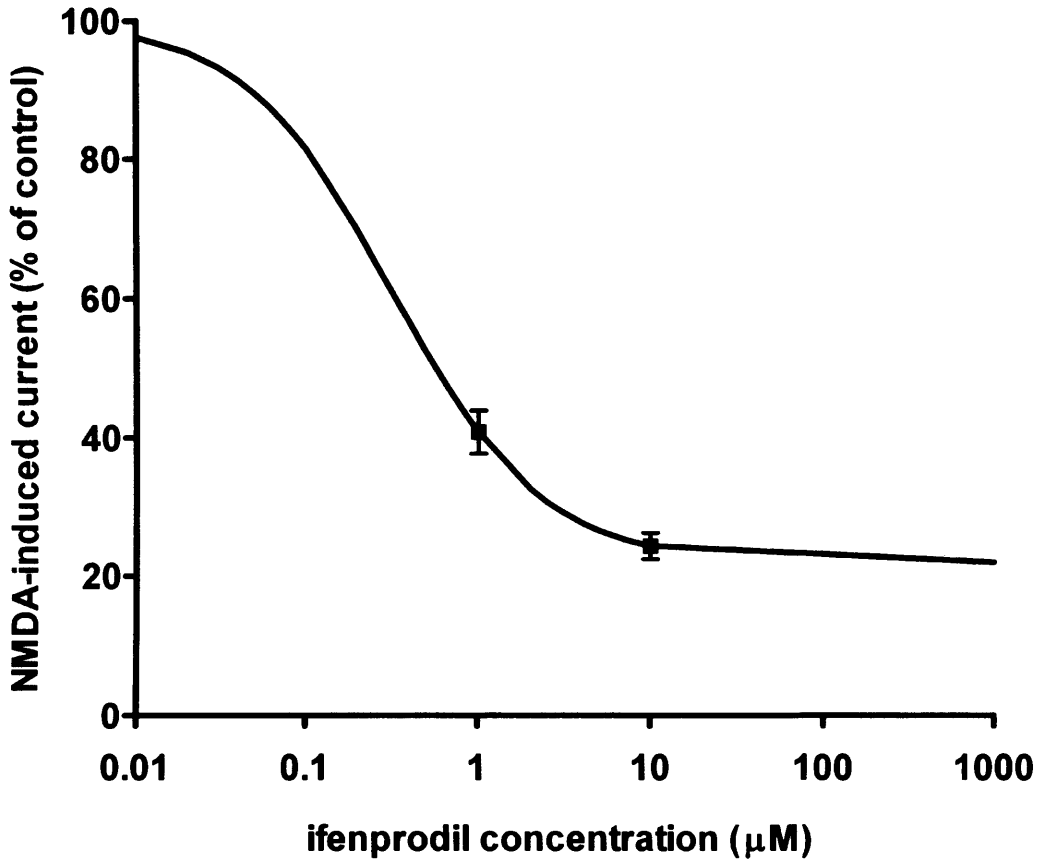

Figure 5.3 Concentration-inhibition curve of ifenprodil inhibition of NMDA receptors

Concentration inhibition curve was obtained for ifenprodil inhibition of NMDA receptors to dopamine cells from P7 rat SNc. The NMDA-induced whole-cell currents were evoked by 250μM NMDA and 10μM glycine. And the coapplocation of 1μM and 10μM ifenprodil significantly reduced the whole-cell current. The IC_{50} for NMDARs on dopaminergic neurons is estimated to be 0.32μM.

5.4 Discussion

To assess the contribution of NR2B-containing NMDARs to macroscopic NMDA evoked currents, we have made use of the fact that ifenprodil selectively blocks recombinant NMDARs assembled with NR1-NR2B subunits (Williams 1993). It has been suggested that dopaminergic neurons in SNc express both NR2B and NR2D subunits (Monyer *et al.* 1994; Standaert *et al.* 1994; Standaert DG 1994; Dunah *et al.* 1998; Albers *et al.* 1999; Chatha *et al.* 2000; Jones & Gibb 2005). As indicated by previous studies, at concentrations of 1μM and 10μM, ifenprodil has little effect on recombinant receptor assemblies composed of NR1-NR2A, NR1-NR2C or NR1-NR2D (Williams 1993; Williams 1995) and on native NR1-NR2D receptors (Momiyama *et al.* 1996). Therefore, ifenprodil was used to confirm the presence of NR2B subunits and to also quantify the contribution of NR2B-containing receptors to the whole-cell NMDAR current.

Previous studies have shown that ifenprodil produces a maximal inhibition of 92% at pH=7.3 for recombinant NR1-NR2B receptors, with IC_{50} values of 0.34μM (Williams 1993), 0.22-0.32μM (Avenet *et al.* 1997), 0.17μM (Chazot & Stephenson 1997; Mott *et al.* 1998; Misra *et al.* 2000), when tested against NMDA- or glutamate- evoked responses. Inspection of the data presented here reveals that the IC_{50} from my experiments is in good agreement with previous data. The predicted maximum block by ifenprodil, however, is 78%, which is significantly smaller than that for recombinant NR1-NR2B NMDA receptors. A possible explanation for this inconsistency is that dopaminergic neurons on dopaminergic neurons express NR1-NR2B diheteromeric receptors and NR1-NR2B-NR2D triheteromeric NMDA receptors. Since the diheteromeric or triheteromeric NMDA receptors have similar ifenprodil sensitivity but the triheteromeric NMDA receptors reduced maximal inhibition (about 50%) (Hatton & Paoletti 2005), NMDA-induced

whole-cell currents from dopaminergic neurons would be expected to have the same ifenprodil IC_{50} as recombinant NR1-NR2B NMDARs. However, it can be hypothesized that the whole-cell current has less maximum block by ifenprodil because of the presence of triheteromeric NMDARs. Because the ifenprodil maximum effect on triheteromeric NR2B-containing NMDARs is approximately 50% (Hatton & Paoletti 2005), a mixture of expression of two kinds of NMDARs can explain the reduced maximum inhibition by ifenprodil in dopaminergic neurons.

The maximum block by ifenprodil on dopaminergic neurons could suggest that 14% of the NMDA-induced whole-cell currents were produced by ifenprodil-insensitive NMDA receptors (e.g. NR1-NR2D), assuming the other 86% of current is produced by diheteromeric NR1-NR2B receptors. One possibility is that all the NMDA current may be produced by a mixture of NR1-NR2B and NR1-NR2B-NR2D receptors. Assuming this is the case, these data suggest there are 75% NR1-NR2B and 25% NR1-NR2B-NR2D receptors in P7 dopamine neurons. The Mg^{2+} sensitivity of the residual currents in the presence of 10 μM ifenprodil (see Mg^{2+} block; Chapter 3) show that the ifenprodil-insensitive NMDA current has less Mg^{2+} sensitivity than that for the normal NMDA-induced before application of 10 μM ifenprodil. The Mg^{2+} IC_{50} values after application of 10μM ifenprodil at -100mV, -80mV and -60mV were 25.1μM, 73.2μM and 229.2μM, respectively. These IC50 values are in the range of Mg^{2+} sensitivity for NR2D-containing NMDARs (Table 3.3). There are two possible explanations for the decrease in Mg^{2+} sensitivity after the application of ifenprodil. First, diheteromeric NR1-NR2D NMDARs might be present on dopaminergic neurons, because NR1-NR2D NMDARs have less Mg^{2+} sensitivity than NR1-NR2B NMDARs (Monyer *et al.* 1994; Kuner & Schoepfer 1996; Hatton & Paoletti 2005). After causing 91% inhibition of NR1-NR2B NMDA receptors, a large proportion of the residual current would be carried

by the NR1-NR2D NMDA receptors, as the residual ifenprodil-insensitive NMDA currents are less Mg^{2+} sensitive. By the same principle, a second explanation could be that after causing 90% inhibition of diheteromeric NR1-NR2B receptors and 50% inhibition of triheteromeric NR1-NR2B-NR2D receptors, the residual NR1-NR2B-NR2D current blocked by ifenprodil, has reduced Mg^{2+} sensitivity. However, the Mg^{2+} sensitivity of recombinant triheteromeric receptors has not been investigated in detail. To investigate the identity of the receptor by a different approach, concentration jump experiments were made on NMDARs of dopaminergic neurons to look at the deactivation and desensitization time course for these NMDARs to investigate which NMDA subtypes might be expressed by dopamine neurons (see concentration jump; chapter 4).

Chapter 6: Memantine inhibition of NMDA-induced whole-cell currents in dopamine neurons.

6.1 Summary

1. Whole-cell patch-clamp recording was used to characterize the voltage-dependence of memantine block of NMDA receptors of P7 rat SNc. NMDA receptor-mediated whole-cell currents were evoked by bath-application of 100 μM NMDA and 10 μM glycine. Coapplication of 5 μM and 50 μM memantine with NMDA and glycine significantly reduced the NMDA-mediated whole cell currents at the holding membrane potential of -60 mV.

2. Two memantine block models were used to characterize the voltage-dependence of memantine block: a sequential block model and a trapping block model. Both models estimate the same voltage-dependent parameter, δ, being 0.55-0.6. Compared with δ for external Mg^{2+} (0.84), this result suggested that NMDA receptors undergo a weaker voltage-dependent block by memantine than by external Mg^{2+}.

3. Memantine and Mg^{2+} are both open channel blockers for NMDA receptors and they might compete for binding. In order to investigate competitive block between memantine and external Mg^{2+}, voltage-ramp experiments were carried out in the presence of 1mM Mg^{2+} and 5 μM memantine or 50 μM memantine to obtain the

NMDA I-V relationships.

4. Two new models were developed to investigate competitive block between external Mg^{2+} and memantine. Fitting NMDA I-V relationships with these models shows that Mg^{2+} and memantine do not compete for binding in the NMDA receptor channel.

6.2 Introduction

Memantine is an uncompetitive NMDA antagonist. It was first synthesized in the 1960s by a researcher at Eli Lilly in order to prepare an agent to lower elevated blood sugar level, and was found to affect the central nervous system (CNS) in 1970s (Parsons *et al.* 1999). In 1989, memantine was found to inhibit NMDA receptors with an IC_{50} of about 1μM at –60mV (Kornhuber *et al.* 1989; Chen & Lipton 1997). In addition, high concentrations of memantine (10-500 μM) block many CNS targets, such as serotonin and dopamine uptake, nicotinic acetylcholine receptors, serotonin receptors and sigma-1 receptors (Danysz *et al.* 1997).

Memantine's effects on NMDARs have been a focus of attention because memantine was recently approved by the European Union and the US FDA for use in moderate to severe Alzheimer's disease (Lipton 2006). In addition, memantine might have other potential therapeutic utility for acute and chronic neurodegenetative diseases including stroke, acute trauma, Parkinson's disease, and Huntington's disease (Parsons *et al.* 1999; Beister *et al.* 2004; Lipton 2006).

It has been suggested that memantine is an NMDAR open channel blocker, which only binds when the NMDAR channel is open. In addition, Mg^{2+} application decreases the

apparent affinity of memantine for NMDA receptors (Sobolevsky *et al.* 1998) and the mutation of "N-site" asparagines (residues on the M2 region of NR1 and NR2 subunits that are crucial for Mg^{2+} block) also affect memantine block (Kashiwagi *et al.* 2002) which suggested that the binding site for memantine overlaps with the Mg^{2+} binding site. At physiological pH, memantine has +1 positive charge, which allows memantine to block NMDA channels in a voltage dependent manner.

Compared with other NMDA receptor open channel blockers, such as MK-801, phencyclidine and ketamine, memantine is well tolerated clinically (Lipton 2006). This may be due to memantine's blocking properties. First, memantine inhibits NMDA receptors with higher affinity when the agonist concentration is higher and has less effect at low concentrations of agonist (Chen & Lipton 1997; Sobolevsky & Koshelev 1998; Lipton 2006). This property allows memantine to have the potential to selectively block NMDA receptors at higher (pathological) levels of glutamate release. Meanwhile, it has no or less effect at normal levels of glutamate release for synaptic transmission. Second, memantine has a moderate unbinding rate for NMDA receptors; too slow an off-rate such as Mk-801 causes the drug to accumulate in the channel, interfering with normal neurotransmission. In contrast, too rapid an off-rate (such as Mg^{2+}) causes an inefficient blockade, especially with membrane depolarization, which rapidly relieves the block of positively charged Mg^{2+}.

Most studies of memantine block have been performed in the absence of Mg^{2+}. It is important to carefully examine the competition between external Mg^{2+} and memantine. Since external Mg^{2+} and memantine both bind in the NMDA receptor channel, then Mg^{2+} and memantine must compete for binding. Therefore, in my experiments, whole-cell patch-clamping recording was used to study voltage-dependent memantine block of

NMDARs in dopaminergic neurons in SNc and the competition between external Mg^{2+} and memantine on NMDA receptors in these neurons was considered.

6.3 Models and curve fitting methods

So far, there are two main memantine block models which have been developed (Sobolevsky *et al.* 1998; Lipton 2006) to explain memantine block of NMDA receptors: a sequential blocking model [Scheme 6.1b] and a trapping block model [Scheme 6.1a]. The main difference between these two models is that in the sequential block model [Scheme 6.1b], memantine as an open channel blocker can only block the NMDA receptor channel open state (AR*) and the binding prevents NMDA channel closure and the channel only can close once memantine unbinds from the NMDA channel. In the trapping block model, however, agonist can unbind before memantine unbinds from the NMDA receptor; the NMDA receptor can close and trap memantine in the NMDAR channel. Then, the trapped memantine needs agonist help to leave the NMDA channel.

In order to investigate the competition between external Mg^{2+} and memantine for block of NMDAR channels, three main models were developed in my experiments to explain memantine block according to the original sequential block and trapping block models: a competition sequential block model [Scheme 6.2], a competition trapping block model [Scheme 6.3] and a competition sequential block model with two agonist binding sites [Scheme 6.4].

It has been shown that similar to memantine's effects on NMDA receptors, external Mg^{2+} is an open channel blocker and blocks NMDA receptors in a voltage dependent manner (Nowak *et al.* 1984; Mayer & Westbrook 1985; Monyer *et al.* 1994). Therefore, in these

new models, external Mg^{2+} was introduced into the original memantine block model and competition with memantine to block NMDA channels in the open state (AR*) was investigated.

Furthermore, in order to investigate whether a desensitized state and whether the number of agonist binding sites affects memantine block, Mg^{2+} block models with an NMDA receptor desensitized state [Scheme 6.2b, 6.3b, 6.4b] and models with two agonist binding sites [Scheme 6.4a, 6.4b] were developed.

In order to use these models to fit my experimental NMDAR I-V relations, the equations for calculating channel open probability and the whole-cell currents were obtained and are shown below.

(a)

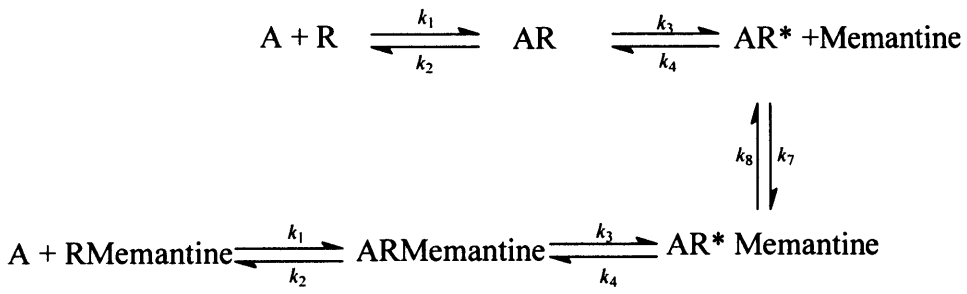

(b)

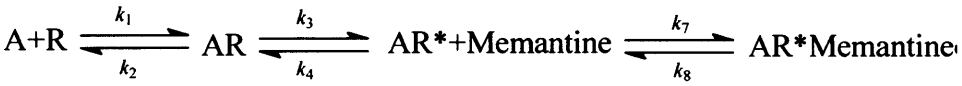

Scheme 6.1. Schematic models of channel blockade of NMDARs by memantine.

(a) Trapping block model: an NMDA receptor (R) must bind agonist molecule (A) to reach state AR. Subsequently, multiple structural rearrangements lead to channel opening (AR*). The blocker molecule then can bind in the open channel (AR*Memantine); the channel can close on the blocker (ARMemantine); and agonist can unbind, trapping the blocker (RMemantine).

(b) Sequential block model: because blocker binding prevents the channel closure conformational change, ARMemantine and Rmemantine states are not accessible in this blocking model.

(a)

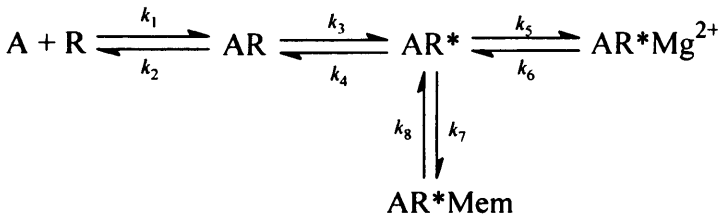

(b)

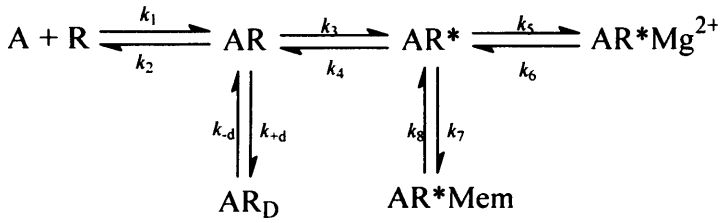

Scheme 6.2. Schematic models of competition block between Mg^{2+} and memantine

(a) Competition sequential block model: Mg^{2+} can compete for the NMDA channel open state with memantine (AR^*Mg^{2+}). In this model, Mg^{2+} binding prevents channel closure; the channel can not close and agonist can not unbind until Mg^{2+} unbinds from the NMDA channel.

(b) In order to understand the effect of a desensitizated state on channel open probability and voltage dependent block by Mg^{2+} and memantine, NMDA receptor desensitization is taken into account by addition of a desensitized state (AR_D) to the model.

(a)

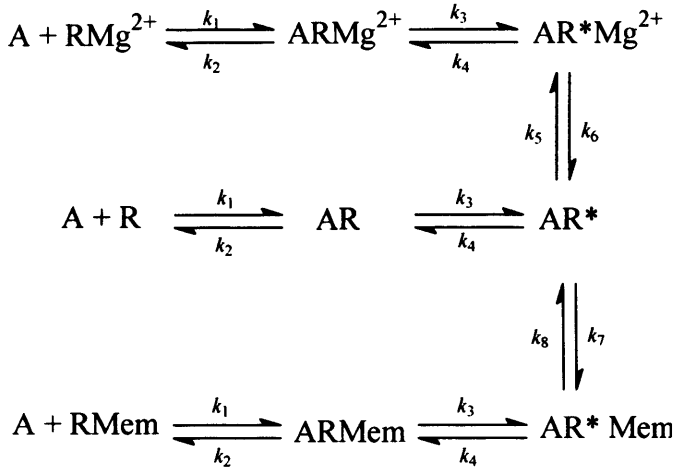

(b)

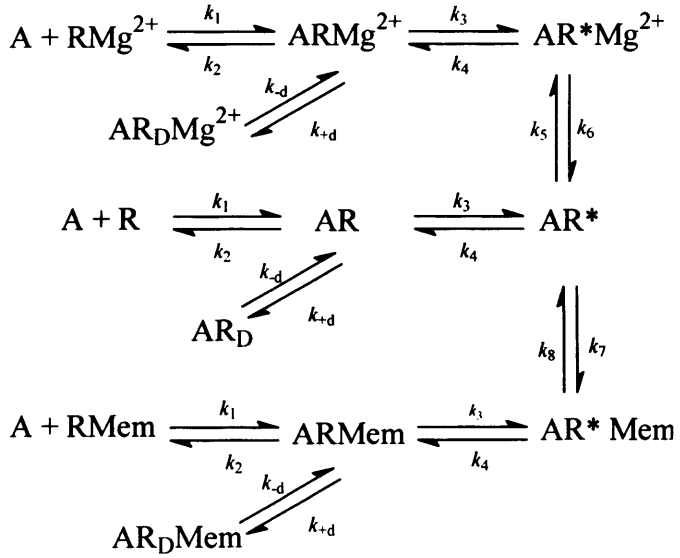

Scheme 6.3. Schematic models of competition trapping block between Mg^{2+} and memantine

(a) Competition trapping block model: In this trapping block model, Mg^{2+} and memantine can compete for the NMDA channel open state and they can produce a trapping block (RMg^{2+}, $ARMg^{2+}$, AR, ARMem, RMem) where the blockers can not leave the NMDA channel without agonist assistance and with the channel in the open state.

(b) Competition trapping block model with desensitized state. In this competition trapping block model, three desensitizated states were introduced into the original trapping block model in order to investigate whether desensitized states have any effect on voltage dependent block by memantine and Mg^{2+}.

(a)

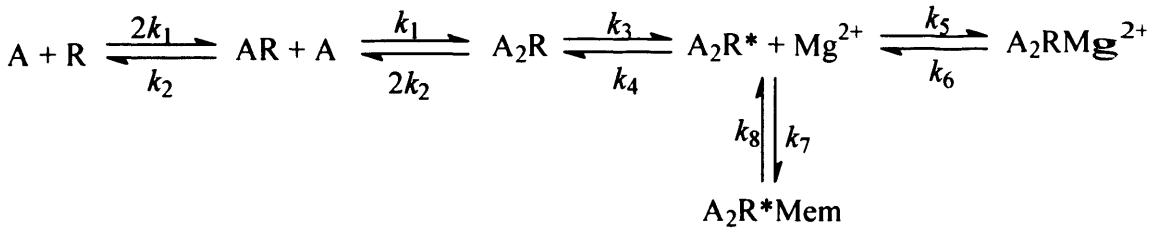

(b)

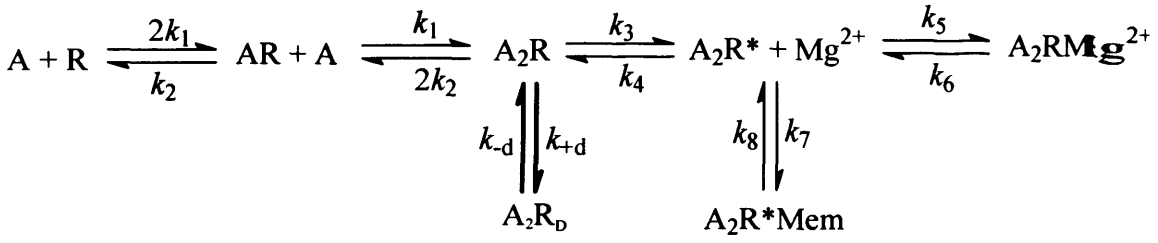

Scheme 6.4. Schematic models of competition sequential block model with two agonist binding sites

Competition sequential block model: in order to investigate whether the number of agonist binding sites will affect the quantification of voltage dependent block by Mg^{2+} and memantine, models with two agonist binding sites were developed and model (b) includes NMDA receptor desensitization (A_2R_D).

For the **competition sequential block model without desensitization** [Scheme 6.2], NMDA channel open probability is expressed by equation 1.

$$P_{open} = \frac{[AR^*]}{[R_{Total}]} = \frac{1}{\frac{k_2}{k_1}\frac{k_4}{k_3}\frac{1}{[A]} + \frac{k_4}{k_3} + 1 + \frac{k_5}{k_6}[Mg^{2+}] + \frac{k_7}{k_8}[Mem]} \quad [1]$$

All the parameters are defined on section 3.1.1.1.

The voltage dependence of Mg^{2+} and memantine block is expressed as relation 2, 3:

$$\frac{k_6}{k_5} = K_{Mg}(0mV)\exp(\frac{\delta_{Mg}VFz}{RT}) \quad [2]$$

$$\frac{k_8}{k_7} = K_{Mem}(0mV)\exp(\frac{\delta_{mem}VFz}{RT}) \quad [3]$$

All the parameters are defined on the section 3.1.1.1.

Thus, the current at any particular voltage is described by equation 4:

$$I_B = N(V_h - V_{rev})\gamma P_{open}$$

$$= \frac{\gamma(V_h - V_{rev})N}{\frac{k_2}{k_1}\frac{k_4}{k_3}\frac{1}{[A]} + \frac{k_4}{k_3} + 1 + \frac{[Mg^{2+}]}{K_{Mg2+}(0mV)\exp(\frac{V\delta^{Mg}zF}{RT})} + \frac{[Mem]}{K_{Mem}(0mV)\exp(\frac{V\delta^{Mem}zF}{RT})}} \quad [4]$$

All the parameters are defined on section 3.1.1.1.

For the **competition sequential block model with a desensitized state** [Scheme 6.2.b], NMDA channel open probability is expressed by equation 5.

$$P_{open} = \frac{[AR^*]}{[R_{Total}]} = \frac{1}{\frac{k_2}{k_1}\frac{k_4}{k_3}\frac{1}{[A]} + \frac{k_4}{k_3} + 1 + \frac{k_{+d}}{k_{-d}}\frac{k_4}{k_3} + \frac{k_5}{k_6}[Mg^{2+}] + \frac{k_7}{k_8}[Mem]} \quad [5]$$

All the parameters are defined on the section 3.1.1.1.

The voltage dependence of Mg^{2+} and memantine block is expressed by relation 2, 3.

Thus, the current at any particular voltage is described by equation 6:

$$I_B = N(V_h - V_{rev})\gamma P_{open} \quad [6]$$

$$= \frac{\gamma(V_h - V_{rev})N}{\frac{k_2}{k_1}\frac{k_4}{k_3}\frac{1}{[A]} + \frac{k_4}{k_3} + 1 + \frac{k_{+d}}{k_{-d}}\frac{k_4}{k_3} + \frac{[Mg^{2+}]}{K_{Mg2+}(0mV)\exp(\frac{V\delta^{Mg}zF}{RT})} + \frac{[Mem]}{K_{Mem}(0mV)\exp(\frac{V\delta^{Mem}zF}{RT})}}$$

All the parameters are defined on the section 3.1.1.1.

For the **competition trapping block model without a desensitized state** [Scheme 6.3.a], NMDA channel open probability is expressed by equation 7.

$$P_{open} = \frac{[AR^*]}{[R_{Total}]} = \frac{1}{(\frac{k_2}{k_1}\frac{k_4}{k_3}\frac{1}{[A]} + \frac{k_4}{k_3} + 1) \quad (\frac{k_5}{k_6}[Mg^{2+}] + \frac{k_7}{k_8}[Mem])} \quad [7]$$

All the parameters are defined on the section 3.1.1.1.

The voltage dependence of Mg^{2+} and memantine block is expressed by relation 2, 3.

Thus, the current at any particular voltage is described by equation 8:

$$I_B = N(V_h - V_{rev})\gamma P_{open} \qquad [8]$$

$$= \frac{\gamma(V_h - V_{rev})N}{(\frac{k_2}{k_1}\frac{k_4}{k_3}\frac{1}{[A]} + \frac{k_4}{k_3} + 1)\ (\frac{[Mg^{2+}]}{K_{Mg2+}(0mV)\exp(\frac{V\delta^{Mg}zF}{RT})} + \frac{[Mem]}{K_{Mem}(0mV)\exp(\frac{V\delta^{Mem}zF}{RT})})}$$

All the parameters are defined on the section 3.1.1.1.

For the **competition trapping block model with a desensitized state** [Scheme 6.3b], NMDA channel open probability is expressed by equation 9.

$$P_{open} = \frac{[AR^*]}{[R_{Total}]} = \frac{1}{(\frac{k_2}{k_1}\frac{k_4}{k_3}\frac{1}{[A]} + \frac{k_4}{k_3} + 1 + \frac{k_{+d}}{k_{-d}}\frac{k_4}{k_3})\ (1 + \frac{k_5}{k_6}[Mg^{2+}] + \frac{k_7}{k_8}[Mem])} \qquad [9]$$

All the parameters are defined on the section 3.1.1.1.

The voltage dependence of Mg^{2+} and memantine block is expressed by relation 2, 3.

Thus, the current at any particular voltage is described by equation 10:

$$I_B = N(V_h - V_{rev})\gamma P_{open} \qquad [10]$$

$$= \frac{\gamma(V_h - V_{rev})N}{(\frac{k_2}{k_1}\frac{k_4}{k_3}\frac{1}{[A]} + \frac{k_4}{k_3} + 1 + \frac{k_{+d}}{k_{-d}}\frac{k_4}{k_3})\ (1 + \frac{[Mg^{2+}]}{K_{Mg2+}(0mV)\exp(\frac{V\delta^{Mg}zF}{RT})} + \frac{[Mem]}{K_{Mem}(0mV)\exp(\frac{V\delta^{Mem}zF}{RT})})}$$

All the parameters are defined on the section 3.1.1.1.

For the **competition sequential block model with one agonist binding site** [Scheme 6.4a], NMDA channel open probability is expressed by equation 11.

$$P_{open} = \frac{[AR^*]}{[R_{Total}]} = \frac{1}{\frac{k_2}{k_1}\frac{k_4}{k_3}\frac{k_2'}{k_1'}\frac{1}{[A]^2} + \frac{k_4}{k_3}\frac{k_2'}{k_1'}\frac{1}{[A]} + \frac{k_4}{k_3} + 1 + \frac{k_5}{k_6}[Mg^{2+}] + \frac{k_7}{k_8}[Mem]} \qquad [11]$$

All the parameters are defined on the section 3.1.1.1. $k_2'=2k_2$ and $k_1'=2k_1$.

The voltage dependence of Mg^{2+} and memantine block is expressed by relation2, 3.

Thus, the current at any particular voltage is described by equation 12:

$$I_B = N(V_h - V_{rev})\gamma P_{open} \qquad [12]$$

$$= \frac{\gamma(V_h - V_{rev})N}{\frac{k_2}{k_1}\frac{k_4}{k_3}\frac{k_2'}{k_1'}\frac{1}{[A]^2} + \frac{k_4}{k_3}\frac{k_2'}{k_1'}\frac{1}{[A]} + \frac{k_4}{k_3} + 1 + \frac{[Mg^{2+}]}{K_{Mg2+}(0mV)\exp(\frac{V\delta^{Mg}zF}{RT})} + \frac{[Mem]}{K_{Mem}(0mV)\exp(\frac{V\delta^{Mem}zF}{RT})}}$$

All the parameters are defined on the section 3.1.1.1.

For the **competition sequential block model with two agonist binding sites and desensitized state** [Scheme 6.4b], NMDA channel open probability is expressed by equation 13.

$$P_{open} = \frac{[AR^*]}{[R_{Total}]} = \frac{1}{\frac{k_2}{k_1}\frac{k_4}{k_3}\frac{k_2'}{k_1'}\frac{1}{[A]^2} + \frac{k_4}{k_3}\frac{k_2'}{k_1'}\frac{1}{[A]} + \frac{k_4}{k_3} + \frac{k_4}{k_3}\frac{k_{d+}}{k_{d-}} + 1 + \frac{k_5}{k_6}[Mg^{2+}] + \frac{k_7}{k_8}[Mem]} \quad [13]$$

All the parameters are defined on the section 3.1.1.1.

The voltage dependence of Mg^{2+} and memantine block is expressed by relation2, 3.

Thus, the current at any particular voltage is described by equation 14:

$$I_B = N(V_h - V_{rev})\gamma P_{open} \quad [14]$$

$$= \frac{\gamma(V_h - V_{rev})N}{\frac{k_2}{k_1}\frac{k_4}{k_3}\frac{k_2'}{k_1'}\frac{1}{[A]^2} + \frac{k_4}{k_3}\frac{k_2'}{k_1'}\frac{1}{[A]} + \frac{k_4}{k_3} + \frac{k_4}{k_3}\times\frac{k_{+d}}{k_{-d}} + 1 + \frac{[Mg^{2+}]}{K_{Mg2+}(0mV)\exp(\frac{V\delta^{Mg}zF}{RT})} + \frac{[Mem]}{K_{Mem}(0mV)\exp(\frac{V\delta^{Mem}zF}{RT})}}$$

All the parameters are defined on the section 3.1.1.1. k_2'=2k_2 and k_1'=2k_1.

During the optimization of the fit to block by Mg^{2+} and memantine, the number of NMDA receptors, N, reversal potential, V_{rev}, K_{Mg}^{2+}(0mV), K_{Mem}(0mV), $\delta_{Mg^{2+}}$ and δ_{mem} were allowed to vary. All values of parameters are shown in Table 6.1. The value of k_2/k_1 was set to be 10 based on previous reports (Benveniste & Mayer 1991; Sobolevsky *et al.* 1998). The values of k_4/k_3 and k_{+d}/k_{-d} are fixed to be 2 and 5, respectively, based on a previous study (Lester & Jahr 1992).

6.4 Results

In all memantine experiments, 10μM glycine and 100μM of NMDA were used to activate the NMDA-induced whole-cell current. 1μM strychnine and 100nM TTX were applied to block glycine receptors and action potentials, respectively. All experiments were carried out at room temperature and drugs were applied by bath perfusion.

6.4.1 Voltage-dependent memantine block of NMDA receptors

In order to characterize the voltage dependent memantine block of NMDA receptors in the absence of external Mg^{2+}, voltage-ramps from –100mV to +40mV were been made in the whole-cell configuration in the presence of NMDA or in the absence of NMDA (control). An example NMDAR current trace from a whole-cell recording is shown in Figure 6.1. Ramps were made in groups of four and averaged data from the 4 ramps were used for analysis. The NMDAR I-V relations were obtained by subtracting averaged NMDA ramps (in the presence of NMDA) from control ramps (in the absence of NMDA).

Figure 6.2A shows an example of the averaged NMDAR I-V relationship obtained in the presence of 100μM NMDA, 10μM glycine and 5μM memantine. The I-V curve shows a weak voltage-dependence of memantine block from +40mV to –70mV and passes maximum inward current at –70mV, then exhibits a negative slope from –70mV to –100mV. Figure 6.2B shows an example of an averaged NMDAR I-V curve evoked by voltage ramps in the presence of 100μM NMDA, 10μM glycine and 50μM memantine. The NMDAR I-V relation for 50μM memantine showed a significant voltage dependence of memantine block, passing maximum inward current at –50mV and exhibits a negative slope from –50mV to -100mV.

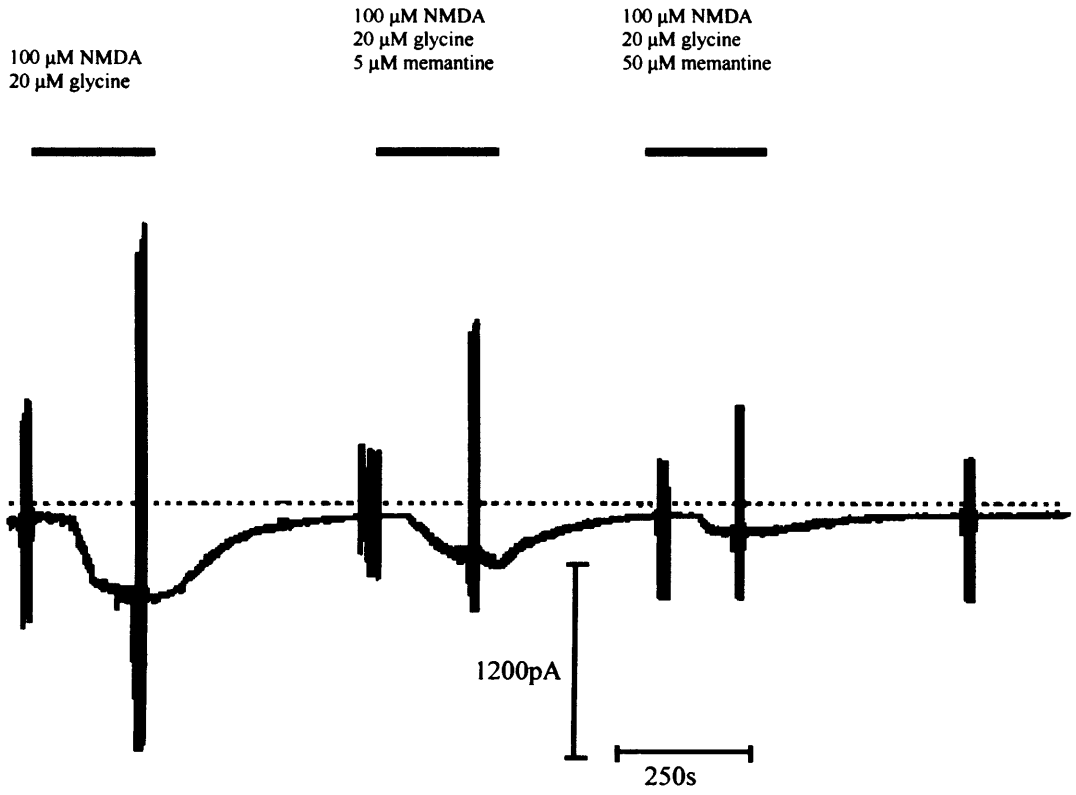

Figure 6.1 Memantine inhibition of NMDA-mediated whole-cell currents at –60mV in the presence of added Mg^{2+}

The first NMDAR response was evoked by 100 μM NMDA, 10μM glycine and coapplication with 5μM or 50μM memantine significantly reduced the NMDA-evoked whole-cell currents, which are shown in the second and third responses, respectively. Upright lines on the NMDAR current trace represent the current traces evoked by voltage-ramps from –100mV to +40mV to study voltage-dependent memantine block of NMDA receptors.

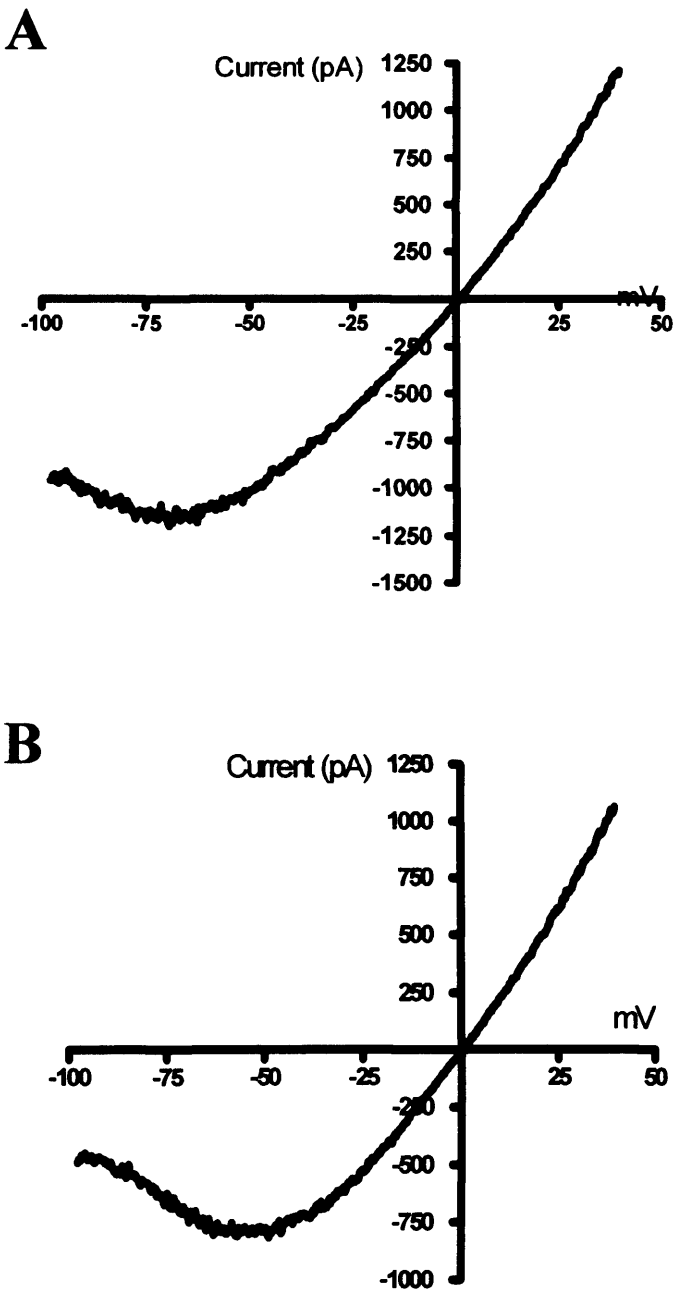

Figure 6.2 Voltage dependent block of NMDA receptors by memantine in the absence of added Mg^{2+}

(A) An example of the NMDA-evoked I-V relation in the presence of 100μM NMDA, 10μM glycine and 5μM memantine. The current curve shows a significant voltage dependent block by memantine and passes maximum inward current about –70mV. (B) From the same cell as illustrated in A, an example of the NMDAR I-V relation evoked by 100μM NMDA, 20μM glycine and 50μM memantine. It exhibits an almost linear relation between –40mV and +50mV and passes maximum current about –50mV, and shows a negative slope between –100mV and –60mV.

Figure 6.3 shows normalized and averaged NMDA I-V relations evoked by 100μM NMDA, 10μM glycine and 5μM or 50μM memantine. The averaged NMDAR I-V curves (n=8) were normalized to the current at +40mV to compare voltage dependent differences between external Mg^{2+} and memantine. It is obvious that NMDA receptors undergo a much stronger voltage-dependent block by 1mM external Mg^{2+} than memantine. In order to investigate the interaction between external Mg^{2+} and memantine, I quantified the voltage-dependent Mg^{2+} block of NMDA receptors in the absence of memantine and the results are shown in Table 6.2. The voltage-dependent Mg^{2+} block parameter δ does not depend on which model was used during the curve fitting and is 0.84. However, the value of K_{Mg2+} (0mV) depends on the model, being 1.1mM for the sequential block model with a desensitized state (Scheme 6.2b), 4.3mM for Scheme 6.2a, and 14.7mM for the trapping block models (Scheme 6.3a and 6.3b). The two-agonist-binding-site model gives similar results to the simple sequential block model. These data are consistent with my previous data about voltage-dependent Mg^{2+} block in chapter 3.

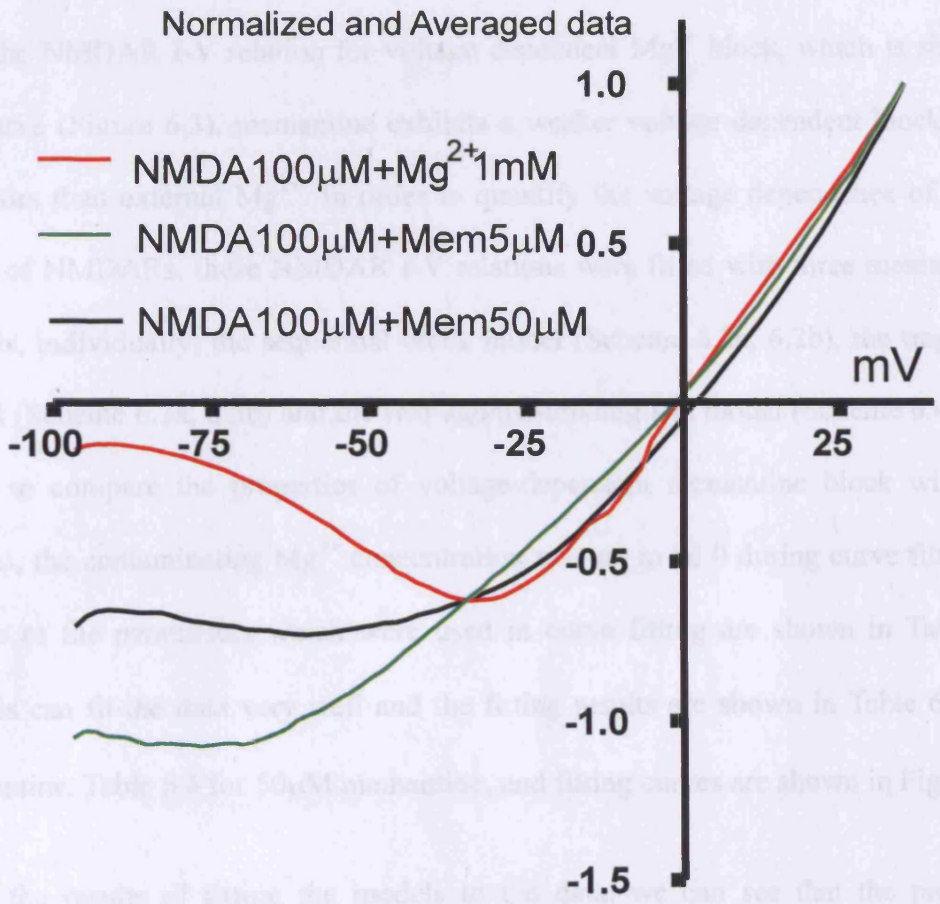

Figure 6.3 Voltage dependent block by memantine and Mg^{2+}

All I-V relations shown in this figure were evoked by voltage ramps from –100mV to +40 mV in the presence of 100μM NMDA and 10 μM glycine. 100nM TTX and 1μM strychnine were added to the external solution to block voltage gated soldium channels and glycine receptors on dopaminergic neurons. Compared to Mg^{2+}, memantine shows a less voltage-dependent block.

For the averaged and normalized NMDAR I-V relations of 5μM and 50μM memantine, maximum inward currents are found at about –75mV and –55mV, respectively. Compared with the NMDAR I-V relation for voltage dependent Mg^{2+} block, which is shown in the red curve (Figure 6.3), memantine exhibits a weaker voltage dependent block of NMDA receptors than external Mg^{2+}. In order to quantify the voltage dependence of memantine block of NMDARs, these NMDAR I-V relations were fitted with three memantine block models, individually; the sequential block model (Scheme 6.2a, 6.2b), the trapping block model (Scheme 6.3a, 6.3b) and the two-agonist-binding-site model (Scheme 6.4a, 6.4b). In order to compare the properties of voltage-dependent memantine block with previous studies, the contaminating Mg^{2+} concentration was set to be 0 during curve fitting and the values of the parameters which were used in curve fitting are shown in Table 6.1. All models can fit the data very well and the fitting results are shown in Table 6.3 for 5μM memantine, Table 6.4 for 50μM memantine, and fitting curves are shown in Figure 6.4.

From the results of fitting the models to the data, we can see that the presence of a desensitized state in the sequential block model which reduces the control P_{open} largely influences the estimated $K_{mem}(0mV)$ value, while the δ value is independent of the desensitized state. In contrast, the presence of a desensitized state does not affect voltage-dependent parameters for the trapping block model. As metioned before, the two-agonist-binding-site model gives similar fitting results to the sequential block model.

Table 6.1 Equilibrium constants used for curve fitting

k_2/k_1	10
k_4/k_3	2
k_{+d}/k_{-d}	5
zF/RT (Mg^{2+})	0.079171
zF/RT (Memantine)	0.039586
Conductance (pS)	50

During optimization of the fit for inhibition by Mg^{2+} and memantine, the number of NMDA receptors, reversal potential, K_{Mg2+}(0mV), K_{Mem}(0mV), δ_{Mg2+} and δ_{mem} were allowed to vary. All values of fixed parameters are shown in Table 6.1. The value of k_2/k_1 was set to be 10 based on previous reports (Benveniste & Mayer 1991; Sobolevsky *et al.* 1998). The values of k_4/k_3 and k_{+d}/k_{-d} are fixed to be 2 and 5, respectively (Lester & Jahr 1992).

Table 6.2 Summary of voltage-dependent parameters of Ki (0mV) and δ for Mg^{2+} action

Models	Sequential block model		Trapping block model		Two binding sites models	
	With desensitization	Without desensitization	With desensitization	Without desensitization	With desensitization	Without desensitization
K_{Mg2+}(0mV)	1.1mM	4.3mM	14.7mM	14.7mM	1.1mM	4.2mM
δ	0.84	0.84	0.84	0.84	0.84	0.84

The data for voltage dependent parameters of Mg^{2+} block of NMDAR are from fitting of averaged and normalized NMDAR I-V curves. The NMDAR I-V relation is obtained from a total of 7 sets of experiments. During curve fitting, reversal potential, K_{Mg2+}(0mV) and δ_{Mg2+} were allowed to vary. The value of k_2/k_1 was set to be 10 based on previous reports (Benveniste & Mayer 1995; Sobolevsky *et al.* 1998). The values of k_4/k_3 and k_{+d}/k_{-d} are fixed to be 2 and 5, respectively (Lester & Jahr 1992).

Table 6.3 Summary of voltage-dependent parameters of *Ki* (0mV) and δ for 5 μM memantine action

models	Sequential block model		Trapping block model		Two binding sites models	
	With desensitization	Without desensitization	With desensitization	Without desensitization	With desensitization	Without desensitization
K_{Mem}(0mV)	2.8 μM	11.5 μM	36.7 μM	36.6 μM	2.73 μM	10.7 μM
δ	0.6	0.6	0.6	0.6	0.6	0.6

The data for voltage dependent parameters of memantine block are from fitting of averaged and normalized NMDAR I-V curves. I-V relations were obtained from a total of 7 sets of experiments. During curve fitting, reversal potential, K_{Mem}(0mV) and δ_{Mem} were allowed to vary. The external Mg^{2+} concentration was fixed to be 0. The value of k_2/k_1 was set to be 10 (Benveniste & Mayer 1991; Sobolevsky *et al.* 1998). The values of k_4/k_3 and k_{+d}/k_{-d} are fixed to be 2 and 5, respectively (Lester & Jahr 1992).

Table 6.4 Summary of voltage-dependent parameters of *Ki* (0mV) and δ for 50 μM memantine action

models	Sequential block model		Trapping block model		Two binding sites models	
	With desensitization	Without desensitization	With desensitization	Without desensitization	With desensitization	Without desensitization
K_{Mem}(0mV)	5.96 μM	24.55 μM	78.7 μM	78.2 μM	5.82 μM	22.8 μM
δ	0.55	0.55	0.55	0.55	0.55	0.55

The data for voltage dependent parameters of memantine block are from fitting of an averaged and normalized NMDAR I-V curve. NMDAR I-V relations were obtained from a total of 7 sets of experiments. During curve fitting, reversal potential, K_{Mem}(0mV) andδ_{Mg} were allowed to vary. The external Mg^{2+} concentration was fixed to be 0. The value of k_2/k_1 was set to be 10 (Benveniste & Mayer 1991; Sobolevsky *et al.* 1998)). The values of k_4/k_3 and K_{+d}/k_{-d} are fixed to be 2 and 5, respectively (Lester & Jahr 1992).

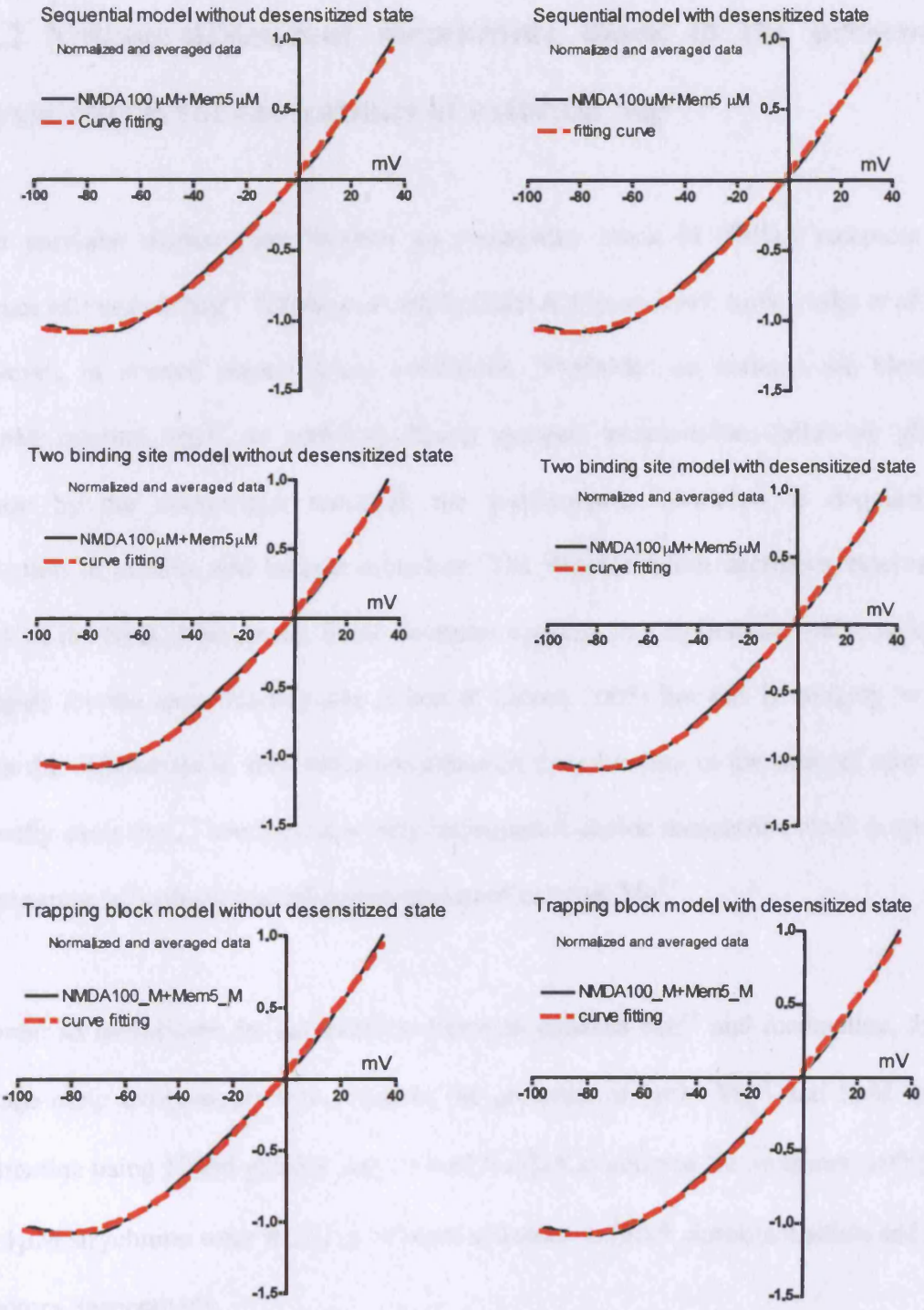

Figure 6.4 Curve fitting results for normalized and averaged NMDAR I-V relations in the absence of added Mg^{2+} which were obtained from 7 sets of experiments. The NMDAR currents were evoked by 100 μM NMDA, 10 μM glycine and 5μM memantine. The results of the curve fitting are summarized in Table 6.3 and 6.4.

6.4.2 Voltage-dependent memantine block in the presence of physiological concentrations of external Mg^{2+}

Most previous studies were focused on memantine block of NMDA receptors in the absence of external Mg^{2+} (Chen *et al.* 1992; Chen & Lipton 1997; Sobolevsky *et al.* 1998). However, in normal physiological conditions, NMDARs on neurons are blocked by 1-3mM external Mg^{2+}. In addition, during synaptic transmission, following glutamate release by the presynaptic terminal, the postsynaptic membrane is depolarized by activation of AMPA and kainate receptors. The depolarization decreases external Mg^{2+} block of the NMDA receptors. Some evidence suggests that memantine and external Mg^{2+} compete for the same binding site (Chen & Lipton 2005) but this is unlikely to be true given the differences in their structure although their binding in the channel may still be mutually exclusive. Therefore, it is very important to define memantine block properties in the presence of a physiological concentration of external Mg^{2+}.

In order to investigate the competition between external Mg^{2+} and memantine, the same voltage-ramp experiments were done in the presence of 1mM Mg^{2+} and 5μM or 50μM memantine using 10μM glycine and 100μM NMDA to activate the receptors. 100nM TTX and 1μM strychnine were added to external solutions to block action potentials and glycine receptors, respectively.

Figure 6.5 shows examples of NMDAR current-voltage relations recorded in the presence of 100μM NMDA, 10μM glycine, 1mM Mg^{2+} and 5μM memantine or 50μM memantine, respectively. Surprisingly, (as previous described by Sobolevsky *et al.*, 1998) the voltage dependent block of NMDA-induced whole-cell currents by 5μM memantine and 1mM

Mg^{2+} is stronger than the block by 50μM memantine and 1mM Mg^{2+}. The NMDAR I-V curves for 5μM memantine and 50μM memantine pass maximum inward currents at –30mV and –45mV, respectively.

In order to investigate competition between external Mg^{2+} and memantine, the NMDA receptor I-V relations were fitted with different models. Since the presence of external Mg^{2+} can not change the binding sites for memantine (unless both could be bound at the same site), δ for external Mg^{2+} and δ for memantine were fixed to be 0.84 and 0.6 during fitting, respectively (the values obtained from fitting each alone). Because both curves were from the same cell, the number of NMDA receptors was set to be the same for both curves during fitting. The results of the fitting are shown in Table 6.5 and Figure 6.6.

Averaged NMDA receptor I-V relations were obtained by averaging a total of 8 sets of experiments (Figure 6.7). Because the two-agonist-binding-site model always gives similar fitting results to the simple sequential model, these averaged NMDA receptor I-V relations were fitted with the competition sequential block model (Scheme 6.2a, 6.2b) and the competition trapping block model (Scheme 6.3a, 6.3b). The δ for Mg^{2+} and δ for memantine were fixed to be 0.84 and 0.6, respectively. The number of NMDA receptors was set to be same for both curves during fitting. The results of the fitting are shown in Table 6.6 and Figure 6.8.

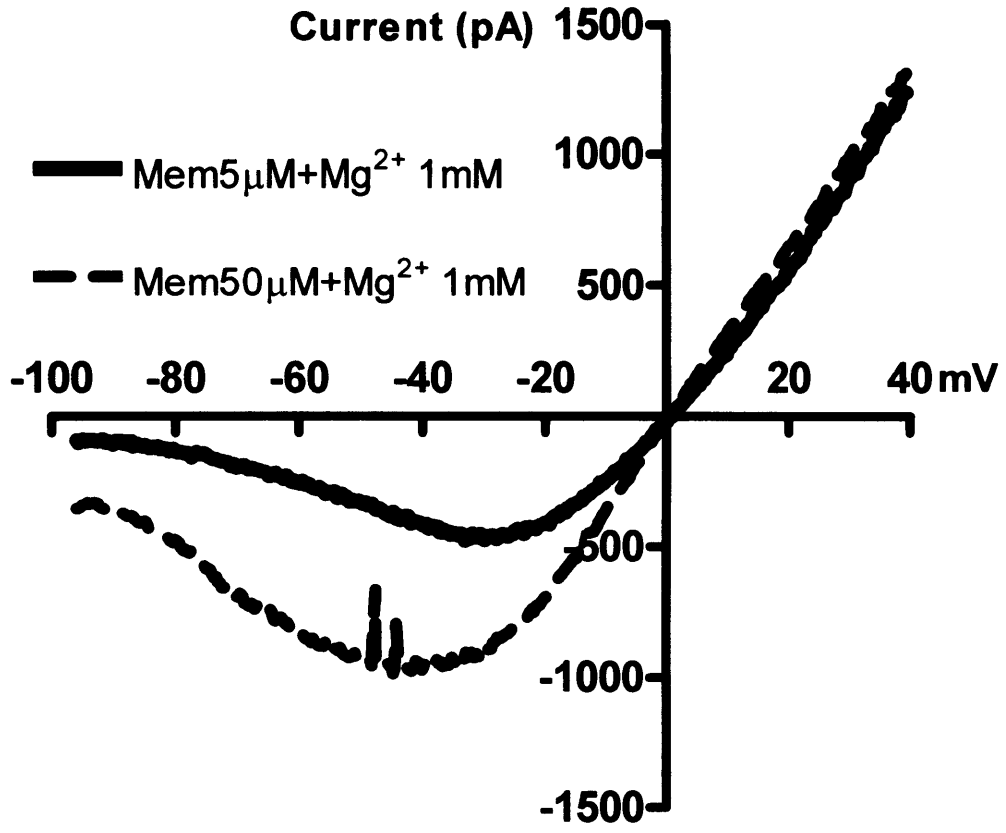

Figure 6.5 Competitive block between external Mg^{2+} and memantine

An example of NMDA I-V relations evoked by 100μM NMDA and 10 μM glycine in the presence of 1mM Mg^{2+}, 5 μM or 50 μM memantine. The intriguing result is that in the presence of 1mM Mg^{2+}, the NMDA I-V curve for 50 μM memantine shows a weaker voltage dependent block than with 5 μM memantine.

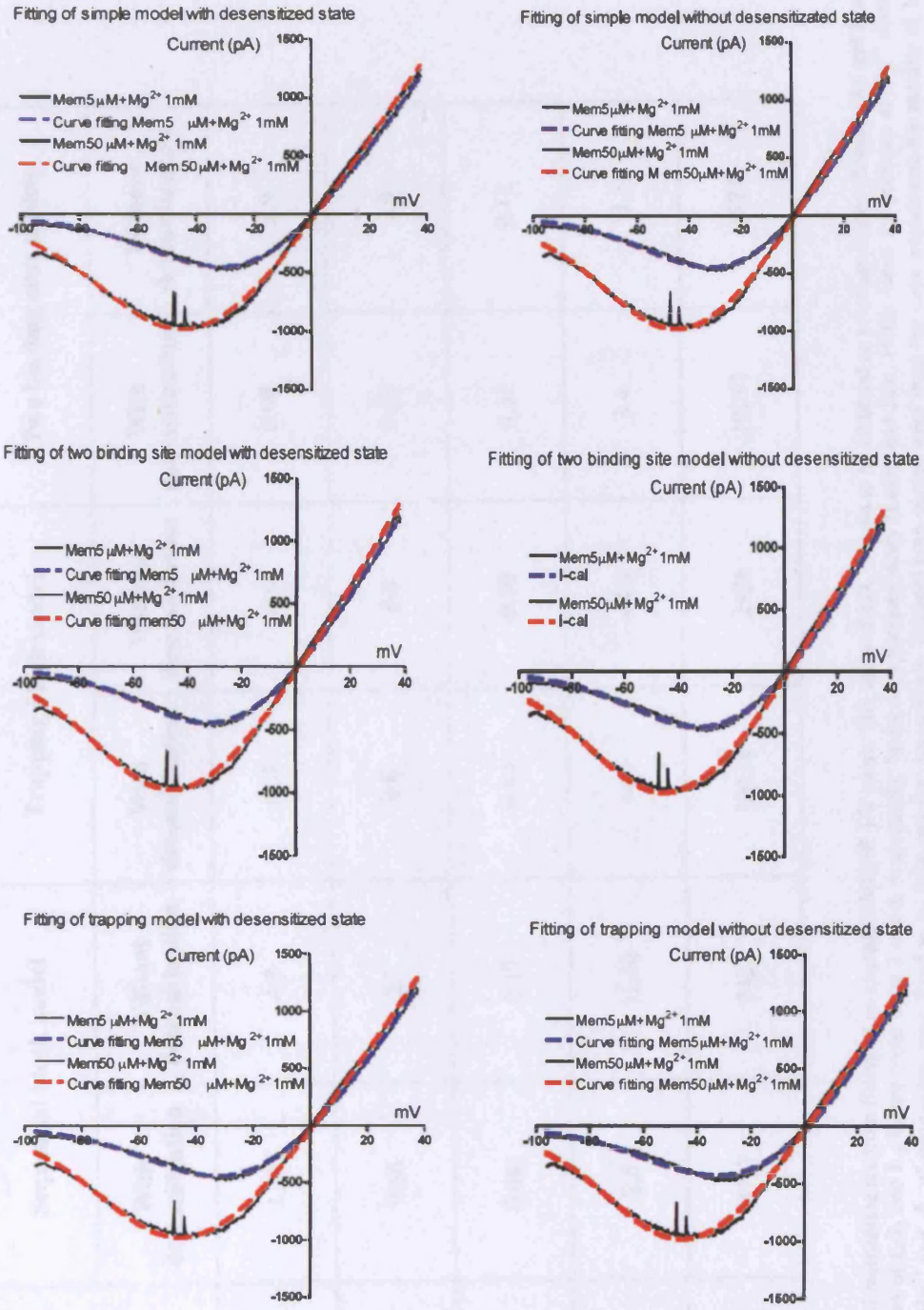

Figure 6.6, Curve fitting results for examplary NMDAR I-V relations, which were evoked by 100 μ M NMDA, 10 μ M glycine and 1mM Mg^{2+} with 5 μM and 50 μM memantine.

Table 6.5 Summary of competition curve fitting results

	Sequential block model		Trapping block model		Two binding sites models	
	With desensitization	**Without desensitization**	**With desensitization**	**Without desensitization**	**With desensitization**	**Without desensitization**
K_{Mem}(0mV) for 5uM Memantine (μM)	1.17	4.8	10.7	6.5	0.98	3.9
K_{Mg2+}(0mV) for 5uM Memantine (mM)	0.56	2.3	8.6	8.6	0.65	2.6
K_{Mem}(0mV) for 50uM Memantine (mM)	0.041	0.17	0.44	0.50	0.31	0.12
K_{Mg2+}(0mV) for 50uM Memantine (mM)	2.8	11.36	44.5	44.5	3.4	13.3
Number of receptors	9757	2424	10434	2926	10091	2571

The data for competition block between Mg^{2+} and memantine are from fitting of an exanple NMDAR I-V curve. The value of k_2/k_1 was set to be 10 based on previous reports (Sobolevsky and Koshelev, 1998, Benveniste and Monyer, 1991). The values of k_4/k_3 and k_d/k_{-d} are fixed to be 2 and 5, respectively, based on a previous study (Lester and Jahr, 1992). Since the presence of Mg^{2+} should not change the binding sites for memantine, δ of Mg^{2+} and δ of memantine were fixed to be 0.84 and 0.6, respectively. Because both curves were from the same experiment, the number of NMDA receptors was set to be the same for both curves during fitting.

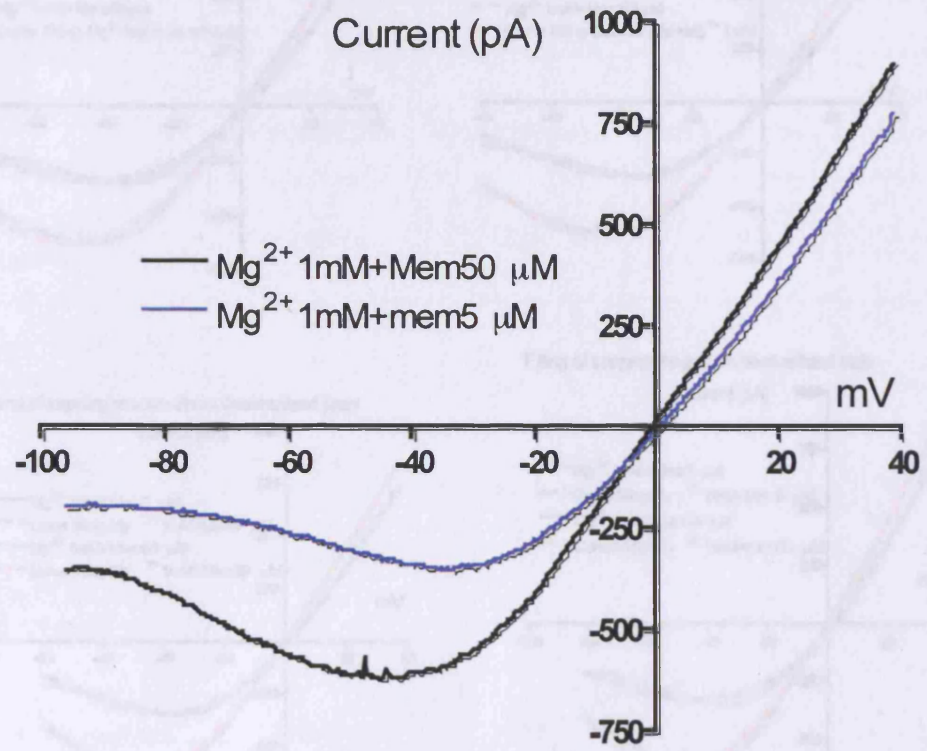

Figure 6.7 NMDAR competition block between Mg^{2+} and memantine

Averaged NMDA I-V relations were evoked by 100μM NMDA and 10μM glycine in the presence of 1mM Mg^{2+} and 5μM or 50μM memantine. These NMDA I-V relations were obtained from a total of 8 sets of experiments.

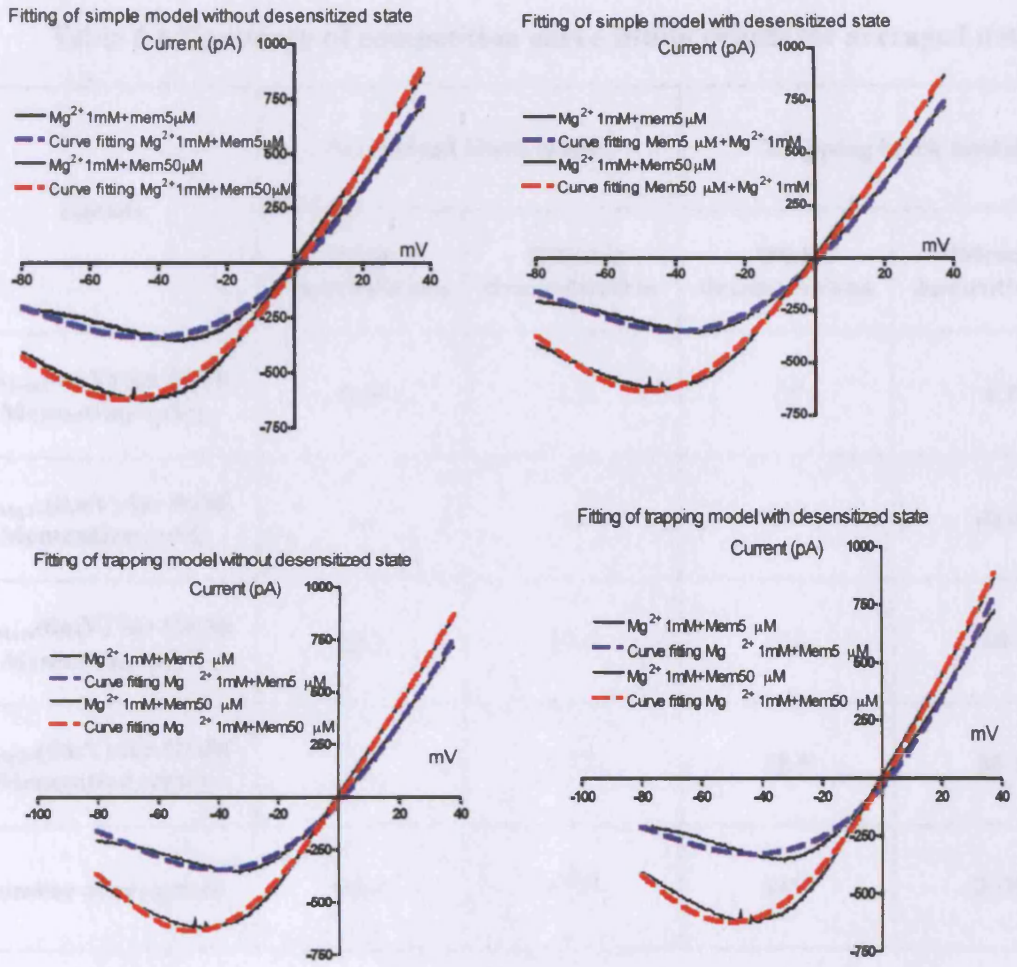

Figure 6.8, Curve fitting results for averaged NMDAR I-V relations, which were obtained by averaging 8 individual recordings in the presence of 100 μM NMDA, 10 μM glycine, 1mM Mg^{2+} and 5 μM or 50 μM memantine.

Table 6.6 Summary of competition curve fitting results for averaged data

models	Sequential block model		Trapping block model	
	With desensitization	Without desensitization	With desensitization	Without desensitization
K_{Mem}(0mV) for 5uM Memantine (μM)	0.68	1.9	7.9	4.2
K_{Mg2+}(0mV) for 5uM Memantine (mM)	1.8	13	24.8	48.6
K_{Mem}(0mV) for 50uM Memantine (μM)	22.3	51.4	314	187
K_{Mg2+}(0mV) for 50uM Memantine (mM)	4	27.7	58.6	86.1
Number of receptors	6664	1777	6987	2139

The data for competition block between Mg^{2+} and memantine are from fitting of averaged NMDAR I-V curves. The value of k_2/k_1 was set to be 10 based on previous reports (Sobolevsky and Koshelev, 1998, Benveniste and monyer, 1991) and the values of k_4/k_3 and k_{+d}/k_{-d} were fixed to be 2 and 5, respectively (Lester and Jahr, 1992). Since the presence of Mg^{2+} does not change the binding sites for memantine, δ of Mg^{2+} and δ of memantine were fixed to be 0.84 and 0.6, respectively. Because both curves were from the same experiments, the number of NMDA receptors was set to be same for both curves during fitting.

6.5 Discussion

6.5.1 Models for estimating voltage-dependent memantine block of NMDA receptors

6.5.1.1 Number of agonist binding reactions in the model does not affect the estimated voltage-dependent parameters of memantine block

In my experiments, three memantine block models were used to fit NMDAR I-V relations to estimate the parameters of voltage-dependent memantine block. These models were the simple sequential block model (Scheme 6.2a and Scheme 6.2b), the trapping block model (Scheme 6.3a and Scheme 6.3b), and the two-agonist-binding-site model (Scheme 6.4a and Scheme 6.4b) (This model was developed from the simple block model to investigate whether the number of agonist binding reactions in the sequential block model will affect the results). In addition, in order to investigate whether a desensitized state will affect the fitting results, each model was fitted with a desensitized state (Scheme 6.2b, Scheme 6.3b and Scheme 6.4b) or without a desensitized state (Scheme 6.2a, Scheme 6.3a and Scheme 6.4a) to the NMDAR I-V relations. The results of the model fitting show that the two-agonist-binding-site model always gives similar fitting results to these obtained with the simple block model (Table 6.2, Table 6.3, Table 6.4, Table 6.5), suggesting that the number of agonist binding reactions in the models does not affect estimation of the blocking parameters. Therefore, in this discussion the results of fitting with the two-agonist-binding-site model fitting are omitted and the difference between the simple block model and the trapping block model considered further.

6.5.1.2 The absence of a desensitized state in the sequential block model over-estimates the K_{mem}(0mV) value but not in the trapping block model.

Tables 2,3,4,5,6 show that when the sequential block model is used to estimate parameters of voltage-dependent memantine block, the estimated K_{mem}(0mV) value is affected by the presence of a desensitized state in the model. The K_{mem}(0mV) value estimated using the model without a desensitized state is about 4 times higher than the value from the model with a desensitized state when the desensitization equilibrium constant (K_d=k_{-d}/k_{+d}) is set to be 0.2. In contrast, the presence of a desensitized state in the sequential block model does not affect estimating the δ value.

However, for the trapping block model, the voltage-dependent blocking parameters, δ and K_{mem}(0mV), are independent of the presence of a desensitized state.

6.5.2 Comparion with previous studies

It is widely accepted that memantine is an NMDA receptor open channel blocker and displays a weakly voltage-dependent block not only in oocyte expression systems but also with native NMDA receptors in different brain regions (Kornhuber *et al.* 1989; Chen *et al.* 1992; Blanpied *et al.* 1997; Chen & Lipton 1997; Sobolevsky *et al.* 1998; Chen *et al.* 1999; Kashiwagi *et al.* 2002; Chen & Lipton 2005; Wrighton *et al.* 2007). Its voltage-dependent parameters, δ and K_{mem}(0mV), from previous studies are shown in Table 6.7.

Table 6.7 Summary of previous studies about voltage-dependent memantine block

Paper	Animal	Cell type	δ	K_{mem}(0mV) (μM)	IC_{50} (-60mV) (μM)	Possible subunits
(Chen & Lipton 2005)	Oocyte	NR1-1a/NR2A	0.84	4.89	0.79	NR1-NR2A
		NR1-1b/NR2A	0.85	6.99	0.94	
		NR1-4a/NR2A	0.84	4.30	0.87	
		NR1-4b/NR2A	0.83	5.37	1.1	
(Wrighton *et al.* 2008)	Oocyte	NR1-NR2A	0.84	-----	1.7	NR1-NR2A
		NR1-NR2D	0.62	-----	0.42	NR1-NR2D
(Kashiwagi *et al.* 2002)	Oocyte	NR1-NR2B	0.89	7.1	0.46	NR1-NR2B
(Blanpied *et al.* 1997)	Cultured neurons NR1-NR2A NR1-NR2B	superior collicular and hippocampal	0.87	14.2	-------	
(Chen & Lipton 1997)	4 day old rat	Retinal ganglia cell	0.82	-----	------	
(Sobolevsky & Koshelev 1998)		CA1 Pyramidal cell	0.73	18.5	-------	
(Sobolevsky *et al.* 1998)	2 weeks old rat	Hippocampal slice	0.73	17.9	------	

6.5.2.1 Comparison of dopamine cell results with recombinant NMDA receptor studies

It is known from previous studies that, similar to voltage-dependent Mg^{2+} block of NMDA receptors, memantine block NMDA receptors is NR2-subunit dependent. The NMDA receptors composed of NR1-NR2A and NR1-NR2B are blocked more strongly by memantine than NMDA receptors formed by NR1-NR2D (Table 6.7). The value of the voltage-dependent parameter δ for NR1-NR2A and NR1-NR2B NMDA receptors is in the range from 0.83 to 0.89 while the value of K_{mem}(0mV) is in the range from 4.3μM to 7.1μM. However, the δ value for the NR1-NR2D NMDA receptor is much less than for NR1-NR2A and NR1-NR2B NMDA receptors, being 0.62 (Wrighton *et al.* 2007).

In my experiments, fitting averaged and normalized NMDA I-V relations obtained in the presence of 100μM NMDA, 10μM glycine and 5 or 50μM memantine gives us an estimate of the voltage-dependence parameter δ to be 0.55-0.6. The value of K_{mem}(0mV) is affected by which model is used during the curve fitting. For the sequential block model, the K_{mem}(0mV) values are 2.8-5.96 μM (with a desensitizated state) and 11.5-24.6 μM (without a desensitized state) while for the trapping block model, the K_{mem}(0mV) values were independent of desensitized states and were found to be 36.6-78 μM. Inspection of my data presented here reveals that the δ value (0.55-0.6) from my experiments is much smaller than the δ value for NR1-NR2A and NR1-NR2B NMDA receptors (0.83-0.89) and is very close to the value for NR1-NR2D recombinant NMDA receptors (0.62) (Wrighton *et al.* 2007). This result supports the idea that dopaminergic neurons in SNc express a mixture of NR2B- and NR2D- containing NMDA receptors. Here we see that the δ value is somewhat

smaller than data from recombinant NR1-NR2D NMDA receptors. This difference might be due to differences in the receptor expression systems or a permeant ion effect, because in my experiments 1mM Ca^{2+} was applied in the external solution while in Wrighton's experiments 1.8mM Ba^{2+} was added instead of Ca^{2+}. In addition, in the present experiments the main intracellular cation is Cs^{+} while in Wrighton's oocyte experiments, this is likely to the K^{+}.

In addition, K_{mem}(0mV) value (2.8-5.96 μM) obtained from the sequential block model with a desensitized state is very similar to data from recombinant NMDA receptors. This result might be because the same sequential block model was also used to fit data from recombinant NMDA receptors in previous studies (Chen & Lipton 1997; Wrighton *et al.* 2008).

6.5.2.2 Comparison with other native NMDA receptors

Table 7 shows that the δ value for voltage-dependent memantine block of native NMDARs is in the range from 0.73 to 0.87 while the K_{mem}(0mV) value is from 14.2-18.5μM. The wide range of δ values might be due to the percentage difference of the native NMDA receptors which have a less voltage-dependent memantine block (NR2C-, NR2D-containing NMDA receptors). Compared with other native NMDA receptors, a smaller δ value was obtained from my experiments. One possible explanation could be a larger percentage of NR2D-containing NMDA receptors is expressed by dopaminergic neurons than neurons in the hippocampal CA1 region or retinal ganglion cells. Another explanation could be that different models were used during estimation of the voltage-dependent memantine block parameters. For example, Blanpied *et al.* (1997) suggested that when

memantine and the agonist are washed off after steady-state block, one-sixth of blocked channels released rather than trapped the blocker and a partial trapping block model was used to fit their data. Also as mentioned before, ionic differences in internal and external solution between experiments also can cause a difference, as Chen *et al.* (1997) reported that when internal CsCl was replaced by NMDG, the δ value was reduced from 0.83 to 0.53 (Chen & Lipton 1997).

Chapter 7: Functional NR2B- and NR2D-containing NMDA receptor channels in P7 rat subthalamic nucleus

7.1 Summary

1. Single-channel recording experiments have been made from outside-out patches which were pulled from P7 rat STN neurons to study the kinetics and composition of NMDA receptors.

2. Application of NMDA (200 μM) and glycine (10 μM) to outside-out patches activated NMDA receptor channels with four different amplitudes: 1.15pA, 2.53pA, 3.14pA, 4pA. Both large- (52 pS and 42 pS) and small- (42 pS and 19 pS) conductance NMDAR channels are expressed by P7 rat STN neurons. Meanwhile, a unique large conductance (66.7 pS) NMDA channel is found.

3. The application of 10 μM ifenprodil reduced the mean open time from 2.78 ± 0.64ms to 2.2 ± 0.98ms and increased the mean shut time from 35.3 ± 15.8ms to 64.9 ± 29ms. Therefore, the decrease in P_{open} (from 0.2 to 0.03) is accounted for by a significant increase in mean shut time and decrease in mean open time. This result suggests that NR2B-containing NMDA receptors are expressed by STN neurons.

4. Analysis of the frequency of direct transitions between the small-conductance states showed that transitions from 42 pS to 19 pS levels occur more frequently than transitions from19 pS to 42 pS. While 32.6% of direct transitions were from 19 to 42 pS, 67.7% were from 42 to 19 pS. This asymmetry of direct transitions is unique to NR2D-containing NMDARs, indicating that STN neurones contain NR2D subunits.

7.2 Introduction

The subthalamic nucleus (STN) is one part of the basal ganglia circuits in the midbrain which play a very important role in controlling movement (Kitai & Deniau 1981; Kita & Kitai 1987; Bolam *et al.* 2000; Chatha *et al.* 2000). The subthalamic nucleus receives its main inputs from the striatum, cortex, thalamus, and brainstem (Kita & Kitai 1994; Chatha *et al.* 2000) and via its glutamatergic projections plays a key role in controlling the output nuclei of the basal ganglia; the substantia nigra pars reticulata (SNr) and the internal segment of the globus pallidus (GPi). In addition, a crucial output to substantia nigra pars compacta mediated by glutamate also has been found which may contribute to excitotoxic dopamine neuron death during Parkinson's disease (Blandini *et al.* 2000).

It has been shown that functional NMDA receptors are expressed by STN neurons (Gotz *et al.* 1997). NMDA-mediated afferent input has an important role in controlling the activity of the STN (Nakanishi *et al.* 1988; Gotz *et al.* 1997). Blockade of STN NMDA receptors interrupts excitation of the GPi after cortical stimulation, suggesting that these receptors are important in physiological modulation of the basal ganglia outflow pathway (Nambu *et al.* 2000). In Parkinson disease (PD), it has been hypothesized (Blandini *et al.* 2000) that one result of the loss of dopamine is an increased excitatory drive from the STN to the

remaining dopamine neurones of the substantia nigra to compensate for the loss of some dopamine neurones by driving the remaining dopamine neurones much harder. The hyperactivity of STN neurons has been already observed in animal models of Parkinsonism and this abnormal activity is partially mediated by NMDA receptors and is reduced by the NMDA antagonist MK-801. These observations suggest that inhibition of NMDA receptors in STN neurons might be of therapeutic benefit in PD (Blandini *et al.* 2000).

Although STN neurones express functional NMDA receptors (Gotz *et al.* 1997), their subunit composition is not known. High levels of NR2D subunit mRNA (Monyer *et al.* 1994; Standaert *et al.* 1994) and low levels of NR2B mRNA are expressed in adult rat STN neurons.

My experiment was to characterize functional NMDA receptor subtypes which are present in STN neurones, and to investigate whether NR2D and NR2B subunits form functional NMDA receptors, using single-channel recordings from outside-out patches. The results support the idea that NR2B- and NR2D-containing NMDA receptors are expressed in subthalamic nucleus neurons. It is of interest to determine the NMDA receptor subtypes in this nucleus. This information is relevant to the use of NMDA receptor antagonists in Parkinson's disease (Del Dotto *et al.* 2001).

7.3 Results

7.3.1 NMDA activates channels with four distinct conductance levels in STN

Application of NMDA (200 μM) and glycine (10 μM) to outside-out patches (n=6) from subthalamic nucleus activated individual NMDA receptor channels with four different amplitudes: 1.15pA, 2.53pA, 3.14pA, 4pA. Two example recordings showing NMDA receptor channel openings to these four amplitudes are shown in Figure 7.1A a, b. The stability of channel amplitudes is shown in Figure 7.1C. In 6 patches, in the presence of 200 μM NMDA and 10 μM glycine, the mean open time was 2.78±0.64ms and the mean open probability was 0.09±0.014. The distribution of channel amplitudes activated by 200 μM NMDA in 3 of 6 patches was fitted with the sum of three Gaussian components (1.15pA, 2.53pA, 3.14pA) (Figure 7.1B) while the other 3 patches also showed unusually large conductance openings (4pA). The measured channel amplitudes correspond to chord conductances (relative areas) of 19.2 ± 1.1pS (5.43 ± 0.43%), 42.1 ± 1.8pS (18.2 ± 9.4%), 52.4 ± 1.4pS (65.1 ± 11.2%), and 66.7 ± 1.0 (34.0 ± 22.1%).

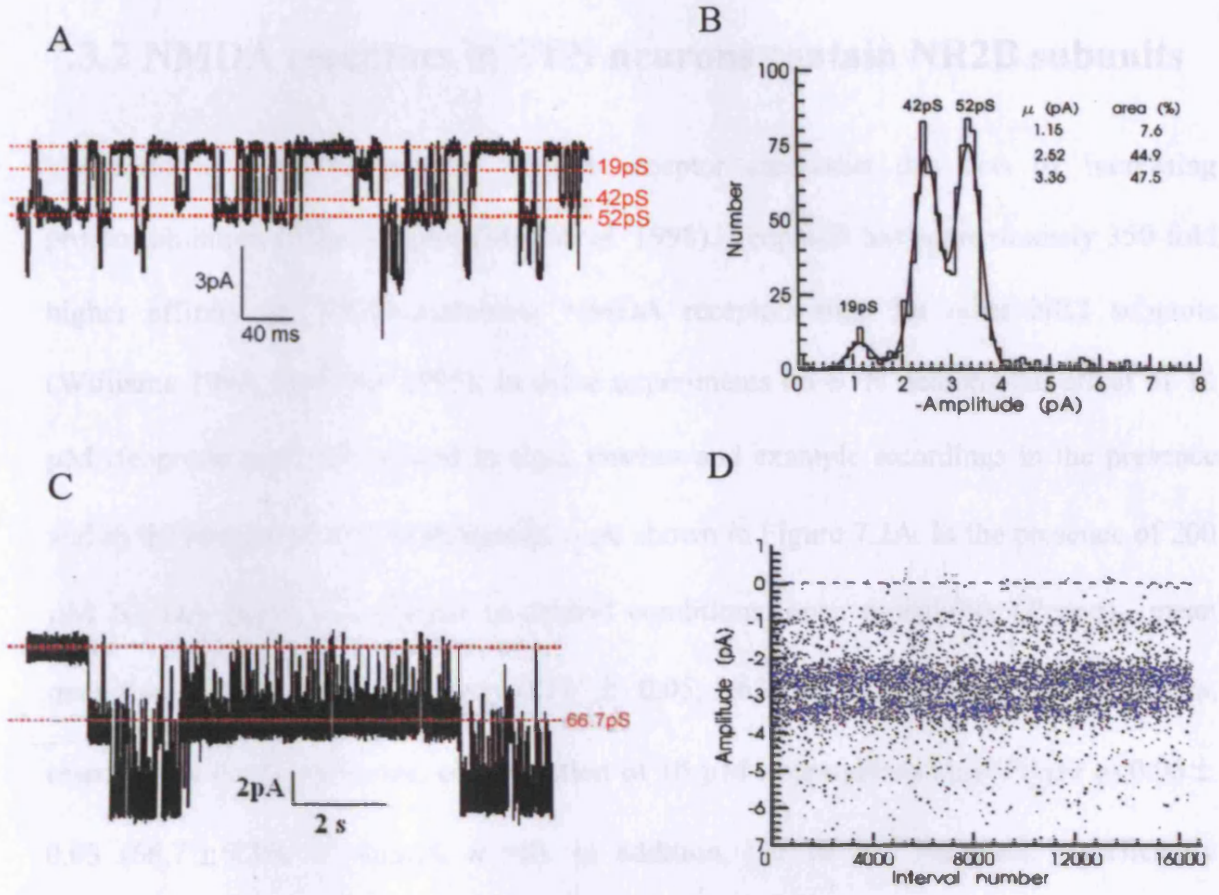

Figure 7.1 Large and small-conductance NMDA receptor channels in STN neurons

A, example currents recorded from outside-out patches from STN neurones at a membrane potential of -60 mV in the presence of 200 μM NMDA and 10 μM glycine showing three different current amplitudes corresponding to the three conductance levels indicated in B;

B, amplitude distribution for the patch illustrated in A, fitted with the sum of three Gaussian components. The standard deviations were constrained to be the same (0.253 pA) for each component. The mean amplitude and relative area of each component are shown on the histogram, and correspond to chord conductances of 19 pS, 42 pS and 52 pS.

C, Example recording from a different patch to that illustrated in A showing a long burst of high-conductance openings with a mean chord conductance of 66.7pS.

D, stability plot of channel amplitudes for one patch throughout the duration of the recording.

7.3.2 NMDA receptors in STN neurons contain NR2B subunits

Ifenprodil is a non-competitive NMDA receptor antagonist that acts by increasing proton-inhibition of the receptor (Mott *et al.* 1998). Ifenprodil has approximately 350-fold higher affinity for NR2B-containing NMDA receptors than for other NR2 subunits (Williams 1993; Williams 1995). In these experiments on STN neurons the effect of 10 μM ifenprodil was investigated in eight patches and example recordings in the presence and in the absence of 10 μM ifenprodil were shown in Figure 7.2A. In the presence of 200 μM NMDA and10 μM glycine in control conditions, open probability (*P*open) mean open time and mean shut time were 0.11 ± 0.05, 2.63 ± 0.52 ms and 35.3 ± 15.8ms, respectively (*n*=8). However, coapplication of 10 μM ifenprodil reduced *P*open to 0.06± 0.03 (66.7±9.3% of control, *n* =8). In addition, the 10 μM ifenprodil significantly decreased the proportion of 54 pS and 67pS channel openings observed in the amplitude distributions and reduced the mean amplitude from –2.99 ± -1.33pA to –2.48 ± -1.1pA (n=8) (Figure 7.2C). The application of 10 μM ifenprodil also reduced the mean open time from 3.78 ± 0.64ms to 2.2 ± 0.98ms and increased the mean shut time from 35.3 ± 15.8ms to 64.9 ± 29ms (an example was shown in Figure 7.2B). Therefore, the decrease in P_{open} is accounted for by a significant increase in mean shut time and decrease in mean open time.

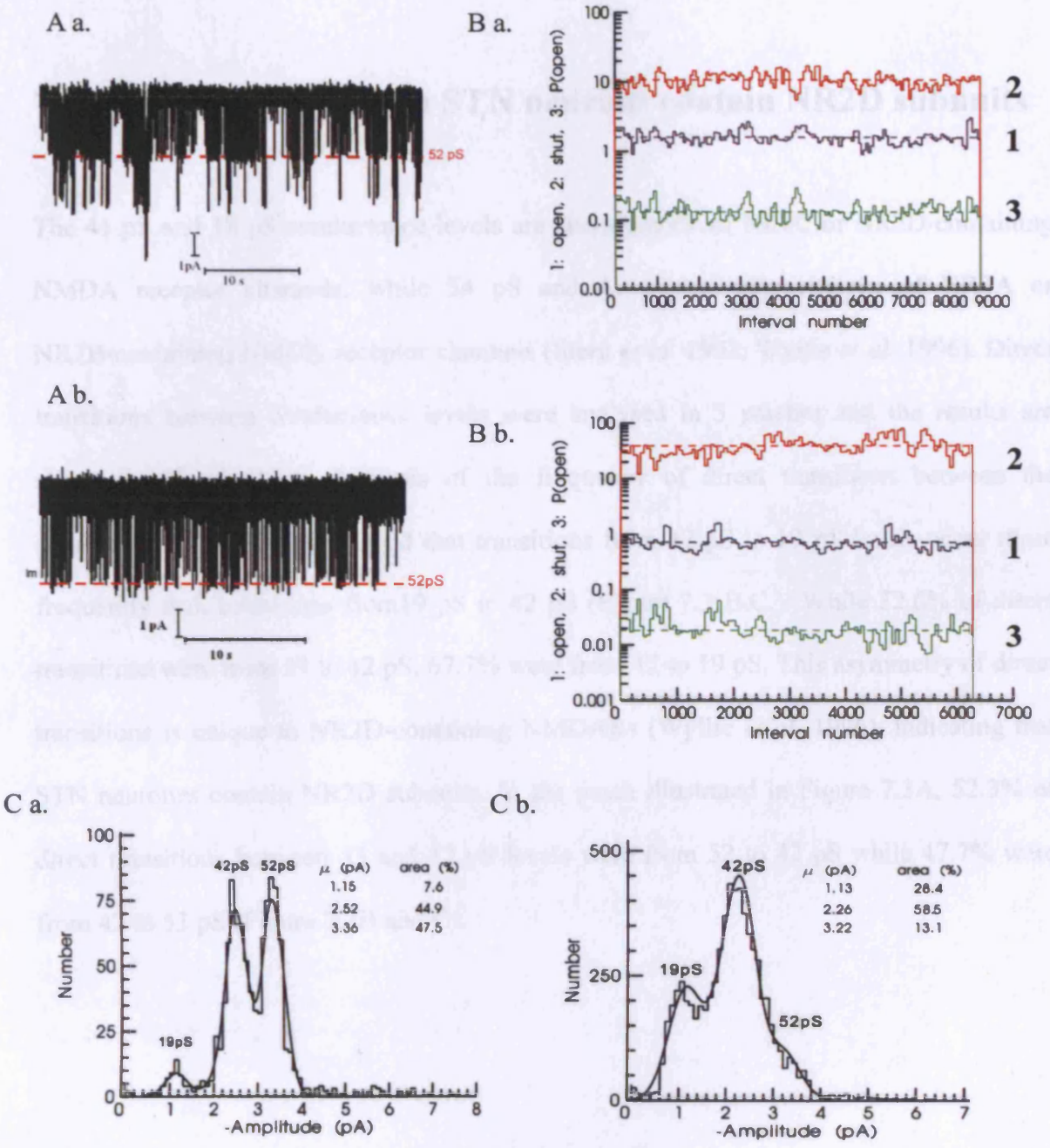

Figure 7.2 Large-conductance NMDA receptor channels in STN neurones contain NR2B subunits

A, example currents recorded *a*, in the presence of 200 μM NMDA; *b*, in the presence of 200 μM NMDA and 10 μM ifenprodil;

B, stability plots of *P*open, mean open time and mean shut time for single-channel currents in a, 200 μM NMDA and b, in the presence of 200 μM NMDA and 10 μM ifenprodil showing that, in this patch, in addition to decreasing channel open time, ifenprodil also decreased P_{open} and increased in channel shut time.

C, example amplitude distributions from the same patch illustrated in B. *a*, in the presence of 200 μM NMDA; *b*, in the presence of 200 μM NMDA and 10 μM ifenprodil, showing that ifenprodil significantly reduces the proportion of high conductance NMDA channel openings. In Ca, there were 1687 openings in a recording period of 120 seconds and in Cb, in the presence of ifenprodil there were 6462 openings in a recording period of 800 seconds.

7.3.3 NMDA receptors in STN neurons contain NR2D subunits

The 41 pS and 18 pS conductance levels are characteristic of NR2C or NR2D-containing NMDA receptor channels, while 54 pS and 41 pS are characteristic of NR2A or NR2B-containing NMDA receptor channels (Stern *et al.* 1992; Wyllie *et al.* 1996). Direct transitions between conductance levels were analysed in 3 patches and the results are shown in Figure 7.3A. Analysis of the frequency of direct transitions between the small-conductance states showed that transitions from 42 pS to 19 pS levels occur more frequently than transitions from19 pS to 42 pS (Figure 7.3 B.C.). While 32.6% of direct transitions were from 19 to 42 pS, 67.7% were from 42 to 19 pS. This asymmetry of direct transitions is unique to NR2D-containing NMDARs (Wyllie *et al.* 1996), indicating that STN neurones contain NR2D subunits. In the patch illustrated in Figure 7.3A, 52.3% of direct transitions between 53 and 42 pS levels were from 52 to 42 pS while 47.7% were from 42 to 53 pS (Figure 7.3B and C).

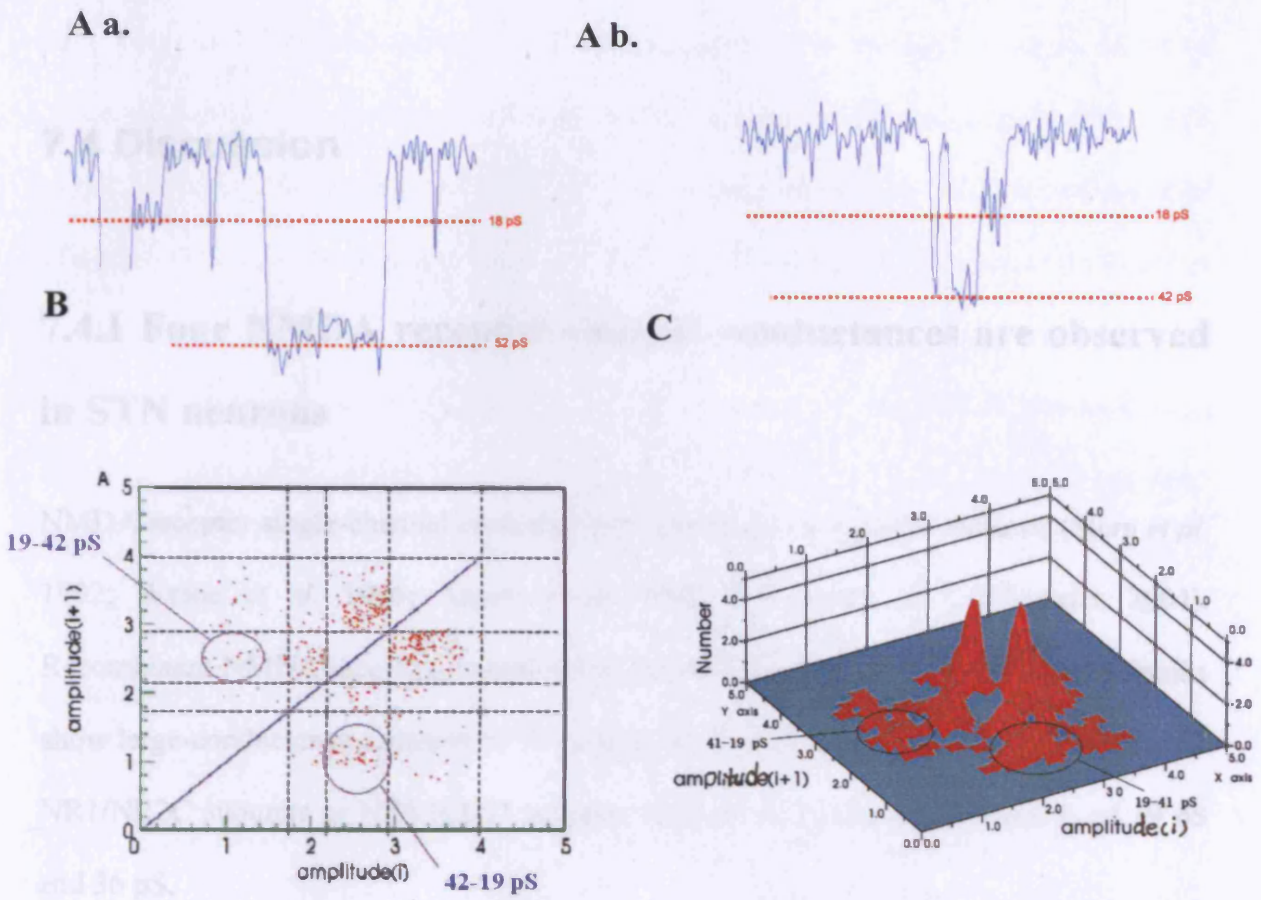

Figure 7.3 NMDA receptors in STN neurones contain NR2D subunits
A, examples of direct transitions a, between 18 pS and 52 pS and b, between18 pS and 42 pS. Transitions were identified using A_{crit} values of 1.72 pA, 2.18 pA and 2.90 pA, calculated from the fit to the amplitude distribution shown in Fig. 1*C*.

B, plot of channel amplitudes before and after direct transitions from the same patch illustrated in *A*. Each point on the graph represents a single direct transition. The density of points illustrates that direct transitions between 42 pS and 52 pS occur with equal frequency, while transitions between 19 pS and 42 pS are asymmetric, occurring more frequently from 42 pS to 19 pS than from 19 pS to 42 pS.

C, Three-dimensional plot of the same data shown in *B*.

7.4 Discussion

7.4.1 Four NMDA receptor channel conductances are observed in STN neurons

NMDA receptor single-channel properties are determined by the NR2 subunits (Stern *et al.* 1992; Wyllie *et al.* 1996; Anson *et al.* 1998; Cull-Candy & Leszkiewicz 2004). Recombinant NMDA receptors composed of NR1/NR2A subunits or NR1/NR2B subunits show large-conductance channels of 38 pS and 50 pS while NMDA receptors composed of NR1/NR2C subunits or NR1/NR2D subunits show small conductance channels of 19 pS and 36 pS.

Functional NMDA receptors have previously been described in midbrain STN neurons with kinetic properties suggestive of NR2B-containing receptors (Gotz *et al.* 1997) although their subunit composition was not investigated. Here single-channel recordings from outside-out patches in P7 rat subthalamic nucleus were made to investigate NMDA receptor subunit composition. The results show that four different channel conductances are found, suggesting the receptor population is not homogeneous. The 19pS and 42pS NMDA channels are similar to NR1-NR2C or NR1-NR2D NMDA channels while the 42pS and 52pS NMDA channels are similar to NR1-NR2A and NR1-NR2B recombinant NMDA channels. In addition, an unusual large conductance NMDA channel (67pS) was observed during application of 200 μM NMDA and 10 μM glycine that was inhibited by ifenprodil (See section 7.3.3). According to previous studies, large conductance channels of 69pS and 62pS have been described in spinal cord motorneurons and interneurons (Palecek *et al.* 1999; Abdrachmanova *et al.* 2000; Green & Gibb 2001). In the

motorneurons, Abdrachmanova *et al.* (2000) suggested that the 69pS channel might be activated during synaptic transmisstion and Green & Gibb (2001) suggested that the 69pS might be a phenomenon associated with the developing spinal cord. Since a medium level of NR3A mRNA is expressed in STN neurons in the adult pig-tail macaque brain (Mueller & Meador-Woodruff 2005) and in rat NR3A protein expression peaked between postnatal days 7 and 10 in the midbrain, it may be that these receptors contain NR3A, although when combined with NR1 and NR2A, NR3A gives mainly 28 pS channels (Perez-Otano *et al.* 2001).

Therefore, observations in my experiments suggest that functional NMDA receptors in STN contain NR2B subunits and either NR2C or NR2D subunits and NR3A subunits might be present in STN but not in all individual NMDA receptors.

7.4.2 Functional NMDA receptors in STN dopaminergic neurones contain NR2D subunits

NR2C and NR2D subunits can be distinguished by analysis of direct transitions between conductance levels (Wyllie *et al.* 1996; Wyllie *et al.* 1998; Cull-Candy & Leszkiewicz 2004). In STN neurons, direct transition analysis showed that transitions from 42 pS to 19 pS levels occur more frequently (67.7%) than transitions from 19 pS to 42 pS (32.6%) that is consistent with the presence of NR2D rather than NR2C subunits (Wyllie *et al.* 1996). This same method which has been used to identify NR2D subunits has been reported by several groups. Misra *et al.* reported that in cerebellum Purkinje cells, 63% of direct transitions between 21pS and 34 pS went from 34pS to 21pS. In another Pukinje cell study, 72% of direct transition between 18pS and 38pS went from 38pS to 18pS (Momiyama *et al.* 1996). In addition, in cerebellar Golgi cells, 64% of direct transitions between 19pS and

39pS went from 39pS to 19pS (Misra *et al.* 2000) which is similar to the single-channel results from dopaminergic neurons in substantia nigra compacta (Jones & Gibb 2005). Our data are in good agreement with previous studies, suggesting the presence of NR2D subunits.

The presence of NR2D rather than NR2C subunits in NMDA receptor channels in STN neurons is also consistent with expression studies. No NR2C mRNA was detected in rat brain STN, but high levels of NR2D mRNA were found in the same experiment (Standaert *et al.* 1994). Our findings support the idea that NR2D subunits form functional NMDA receptors in STN neurones. Thus, NR2D-containing NMDA receptors may provide a novel therapeutic target in the basal ganglia.

7.4.3 Functional NMDA receptors in STN neurones contain NR2B subunits

Ifenprodil is a non-competitive NMDA receptor antagonist with high affinity for NR2B-containing NMDA receptors rather than those containing NR2A, NR2C or NR2D subunits (Williams 1993; Williams 1995; Cull-Candy & Leszkiewicz 2004). In the presence of saturating concentraions of agonist, NMDA or glutamate, 10 μM ifenprodil causes about 92% inhibition of NR1-NR2B mediated whole-cell current (Williams 1993; Mott *et al.* 1998) but only 50% inhibition for triheteromeric NR2B-containing receptors (Hatton & Paoletti 2005). In STN neurones, 10 μM ifenprodil reduced open probability of single-channel openings by 67%, suggesting a mixed population of NMDA receptors (diheteromeric and triheteromeric NR2B-containing NMDA receptors are expressed by P7 rat STN neurons. The same situation has been found in several brain regions such as

dopaminergic neurons in SNc (Jones & Gibb 2005) and Golgi cells in cerebellum (Brickley *et al.* 2003) . Interestingly, in my experiements a large conductance NMDA receptor (67pS) has been found in 3 of 6 patches from STN neurons and the application of 10 μM ifenprodil significantly reduced the open probability of this large conductance channel. Such a large conductance channel has not been described in SNc or cerebellar Golgi or Purkinje cells. It could be that the large conductance NMDA receptor might be the NR2B-containing NMDA receptor. In addition, direct transitions from 52pS to 19pS have been found in my experiments, suggesting triheteromeric NMDA receptors might be expressed by STN neurons.

In summary, we have shown that NMDA receptors in STN neurons contain NR2D and NR2B subunits. They might be a mixed population of diheteromeric NR1-NR2B NMDA receptor and triheteromeric NR1-NR2B-NR2D NMDA receptors.

Chapter 8: Future experiments

Since Parkinson's Disease is generally considered a disease of late middle age with the average age of onset at around 60 years of age, it is necessary to know the NMDA receptor composition on dopaminergic neurons of adult animals (in rats more than 6 weeks old). In addition, the NMDA receptor composition in SNc in animals with Parksinson's disease models is of interest. This information may contribute to revealing the pathogenetic mechanism underlying Parkinson's disease and also they can provide more accurate therapeutic target information for Parkinson's disease. Therefore, to extend this project, the NMDAR composition of SNc on adult animals and animals with Parkinson's disease (Parkinson's disease models) could be investigated using similar methods to those described in this thesis.

In addition, some relatively selective NMDA antagonists have been reported recently, such as UBP-141, PPDA and PBPD (Morley *et al.* 2005). It has been suggested that the PPDA and PBPD would have roughly 40-100 fold higher selectivity for NR2D subunits than NR2A and NR2B (Feng *et al.* 2004). Therefore, these drugs might be used in PD models to determine possible synaptic functions of NR2D-containing NMDA receptors (Brothwell *et al.* 2008).

In P7 subthalamic neurons, analysis of NMDA receptor single-channel properties revealed firstly, that activation of NMDA receptors produced a high conductance pattern of single-channel activity characterized by 42 pS and 52 pS single-channel currents and a low conductance pattern of single-channel activity characterized by 18 pS and 42 pS

single-channel currents. In addition, an unusual conductance, 68 pS single-channel current, was observed. Secondly, 10 μM ifenprodil significantly reduced NMDA receptor open probability by $66.7 \pm 9.3\%$, suggesting that NR2B-containing NMDA receptors are present on P7 STN neurons. Finally, direct transition analysis between open levels suggests that NR2D-containing NMDA receptors are expressed by P7 STN neurons. These findings were consistent with evidence showing that mRNA (Monyer *et al.* 1994; Standaert *et al.* 1994) and protein (Dunah *et al.* 1996; Dunah *et al.* 1998) encoding high levels of NR2D and low levels of NR2B subunits are expressed in STN neurons.

Since both NR2A- and NR2B-containing NMDA receptors show a similar large-conductance pattern of single-channel activity, which are 50 pS and 40 pS, it is necessary to know if functional NR2A-containing NMDA receptors are present on P7 rat STN neurons. It has been shown that high affinity Zn^{2+} inhibition of NR2A-containing NMDA receptors (Chen *et al.* 1997; Paoletti *et al.* 1997) can be removed by chelating extracellular contaminating Zn^{2+} with TPEN (N,N,N',N'-tetrakis-(2-pyridilmethyl)-ethylenediamine), a non-reducing metal chelating agent (Paoletti *et al.* 1997). The effect of TPEN is described as a potentiation of macroscopic currents produced by NMDA receptors in cultured cells and by NR1a/NR2A recombinant NMDA receptors expressed in HEK 293 cells and Xenopus oocytes (Paoletti *et al.* 1997) but not by NR1a/NR2A receptors expressed in Chinese hamster ovary (CHO) cells (Brimecombe et al., 1997). If a sub-population of NR2A-containing NMDA receptors with high Zn^{2+} sensitivity is present in P7 STN neurons then an increase in single-channel activity will be expected after contaminating Zn^{2+} is removed by adding TPEN or inhibition may be seen when extra Zn^{2+} is added to the external solution. Similar approaches could be used to assess the potential contribution of NR2A subunits to NMDA receptors in P7 rat STN neurons and the results compared with similar results from adult

neurons.

Chapter 9: References

Abdrachmanova, G., J. Teisinger, V. Vlachova & L. Vyklicky, Jr. (2000). "Molecular and functional properties of synaptically activated NMDA receptors in neonatal motoneurons in rat spinal cord slices." Eur J Neurosci **12**(3): 955-63.

Albers, D. S., S. W. Weiss, M. J. Iadarola & D. G. Standaert (1999). "Immunohistochemical localization of N-methyl-D-aspartate and alpha-amino-3-hydroxy-5-methyl-4-isoxazolepropionate receptor subunits in the substantia nigra pars compacta of the rat." Neuroscience **89**(1): 209-20.

Alexander, G. E. & M. D. Crutcher (1990). "Functional architecture of basal ganglia circuits: neural substrates of parallel processing." Trends Neurosci **13**(7): 266-71.

Andersson, O., A. Stenqvist, A. Attersand & G. von Euler (2001). "Nucleotide sequence, genomic organization, and chromosomal localization of genes encoding the human NMDA receptor subunits NR3A and NR3B." Genomics **78**(3): 178-84.

Anson, L. C., P. E. Chen, D. J. Wyllie, D. Colquhoun & R. Schoepfer (1998). "Identification of amino acid residues of the NR2A subunit that control glutamate potency in recombinant NR1/NR2A NMDA receptors." J Neurosci **18**(2): 581-9.

Antonov, S. M. & J. W. Johnson (1999). "Permeant ion regulation of N-methyl-D-aspartate receptor channel block by Mg(2+)." Proc Natl Acad Sci U S A **96**(25): 14571-6.

Armstrong, N., Y. Sun, G. Q. Chen & E. Gouaux (1998). "Structure of a glutamate-receptor ligand-binding core in complex with kainate." Nature **395**(6705): 913-7.

Ascher, P. & L. Nowak (1988). "The role of divalent cations in the N-methyl-D-aspartate responses of mouse central neurones in culture." J Physiol **399**: 247-66.

Avenet, P., J. Leonardon, F. Besnard, D. Graham, H. Depoortere & B. Scatton (1997). "Antagonist properties of eliprodil and other NMDA receptor antagonists at rat NR1A/NR2A and NR1A/NR2B receptors expressed in Xenopus oocytes." Neurosci Lett **223**(2): 133-6.

Banke, T. G., S. M. Dravid & S. F. Traynelis (2005). "Protons trap NR1/NR2B NMDA receptors in a nonconducting state." J Neurosci **25**(1): 42-51.

Banke, T. G. & S. F. Traynelis (2003). "Activation of NR1/NR2B NMDA receptors." Nat Neurosci **6**(2): 144-52.

Barbour, B. (2001). "An evaluation of synapse independence." J Neurosci **21**(20): 7969-84.

Bayer, K. U., P. De Koninck, A. S. Leonard, J. W. Hell & H. Schulman (2001). "Interaction with the NMDA receptor locks CaMKII in an active conformation." Nature **411**(6839): 801-5.

Beister, A., P. Kraus, W. Kuhn, M. Dose, A. Weindl & M. Gerlach (2004). "The N-methyl-D-aspartate antagonist memantine retards progression of Huntington's disease." J Neural Transm Suppl(68): 117-22.

Benveniste, M. & M. L. Mayer (1991). "Kinetic analysis of antagonist action at N-methyl-D-aspartic acid receptors. Two binding sites each for glutamate and glycine." Biophys J **59**(3): 560-73.

Benveniste, M. & M. L. Mayer (1995). "Trapping of glutamate and glycine during open channel block of rat hippocampal neuron NMDA receptors by 9-aminoacridine." J Physiol **483 (Pt 2)**: 367-84.

Berendse, H. W. & H. J. Groenewegen (1990). "Organization of the thalamostriatal projections in the rat, with special emphasis on the ventral striatum." J Comp Neurol **299**(2): 187-228.

Blanchet, P. J., S. Konitsiotis, E. R. Whittemore, Z. L. Zhou, R. M. Woodward & T. N. Chase (1999). "Differing effects of N-methyl-D-aspartate receptor subtype selective antagonists on dyskinesias in levodopa-treated 1-methyl-4-phenyl-tetrahydropyridine monkeys." J Pharmacol Exp Ther **290**(3): 1034-40.

Blandini, F., G. Nappi, C. Tassorelli & E. Martignoni (2000). "Functional changes of the basal ganglia circuitry in Parkinson's disease." Prog Neurobiol **62**(1): 63-88.

Blanpied, T. A., F. A. Boeckman, E. Aizenman & J. W. Johnson (1997). "Trapping channel block of NMDA-activated responses by amantadine and memantine." J Neurophysiol **77**(1): 309-23.

Bliss, T. V. & G. L. Collingridge (1993). "A synaptic model of memory: long-term potentiation in the hippocampus." Nature **361**(6407): 31-9.

Bolam, J. P., J. J. Hanley, P. A. Booth & M. D. Bevan (2000). "Synaptic organisation of the basal ganglia." J Anat **196 (Pt 4)**: 527-42.

Brickley, S. G., C. Misra, M. H. Mok, M. Mishina & S. G. Cull-Candy (2003). "NR2B and NR2D subunits coassemble in cerebellar Golgi cells to form a distinct NMDA receptor subtype restricted to extrasynaptic sites." J Neurosci **23**(12): 4958-66.

Brothwell, S. L., J. L. Barber, D. T. Monaghan, D. E. Jane, A. J. Gibb & S. Jones (2008). "NR2B- and NR2D-containing synaptic NMDA receptors in developing rat substantia nigra pars compacta dopaminergic

neurones." J Physiol **586**(Pt 3): 739-50.
Cathala, L., C. Misra & S. Cull-Candy (2000). "Developmental profile of the changing properties of NMDA receptors at cerebellar mossy fiber-granule cell synapses." J Neurosci **20**(16): 5899-905.
Chatha, B. T., V. Bernard, P. Streit & J. P. Bolam (2000). "Synaptic localization of ionotropic glutamate receptors in the rat substantia nigra." Neuroscience **101**(4): 1037-51.
Chatterton, J. E., M. Awobuluyi, L. S. Premkumar, H. Takahashi, M. Talantova, Y. Shin, J. Cui, S. Tu, K. A. Sevarino, N. Nakanishi, G. Tong, S. A. Lipton & D. Zhang (2002). "Excitatory glycine receptors containing the NR3 family of NMDA receptor subunits." Nature **415**(6873): 793-8.
Chazot, P. L. & F. A. Stephenson (1997). "Molecular dissection of native mammalian forebrain NMDA receptors containing the NR1 C2 exon: direct demonstration of NMDA receptors comprising NR1, NR2A, and NR2B subunits within the same complex." J Neurochem **69**(5): 2138-44.
Cheffings, C. M. & D. Colquhoun (2000). "Single channel analysis of a novel NMDA channel from Xenopus oocytes expressing recombinant NR1a, NR2A and NR2D subunits." J Physiol **526 Pt 3**: 481-91.
Chen, B. S., S. Braud, J. D. Badger, 2nd, J. T. Isaac & K. W. Roche (2006). "Regulation of NR1/NR2C N-methyl-D-aspartate (NMDA) receptors by phosphorylation." J Biol Chem **281**(24): 16583-90.
Chen, H. S. & S. A. Lipton (1997). "Mechanism of memantine block of NMDA-activated channels in rat retinal ganglion cells: uncompetitive antagonism." J Physiol **499 (Pt 1)**: 27-46.
Chen, H. S. & S. A. Lipton (2005). "Pharmacological implications of two distinct mechanisms of interaction of memantine with N-methyl-D-aspartate-gated channels." J Pharmacol Exp Ther **314**(3): 961-71.
Chen, H. S., J. W. Pellegrini, S. K. Aggarwal, S. Z. Lei, S. Warach, F. E. Jensen & S. A. Lipton (1992). "Open-channel block of N-methyl-D-aspartate (NMDA) responses by memantine: therapeutic advantage against NMDA receptor-mediated neurotoxicity." J Neurosci **12**(11): 4427-36.
Chen, N., A. Moshaver & L. A. Raymond (1997). "Differential sensitivity of recombinant N-methyl-D-aspartate receptor subtypes to zinc inhibition." Mol Pharmacol **51**(6): 1015-23.
Chen, P. E., A. R. Johnston, M. H. Mok, R. Schoepfer & D. J. Wyllie (2004). "Influence of a threonine residue in the S2 ligand binding domain in determining agonist potency and deactivation rate of recombinant NR1a/NR2D NMDA receptors." J Physiol **558**(Pt 1): 45-58.
Chen, P. E. & D. J. Wyllie (2006). "Pharmacological insights obtained from structure-function studies of ionotropic glutamate receptors." Br J Pharmacol **147**(8): 839-53.
Chen, Y., J. E. Chad, R. C. Cannon & H. V. Wheal (1999). "Reduced Mg2+ blockade of synaptically activated N-methyl-D-aspartate receptor-channels in CA1 pyramidal neurons in kainic acid-lesioned rat hippocampus." Neuroscience **88**(3): 727-39.
Choi, D. W. (1992). "Excitotoxic cell death." J Neurobiol **23**(9): 1261-76.
Clark, B. A., M. Farrant & S. G. Cull-Candy (1997). "A direct comparison of the single-channel properties of synaptic and extrasynaptic NMDA receptors." J Neurosci **17**(1): 107-16.
Clements, J. D., R. A. Lester, G. Tong, C. E. Jahr & G. L. Westbrook (1992). "The time course of glutamate in the synaptic cleft." Science **258**(5087): 1498-501.
Collingridge, G. (1987). "Synaptic plasticity. The role of NMDA receptors in learning and memory." Nature **330**(6149): 604-5.
Collingridge, G. L., C. E. Herron & R. A. Lester (1988). "Frequency-dependent N-methyl-D-aspartate receptor-mediated synaptic transmission in rat hippocampus." J Physiol **399**: 301-12.
Colquhoun, D. (2007). "What have we learned from single ion channels?" J Physiol **581**(Pt 2): 425-7.
Colquhoun, D. & A. G. Hawkes (1977). "Relaxation and fluctuations of membrane currents that flow through drug-operated channels." Proc R Soc Lond B Biol Sci **199**(1135): 231-62.
Colquhoun, D. & B. Sakmann (1981). "Fluctuations in the microsecond time range of the current through single acetylcholine receptor ion channels." Nature **294**(5840): 464-6.
Conn, P. J. & J. P. Pin (1997). "Pharmacology and functions of metabotropic glutamate receptors." Annu Rev Pharmacol Toxicol **37**: 205-37.
Constantine-Paton, M. (1990). "NMDA receptor as a mediator of activity-dependent synaptogenesis in the developing brain." Cold Spring Harb Symp Quant Biol **55**: 431-43.
Counihan, T. J., G. B. Landwehrmeyer, D. G. Standaert, C. M. Kosinski, C. R. Scherzer, L. P. Daggett, G. Velicelebi, A. B. Young & J. B. Penney, Jr. (1998). "Expression of N-methyl-D-aspartate receptor subunit mRNA in the human brain: mesencephalic dopaminergic neurons." J Comp Neurol **390**(1): 91-101.
Cull-Candy, S., S. Brickley & M. Farrant (2001). "NMDA receptor subunits: diversity, development and disease." Curr Opin Neurobiol **11**(3): 327-35.
Cull-Candy, S. G. & D. N. Leszkiewicz (2004). "Role of distinct NMDA receptor subtypes at central synapses." Sci STKE **2004**(255): re16.
Dalby, N. O. & I. Mody (2003). "Activation of NMDA receptors in rat dentate gyrus granule cells by spontaneous and evoked transmitter release." J Neurophysiol **90**(2): 786-97.
Danysz, W., C. G. Parsons, J. Kornhuber, W. J. Schmidt & G. Quack (1997). "Aminoadamantanes as NMDA receptor antagonists and antiparkinsonian agents--preclinical studies." Neurosci Biobehav Rev **21**(4): 455-68.
Das, S., Y. F. Sasaki, T. Rothe, L. S. Premkumar, M. Takasu, J. E. Crandall, P. Dikkes, D. A. Conner, P. V. Rayudu, W. Cheung, H. S. Chen, S. A. Lipton & N. Nakanishi (1998). "Increased NMDA current and spine density in

mice lacking the NMDA receptor subunit NR3A." Nature **393**(6683): 377-81.
Del Dotto, P., N. Pavese, G. Gambaccini, S. Bernardini, L. V. Metman, T. N. Chase & U. Bonuccelli (2001). "Intravenous amantadine improves levadopa-induced dyskinesias: an acute double-blind placebo-controlled study." Mov Disord **16**(3): 515-20.
Dempsey, R. J., M. K. Baskaya & A. Dogan (2000). "Attenuation of brain edema, blood-brain barrier breakdown, and injury volume by ifenprodil, a polyamine-site N-methyl-D-aspartate receptor antagonist, after experimental traumatic brain injury in rats." Neurosurgery **47**(2): 399-404; discussion 404-6.
Di, X., R. Bullock, J. Watson, P. Fatouros, B. Chenard, F. White & F. Corwin (1997). "Effect of CP101,606, a novel NR2B subunit antagonist of the N-methyl-D-aspartate receptor, on the volume of ischemic brain damage off cytotoxic brain edema after middle cerebral artery occlusion in the feline brain." Stroke **28**(11): 2244-51.
Didier, M., M. Xu, S. A. Berman & S. Bursztajn (1995). "Differential expression and co-assembly of NMDA zeta 1 and epsilon subunits in the mouse cerebellum during postnatal development." Neuroreport **6**(16): 2255-9.
Difiglia, M., T. Pasik & P. Pasik (1980). "Ultrastructure of Golgi-impregnated and gold-toned spiny and aspiny neurons in the monkey neostriatum." J Neurocytol **9**(4): 471-92.
Dingledine, R., K. Borges, D. Bowie & S. F. Traynelis (1999). "The glutamate receptor ion channels." Pharmacol Rev **51**(1): 7-61.
Dunah, A. W., J. Luo, Y. H. Wang, R. P. Yasuda & B. B. Wolfe (1998). "Subunit composition of N-methyl-D-aspartate receptors in the central nervous system that contain the NR2D subunit." Mol Pharmacol **53**(3): 429-37.
Dunah, A. W. & D. G. Standaert (2003). "Subcellular segregation of distinct heteromeric NMDA glutamate receptors in the striatum." J Neurochem **85**(4): 935-43.
Dunah, A. W., R. P. Yasuda, Y. H. Wang, J. Luo, M. Davila-Garcia, M. Gbadegesin, S. Vicini & B. B. Wolfe (1996). "Regional and ontogenic expression of the NMDA receptor subunit NR2D protein in rat brain using a subunit-specific antibody." J Neurochem **67**(6): 2335-45.
Edwards, F. A., A. Konnerth, B. Sakmann & T. Takahashi (1989). "A thin slice preparation for patch clamp recordings from neurones of the mammalian central nervous system." Pflugers Arch **414**(5): 600-12.
Erreger, K., S. M. Dravid, T. G. Banke, D. J. Wyllie & S. F. Traynelis (2005). "Subunit-specific gating controls rat NR1/NR2A and NR1/NR2B NMDA channel kinetics and synaptic signalling profiles." J Physiol **563**(Pt 2): 345-58.
Farrant, M., D. Feldmeyer, T. Takahashi & S. G. Cull-Candy (1994). "NMDA-receptor channel diversity in the developing cerebellum." Nature **368**(6469): 335-9.
Fellin, T., O. Pascual, S. Gobbo, T. Pozzan, P. G. Haydon & G. Carmignoto (2004). "Neuronal synchrony mediated by astrocytic glutamate through activation of extrasynaptic NMDA receptors." Neuron **43**(5): 729-43.
Feng, B., H. W. Tse, D. A. Skifter, R. Morley, D. E. Jane & D. T. Monaghan (2004). "Structure-activity analysis of a novel NR2C/NR2D-preferring NMDA receptor antagonist: 1-(phenanthrene-2-carbonyl) piperazine-2,3-dicarboxylic acid." Br J Pharmacol **141**(3): 508-16.
Fischer, G., V. Mutel, G. Trube, P. Malherbe, J. N. Kew, E. Mohacsi, M. P. Heitz & J. A. Kemp (1997). "Ro 25-6981, a highly potent and selective blocker of N-methyl-D-aspartate receptors containing the NR2B subunit. Characterization in vitro." J Pharmacol Exp Ther **283**(3): 1285-92.
Forsythe, I. D. & G. L. Westbrook (1988). "Slow excitatory postsynaptic currents mediated by N-methyl-D-aspartate receptors on cultured mouse central neurones." J Physiol **396**: 515-33.
Fujisawa, S. & C. Aoki (2003). "In vivo blockade of N-methyl-D-aspartate receptors induces rapid trafficking of NR2B subunits away from synapses and out of spines and terminals in adult cortex." Neuroscience **121**(1): 51-63.
Furukawa, Y., M. Okada, N. Akaike, T. Hayashi & J. Nabekura (2000). "Reduction of voltage-dependent magnesium block of N-methyl-D-aspartate receptor-mediated current by in vivo axonal injury." Neuroscience **96**(2): 385-92.
Gibb, A. J. & D. Colquhoun (1991). "Glutamate activation of a single NMDA receptor-channel produces a cluster of channel openings." Proc Biol Sci **243**(1306): 39-45.
Gibb, A. J. & D. Colquhoun (1992). "Activation of N-methyl-D-aspartate receptors by L-glutamate in cells dissociated from adult rat hippocampus." J Physiol **456**: 143-79.
Gotti, B., D. Duverger, J. Bertin, C. Carter, R. Dupont, J. Frost, B. Gaudilliere, E. T. MacKenzie, J. Rousseau, B. Scatton & et al. (1988). "Ifenprodil and SL 82.0715 as cerebral anti-ischemic agents. I. Evidence for efficacy in models of focal cerebral ischemia." J Pharmacol Exp Ther **247**(3): 1211-21.
Gotz, T., U. Kraushaar, J. Geiger, J. Lubke, T. Berger & P. Jonas (1997). "Functional properties of AMPA and NMDA receptors expressed in identified types of basal ganglia neurons." J Neurosci **17**(1): 204-15.
Green, G. M. & A. J. Gibb (2001). "Characterization of the single-channel properties of NMDA receptors in laminae I and II of the dorsal horn of neonatal rat spinal cord." Eur J Neurosci **14**(10): 1590-602.
Haber, S. N. (2003). "The primate basal ganglia: parallel and integrative networks." J Chem Neuroanat **26**(4): 317-30.
Hajos, M. & S. A. Greenfield (1993). "Topographic heterogeneity of substantia nigra neurons: diversity in intrinsic membrane properties and synaptic inputs." Neuroscience **55**(4): 919-34.

Hallett, P. J. & D. G. Standaert (2004). "Rationale for and use of NMDA receptor antagonists in Parkinson's disease." Pharmacol Ther **102**(2): 155-74.
Hamani, C., J. A. Saint-Cyr, J. Fraser, M. Kaplitt & A. M. Lozano (2004). "The subthalamic nucleus in the context of movement disorders." Brain **127**(Pt 1): 4-20.
Hatton, C. J. & P. Paoletti (2005). "Modulation of triheteromeric NMDA receptors by N-terminal domain ligands." Neuron **46**(2): 261-74.
Hayashi, Y. & A. K. Majewska (2005). "Dendritic spine geometry: functional implication and regulation." Neuron **46**(4): 529-32.
Herron, C. E., R. A. Lester, E. J. Coan & G. L. Collingridge (1986). "Frequency-dependent involvement of NMDA receptors in the hippocampus: a novel synaptic mechanism." Nature **322**(6076): 265-8.
Hess, S. D., L. P. Daggett, C. Deal, C. C. Lu, E. C. Johnson & G. Velicelebi (1998). "Functional characterization of human N-methyl-D-aspartate subtype 1A/2D receptors." J Neurochem **70**(3): 1269-79.
Hollmann, M., C. Maron & S. Heinemann (1994). "N-glycosylation site tagging suggests a three transmembrane domain topology for the glutamate receptor GluR1." Neuron **13**(6): 1331-43.
Holt, D. J., A. M. Graybiel & C. B. Saper (1997). "Neurochemical architecture of the human striatum." J Comp Neurol **384**(1): 1-25.
Horak, M., K. Vlcek, M. Petrovic, H. Chodounska & L. Vyklicky, Jr. (2004). "Molecular mechanism of pregnenolone sulfate action at NR1/NR2B receptors." J Neurosci **24**(46): 10318-25.
Hu, B. & C. W. Bourque (1992). "NMDA receptor-mediated rhythmic bursting activity in rat supraoptic nucleus neurones in vitro." J Physiol **458**: 667-87.
Ishii, T., K. Moriyoshi, H. Sugihara, K. Sakurada, H. Kadotani, M. Yokoi, C. Akazawa, R. Shigemoto, N. Mizuno, M. Masu & et al. (1993). "Molecular characterization of the family of the N-methyl-D-aspartate receptor subunits." J Biol Chem **268**(4): 2836-43.
Jahr, C. E. & C. F. Stevens (1990). "A quantitative description of NMDA receptor-channel kinetic behavior." J Neurosci **10**(6): 1830-7.
Janssen, W. G., P. Vissavajjhala, G. Andrews, T. Moran, P. R. Hof & J. H. Morrison (2005). "Cellular and synaptic distribution of NR2A and NR2B in macaque monkey and rat hippocampus as visualized with subunit-specific monoclonal antibodies." Exp Neurol **191 Suppl 1**: S28-44.
Johnson, J. W. & P. Ascher (1987). "Glycine potentiates the NMDA response in cultured mouse brain neurons." Nature **325**(6104): 529-31.
Johnson, J. W. & P. Ascher (1990). "Voltage-dependent block by intracellular Mg2+ of N-methyl-D-aspartate-activated channels." Biophys J **57**(5): 1085-90.
Jones, S. & A. J. Gibb (2005). "Functional NR2B- and NR2D-containing NMDA receptor channels in rat substantia nigra dopaminergic neurones." J Physiol **569**(Pt 1): 209-21.
Kampa, B. M., J. Clements, P. Jonas & G. J. Stuart (2004). "Kinetics of Mg2+ unblock of NMDA receptors: implications for spike-timing dependent synaptic plasticity." J Physiol **556**(Pt 2): 337-45.
Kashiwagi, K., T. Masuko, C. D. Nguyen, T. Kuno, I. Tanaka, K. Igarashi & K. Williams (2002). "Channel blockers acting at N-methyl-D-aspartate receptors: differential effects of mutations in the vestibule and ion channel pore." Mol Pharmacol **61**(3): 533-45.
Kawaguchi, Y., C. J. Wilson, S. J. Augood & P. C. Emson (1995). "Striatal interneurones: chemical, physiological and morphological characterization." Trends Neurosci **18**(12): 527-35.
Kelley, A. E., V. B. Domesick & W. J. Nauta (1982). "The amygdalostriatal projection in the rat--an anatomical study by anterograde and retrograde tracing methods." Neuroscience **7**(3): 615-30.
Kern, D. S. & R. Kumar (2007). "Deep brain stimulation." Neurologist **13**(5): 237-52.
Kew, J. N. & J. A. Kemp (2005). "Ionotropic and metabotropic glutamate receptor structure and pharmacology." Psychopharmacology (Berl) **179**(1): 4-29.
Kew, J. N., G. Trube & J. A. Kemp (1996). "A novel mechanism of activity-dependent NMDA receptor antagonism describes the effect of ifenprodil in rat cultured cortical neurones." J Physiol **497 (Pt 3)**: 761-72.
Kirson, E. D., C. Schirra, A. Konnerth & Y. Yaari (1999). "Early postnatal switch in magnesium sensitivity of NMDA receptors in rat CA1 pyramidal cells." J Physiol **521 Pt 1**: 99-111.
Kita, H. & S. T. Kitai (1987). "Efferent projections of the subthalamic nucleus in the rat: light and electron microscopic analysis with the PHA-L method." J Comp Neurol **260**(3): 435-52.
Kita, H. & S. T. Kitai (1994). "The morphology of globus pallidus projection neurons in the rat: an intracellular staining study." Brain Res **636**(2): 308-19.
Kitai, S. T. & J. M. Deniau (1981). "Cortical inputs to the subthalamus: intracellular analysis." Brain Res **214**(2): 411-5.
Kohr, G., V. Jensen, H. J. Koester, A. L. Mihaljevic, J. K. Utvik, A. Kvello, O. P. Ottersen, P. H. Seeburg, R. Sprengel & O. Hvalby (2003). "Intracellular domains of NMDA receptor subtypes are determinants for long-term potentiation induction." J Neurosci **23**(34): 10791-9.
Komuro, H. & P. Rakic (1993). "Modulation of neuronal migration by NMDA receptors." Science **260**(5104): 95-7.
Kornhuber, J., J. Bormann, W. Retz, M. Hubers & P. Riederer (1989). "Memantine displaces [3H]MK-801 at therapeutic concentrations in postmortem human frontal cortex." Eur J Pharmacol **166**(3): 589-90.

Krapivinsky, G., L. Krapivinsky, Y. Manasian, A. Ivanov, R. Tyzio, C. Pellegrino, Y. Ben-Ari, D. E. Clapham & I. Medina (2003). "The NMDA receptor is coupled to the ERK pathway by a direct interaction between NR2B and RasGRF1." Neuron **40**(4): 775-84.

Kuner, T. & R. Schoepfer (1996). "Multiple structural elements determine subunit specificity of Mg2+ block in NMDA receptor channels." J Neurosci **16**(11): 3549-58.

Kuppenbender, K. D., D. S. Albers, M. J. Iadarola, G. B. Landwehrmeyer & D. G. Standaert (1999). "Localization of alternatively spliced NMDAR1 glutamate receptor isoforms in rat striatal neurons." J Comp Neurol **415**(2): 204-17.

Kuramoto, T., T. Maihara, M. Masu, S. Nakanishi & T. Serikawa (1994). "Gene mapping of NMDA receptors and metabotropic glutamate receptors in the rat (Rattus norvegicus)." Genomics **19**(2): 358-61.

Laurie, D. J., J. Putzke, W. Zieglgansberger, P. H. Seeburg & T. R. Tolle (1995). "The distribution of splice variants of the NMDAR1 subunit mRNA in adult rat brain." Brain Res Mol Brain Res **32**(1): 94-108.

Laurie, D. J. & P. H. Seeburg (1994). "Regional and developmental heterogeneity in splicing of the rat brain NMDAR1 mRNA." J Neurosci **14**(5 Pt 2): 3180-94.

Layer, R. T., P. Popik, T. Olds & P. Skolnick (1995). "Antidepressant-like actions of the polyamine site NMDA antagonist, eliprodil (SL-82.0715)." Pharmacol Biochem Behav **52**(3): 621-7.

Lester, R. A. & C. E. Jahr (1992). "NMDA channel behavior depends on agonist affinity." J Neurosci **12**(2): 635-43.

Li, J. H., Y. H. Wang, B. B. Wolfe, K. E. Krueger, L. Corsi, G. Stocca & S. Vicini (1998). "Developmental changes in localization of NMDA receptor subunits in primary cultures of cortical neurons." Eur J Neurosci **10**(5): 1704-15.

Li, S., X. Tian, D. M. Hartley & L. A. Feig (2006). "Distinct roles for Ras-guanine nucleotide-releasing factor 1 (Ras-GRF1) and Ras-GRF2 in the induction of long-term potentiation and long-term depression." J Neurosci **26**(6): 1721-9.

Lipton, S. A. (2006). "Paradigm shift in neuroprotection by NMDA receptor blockade: memantine and beyond." Nat Rev Drug Discov **5**(2): 160-70.

Lozovaya, N., S. Melnik, T. Tsintsadze, S. Grebenyuk, Y. Kirichok & O. Krishtal (2004). "Protective cap over CA1 synapses: extrasynaptic glutamate does not reach the postsynaptic density." Brain Res **1011**(2): 195-205.

Magleby, K. L. & C. F. Stevens (1972). "A quantitative description of end-plate currents." J Physiol **223**(1): 173-97.

Mayer, M. L. (2006). "Glutamate receptors at atomic resolution." Nature **440**(7083): 456-62.

Mayer, M. L. & N. Armstrong (2004). "Structure and function of glutamate receptor ion channels." Annu Rev Physiol **66**: 161-81.

Mayer, M. L. & G. L. Westbrook (1985). "The action of N-methyl-D-aspartic acid on mouse spinal neurones in culture." J Physiol **361**: 65-90.

Mayer, M. L. & G. L. Westbrook (1987). "Permeation and block of N-methyl-D-aspartic acid receptor channels by divalent cations in mouse cultured central neurones." J Physiol **394**: 501-27.

Mayer, M. L., G. L. Westbrook & P. B. Guthrie (1984). "Voltage-dependent block by Mg2+ of NMDA responses in spinal cord neurones." Nature **309**(5965): 261-3.

McGeorge, A. J. & R. L. Faull (1989). "The organization of the projection from the cerebral cortex to the striatum in the rat." Neuroscience **29**(3): 503-37.

Misra, C., S. G. Brickley, M. Farrant & S. G. Cull-Candy (2000). "Identification of subunits contributing to synaptic and extrasynaptic NMDA receptors in Golgi cells of the rat cerebellum." J Physiol **524 Pt 1**: 147-62.

Misra, C., S. G. Brickley, D. J. Wyllie & S. G. Cull-Candy (2000). "Slow deactivation kinetics of NMDA receptors containing NR1 and NR2D subunits in rat cerebellar Purkinje cells." J Physiol **525 Pt 2**: 299-305.

Mitchell, I. J. & C. B. Carroll (1997). "Reversal of parkinsonian symptoms in primates by antagonism of excitatory amino acid transmission: potential mechanisms of action." Neurosci Biobehav Rev **21**(4): 469-75.

Mohrmann, R., G. Kohr, H. Hatt, R. Sprengel & K. Gottmann (2002). "Deletion of the C-terminal domain of the NR2B subunit alters channel properties and synaptic targeting of N-methyl-D-aspartate receptors in nascent neocortical synapses." J Neurosci Res **68**(3): 265-75.

Momiyama, A., D. Feldmeyer & S. G. Cull-Candy (1996). "Identification of a native low-conductance NMDA channel with reduced sensitivity to Mg2+ in rat central neurones." J Physiol **494 (Pt 2)**(Pt 2): 479-92.

Monyer, H., N. Burnashev, D. J. Laurie, B. Sakmann & P. H. Seeburg (1994). "Developmental and regional expression in the rat brain and functional properties of four NMDA receptors." Neuron **12**(3): 529-40.

Monyer, H., R. Sprengel, R. Schoepfer, A. Herb, M. Higuchi, H. Lomeli, N. Burnashev, B. Sakmann & P. H. Seeburg (1992). "Heteromeric NMDA receptors: molecular and functional distinction of subtypes." Science **256**(5060): 1217-21.

Moriyoshi, K., M. Masu, T. Ishii, R. Shigemoto, N. Mizuno & S. Nakanishi (1991). "Molecular cloning and characterization of the rat NMDA receptor." Nature **354**(6348): 31-7.

Morley, R. M., H. W. Tse, B. Feng, J. C. Miller, D. T. Monaghan & D. E. Jane (2005). "Synthesis and pharmacology of N1-substituted piperazine-2,3-dicarboxylic acid derivatives acting as NMDA receptor antagonists." J Med Chem **48**(7): 2627-37.

Mott, D. D., J. J. Doherty, S. Zhang, M. S. Washburn, M. J. Fendley, P. Lyuboslavsky, S. F. Traynelis & R.

Dingledine (1998). "Phenylethanolamines inhibit NMDA receptors by enhancing proton inhibition." Nat Neurosci **1**(8): 659-67.
Mueller, H. T. & J. H. Meador-Woodruff (2005). "Distribution of the NMDA receptor NR3A subunit in the adult pig-tail macaque brain." J Chem Neuroanat **29**(3): 157-72.
Nakanishi, H., H. Kita & S. T. Kitai (1988). "An N-methyl-D-aspartate receptor mediated excitatory postsynaptic potential evoked in subthalamic neurons in an in vitro slice preparation of the rat." Neurosci Lett **95**(1-3): 130-6.
Nambu, A., H. Tokuno, I. Hamada, H. Kita, M. Imanishi, T. Akazawa, Y. Ikeuchi & N. Hasegawa (2000). "Excitatory cortical inputs to pallidal neurons via the subthalamic nucleus in the monkey." J Neurophysiol **84**(1): 289-300.
Nash, J. E., M. P. Hill & J. M. Brotchie (1999). "Antiparkinsonian actions of blockade of NR2B-containing NMDA receptors in the reserpine-treated rat." Exp Neurol **155**(1): 42-8.
Neher, E. & B. Sakmann (1976). "Single-channel currents recorded from membrane of denervated frog muscle fibres." Nature **260**(5554): 799-802.
Nevian, T. & B. Sakmann (2004). "Single spine Ca2+ signals evoked by coincident EPSPs and backpropagating action potentials in spiny stellate cells of layer 4 in the juvenile rat somatosensory barrel cortex." J Neurosci **24**(7): 1689-99.
Nowak, L., P. Bregestovski, P. Ascher, A. Herbet & A. Prochiantz (1984). "Magnesium gates glutamate-activated channels in mouse central neurones." Nature **307**(5950): 462-5.
Okiyama, K., D. H. Smith, W. F. White, K. Richter & T. K. McIntosh (1997). "Effects of the novel NMDA antagonists CP-98,113, CP-101,581 and CP-101,606 on cognitive function and regional cerebral edema following experimental brain injury in the rat." J Neurotrauma **14**(4): 211-22.
Ozawa, S., H. Kamiya & K. Tsuzuki (1998). "Glutamate receptors in the mammalian central nervous system." Prog Neurobiol **54**(5): 581-618.
Palecek, J. I., G. Abdrachmanova, V. Vlachova & L. Vyklick, Jr. (1999). "Properties of NMDA receptors in rat spinal cord motoneurons." Eur J Neurosci **11**(3): 827-36.
Paoletti, P., P. Ascher & J. Neyton (1997). "High-affinity zinc inhibition of NMDA NR1-NR2A receptors." J Neurosci **17**(15): 5711-25.
Paoletti, P. & J. Neyton (2007). "NMDA receptor subunits: function and pharmacology." Curr Opin Pharmacol **7**(1): 39-47.
Paoletti, P., J. Neyton & P. Ascher (1995). "Glycine-independent and subunit-specific potentiation of NMDA responses by extracellular Mg2+." Neuron **15**(5): 1109-20.
Paoletti, P., F. Perin-Dureau, A. Fayyazuddin, A. Le Goff, I. Callebaut & J. Neyton (2000). "Molecular organization of a zinc binding n-terminal modulatory domain in a NMDA receptor subunit." Neuron **28**(3): 911-25.
Parent, A. & L. N. Hazrati (1995). "Functional anatomy of the basal ganglia. I. The cortico-basal ganglia-thalamo-cortical loop." Brain Res Brain Res Rev **20**(1): 91-127.
Parsons, C. G., W. Danysz & G. Quack (1999). "Memantine is a clinically well tolerated N-methyl-D-aspartate (NMDA) receptor antagonist--a review of preclinical data." Neuropharmacology **38**(6): 735-67.
Patneau, D. K. & M. L. Mayer (1990). "Structure-activity relationships for amino acid transmitter candidates acting at N-methyl-D-aspartate and quisqualate receptors." J Neurosci **10**(7): 2385-99.
Penney, J. B., Jr. & A. B. Young (1986). "Striatal inhomogeneities and basal ganglia function." Mov Disord **1**(1): 3-15.
Perez-Otano, I., C. T. Schulteis, A. Contractor, S. A. Lipton, J. S. Trimmer, N. J. Sucher & S. F. Heinemann (2001). "Assembly with the NR1 subunit is required for surface expression of NR3A-containing NMDA receptors." J Neurosci **21**(4): 1228-37.
Perin-Dureau, F., J. Rachline, J. Neyton & P. Paoletti (2002). "Mapping the binding site of the neuroprotectant ifenprodil on NMDA receptors." J Neurosci **22**(14): 5955-65.
Pina-Crespo, J. C. & A. J. Gibb (2002). "Subtypes of NMDA receptors in new-born rat hippocampal granule cells." J Physiol **541**(Pt 1): 41-64.
Prybylowski, K., G. Rumbaugh, B. B. Wolfe & S. Vicini (2000). "Increased exon 5 expression alters extrasynaptic NMDA receptors in cerebellar neurons." J Neurochem **75**(3): 1140-6.
Qian, A., S. M. Antonov & J. W. Johnson (2002). "Modulation by permeant ions of Mg(2+) inhibition of NMDA-activated whole-cell currents in rat cortical neurons." J Physiol **538**(Pt 1): 65-77.
Qian, A., A. L. Buller & J. W. Johnson (2005). "NR2 subunit-dependence of NMDA receptor channel block by external Mg2+." J Physiol **562**(Pt 2): 319-31.
Radad, K., G. Gille & W. D. Rausch (2005). "Short review on dopamine agonists: insight into clinical and research studies relevant to Parkinson's disease." Pharmacol Rep **57**(6): 701-12.
Roche, K. W., S. Standley, J. McCallum, C. Dune Ly, M. D. Ehlers & R. J. Wenthold (2001). "Molecular determinants of NMDA receptor internalization." Nat Neurosci **4**(8): 794-802.
Rumbaugh, G., K. Prybylowski, J. F. Wang & S. Vicini (2000). "Exon 5 and spermine regulate deactivation of NMDA receptor subtypes." J Neurophysiol **83**(3): 1300-6.
Schorge, S. & D. Colquhoun (2003). "Studies of NMDA receptor function and stoichiometry with truncated and

tandem subunits." J Neurosci 23(4): 1151-8.
Scimemi, A., A. Fine, D. M. Kullmann & D. A. Rusakov (2004). "NR2B-containing receptors mediate cross talk among hippocampal synapses." J Neurosci 24(20): 4767-77.
Shalaby, I. A., B. L. Chenard, M. A. Prochniak & T. W. Butler (1992). "Neuroprotective effects of the N-methyl-D-aspartate receptor antagonists ifenprodil and SL-82,0715 on hippocampal cells in culture." J Pharmacol Exp Ther 260(2): 925-32.
Sheng, M., J. Cummings, L. A. Roldan, Y. N. Jan & L. Y. Jan (1994). "Changing subunit composition of heteromeric NMDA receptors during development of rat cortex." Nature 368(6467): 144-7.
Sigworth, F. J. & S. M. Sine (1987). "Data transformations for improved display and fitting of single-channel dwell time histograms." Biophys J 52(6): 1047-54.
Sobolevsky, A. & S. Koshelev (1998). "Two blocking sites of amino-adamantane derivatives in open N-methyl-D-aspartate channels." Biophys J 74(3): 1305-19.
Sobolevsky, A. I., S. G. Koshelev & B. I. Khodorov (1998). "Interaction of memantine and amantadine with agonist-unbound NMDA-receptor channels in acutely isolated rat hippocampal neurons." J Physiol 512 (Pt 1): 47-60.
Spruston, N., P. Jonas & B. Sakmann (1995). "Dendritic glutamate receptor channels in rat hippocampal CA3 and CA1 pyramidal neurons." J Physiol 482 (Pt 2): 325-52.
Standaert DG, T. C., Young AB, Penney JB Jr. (1994). "Organization of N-methyl-D-aspartate glutamate receptor gene expression in the basal ganglia of the rat." J Comp Neurol 343(1)(May 1): 1-16.
Standaert, D. G., C. M. Testa, A. B. Young & J. B. Penney, Jr. (1994). "Organization of N-methyl-D-aspartate glutamate receptor gene expression in the basal ganglia of the rat." J Comp Neurol 343(1): 1-16.
Stephenson, F. A. (2001). "Subunit characterization of NMDA receptors." Curr Drug Targets 2(3): 233-9.
Stern, P., P. Behe, R. Schoepfer & D. Colquhoun (1992). "Single-channel conductances of NMDA receptors expressed from cloned cDNAs: comparison with native receptors." Proc Biol Sci 250(1329): 271-7.
Stern, P., M. Cik, D. Colquhoun & F. A. Stephenson (1994). "Single channel properties of cloned NMDA receptors in a human cell line: comparison with results from Xenopus oocytes." J Physiol 476(3): 391-7.
Stocca, G. & S. Vicini (1998). "Increased contribution of NR2A subunit to synaptic NMDA receptors in developing rat cortical neurons." J Physiol 507 (Pt 1): 13-24.
Strecker, G. J., M. B. Jackson & F. E. Dudek (1994). "Blockade of NMDA-activated channels by magnesium in the immature rat hippocampus." J Neurophysiol 72(4): 1538-48.
Takano, H., O. Onodera, H. Tanaka, H. Mori, K. Sakimura, T. Hori, H. Kobayashi, M. Mishina & S. Tsuji (1993). "Chromosomal localization of the epsilon 1, epsilon 3 and zeta 1 subunit genes of the human NMDA receptor channel." Biochem Biophys Res Commun 197(2): 922-6.
Tamura, Y., Y. Sato, T. Yokota, A. Akaike, M. Sasa & S. Takaori (1993). "Ifenprodil prevents glutamate cytotoxicity via polyamine modulatory sites of N-methyl-D-aspartate receptors in cultured cortical neurons." J Pharmacol Exp Ther 265(2): 1017-25.
Tanner, C. M. (1992). "Occupational and environmental causes of parkinsonism." Occup Med 7(3): 503-13.
Tepper, J. M., S. F. Sawyer & P. M. Groves (1987). "Electrophysiologically identified nigral dopaminergic neurons intracellularly labeled with HRP: light-microscopic analysis." J Neurosci 7(9): 2794-806.
Thomas, C. G., A. J. Miller & G. L. Westbrook (2006). "Synaptic and extrasynaptic NMDA receptor NR2 subunits in cultured hippocampal neurons." J Neurophysiol 95(3): 1727-34.
Toulmond, S., A. Serrano, J. Benavides & B. Scatton (1993). "Prevention by eliprodil (SL 82.0715) of traumatic brain damage in the rat. Existence of a large (18 h) therapeutic window." Brain Res 620(1): 32-41.
Tovar, K. R. & G. L. Westbrook (2002). "Mobile NMDA receptors at hippocampal synapses." Neuron 34(2): 255-64.
Traynelis, S. F., M. Hartley & S. F. Heinemann (1995). "Control of proton sensitivity of the NMDA receptor by RNA splicing and polyamines." Science 268(5212): 873-6.
Traynelis, S. F., R. A. Silver & S. G. Cull-Candy (1993). "Estimated conductance of glutamate receptor channels activated during EPSCs at the cerebellar mossy fiber-granule cell synapse." Neuron 11(2): 279-89.
Unwin, N. (1989). "The structure of ion channels in membranes of excitable cells." Neuron 3(6): 665-76.
Vargas-Caballero, M. & H. P. Robinson (2004). "Fast and slow voltage-dependent dynamics of magnesium block in the NMDA receptor: the asymmetric trapping block model." J Neurosci 24(27): 6171-80.
Vicini, S. & G. Rumbaugh (2000). "A slow NMDA channel: in search of a role." J Physiol 525 Pt 2(283): 283.
Vicini, S., J. F. Wang, J. H. Li, W. J. Zhu, Y. H. Wang, J. H. Luo, B. B. Wolfe & D. R. Grayson (1998). "Functional and pharmacological differences between recombinant N-methyl-D-aspartate receptors." J Neurophysiol 79(2): 555-66.
Wang, L. Y. & J. F. MacDonald (1995). "Modulation by magnesium of the affinity of NMDA receptors for glycine in murine hippocampal neurones." J Physiol 486 (Pt 1)(Pt 1): 83-95.
Washio, H., K. Takigachi-Hayashi & S. Konishi (1999). "Early postnatal development of substantia nigra neurons in rat midbrain slices: hyperpolarization-activated inward current and dopamine-activated current." Neurosci Res 34(2): 91-101.
Watanabe, M., Y. Inoue, K. Sakimura & M. Mishina (1993). "Distinct distributions of five N-methyl-D-aspartate receptor channel subunit mRNAs in the forebrain." J Comp Neurol 338(3): 377-90.

Watanabe, M., M. Mishina & Y. Inoue (1994). "Distinct distributions of five NMDA receptor channel subunit mRNAs in the brainstem." J Comp Neurol **343**(4): 520-31.
Watanabe, M., M. Mishina & Y. Inoue (1994). "Distinct spatiotemporal expressions of five NMDA receptor channel subunit mRNAs in the cerebellum." J Comp Neurol **343**(4): 513-9.
Weiss, D. S. & K. L. Magleby (1989). "Gating scheme for single GABA-activated Cl- channels determined from stability plots, dwell-time distributions, and adjacent-interval durations." J Neurosci **9**(4): 1314-24.
Wenzel, A., J. M. Fritschy, H. Mohler & D. Benke (1997). "NMDA receptor heterogeneity during postnatal development of the rat brain: differential expression of the NR2A, NR2B, and NR2C subunit proteins." J Neurochem **68**(2): 469-78.
Williams, K. (1993). "Ifenprodil discriminates subtypes of the N-methyl-D-aspartate receptor: selectivity and mechanisms at recombinant heteromeric receptors." Mol Pharmacol **44**(4): 851-9.
Williams, K. (1995). "Pharmacological properties of recombinant N-methyl-D-aspartate (NMDA) receptors containing the epsilon 4 (NR2D) subunit." Neurosci Lett **184**(3): 181-4.
Wollmuth, L. P., T. Kuner & B. Sakmann (1998). "Adjacent asparagines in the NR2-subunit of the NMDA receptor channel control the voltage-dependent block by extracellular Mg2+." J Physiol **506 (Pt 1)**(Pt 1): 13-32.
Wollmuth, L. P., T. Kuner & B. Sakmann (1998). "Intracellular Mg2+ interacts with structural determinants of the narrow constriction contributed by the NR1-subunit in the NMDA receptor channel." J Physiol **506 (Pt 1)**(Pt 1): 33-52.
Wollmuth, L. P. & A. I. Sobolevsky (2004). "Structure and gating of the glutamate receptor ion channel." Trends Neurosci **27**(6): 321-8.
Wolosker, H. (2006). "D-serine regulation of NMDA receptor activity." Sci STKE **2006**(356): pe41.
Wrighton, D. C., E. J. Baker, P. E. Chen & D. J. Wyllie (2007). "Mg2+ and memantine block of rat recombinant NMDA receptors containing chimeric NR2A/2D subunits expressed in Xenopus laevis oocytes." J Physiol.
Wrighton, D. C., E. J. Baker, P. E. Chen & D. J. Wyllie (2008). "Mg2+ and memantine block of rat recombinant NMDA receptors containing chimeric NR2A/2D subunits expressed in Xenopus laevis oocytes." J Physiol.
Wyllie, D. J., P. Behe & D. Colquhoun (1998). "Single-channel activations and concentration jumps: comparison of recombinant NR1a/NR2A and NR1a/NR2D NMDA receptors." J Physiol **510 (Pt 1)**(Pt 1): 1-18.
Wyllie, D. J., P. Behe, M. Nassar, R. Schoepfer & D. Colquhoun (1996). "Single-channel currents from recombinant NMDA NR1a/NR2D receptors expressed in Xenopus oocytes." Proc Biol Sci **263**(1373): 1079-86.
Yung, W. H., M. A. Hausser & J. J. Jack (1991). "Electrophysiology of dopaminergic and non-dopaminergic neurones of the guinea-pig substantia nigra pars compacta in vitro." J Physiol **436**: 643-67.
Zeevalk, G. D. & W. J. Nicklas (1990). "Action of the anti-ischemic agent ifenprodil on N-methyl-D-aspartate and kainate-mediated excitotoxicity." Brain Res **522**(1): 135-9.
Zhang, X. X., B. S. Bunney & W. X. Shi (2000). "Enhancement of NMDA-induced current by the putative NR2B selective antagonist ifenprodil." Synapse **37**(1): 56-63.
Zhu, Y. & A. Auerbach (2001). "K(+) occupancy of the N-methyl-d-aspartate receptor channel probed by Mg(2+) block." J Gen Physiol **117**(3): 287-98.
Zhu, Y. & A. Auerbach (2001). "Na(+) occupancy and Mg(2+) block of the n-methyl-d-aspartate receptor channel." J Gen Physiol **117**(3): 275-86.